INTERNATIONAL HELLENIC UNIVERSITY

SCHOOL OF ENGINEERING

DEPARTMENT OF INFORMATION AND ELECTRONIC ENGINEERING

BACHELOR THESIS

«Comparative Study of Electronic Circuits for Bacterial Identification»

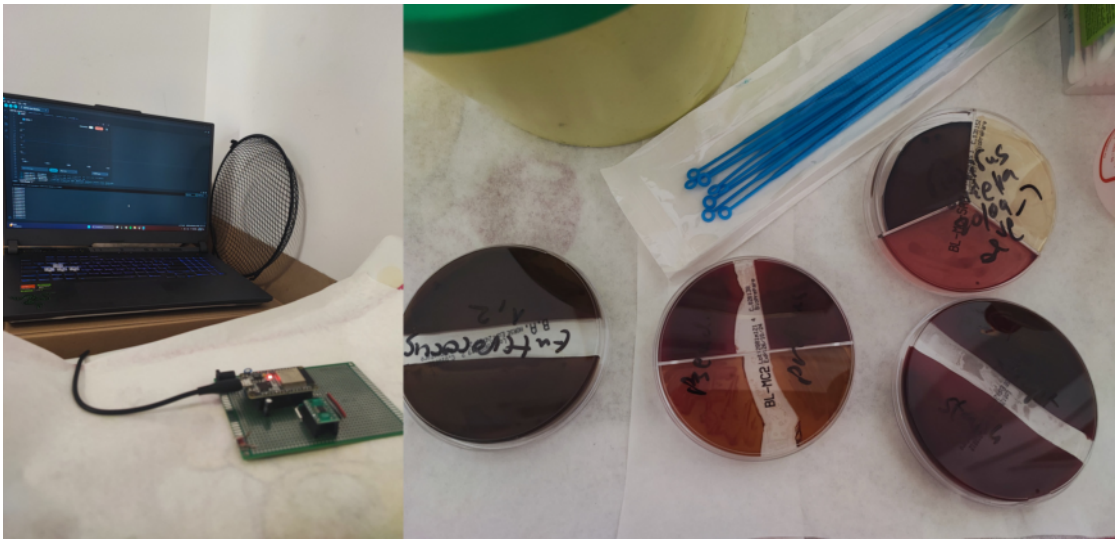

Student
Dimitrios D. Koliouskas
Student Number: 518060

Supervisor
Dr. Argyrios T. Hatzopoulos
Assistant Professor

Co-Supervisor
Vasileios Delimaras
Ph.D. Candidate

September 17, 2024

Thesis Title: Comparative Study of Electronic Circuits for Bacterial Identification
Thesis number: 23315
Student's full name: Dimitrios D. Koliouskas
Supervisor's full name: Argyrios T. Hatzopoulos
Co-Supervisor's full name: Vasileios Delimaras
Thesis ascension date: 04/11/2023
Thesis publish date: 17/09/2024

I hereby certify that I am the author of this paper and that any assistance I may have received in its preparation is fully acknowledged and referenced in the paper. Furthermore, I have recorded all sources that have been used; ideas, images and text, whether quoted verbatim or paraphrased. Furthermore, I certify that this thesis prepared by me, meets the standards required for submission as a thesis at the Department of Information and Electronic Engineering, International Hellenic University (IHU).

The approval of this thesis by the Department of Information and Electronic Engineering of the International Hellenic University does not necessarily indicate that the views expressed by the author are endorsed by the Department.

«In memory of my beloved father...»

Preface

During my final semesters at university, I came to the realization that studying, researching and innovating fulfilled me. Furthermore, I often found myself engaged in contemplating a multitude of concepts pertaining to technological advancement. All the above made me realise that my thesis should be based on research.
To be more precise, my thesis would comprise both a theoretical and a practical part. I am eager to see the final result implemented in practice, rather than merely studying it theoretically.

I resolved that the project would be interdisciplinary in nature and that the various components would be integrated in a coherent manner. At the outset, a number of ideas, plans and proposals were formulated with respect to a range of disciplines, including robotics, automatic control systems, analogue and digital electronics, machine learning, computer vision, artificial neural networks and artificial intelligence, optimisation algorithms and dielectrophoresis. All of these disciplines would coexist in the field of biomedicine.

Ultimately, as the project remains at the undergraduate level, some of the aforementioned areas were combined, while the remainder will be reserved for future research and publications. The benefits accrued during this period as a result of this process are manifold.
It is worth mentioning that this research reinforced my enthusiasm for pursuing a career in biomedical engineering.

Abstract

This bachelor thesis addresses the nexus of innovation and interdisciplinary inquiry in two interconnected domains; technology and healthcare.
On the one hand, this thesis concentrates on the domains of electronic engineering and programming. Concerning the field of electronics, the primary focus is on micro-scale and interconnected circuits, whereas concerning the domain of programming, stress is placed on microcontroller programming and graph creation.
On the other hand, concerning the health sector, I focused on the field of microbiology and more precisely, on bacteria.
The objective of this research is to develop an affordable device responsible for the rapid and accurate identification of bacteria.

In the initial phase of the study, a comparison is made between various circuits and electronic capacitance devices to identify the optimal one. More particularly, the Interdigitated/Interdigital electrodes intended for use as sensors will be subjected to analysis. Upon completion of the experiments and attainment of the anticipated outcomes, the design of the printed circuit board will commence. Concurrently, cultures of six distinct bacterial strains, comprising three Gram-positive and three Gram-negative organisms, will be prepared. Once the device is ready for use, experiments will be conducted in a microbiology laboratory with appropriate equipment and answers to the first question in microbiology will be given; are the bacteria analyzed Gram positive or Gram negative? In this instance, the objective is to ascertain whether there are disparate electrical properties between Gram-positive and Gram-negative bacteria, with a specific focus on their capacitance values. Subsequently, the disparate electrical properties of the various bacterial types will be evaluated in comparison to one another.

The research was fruitful and more importantly, the device was successfully created. This achievement can be regarded as a significant milestone in the field of technology, particularly because improvements in the healthcare industry can be made.

Keywords: Bacterial Identification, Electronic Circuits, Interdigitated/Interdigital Electrodes, Capacitance Measurement, Gram-Positive and Gram-Negative Bacteria, Biosensors, Biomedical Engineering, Innovative Bacterial Detection, Capacitance-Based Biosensing, Microcontroller Integration in Microbiology, Cost-Effective Bacterial Identification.

«Συγκριτική Μελέτη Ηλεκτρονικών Διατάξεων για Ταυτοποίηση Βακτηρίων»

«Δημήτριος Δ. Κολιούσκας»

Περίληψη

Το θέμα της παρούσας ερευνητικής Διπλωματικής Εργασίας αφορά την καινοτομία και την διεπιστημονικότητα δύο εκ των κυριότερων τομέων της καθημερινότητας, της τεχνολογίας και του κλάδου υγείας.
Όσον αφορά την τεχνολογία, η εργασία επικεντρώνεται στον τομέα της ηλεκτρονικής μηχανικής και στον τομέα του προγραμματισμού. Στο κομμάτι της ηλεκτρονικής δίνεται βάση κυρίως στη μικροκλίμακα και στα διασυνδεδεμένα κυκλώματα, ενώ στο κομμάτι του προγραμματισμού, δίνεται βάση, κυρίως, στον προγραμματισμό μικροελεγκτών και την δημιουργία γραφημάτων.
Από την άλλη, όσον αφορά τον κλάδο υγείας, η εργασία επικεντρώνεται στον τομέα της μικροβιολογίας σε ό,τι αφορά τα βακτήρια.
Τελικός στόχος της εργασίας αυτής, είναι η δημιουργία μιας φθηνής (συγκριτικά με τις υπόλοιπες μεθόδους) συσκευής που θα χρησιμοποιείται για την αποτελεσματική ταυτοποίηση των βακτηρίων.

Αρχικά, συγκρίνονται διάφορα κυκλώματα και ηλεκτρονικές διατάξεις χωρητικότητας ώστε να βρεθεί το βέλτιστο μεταξύ τους. Στη συνέχεια, θα αναλυθούν τα διασυνδεδεμένα/διαψηφιακά ηλεκτρόδια που θα χρησιμοποιηθούν ως αισθητήρια. Όταν ολοκληρωθούν τα πειράματα και βρεθούν τα προσδοκόμενα αποτελέσματα, θα σχεδιαστεί η πλακέτα τυπωμένου κυκλώματος. Ταυτόχρονα θα ετοιμάζονται καλλιέργειες 6 διαφορετικών βακτηρίων, 3 θετικά κατά Gram και 3 αρνητικά κατά Gram. Όταν πλέον θα είναι έτοιμη η συσκευή, θα ακολουθήσουν πειράματα σε μικροβιολογικό εργαστήριο με κατάλληλο εξοπλισμό για να απαντηθεί το πρώτο ερώτημα που τίθεται στη μικροβιολογία, είναι τα βακτήρια που αναλύονται θετικά κατά Gram ή αρνητικά κατά Gram; Στην προκειμένη, αν έχουν διαφορετικές ηλεκτρικές ιδιότητες τα θετικά κατά Gram βακτήρια από τα αρνητικά κατά Gram βακτήρια και συγκεκριμένα αν έχουν διαφορετικές τιμές χωρητικότητας. Έπειτα, θα δοκιμαστούν για τις διαφορετικές ηλεκτρικές ιδιότητες οι διαφορετικοί τύποι βακτηρίων μεταξύ τους.

Τα αποτελέσματα της έρευνας ήταν τα αναμενόμενα και δημιουργήθηκε επιτυχώς η χρήσιμη αυτή συσκευή. Η μέρα των επιτυχών αποτελεσμάτων θεωρείται σημαντική μέρα για την ανάπτυξη της τεχνολογίας και ιδίως την διευκόλυνση του κλάδου υγείας.

Λέξεις-κλειδιά: Ταυτοποίηση Βακτηρίων, Ηλεκτρονικά Κυκλώματα, Διασυνδεδεμένα/Διαψηφιακά Ηλεκτρόδια, Μέτρηση χωρητικότητας, Gram-Θετικά και Gram-Αρνητικά Βακτήρια, Βιοαισθητήρες, Βιοϊατρική Μηχανική, Καινοτόμος Εντοπισμός Βακτηρίων, Βιοανίχνευση Βάσει της Χωρητικότητας, Ενσωμάτωση Μικροελεγκτών στη Μικροβιολογία, Οικονομικά Αποδοτική Ταυτοποίηση Βακτηρίων.

Acknowledgements

I would like to express my gratitude to my family and particularly to my mother. I am grateful for both her psychological and financial support.

I would also like to express my gratitude to my esteemed colleague, Stefanos Fr. Koufidis (Ph.D. Candidate at Imperial College London), for his invaluable guidance in the scientific editing of this paper.

In addition, I would like to extend my gratitude to Dr. Varlamis G. Sotirios, who kindly provided me with laboratory instruments in his private microbiological laboratory and for his guidance in the field of healthcare, thus facilitating the completion of tasks that would otherwise have been left for future research and study.

Furthermore, I would be remiss if I did not express my sincerest gratitude to the supervisor of this thesis, Dr. Argyrios T. Hatzopoulos. Throughout the years of my studies in a variety of subjects, he taught me a lot and he bestowed upon me a great deal of trust for a research topic as a final project.

In conclusion, I would like to salute Ph.D. candidate Delimaras Vassileios, who served as the responsible co-supervisor of this thesis and my mentor.
His significant contribution to my intellectual and scientific development has made me more optimistic. Thanks to him, I have learned to pursue my dreams and try to become the best version of myself. Without his presence, this research would not have been so fruitful.
As a result of our multifaceted interactions, which encompassed both educational and scientific discourse, as well as personal communication, a profound enthusiasm for the subject matter was instilled within me. A passion for the pursuit of knowledge.

Contents

List of Figures

List of Tables

List of Appendices

Appendix A: BACTERIA AND THEIR IDENTIFICATION METHODS

Appendix B: AD7745

Appendix E: MATLAB CODE USED FOR GRAPHS IN CHAPTER 7

List of Acronyms

ADC	Analog-to-Digital Converter
AD7745ARUZ	Specific integrated circuit used in the design
CAPDAC	Capacitive Digital-to-Analog Converter
CDC	Capacitance-to-Digital Converter
CRISPR	Clustered Regularly Interspaced Short Palindromic Repeats
DC	Direct Current
DEP	Dielectrophoresis
DNA	Deoxyribonucleic Acid
DNase	Thermolabile Nuclease
DNL	Differential Nonlinearity
EC	Electrolyte Conductivity
ELISA	Enzyme-Linked Immunosorbent Assay
ESR	Equivalent Series Resistance
fF	Femtofarads
IC	Integrated Circuit
IHU	International Hellenic University
I2C	Inter-Integrated Circuit
IDAM	Interdigitated Microelectrode Arrays
IDE	Integrated Development Environment
IDEs	Interdigitated Electrode Arrays
IDES	Interdigitated Electrode Structures
IDTs	Interdigitated Transducers
IR	Infrared
LPS	Lipopolysaccharide (component of bacterial cell walls)
MALDI-TOF MS	Matrix-Assisted Laser Desorption/Ionization Time-of-Flight Mass Spectrometry

MIDCAP	Multi-finger Interdigitated Capacitor
MIPs	Molecularly Imprinted Polymers
MS	Mass Spectrometry
MUT	Material Under Test
NMOS	N-Channel Metal-Oxide-Semiconductor
O-NPG	Ortho-Nitrophenyl-β-Galactopyranoside
PCB	Printed Circuit Board
PCR	Polymerase Chain Reaction
PHIL	Public Health Image Library
PFGE	Pulse-Field Gel Electrophoresis
PMOS	P-Channel Metal-Oxide-Semiconductor
PSR	Power Supply Rejection
RDY	Ready (signal pin in I2C communication)
RMS	Root Mean Square
SAW	Surface Acoustic Wave
SCL	Serial Clock Line
SDA	Serial Data Line
Si	Silicon
SiO_2	Silicon Dioxide
SMD	Surface-Mount Device
SMD-to-DIP	Surface-Mount Device to Dual In-Line Package
UV	Ultraviolet (a form of electromagnetic radiation)
VDD	Voltage Drain Drain (power supply pin)
WGS	Whole Genome Sequencing

Chapter 1

Introduction

1.1 Introduction

This chapter establishes the foundation for the thesis by examining the fundamental concepts of microbiology, with a particular emphasis on the classification and identification of bacteria. This section critically examines the conventional approaches used in bacterial identification and more particularly, their shortcomings with regards to cost-effectiveness, accuracy, and time efficiency. In this chapter, we will focus on the need for innovation in this field, emphasizing the potential of electronic circuits to transform the bacterial identification process. In fact, this chapter presents a revolutionary method that combines microbiological analysis with electronic engineering concepts.
After providing a brief introduction to microorganisms and bacteria, we will analyze the various and different methods of classification and identification of bacteria. Then, we will shed light on the main problem that exists in microbiology laboratories and clinics regarding the identification of bacteria, by providing information drawn from modern studies. Then, we will focus on the implementation of an innovative way of bacterial identification, as well as on the objective and expected results of this work. The theoretical and experimental procedures follow in detail. At the end of the thesis, conclusions will be made and ideas for future research and development will be proposed.

1.2 Microbiology

1.2.1 Biology and the Microworld

Biology is the science that examines life and the processes that keep it going. In this discipline, every aspect of life's physicochemical makeup is explored. Due to the current tendency towards interdisciplinary inquiry and the integration of scientific knowledge from various fields, the fields of biology and other scientific disciplines have a lot in common.

Microbiology is the study of a broad range of often tiny, fundamental life things, such as bacteria, viruses, and archaea. It is sometimes referred to as the study of microorganisms or microbes. This field deals with the construction, classification, and utilization of such organisms as well as techniques for influencing and controlling their behavior.

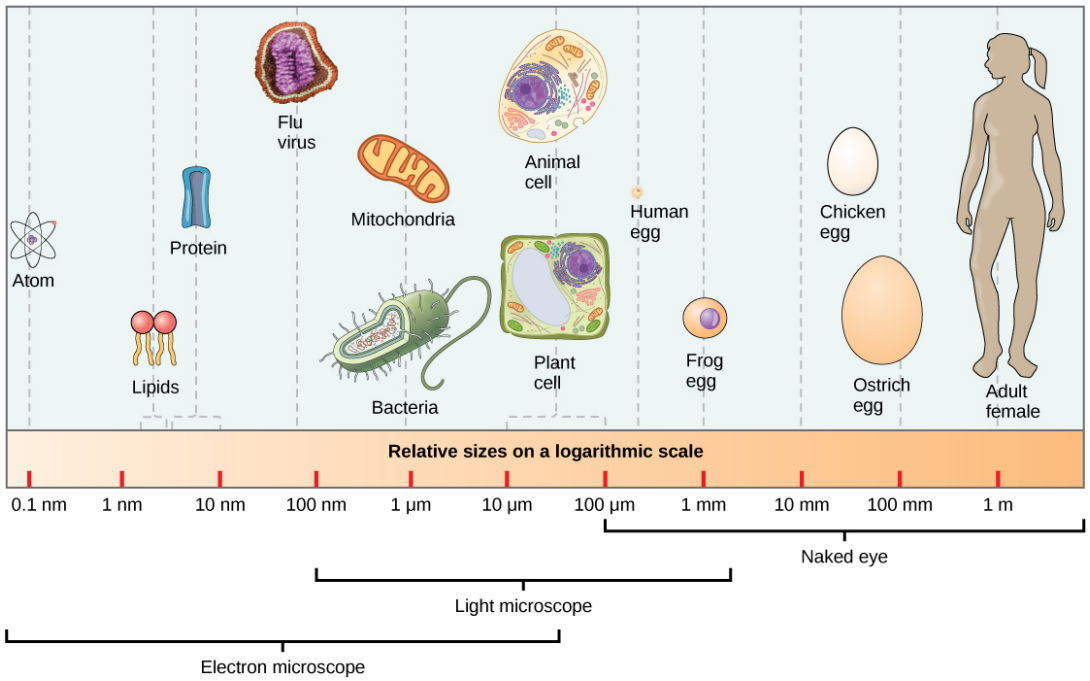

Figure 1.1: A logarithmic scale of microbes
Source: LibreTexts / Biology / 4.2: Prokaryotic Cells

1.2.2 Microorganisms and Bacteria

The tiny creatures known as microorganisms, sometimes referred to as microbes, can be either single cells or colonies of cells. Microbes may be highly diverse since they make up the bulk of unicellular organisms in all three realms of life. Bacteria and Archaea are the only domains that include microorganisms. The third category, Eukaryota, includes all multicellular organisms as well as a sizable number of protozoans and unicellular protists. It is worth mentioning that protists share a relationship with both living things and green plants. Last but not least, there are many tiny multicellular organisms that are not normally thought of as microbes, including micro-animals, certain fungi, and some types of algae.
The relationship between microbes and daily living is complex. In addition to being present on the interior and external surfaces of the human body, microbes are also widely distributed in the soil, seas, and air. Even though they are usually invisible, microorganisms are numerous and their presence is evident. On the one hand, they can spread disease or cause material decay and on the other hand, they can ferment substances, like sugar for instance, leading to the fermentation of wine and beer. They are even able to produce valuable products like antibiotics and insulin. Given that microorganisms convert leftover animal and plant material into more easily recycled forms, we can deduce that they are of utmost importance for our planet's ecology.

Bacteria, or a single bacterium, refers to any of a group of microscopic single-celled organisms that are widespread on Earth and may be found in almost every ecosystem, from deep-sea vents to human digestive tracts. Prokaryotes, which are unicellular living organisms, include bacteria. They lack an internal structure, including a membrane-bound nucleus. For at least 75 percent of its history, prokaryotes have dominated life on Earth and have evolved to fill almost all of its biological niches. They can

use nearly every organic molecule as well as certain inorganic materials as nourishment, and they have highly diverse metabolic capabilities. The majority of bacteria are benign ecological organisms whose metabolic functions sustain higher life forms, even though some of them can cause diseases. Other bacteria coexist with plants and invertebrates as symbionts, carrying out vital functions for their hosts including fixing nitrogen and breaking down cellulose. In the absence of prokaryotes, the soil would not be productive and organic matter would decay considerably more slowly. Certain bacteria are used in the preparation of several meals, substances, and pharmaceuticals. Studies of the interactions between different bacterial species continue to offer novel insights into the processes that led to the origin of life on Earth. Despite having far smaller and simpler cells than eukaryotic cells, the bacterial kingdom has an immensely diverse assortment of animals that differ in size, form, habitat, and metabolism. Since they are simpler to isolate in pure culture than many different forms of free-living bacteria, studies of bacteria that cause disease have made a substantial contribution to our understanding of them. At this point, we would like to highlight that many free-living bacteria are very different from those that have evolved to live on mammals as parasites or symbionts. For that reason, no generalizations about the make-up or structure of bacteria should be made. Three different species of bacteria—Bacillus, Vibrio, Spirillum, and Spirochetes—can have one of three basic shapes: spherical (Coccus), rod-like (Bacillus), or curved (Spirillum). Bacteria can have a wide range of real morphologies, and cells can be stretched or compressed in one dimension. Bacteria that do not separate from one another during cell division form recognizable clusters that make them easier to identify.

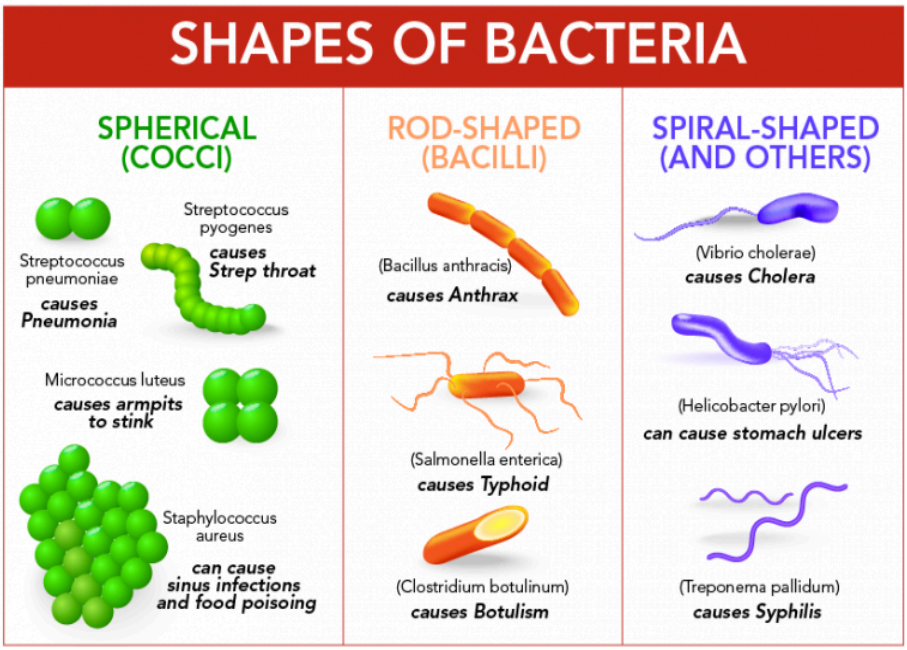

Figure 1.2: Different shapes of bacteria
Source: Let's Talk Science / Introduction to Bacteria

1.3 Bacterial Classification and Identification

Scientists argue that in a handful of soil in a person's hands or in a glass filled with water, there are about a million different kinds of bacteria. Although most of these cannot be grown in a laboratory to

be studied in detail, there remain hundreds of thousands of different species that can be. For that reason, various ways of classifying and identifying them have been developed. The science of classifying living organisms is called taxonomy. We have been employing taxonomy since the Swedish botanist Carl Von Linné, or Linneus, established a system for classification using taxonomic categories in the 18th century. He wanted to minimize the chaos caused by new species being continually discovered and provide a structure for defining and identifying these species. In the bacterial hypothesis, classification is the name given to specifically developed methods for identifying bacteria. Identification is aimed at classifying the microorganism into a specific genus, species, serotype, biotype and resistance species. The reference to the name of the bacteria is made in two words, the first specifying the genus and the second specifying the species. Names should be presented in italics, e.g. *Staphylococcus aureus* (see Figure 1.3). There are 3 main categories of bacterial classification: the phenotypic, the analytical and the genotypic.

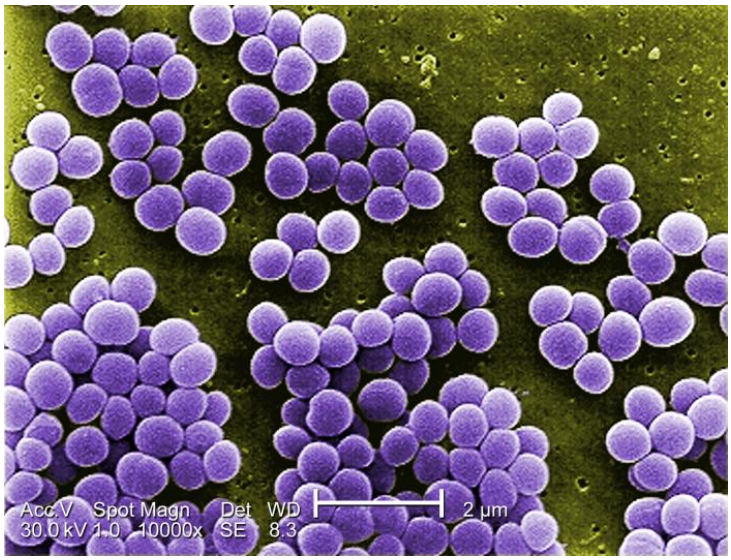

Figure 1.3: A high magnification of 10,000X of *Staphylococcus aureus* bacteria
Source:: Centers for Disease Control and Prevention(CDC) / Public Health Image Library (PHIL)

1.3.1 Phenotypic Classification

Phenotypic classification, which is the traditional classification, is based on morphology and refers to observable characteristics such as size, shape and colour. It was developed in the 1900s-1950s. Scientists were based on observing microscopic and macroscopic morphological characteristics of bacteria. There are the following identification methods: Gram staining, bacterial cell morphology and regulation, different types of colours, culture characteristics, growth requirements, biochemical reactions, serological systems, antibiograms and fully or semi-automatic identification methods (Vitek, Phoenix, etc.). More specifically, using Gram's stain (the method was developed by Hans Christian Gram in 1884) depending on whether the cell wall was purple or pink, we distinguished between Gram positive and Gram negative bacteria. In this way, it was possible to determine how much peptidoglycan their cell wall contained. Positive Gram organisms have a thin wall of peptidoglycan retaining a lot of crystalline violet staining and thus displaying a vivid blue under the microscope. Negative Gram organisms, on the other hand, have an even thinner layer of peptidoglycan, which does not retain the

blue staining. Even this slight simplification of the separation, into positive and negative Gram, serves to explain their behaviour. Gram-positive bacteria have large peptidoglycan structures. As already mentioned, this explains the different staining with Gram staining. Some Gram-positive bacteria can also produce spores in cases where the environment is harsh, for instance, in environments where there is a lack of carbon and nitrogen. For that reason, the bacteria can survive in harsh environments thanks to their spores, which can also lead to reinfections (such as *pseudomembranous colitis* from *Clostridium difficile*). In addition to a thin layer of peptidoglycan, Gram-negative bacteria also have an additional membrane known as the outer cytoplasmic membrane. This adds another permeability barrier and necessitates the use of transport mechanisms to cross the membrane. The cytoplasmic membrane of Gram-negative bacteria is composed mainly of endotoxin. It is essential for bacteria to possess this component. The endotoxin consists of the species-specific antigen. O (also a polysaccharide), the highly conserved polysaccharide core and the lipid part A. Endotoxins are associated with cells, unlike exotoxins which are generated, however they can also be shed after cell division or cell death. The lipid A portion of the endotoxin is responsible for the potentially fatal condition of sepsis. Disorientation, fever, drop in blood pressure and eventually multiorgan failure are clinical signs of sepsis. Endotoxin, also known as Lipopolysaccharide (component of bacterial cell walls) (LPS). [1] The bacilli cell morphology and regulation refers to the types: bacilli, cocci and spirilla. They are recognized by their shape, the bacteria that are rod-shaped are called bacilli, those that are spherical cocci and those that are spiral or multi-curved shaped spirilla. As we mentioned before, different types of staining can occur with fast acid staining, capsule staining, spore staining, flagella staining and many others. Some microbes, have very distinct color characteristics, such as the genus *Mycobacterium* (see on Appendix A, Figure A.1) which can be detected by fast acid. The characteristics of a culture (colonial morphology) are observed in how it grows on agar in the laboratory. Here too, size, shape, colour and even smell are noted. For example, *streptococci* colonies tend to be smaller than most other types and *Serratia marcescens* (see on Appendix A, Figure A.2) typically appears red at 22 degrees Celsius. They can be tested for haemolytic properties in blood agar, determining whether the bacteria produce toxic by-products capable of destroying red blood cells. For example, *Streptococcus pyogens* (see on Appendix A, Figure A.3), the cause of pharyngitis, is a Gram-positive bacterium that forms long chains of cocci and grows as small, white, haemolytic colonies on blood agar plates. The method that observes the growth requirements of bacteria refers to the fact that they can be grouped based on their need for oxygen to grow. In terms of serological systems, a complement to biochemical identification, specific antisera detect either carbohydrate or protein antigens, from bacteria (Enzyme-Linked Immunosorbent Assay (ELISA), agglutination) and this leads to rapid identification of clinical data. The aforementioned phenotypic characterizations are used merely to begin the process of identifying bacteria so that they can be investigated more thoroughly than others. These are their biochemical reactions and properties, such as their ability to ferment carbohydrates, which carbon sources they can use for their growth and the presence or absence of various enzymes such as lipases, proteases or nucleases. These techniques have also been used to subdivide groups of organisms beyond the species level down to a specific strain. Examining the genetic makeup of an organism, especially in the case of an epidemic, is called biotyping. Many bacteria also have antigens, which may be a toxin or other substance that causes an immune response in the organism. The grouping of bacteria based on these antigens is called serotyping. Using serotyping, scientists can work in reverse using antibodies to detect which antigens are present, allowing them to limit the bacteria's capabilities. Serotyping is a powerful tool

for classification, especially for species that are difficult to culture, difficult to test biochemically, or that need to be identified quickly, such as during an outbreak. Scientists can also be assisted by the use of phage typing since they can have access to the bacteriophages to which bacteria may be sensitive.

The most important method would be biochemical identification since it is useful for enzyme production. There are many types of enzyme assays, which are tested for their presence in the microorganism being tested. The basic tests for these enzymes are called: catalase, oxidase, optokinin, bacitracin, X/V growth factors, thermosensitive nuclease (extracellular Thermolabile Nuclease (DNase)), acycline, indole, indole, motility, urease, coagulase (pectase), Ortho-Nitrophenyl-β-Galactopyranoside (O-NPG). More precisely, there are several other types of tests, such as carbohydrate utilization mentioned above, glucose oxidation/fermentation, phenylalanine deamination, lysine decarboxylation, three sugar utilization test, etc. The catalase assay, tests for the presence of the enzyme catalase, using 3% H2O2 (produced during the breakdown of carbohydrates) and microbial culture on a slide. Thus, if H2O2 is broken down into H2O and O producing bubbles, then it is catalase positive (see on Appendix A, Figure A.4). Oxidase test, checks if the enzyme cytochrome oxidase is present, using o-phenylenediamine hydrochloride in solution, tablets, strips or strips and fresh colonies. If NADH (due to the enzyme) is converted to NAD + H2O, then a blue colour appears in 10 minutes. Then it is positive to oxidase (see on Appendix A, Figure A.5). In the optochin test, it tests the sensitivity of the microorganism to optochin (otherwise ethyl hydrocupreinehydrochloride) which activates autolytic enzymes of the microorganism and thereby induces its lysis. Hematous agar, optochin tablets, incubation in 5% CO2 for 24 hours are used. If the inhibition zone of the microorganism is greater than or equal to 10 thousand, it is positive to optochin. This test is particularly useful in the crude discrimination of *pneumococci/a-hemolytic streptococci* (see on Appendix A, Figure A.6). The bacitracin test, tests the sensitivity of the microorganism to the antibiotic bacitracin. It uses blood agar, bacitracin tablets and incubation for 24 hours. If there is growth inhibition then they are positive to bacitracin. Very useful test in distinguishing group A *beta-hemolytic streptococcus* (GAS) from other *beta-hemolytic streptococci* (see on Appendix A, Figure A.7). The X/V growth factors test, the dependence of haemophiliacs on the factors, X(protoporphyrin) and Y(amine) found in the blood, is tested for growth. Blood-free material and tablets impregnated with X/V/XV factors at a distance of 3,5 mm are used. Incubation in 5% CO2 18-24. A check is made for growth around the discs (i.e. dependence on the specific agent) (see on Appendix A, Figure A.8). The (DNase) assay, tests for the presence of extracellular DNase that hydrolyzes, HCL-insoluble Deoxyribonucleic Acid (DNA), into soluble oligonucleotides. DNA material is used and incubated for 18-24 hours. After incubation, the culture is flooded with 1M (3,6%) HCL. Check for clear algae around the positive control and the tested micro-organism. If there is presence of clear aloes then they are DNase positive, otherwise if there is absence of clear aloes or the aloe is less than the stigma (CNS, etc.) (see on Appendix A, Figure A.9). The esculin test, tests the ability of the microorganism to hydrolyze, in the presence of bile, colourless esculin into glucose and esculin which in the presence of Fe++ produces a black complex. Use of a tyrosine agar in dish or tubes or a tyrosine broth and incubation from 4 to 24 hours. If there is production of black colour it is positive to esculin. One such example is *enterococcus* (see on Appendix A, Figure A.10). The indole test, tests the ability of the microorganism to produce the enzyme tryptophanase which hydrolyzes the amino acid tryptophan into indole and aldehyde. Peptone broth with 1% tryptophan, incubation for 18-24 hours and Kovacs reagent (p dimethylamino benzaldehyde, amyl alcohol, HCL) is used. If a pink ring appears

on the surface, then it is indole positive, for example *E. coli.* If a colourless ring appears on the surface, then they are indole negative. For example *Klebsiella spp* (see on Appendix A, Figure A.11). The motility test, tests the ability of microorganisms, mainly bacteria and rarely granules, to move due to the presence of flagella. Semi-liquid agar in a tube, with or without dye, inoculation by deep inoculation and incubation for 18-24 hours at 35-37°C is used. If there is diffusion and blurring of the material, then it is positive in mobility. The result of this test, of course, depends on the incubation conditions, e.g. *Y. enterocolitica mobile* at 20-25°C and immobile at 30°C(see on Appendix A, Figure A.12). The urease test tests the ability of the microorganisms to break down urea into two molecules of ammonia with their urease enzyme, resulting in an increase in the pH of the material. Use urea broth with urea and phenol red indicator at pH 6,8, incubated for 18 to 24 hours at 35 to 37°C. If a pink color appears from the change in indicator with an increase in pH to 8.4, then it is urease-positive. For example, *Proteus spp* and *Helicobacter/campylobacters* (see on Appendix A, Figure A.13). The coagulase (pectase) assay, tests the ability of staphylococci to cause plasma clotting by means of the enzyme coagulase which they produce in two forms the cell wall-bound (clumping factor) and the free one released by the microorganism. A plaque test is used for the bound (*staphylococcus* suspension + anaerobic plasma or latex particle reagent). If there is production of clumps, they are coagulase positive. On the other hand, a tube test for free (*staphylococcus* suspension + human or commercial plasma suitably diluted with conglomerate plasma, incubated for 4 hours) is used. If there is coagulum production, they are coagulase positive (see on Appendix A, Figure A.14). Finally, the O-NPG assay, tests for the presence of b-galactosidase in the microorganism which, together with permease, causes the breakdown of lactose into galactose and glucose. The permease introduces the lactose into the cell, while the galactosidase breaks it down. Some microorganisms have only galactosidase and are unable to break down lactose (slow fermenters). O-NPG solution (which has the same structure as lactose) is used, incubated for 18-24 hours at 35-37°C. If a yellow colour appears, they are O-NPG positive). Such an example is the lactose-slow fermenting *enterobacteria* and *neisseria* (see on Appendix A, Figure A.15).

Below, 3 tables are attached as an example of the phenotypic classification method of bacteria. Tables 1.3.1, 1.3.2 and 1.3.3 illustrate charecteristics, date and examples of Gram-Positive, Gram-Negative and miscellaneous bacteria respectively.

Table 1.3.1: Gram Positive Bacteria [1]

Name	Morphology	O_2 Requirements	Commensal	Reservoirs / Sites of colonization, Transmission	Types of Infections
Staphylococci	Cocci in grape-like clusters	facultative anaerobe	Yes	Skin, nares / endogenous, direct contact, aerosol	Soft tissue, bone, joint, endocarditis, food poisoning
Streptococci	Cocci in pairs, chains	facultative anaerobe	Some species	Oropharynx, skin / endogenous, direct contact, aerosol	Skin, pharyngitis, endocarditis, toxic shock
Pneumonococci	Diplococci, lancet shaped	facultative anaerobe	Yes / No	Oropharynx, sinus / aerosol	Pneumonia, otitis, sinusitis, meningitis
Enterococci	Cocci in pairs, chains	facultative anaerobe	Yes	GI tract / endogenous, direct contact	UTI, GI, catheter-related infections
Bacilli	Rods, spore-forming	aerobic	Yes / No	Soil, air, water, animals / aerosol, contact	Anthrax, food poisoning, catheter-related infections
Clostridia	Rods, spore formers	anaerobic	Some Species	GI tract, soil / Breach of skin, endogenous, ingestion	Tetanus, diarrhea, gas gangrene, botulism
Corynebacterium	Rods, nonspore forming	facultative anaerobe	Some species	Skin	Catheter-related infections, diphtheria
Listeria	Rods, nonspore formers	facultative anaerobe	No	Animals, food products / Ingestion	Meningitis
Actinomyces	Irregular, filamentous, form sulfur granules	anaerobic	Yes	GI tract / endogenous	Skin, soft tissue

Table 1.3.2: Gram Negative Bacteria [1]

Name	Morphology	O_2 Requirements	Commensal	Reservoirs / Sites of colonization, Transmission	Types of Infections
Entero-bacteriaceae (E. coli, klebsiella, salmonella, shigella)	Rods	facultative anaerobe	Some species	GI tract, animals / Endogenous, fecal oral	Diarrhea, uninary tract, food poisoning, sepsis
Bacteroides	Rods	anaerobic	Yes	GI tract / Endogenous	Abscesses
Pseudomonas	Rods	aerobic	No	Water, soil / Endogenous, breach of skin barrier	Infections in immunocompromised hosts, Cystic Fibrosis
Vibrio (cholera)	Rods, curved shap	micro-aerophilic	No	Water / Contaminated food, water	Diarrhea
Campylobacter	Rods, curved shape	micro-aerophilic	No	Food / Ingestion of contaminated food	Diarrhea, Bacteremia
Legionella	Rods, poorly stained	micro-aerophilic	No	Water Inhalation of aerosol	Pneumonia, febrile illness
Neisseriam	Cocci, kidney-bean shaped	Micro-aerophilic	No (*N. meningitidis* sometimes)	Humans / Sexual, aerosol	Meningitis, pelvic inflammatory disease
Hemophilus	Coccobacillary-pleomorphic	facultative anaerobe	Some species	Respiratory tract / Endogenous, aerosol	Respiratory, sinusitis, otitis, meningitis
Bartonella	Small, pleo-morphic rods	aerobic/micro-aerophilic	No	Cats, fleas, lice / cat bites, lice or fleas?	Cat scratch disease, endocarditis, bacillary angiomatosis

Table 1.3.3: Miscellaneous Bacteria [1]

Name	**Morphology**	**O_2 Requirements**	**Commensal**	**Reservoirs / Sites of colonization, Transmission**	**Types of Infections**
Helicobacter	Not visible on Gram stain - helical (corkscrew) shaped	microaerophilic	Yes	Stomach / Endogenous, Fecal-oral	peptic ulcer disease, gastric ulcer
Mycobacteria	Rods, Weakly Gram positive, Acid fast stain positive	aerobic	No	Lungs / Fomites	Tuberculosis
Treponemes	Not visible on Gram stain, spiral shaped on dark field exam	Non-culturable on routine media	No	Humans / Sexual transmission	Syphilis
Borrelia	Not visible on Gram stain, spiral shaped on dark field exam	Non-culturable on routine media	No	Rodents, Ticks / Tick bites	Lyme, Relapsing fever
Mycoplasma	Not visible on Gram stain, no cell wall, pleomorphic	Non-culturable on routine media	Some species	Humans / aerosol	respiratory tract infections
Rickettsia / Ehrlichia	Obligate intracellular (Gram negative but not visible on Gram stain)	Non-culturable on routine media	No	Ticks, Mites / Transmitted from the feces on infected lice, fleas, ticks	Cause a variety of illnesses including systemic vasculitis (e.g. Rocky Mountain Spotted Fever), rash, pneumonia

1.3.2 Analytical Classification

Analytical classification includes whole-cell lipid analysis, cell wall fatty acid analysis, whole-cell protein analysis by mass spectrometry and the presence of cellular enzymes by multi-field enzyme electrophoresis. Analytical classification can be labour intensive at the time of work, requiring expensive equipment and specialised training. For these reasons, analytical classification is usually performed in specialised laboratories.

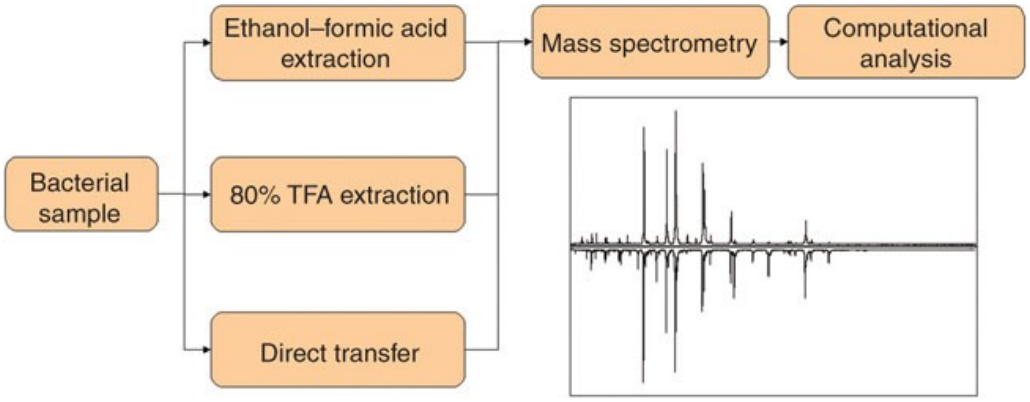

Figure 1.4: A bacterial sample subjected to a protein extraction and the final analysis by mass spectrometry [2]

1.3.3 Genotypic Classification

Genotypic classification, which is a molecular method, is the most accurate method for classifying bacteria. This means using bacterial DNA to determine the species or family to which the bacteria may belong. Originally, scientists used the guaranin or cytosine ratio to classify bacteria. Using DNA-DNA hybridization, scientists measure the degree of genetic similarity between bacterial isolates. Scientists can also extract DNA from an organism and expose it to species-specific molecular probes. If the nucleic acid probe binds to the DNA, then it is likely that the organism has been identified. In addition, some bacteria carry plasmids, which are small circular segments of DNA that replicate independently of the chromosome. There are also Polymerase Chain Reaction (PCR) methods, Pulse-Field Gel Electrophoresis (PFGE) which is the most commonly used molecular analysis and fingerprinting methods (DNA sequencing, plasmid analysis). Finally, while the genetic composition of bacteria can vary drastically between species, their ribosomal genes are remarkably well conserved. Scientists commonly use 16S ribosomal RNA 16S sequences to determine taxonomic relationships among strains of prokaryotes. This is why in situations such as an outbreak or an epidemiological investigation, scientists can use plasmid analysis or ribotyping to quickly identify bacteria. The evaluation of the results of these molecular techniques should be handled by personnel with experience, after having been combined with results from traditional methods, and communication with clinicians is considered necessary.

1.3.4 Final Analysis and Organisation

The above-mentioned classification system is a strong starting point. Using all the techniques described, scientists can organize bacteria into categories and predict their pathogenic capabilities. Some

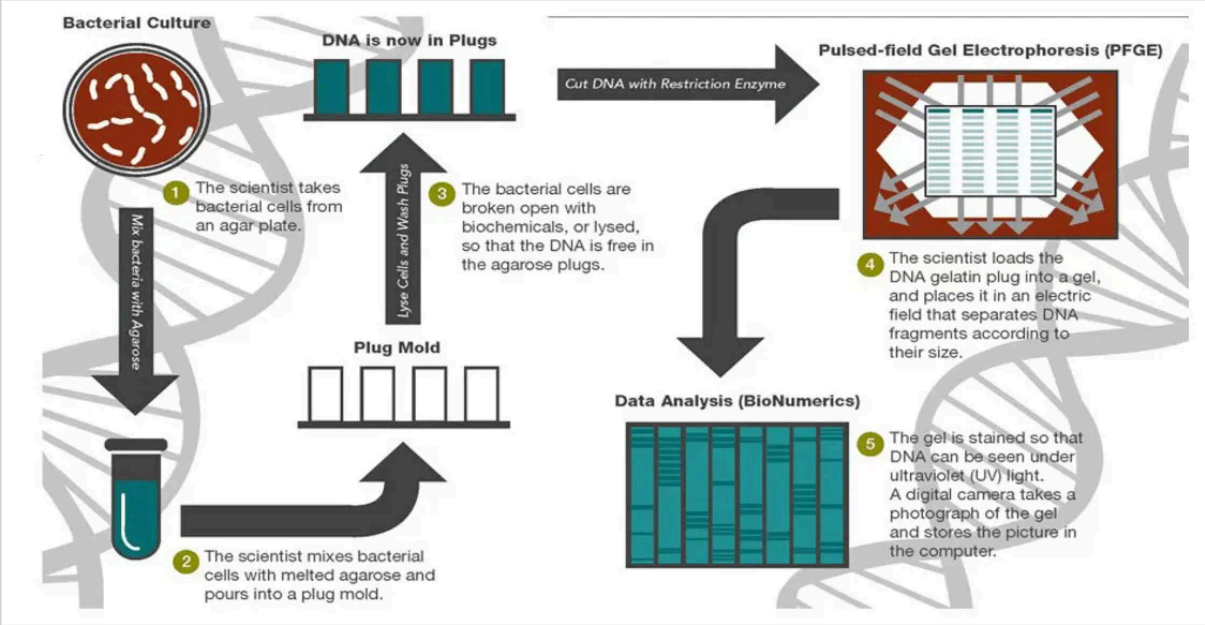

Figure 1.5: The methodology of PFGE, the most accurate and used molecular analysis
Source: Centers for Disease Control and Prevention (CDC) / PulseNet / Whole Genome Sequencing

of these categories for medically important bacteria are as follows. First, Aerobic Gram-Positive Cocci, which can be further subdivided into catalase-positive (e.g. *Staphylococcus*), catalase-negative cocci (e.g. *Enterococcuus*, *Streptococcus*). Next, Aerobic Gram-Positive Rods, which can be grouped into Actinomycetes with cell wall mycolic acids, Antimycetes without cell wall mycolic acids and miscellaneous Gram-Positive Rods. Then aerobic Gram-negative Rods/Cocci/Curved Rods, which include a wide variety of pathogens. Finally, the anaerobic Gram-Positive and Gram-Negative bacteria are further grouped according to their shape (cocci or rods).

1.4 Main Problem

1. **Phenotypic Methods**
   Phenotypic methods remain the bedrock for bacterial identification, relying on the evaluation of physical and biochemical characteristics. These include Gram staining, morphology under a microscope, nutrient utilization, and enzyme activity assays.

   Challenges-Problems:

   - **Time Consumption:** Cultivation-based identification methods can be exceedingly slow, with some bacteria requiring specific growth media and conditions. This can extend the identification process from days to weeks, which is impractical in urgent clinical scenarios.
   - **Specificity and Sensitivity:** The reliance on observable traits that may be shared across multiple species often results in non-specific identification. This ambiguity can lead to misdiagnosis and inappropriate treatment, particularly with bacteria that exhibit atypical phenotypic traits under stress or mutation.

- **Skill and Labor Requirements:** Phenotypic identification demands considerable expertise in microbiological techniques and interpretation of results, necessitating extensive training and experience. This requirement for highly skilled personnel increases the cost and limits the scalability of these methods in less equipped laboratories. [3]

2. **Analytical Methods**
   Modern analytical methods such as Mass Spectrometry (MS) and various forms of chromatography aim to identify bacteria by analyzing their molecular components. These methods are praised for their precision but come with significant limitations.

   Challenges-Problems:

   - **Cost of Infrastructure:** The initial setup for high-throughput equipment like mass spectrometers is financially demanding, often running into hundreds of thousands of dollars. Additionally, operational costs including maintenance, calibration, and consumables further strain budgets, particularly in underfunded institutions.
   - **Complexity and Technical Demand:** Running these instruments requires highly specialized knowledge, not only to operate the equipment but also to interpret the complex data they produce. This steep learning curve limits their use to well-funded, high-tech laboratories.
   - **Preparatory Procedures:** Analytical methods often require extensive and meticulous sample preparation to avoid contamination and ensure the integrity of the sample. This preparation can be labor-intensive and prone to human error, which can compromise the accuracy of the results. [4]

3. **Genotypic Methods**
   Genotypic identification methods, such as PCR, DNA sequencing, and whole-genome sequencing, offer a revolutionary approach by analyzing the genetic material of bacteria. These methods are known for their accuracy but face several practical challenges.

   Challenges-Problems:

   - **Financial Implications:** Despite decreasing costs of sequencing technologies, the expense remains prohibitive for routine use in many settings. The cost of consumables, along with the need for continual updates to software and hardware, poses a significant barrier.
   - **Analytical Expertise:** The analysis of genetic data requires not only sophisticated equipment but also access to bioinformatics tools and expertise. The lack of standardized software and trained personnel can delay and complicate the interpretation of results, limiting its practicality in real-time decision-making.
   - **Turnaround Time and Workflow Integration:** Although faster than some traditional methods, genotypic techniques still require significant setup and processing time. Integrating these methods into standard laboratory workflows remains a challenge, particularly in hospitals where rapid decision-making is critical. [5]

Conclusion
Traditional methods of bacterial identification are fraught with challenges, including high costs, significant time requirements, and a need for specialized personnel and equipment. These limitations underscore the necessity for advancements in bacterial identification technologies that are faster, more cost-effective, and accessible to a wider range of healthcare and research settings.

1.4.1 Existing Solutions to Bacterial Identification Problems

In response to the challenges posed by traditional bacterial identification methods, significant advancements have been made in recent years to develop innovative solutions that address issues related to time consumption, accuracy, and cost.

1. **WGS**: Whole Genome Sequencing (WGS) provides a comprehensive approach to bacterial identification by sequencing the entire genome of a microorganism. This method has revolutionized the field by allowing for the identification of novel bacterial species, tracking antibiotic resistance, and understanding bacterial evolution at an unprecedented level of detail.

   Advantages:

   - **High-Resolution Data:** WGS offers unparalleled accuracy and reliability, surpassing traditional methods. It is particularly useful in clinical settings where precise identification can inform treatment decisions and track outbreaks.
   - **Novel Bacterial Identification:** The ability to sequence entire genomes enables the identification of previously unknown bacterial species, expanding the scope of microbial discovery.
   - **Antibiotic Resistance Tracking:** WGS allows for detailed monitoring of antibiotic resistance genes, which is critical in managing antimicrobial resistance in healthcare settings. [6]

2. **MALDI-TOF MS**
   Matrix-Assisted Laser Desorption/Ionization Time-of-Flight Mass Spectrometry (MALDI-TOF MS) is a mass spectrometry technique that has been widely adopted in clinical microbiology for the rapid identification of bacteria. It works by ionizing bacterial proteins and measuring their mass-to-charge ratio, allowing for quick identification based on a comparison with known spectra.

   Advantages:

   - **Speed and Efficiency:** This method is significantly faster and more cost effective than traditional biochemical assays, providing results within minutes rather than days.
   - **Direct Identification from Clinical Samples:** MALDI-TOF MS can identify a broad range of bacteria directly from clinical samples, minimizing the need for time-consuming culture processes.

- **Cost-Effective:** The operational costs of MALDI-TOF MS are lower than those of many molecular methods, making it a valuable tool in resource-limited settings. [7]

3. **CRISPR-Based Diagnostics**
   Clustered Regularly Interspaced Short Palindromic Repeats (CRISPR) technology, originally developed for gene editing, has been adapted for use in diagnostics. CRISPR-based tests can detect specific bacterial DNA sequences with high sensitivity and specificity, offering a novel method for bacterial identification.

   Advantages:

   - **Rapid and Highly Accurate:** CRISPR diagnostics provide quick results with high accuracy, enabling rapid decision-making in clinical settings.
   - **Point-of-Care Testing:** These diagnostics can be performed at the point of care, reducing the need for laboratory-based testing and expediting treatment initiation.
   - **Antibiotic Resistance Detection:** CRISPR-based diagnostics are particularly valuable for detecting antibiotic-resistant bacteria, where traditional methods may fall short. [8]

1.5 Thesis Aim

The researcher came up with a new and innovative method of identifying bacteria through their electrical properties. Assuming that since bacteria are created with different shapes and colors, they are made up of different chemical compounds. Thus, bacteria that are different from each other have different electrical properties. This identification method will be created when several steps are successfully completed, which will also be explained in the final conclusions as further future study. For now, a comparative study of three electronic circuits will be done in terms of their capacitance and conductivity, so that the most efficient and most accurate one can be found. This study will be done on experimental boards, i.e. breadboards. Then, they will be designed in a special program and implemented on a board as a Printed Circuit Board (PCB). Finally, after a special sensor (interdigitated/interdigital electrode) is placed on the board of the most effective circuit, the researcher/author will be taken to a special room of a microbiology laboratory, with the appropriate assistance of medical-microbiologist specialists, to follow the corresponding experiments on six different cultures of different bacteria among them. The final objective and ultimate goal is to record different electrical properties (capacitance and conductivity) both in one with the other (as they will be different types of bacteria) and in the 3 Gram-Positive from the 3 Gram-Negative bacteria (which the bacteria in the triads with each other should give the same results).

1.6 Thesis Structure

The process of integrating and creating this innovative idea starts with ordering the components, which are a microcontroller, a power supply, a punched board, 2 resistors, 2 capacitors, some female pin headers, a Direct Current (DC) power jack to connect the power supply to the microcontroller and a Capacitance to Digital Converter.

Next will be soldering the components onto the board and later programming for the microcontroller code.

Finally, measurements will be taken in a suitable microbiology laboratory where all safety protocols for protection, disinfection and sterilization will be followed as the materials and the researcher will be exposed to an environment with bacteria and fungi.

Chapter 1 discusses a general theory of the microcosm, microbiology and bacteria, as well as the objectives of the researcher. Problems with existing methods of bacterial identification and the most recent innovative efforts of other researchers are mentioned.

In chapter 2 a literature review is provided, analyzing the papers that made the author think of this project.

Chapter 3 analyses the 3 electronic circuits for capacitance measurement, on which the comparative study will be done later.

Chapter 4 provides critical information about the IC (AD7745) used for the capacitance measurement in the circuit that is chosen for the final experiments.

Chapter 5 details the interdigitated/interdigital electrodes that will be used as sensors in the circuit that is deemed best and discusses their use widely as biosensors.

There are also subsections addressing the chemical elements of which they are composed (so that the most suitable one can be compared and purchased) and the process of disinfecting them after each particular culture of bacteria is placed on them.

Chapter 6 presents the overall integrated and final circuit that will be used as a biosensor to create an innovative and inexpensive method for bacterial identification.

In the 7^{th} chapter the comparative study between the 3 circuits is done theoretically and then in the laboratories of the school, (In Vitro Study).

Then, the research in the microbiological laboratory on bacteria (In Vivo Study) is presented, which is the aim of this research thesis.

Finally, chapter 8^{th} presents a final overview on the results and the conclusions of the research.

Suggestions for improvement for future research are also listed.

1.7 Epilogue

In conclusion, Chapter 1 has provided a comprehensive overview of the current state of bacterial identification techniques, highlighting significant shortcomings and challenges that necessitate the development of novel strategies. The chapter presents a compelling rationale for the research's focus on developing a novel electrical circuit-based technique for bacterial identification, which paves the way

for the subsequent chapters. In order to comprehend the trajectory and potential ramifications of this research in both scientific and practical contexts, it is essential to have a thorough understanding of its fundamental principles. The project is expected to make a significant contribution to the fields of electronic/electrical engineering and microbiology.

Chapter 2

Literature Review

2.1 Introduction

The field of biomedical engineering offers considerable scope for multidisciplinary research, particularly in the context of addressing complex challenges such as bacterial detection. The necessity for more efficacious, expeditious, and precise detection methodologies prompted the author to pursue this subject, as they believe it may have a significant impact on environmental monitoring, food safety, and clinical diagnostics. The existing bacterial identification techniques are frequently constrained by their complexity and time efficiency, which underscores the need for innovation through the use of biosensor technology. The objective of this doctoral research at the International Hellenic University's Department of Information and Electronic Engineering was to investigate novel methodologies for bacterial identification utilizing electronic circuits, with a particular focus on Interdigitated Electrode Arrays (IDEs). This literature review examines the fundamental studies that informed the author's ideas and the design of his study. [9]

2.2 The Role of IDEs in Biosensing

The principal focus of the author's study is the utilization of IDEs for the identification of bacteria. IDEs are distinguished by an interdigitated electrode configuration that optimizes the accessible surface area for interaction with biological materials, thereby enhancing sensitivity. In regard to the efficacy of these electrodes in detecting bacteria through alterations in conductivity or impedance, the design is of paramount importance.

The initial development of nanoscale Integrated Circuit (IC) devices for biochemical sensing applications was conducted by Van Gerwen et al. (1997) in their seminal work. The study demonstrated that the IDEs were capable of detecting minute alterations in impedance resulting from the attachment of macromolecules, such as DNA or antigens, by reducing the electrode spacing to 250 nm. He was intrigued by this exact detection capability, as it provided a model for the creation of extremely sensitive sensors that could recognize bacterial infections using similar processes. The author was particularly drawn to the potential of nanoscale technology in advancing the objective of developing a highly sen-

sitive sensor capable of real-time bacterial identification. [10]

2.3 Conductivity and Impedance Measurements in Bacterial Detection

Another essential component of our approach is the utilization of electrical measurements, specifically those related to conductivity and impedance changes, for the identification of bacterial presence. The work of Sheppard et al. (1993), which investigated the use of microfabricated IDEs for detecting the electrical conductivity of solutions, had a significant impact on the development of this strategy. The study provided valuable insights into the impact of electrode design on sensor sensitivity, establishing a link between electrode geometry and impedance. The concept of utilizing electrical characteristics to identify bacterial interactions with the IDE surface was influenced by our findings. This made us prioritize optimizing electrode design to ensure that the IDEs could detect subtle variations in electrical conductivity throughout the bacterial identification process. [11]

2.4 Applying IDEs for Bacterial Detection: A Step Towards Innovation

In their 2008 study, Lu and colleagues provided a compelling illustration of how antibody-modified IDEs may facilitate real-time bacterial identification. Their work on Escherichia coli detection underscored the practical applicability of IDEs in bacterial detection. In order to identify individual E. coli bacteria, this study combined electrical measuring methods with antibody specificity, indicating that a biosensor of this kind might provide rapid, highly sensitive diagnoses. This work demonstrated how IDEs may be modified for medical applications, such as the identification of bacterial infections in clinical settings, which prompted further investigation by the author. After observing the efficacy of Lu et al.'s study, he postulated that a similar approach could be employed to identify a range of bacterial diseases. He then proceeded to enhance this methodology by focusing on the electrical circuitry that underpins these interactions. [12]

2.5 Enhancing Sensitivity Through Nanoscale Electrode Design

The direction of this thesis was also informed by the work of Van Gerwen et al. (1997), which focused on the fabrication of nanoscale electrodes. The findings demonstrated that reducing the electrode size enhanced sensitivity while mitigating the impact of bulk solution conductivity, thereby facilitating a more detailed examination of the molecular layer at the electrode surface. The construction of a highly sensitive biosensor necessitated the capacity to discern low-concentration bacterial populations, prompting the author to consider the potential benefits of further miniaturization of electrode arrays in this regard. Furthermore, the manufacturing techniques employed, notably deep Ultraviolet (a form of electromagnetic radiation) (UV) lithography, offered a viable, scalable approach to fabricating reliable, high-precision electrodes, which he sought to incorporate into his subsequent investigations. [10]

Our approach to optimizing electrode geometry was also informed by Grover's (2000) study on enhancing the efficiency of integrated device (IDE) design. Grover's research demonstrated that surface area and electrode spacing have a direct impact on sensor performance, particularly concerning sensitivity and signal stability. This was particularly relevant to the author's objective of developing an IDE sensor capable of detecting microorganisms in challenging environments, such as human fluids or contaminated water. The objective was to enhance the biosensing capabilities of the IDEs by optimizing their geometric characteristics through an analysis of Grover's work. [13]

2.6 Motivation and Future Directions

The objective of this initiative is to utilize a multidisciplinary approach to address significant challenges in bacterial detection. Despite the efficacy of conventional techniques for identifying bacteria, they often necessitate a significant investment of time and financial resources. The objective of the author's study is to circumvent these limitations by developing a biosensor that can be employed in a multitude of biological and environmental applications, exhibiting not only rapid and precise detection capabilities but also versatility in its applications.

His study was informed by the papers discussed here, which also provided inspiration for his focus on IDE-based bacterial detection. The potential of IDEs in biosensing was underscored by the contributions of Lu et al. on the utilization of IDEs for E. coli detection, Sheppard on conductivity measurements, and Van Gerwen on nanoscale enhancements. The author's study trajectory was informed by the unique perspectives and technical methodologies presented in each of these investigations.

The continued downsizing of IDE-based biosensors, the creation of superior electrode materials, and the integration of these sensors with microfluidic systems for real-time, point-of-care diagnostics will collectively shape the future trajectory of this technology. Furthermore, there is an increasing demand for more resilient sensors that are capable of functioning in challenging conditions, such as those encountered in industrial settings or within human tissue. The utilization of IDE technology in this study is intended to facilitate the attainment of these objectives, namely the provision of expedient, dependable and precise methods for the detection of bacteria.

2.7 Epilogue

This literature review presents a summary of the key papers that informed the author's thesis study on bacterial detection with IDEs. The reviewed publications offer valuable insights into the functioning, design, and utilization of IDEs in biosensing, with a particular focus on enhancing specificity and sensitivity. The author's initiative, which aims to enhance the state of the art in biosensing technology through improvements in electrode design and the incorporation of novel detection methods, has its theoretical and technological foundation in these fundamental investigations.

Chapter 3

Electronic Circuits

3.1 Introduction

This chapter presents a comprehensive comparison of three capacitance-measuring circuits, accompanied by a detailed examination of the technical aspects of the study. Following a comprehensive evaluation of the available alternatives, the circuits were selected for their potential utility in bacterial identification. The chapter presents a comprehensive examination of the design principles, theoretical foundations, and practical implications associated with each circuit. Furthermore, it examines the technological challenges associated with utilizing these circuits in a microbiological context, including aspects such as sensitivity, precision, and component integration. The objective of this chapter is to establish a robust technical foundation that will inform the selection of the most suitable circuit for the research's experimental phases.

3.2 Capacitive-Sensor Interfaces

A comprehensive examination of three distinct circuits is presented, each analyzed individually. Subsequently, a comparative analysis will be conducted to identify the optimal circuit for utilization in the final microbiology laboratory experiments.

3.2.1 A Method for Capacitance Measurement Based on the Principle of Double Diffusion

This technique is employed in capacitive sensors for the measurement of minute alterations in capacitance. In this technique, a 24-bit Analog-to-Digital Converter (ADC) is employed to facilitate high resolution. The double-differentiation technique ensures that the capacitance measured is independent of the original capacitance of the sensor. Furthermore, the technique has the advantage of eliminating parasitic capacitance that may arise from the sensor terminals and the interconnect leads to the rest of the circuit. [14] [15]

Figure 3.1 illustrates the circuit's block diagram. The excitation signal is applied to both the capacitance sensor and a reference capacitance. [14] [15]

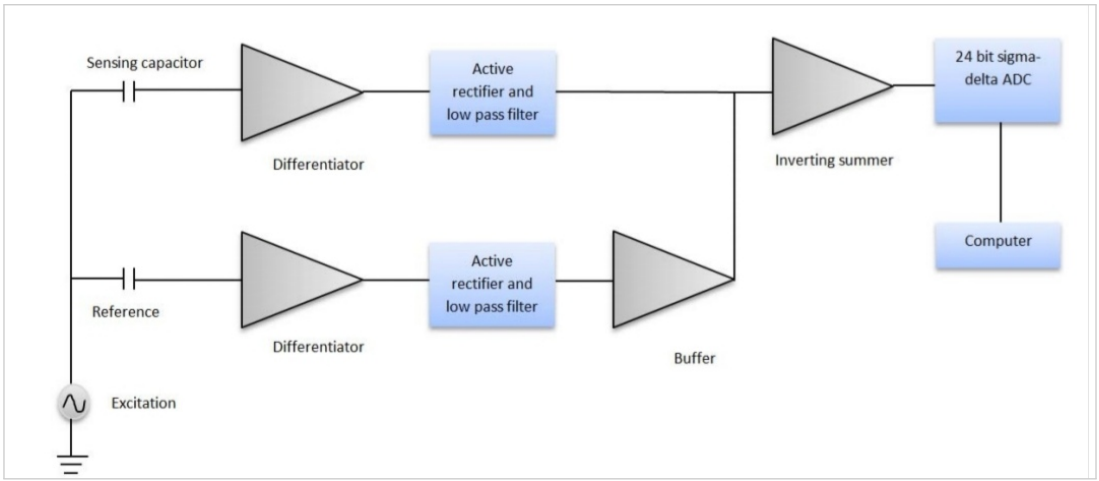

Figure 3.1: Schematic Diagram for measuring capacitance using double differential principle [14]

As an alternative to the reference capacitor, a gyrator phase-shifting circuit, designed to act as a variable capacitor as shown in Figure 3.2, could be employed. Typically, when all the elements of a gyrator circuit are resistors, and a capacitor is substituted for either R_2 or R_4, the resulting circuit is equivalent to that of an inductor. In this instance, however, the resistor was replaced with capacitor C_1, resulting in a high linearity variable capacitor circuit. [14] [16] [15]

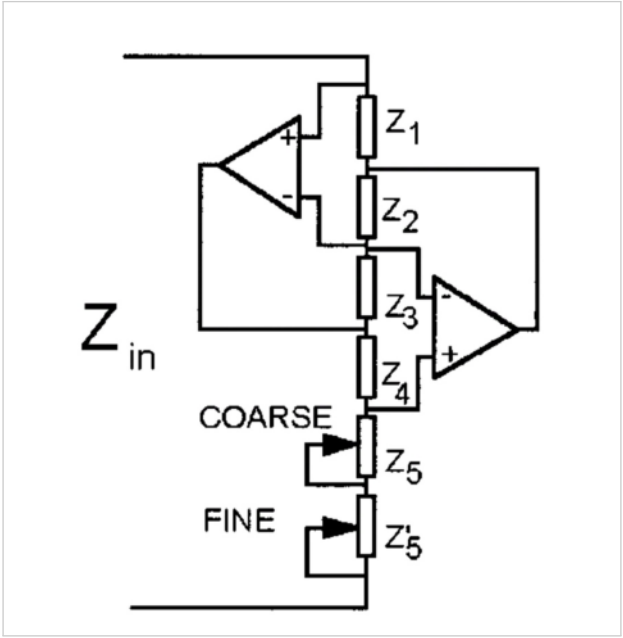

Figure 3.2: Gyrator circuit used to construct a reference capacitor [16]

In each branch of the circuit depicted in Figure 3.2, comprising the sensor capacitance and the reference capacitor, a precision full-wave rectifier and a low-pass filter is employed to convert the output of the differentiator to a direct current DC voltage, as well as to minimize error. The DC output voltages from each branch are then combined algebraically in a step-summing adder. In practice, one input of the adder is subtracted from the other, with the assistance of an inverting amplifier stage that has a gain of -1 and reverses the sign at one of the two inputs of the adder. The resulting output from the adder is fed into a 24-bit sigma-delta analog-to-digital converter. This is achieved by converting the time-varying output to an average DC value of the signal. Subsequently, the output of the ADC is stored in the computer's memory. Two measurements are required: one with no material to be measured (zero or near-zero output) and one with material to be measured on the sensor. The change in capacitance, which is independent of the original capacitance of the sensor, can then be calculated. [14] [15]

The circuit is depicted in greater detail in Figure 3.3, in which the output of each differentiator is represented by the following relationships:

$$V_o(V_1) = -j \cdot \omega \cdot R_1 \cdot C_1 \cdot V_1$$

and

$$V_o(V_2) = -j \cdot \omega \cdot R_2 \cdot C_{\text{ref}} \cdot V_1$$

Subsequently, the outputs of full-wave precision rectifiers are provided as follows:

$$V_o(V_3) = V_m \cdot k_1 \cdot R_1 \cdot C_1$$

and

$$V_o(V_4) = V_m \cdot k_2 \cdot R_2 \cdot C_{\text{ref}}$$

In this context, V_m represents the peak value of the input signal V_1. The initial capacitance of the sensor, C_1, is also a key parameter. Additionally, C_ref denotes the adjusted value of the variable capacitor implemented with the gyrator. The constants k_1 and k_2 are also of significance, as they depend on the ripple factor of the low-pass filters. [16] [15]

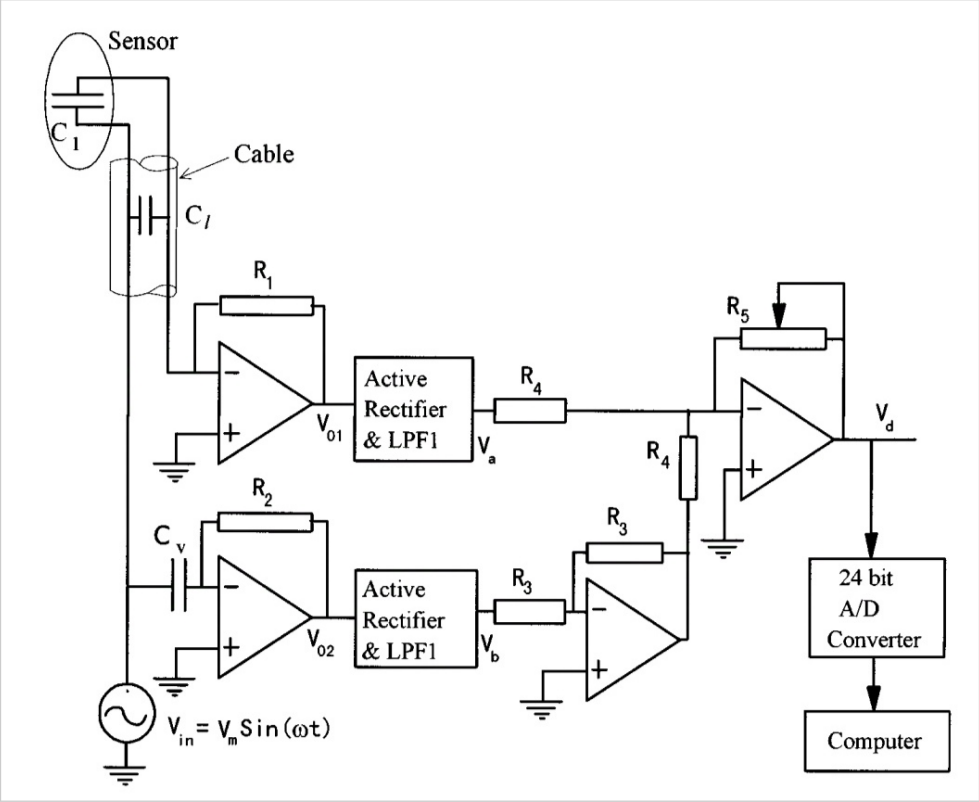

Figure 3.3: Schematic diagram of the designed interface circuit [16]

The initial step is to calibrate the circuit. This is achieved by adjusting the gyrator through its component R_2, which resets the output of the adder to zero. This will be accomplished when the condition C_1 = C_ref is satisfied. At this juncture, the adder's output voltage will be equal to:

$$V_{o1_{(\mathrm{UB})}} = (k_1 \cdot R_1 \cdot C_1 - k_2 \cdot R_2 \cdot C_{\mathrm{ref}}) \cdot C_{\mathrm{UB}} \cdot V_m$$

In this context, G_UB is the profit of the adder. If a material to be measured is now placed in the sensor, then its capacitance will increase by ΔC, resulting in an output from the adder that is equal to:

$$V_{o2_{(\mathrm{UB})}} = (k_1 \cdot R_1 \cdot (C_1 + \Delta C) - k_2 \cdot R_2 \cdot C_{\mathrm{ref}}) \cdot G_{\mathrm{UB}} \cdot V_m$$

The differential measurement achieved in this manner results in a measurable voltage at the output of the adder. The use of a 24-bit ADC ensures the attainment of high accuracy when measuring any small voltage resulting from the output of the adder.

The distinction between the two equations presented above for the output of the adder yields the following mathematical expression:

$$\Delta C = \frac{1 \cdot \left(V_{o2_{(\mathrm{UB})}} - V_{o1_{(\mathrm{UB})}}\right) / V_m}{k_1 \cdot R_1}$$

In practice, it is not feasible to entirely eliminate the ripple voltage at the output of low-pass filters. Nevertheless, this methodology facilitates the generation of a differential measurement, thereby circumventing the inaccuracies that are typically associated with the ripple voltage. The resulting output voltage will be read by a 24-bit sigma-delta ADC, which is characterized by low noise and a sampling frequency defined as f_s. If the voltage to be measured is a repetitive and time-varying function with a frequency of f_{out} and n samples are taken from it, then it can be demonstrated that the mean of these is directly proportional to the DC value of the signal when the following relationship exists:
For $f_{\text{out}} > f_{\text{S}}$:

$$f_s = \frac{n \cdot f_{\text{out}}}{n^2 + 1}$$

Accordingly, the sampling frequency should be set to a value that satisfies the following condition. [16] [15]

The capacitance resulting from the conductors connecting the sensor to the circuit is designated as C_{stray}. Consequently, the value C_1 in the aforementioned circuit analysis relations can be replaced with $C_{stray} + C_1$. In the event that the physical position of the connecting conductors remains unaltered, the parasitic capacitance will retain a constant value. Consequently, it can be replaced with (C_1 + ΔC + C_{stray}), in place of (C_1 + ΔC). In light of the aforementioned considerations, the following equations can be derived:

$$V_{o1_{(\text{UB})}} = \left(k_1 \cdot R_1 \cdot (C_1 + C_{\text{stray}}) - k_2 \cdot R_2 \cdot C_{\text{ref}}\right) \cdot G_{\text{UB}} \cdot V_m$$

Similarly, when the material to be measured is placed on the sensor, a change in the differential capacitance (ΔC) occurs, resulting in a shift in the equation between the measured variables.

$$V_{o2_{(\text{UB})}} = \left(k_1 \cdot R_1 \cdot (C_1 + \Delta C + C_{\text{stray}}) - k_2 \cdot R_2 \cdot C_{\text{ref}}\right) \cdot G_{\text{UB}} \cdot V_m$$

The distinction between these two equations will once more yield the identical relationship for the capacitance alteration, ΔC, as that which was identified when the parasitic C_stray capacitance was not incorporated. It can therefore be assumed that the double diffusion method has an important feature, namely that it automatically eliminates the parasitic capacitance of the conductors without the need for a special method to be developed for this purpose. [16] [15]

In the case of capacitive sensors operating in the picofarad range, a high-resolution change in capacitance, ΔC, of approximately 10^{-18} picofarads can be observed. The output is independent of the initial value of the sensor capacitance and exhibits high accuracy. The circuit has a straightforward configuration, minimal expense, and adaptability for diverse applications and investigations. In this instance, it is employed for the measurement of bacterial capacitance. [16] [15]

3.2.2 A method for measuring capacitance utilising a current-to-voltage converter (Current Sense Amplifier)

Furthermore, this paper will present an additional differential measurement technique. In a previous study, M. R. Haider et al. [17] proposed a low-power circuit for the measurement of small capacitances with high resolution and a high degree of linearity. It is conceivable that this capacitance measurement technique could be employed in biomedical applications. The differential circuit measurement technique facilitates the elimination of distortion from even-order harmonics. [14] [15]

The circuit employs two current sense amplifiers, two rectifiers comprising P-Channel Metal-Oxide-Semiconductor (PMOS) transistors in a diode configuration, and an instrumentation amplifier. A schematic diagram of the circuit is provided in the accompanying Figure 3.4. The circuit incorporates a reference capacitor, typically in the picofarad range, and a capacitance sensor. The excitation signal is applied to the common terminal of both capacitors. The remaining terminal of the capacitors is linked to each of the two current-to-voltage converters (current sense amplifiers). The current flowing through the sensor is contingent upon the capacitance variation of the sensor. The current is then detected by the current-to-voltage converter. The output of the current-to-voltage converter is connected in a diode configuration to the PMOS rectifier, which is used to convert the alternating current to direct current. The rationale behind the selection of PMOS transistors over N-Channel Metal-Oxide-Semiconductor (NMOS) is their superior performance in terms of 1/f noise, also known as flicker or pink noise. [14] [17] [15]

The resulting DC signal from the two rectifiers is then driven differentially to the inputs of an adjustable-gain instrumentation amplifier. The variable gain allows for the sensitivity to be increased or decreased as required. The circuit is capable of inducing a change of 1.32 mV at its output for a change of 1 fF. This technique is particularly suited to the measurement of very small capacitances in the fF range (10^{-15} F). Due to its high common-mode rejection ratio (CMRR), the circuit is also suitable for use in biomedical sensor applications. [14] [15]

The circuit is depicted in great detail in the accompanying figure 3.5.

The circuit has been designed for the differential measurement of any capacitance variation from any capacitive sensor, the nominal value of which is within the range of 5 pF. In single-ended measurements, a capacitor with a nominal value of 5 pF is employed as a reference. Consequently, the two capacitors (the sensor and the reference capacitor) are configured in a manner that one of their two terminals is shared between both capacitors. The remaining two terminals are linked to the inverting input, as illustrated in the accompanying Figure 3.5. The non-inverting terminals of the two operational amplifiers are connected to a reference voltage that is situated at a point approximately midway through the common input signal range. [17] [15]

An excitation signal is applied to the sensor's common terminal and the reference capacitor.

$$V = V_{\text{amp}} \cdot \cos(\omega t + \varphi)$$

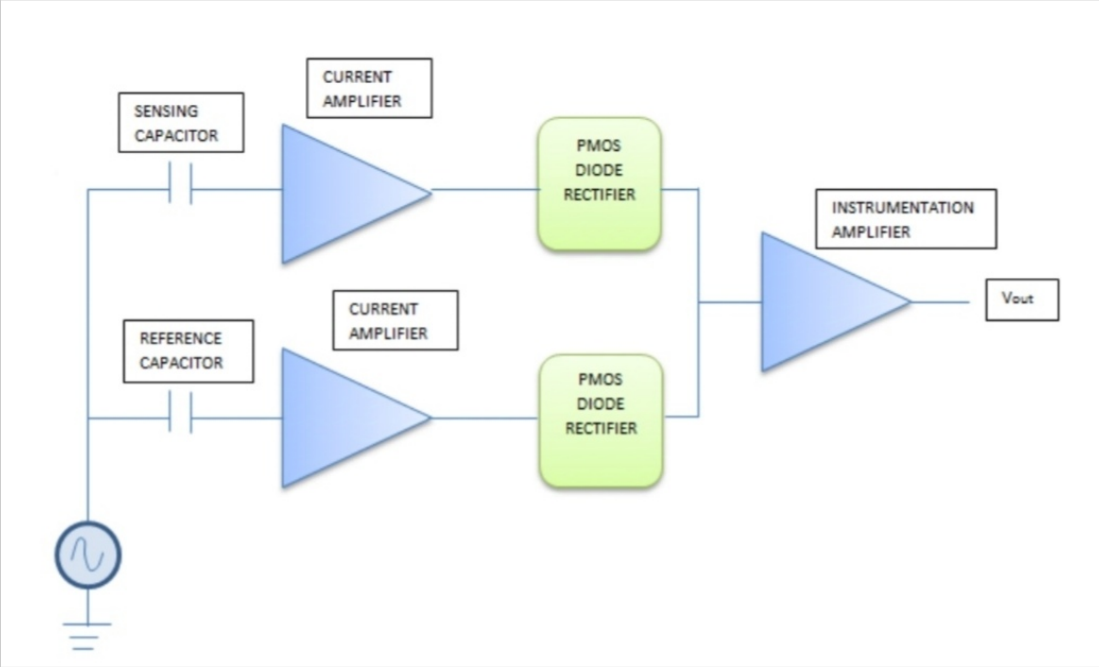

Figure 3.4: Schematic Diagram for Sensor Read-out Circuit [14]

The capacitance variation gives rise to the generation of two distinct current signals. If the nominal value of the reference and sensor capacitors is expressed as C, then the currents flowing through these capacitors can be written as follows:

$$i_{\text{ref}} = C \cdot \frac{dV_p}{dt}$$

$$i_{\text{sens}} = (C \pm \Delta C) \cdot \frac{dV_p}{dt}$$

In this context, V_p represents the amplitude of the excitation signal, while ΔC denotes the change in capacitance of the sensor.

Subsequently, the generated currents are fed into two current-to-voltage converters. Each amplifier is comprised of an operational amplifier and a feedback capacitor (C_f). The resistor R_f is employed in parallel with C_f to regulate the bias point of the output of each amplifier (current sense amplifier), as illustrated in Figure 3.6.

If the frequency of the input signal is represented by $\omega \gg \frac{1}{C_f \cdot R_f}$, then the transfer function of the amplifier can be expressed as follows:

$$H(\omega) \approx -\frac{C_1}{C_f}$$

In this context, C_1 and C_f represent the input and feedback capacitors of the amplifier.

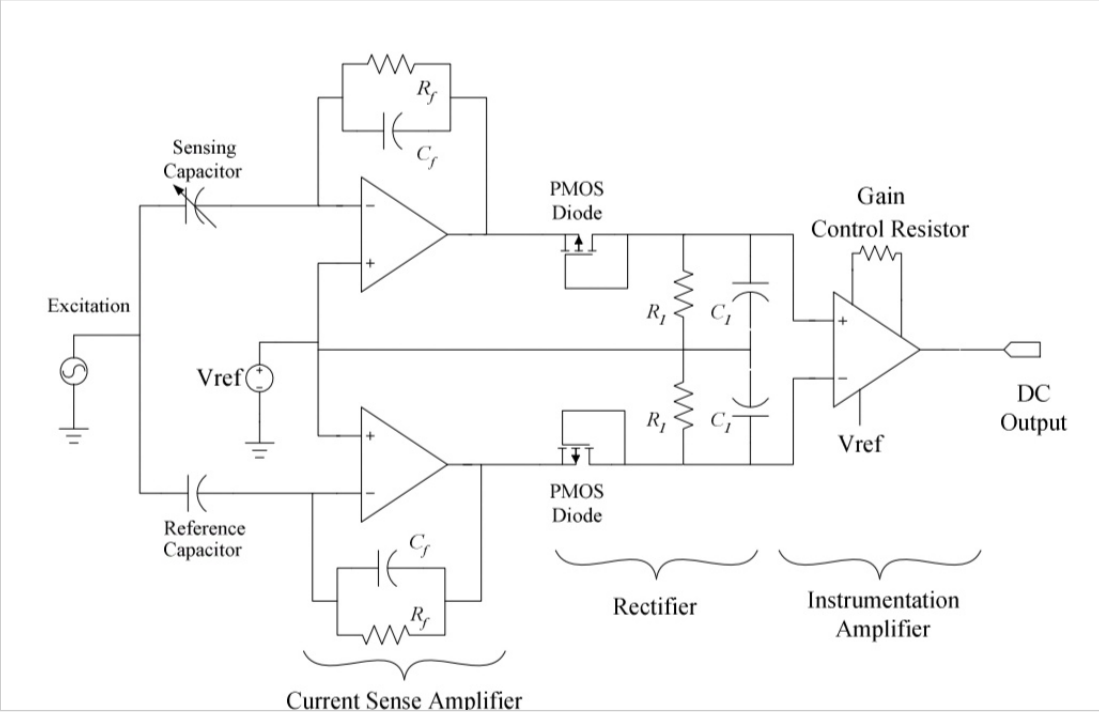

Figure 3.5: Schematic of Sensor Read-out Circuit [17]

By employing the transfer function, the output voltages resulting from the reference capacitor and the capacitance of the sensor can be expressed as follows:

$$V_{\text{out(ref)}} = -\frac{C}{C_f} \cdot V$$

$$V_{\text{out(sens)}} = -\frac{C \pm \Delta C}{C_f} \cdot V$$

As can be seen from the above relations, it is evident that the change in capacitance modulates the amplitude of the excitation signal. As illustrated in the accompanying Figure 3.5, the two output signals are subsequently driven through a diode rectifier. In this configuration, a PMOS rectifier is employed in a diode configuration. The rationale for utilizing a PMOS in lieu of an NMOS, as previously discussed, is due to the reduced 1/f noise (or flicker or pink noise) exhibited by the former in comparison to its NMOS counterpart. The values of the diode rectifier, R_1 and C_1, are selected in accordance with the condition that the time constant $\tau = R_1 \cdot C_1$ satisfies the following equation:

$$\frac{1}{f_{\text{exc}}} < \tau < \frac{1}{f_{\text{sens}}}$$

In this context, the symbols "f_exc" and "f_sens" represent the frequency of the excitation signal and the frequency of change of the capacitance sensor, respectively. The differential output of the aforementioned diode rectifiers can be expressed as follows:

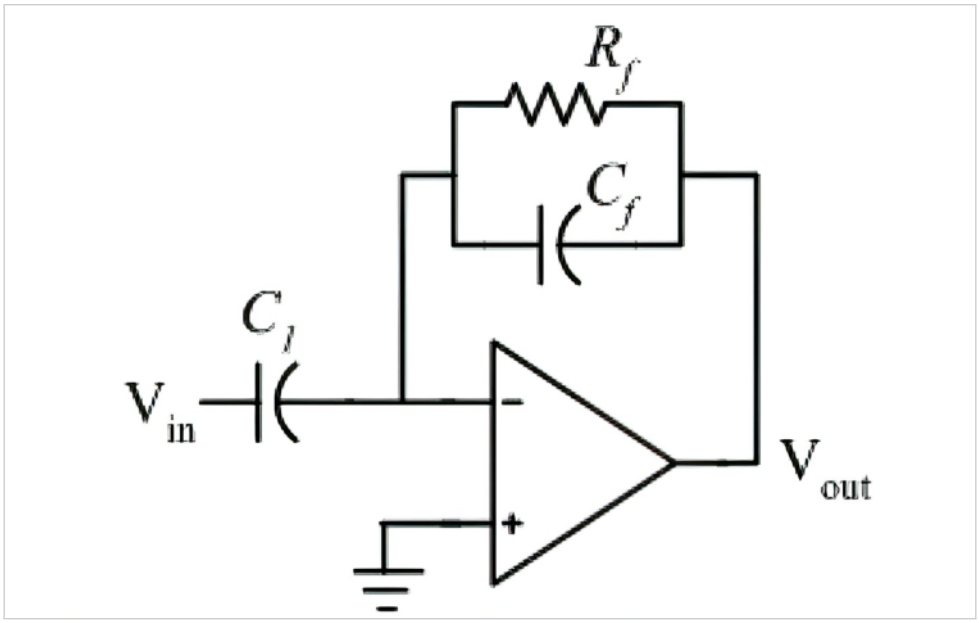

Figure 3.6: Schematic of Current Sense Amplifier [17]

$$V_{\text{diff}} = \pm \frac{\Delta C}{C_f} \cdot \alpha \cdot V_{\text{amp}}$$

In this context, α represents the attenuation factor resulting from the diode rectifier. [17] [15]

The outputs of the two diode rectifiers are then fed to the inputs of an instrumentation amplifier, which serves to amplify the differential V_diff variation of these two outputs.

In an instrumentation amplifier of the type illustrated in Figure 3.7.

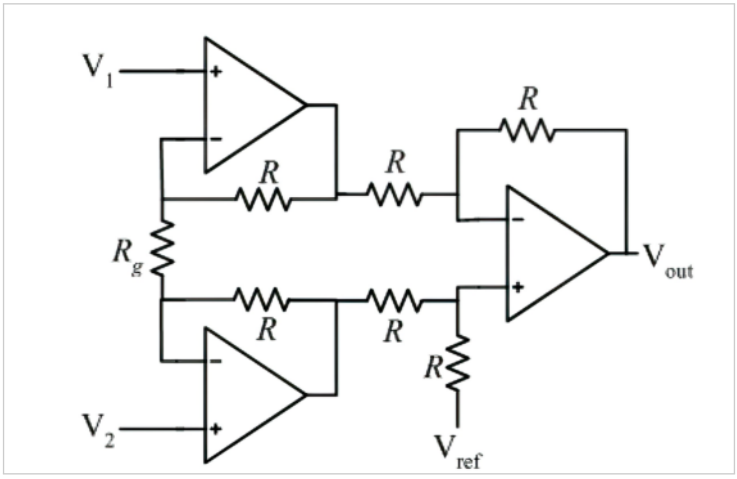

Figure 3.7: Schematic of Instrumentation Amplifier [17]

The output voltage V_out is determined by the ratio of the gain to the differential input.

$$V_{\text{out}} = \left(1 + \frac{2R}{R_c}\right)(V_2 - V_1)$$

In the aforementioned relation, if we introduce the differential variation V_diff of the outputs resulting from the two rectifiers as the input, we obtain the relation for the final output of the circuit, as detailed below:

$$V_{\text{out}} = \left(1 + \frac{2R}{R_c}\right)\left(\pm\frac{\Delta C}{C_f} \cdot \alpha \cdot V_{\text{amp}}\right)$$

It is possible to enhance the gain of the instrumentation amplifier and, consequently, the sensitivity of the system by reducing the value of R_c. Furthermore, the sensitivity of the circuit can be enhanced by reducing the value of the feedback capacitor, C_f. However, in this instance, the frequency of the excitation signal must be increased in order to satisfy the aforementioned condition, $\omega \gg \frac{1}{C_f \cdot R_f}$. It should be noted that a very small value of C_f is susceptible to influence from the parasitic capacitances of its actuators.

3.2.3 Capacitance to Digital Converter for High Accuracy Measurements

The author, having conducted thorough study and research, elected to devise a circuit of minimal complexity and cost, utilizing the AD7745 IC. This was selected due to its exemplary capacitance measurement functionality, offering exceptional precision at low values. The following chapter will provide a comprehensive analysis of the capacitance-to-digital converter.

In essence, the following circuit is a capacitance measurement circuit based on the AD7745 integrated circuit. The circuit is relatively straightforward to design and is compact with high accuracy. Communication with the microcontroller is facilitated through the Inter-Integrated Circuit (I2C) protocol.

The circuit schematic and the PCB files, created with Altium Designer software, will be presented in the following section. Furthermore, the code for programming the microcontroller will be presented, accompanied by a comprehensive explanation of its functionality.

Schematic

As illustrated in the accompanying Figure 3.9, the circuit comprises the Specific integrated circuit used in the design (AD7745ARUZ) IC (specifically from Analog Devices), two capacitors (100nF and 10uF, respectively) placed in parallel with each other and connected to the power supply, two resistors (10k each), and two sensors (C+ and C-). In this instance, for the particular experiments, only one of the two sensors will be employed. In all other instances, the device is powered from a source ranging from 2.7V to 5.25V via the ESP32-S3 microcontroller. In addition, the same microcontroller is responsible for the I2C bus protocol.

In practice, the ESP32-S3 will be powered by a 5V and 3A power supply, which will then supply power to the AD7745. With regard to the I2C bus, it is merely necessary to connect pins 1, 16 and 2, which correspond to Serial Clock Line (SCL)[1], Serial Data Line (SDA)[2] and Ready (signal pin in I2C com-

[1](used in I2C communication)
[2](used in I2C communication)

munication) (RDY), to the corresponding pins on the ESP32-S3. The selection of these pins on the microcontroller is made by the programmer.

More precisely, the circuit under consideration was specifically designed for the purpose of measuring the capacitance of bacteria and is intended to be used for the accurate measurement of capacitance. The AD7745ARUZ, a high-resolution, low-noise capacitance-to-digital converter (CDC), will be employed for this purpose. The AD7745ARUZ is the optimal choice for this application, as it exhibits a high degree of precision in the detection of extremely low capacitance values, as low as a few Femtofarads (fF). The C+ terminal, which serves as the interface for capacitance measurement, is connected to the single-ended capacitive input within the design. In the absence of active driving of the SDA and SCL lines by the master or slave, the resistors R1 and R2 function as pull-up resistors for the I2C bus, maintaining the lines in their designated states. The objective of the capacitors C1 (100nF) and C2 (10uF) is to provide a decoupling function for the power supply. The voltage supply ensures that the AD7745ARUZ receives a consistent voltage, which is essential for maintaining the precision of the capacitance measurements. The filters serve to eliminate noise from the circuit.
In order to facilitate effective noise filtering across a range of frequencies, the capacitors are arranged in parallel. C1 serves to filter out noise of a higher frequency, while C2 is responsible for filtering noise of a lower frequency. The parallel configuration assists in preserving the integrity of the sensitive measurements by minimizing fluctuations in the power supply.
The circuit has been meticulously designed with the objective of optimising the performance of the AD7745ARUZ in a low-capacitance, high-precision measurement configuration. This ensures the accurate identification of the minute capacitance fluctuations induced by bacterial activity.

I^2C Protocol

The Inter-Integrated Circuit (I^2C) protocol, initially developed by Philips Semiconductor in 1982, is a widely utilized serial communication bus. The I^2C protocol may facilitate communication between microcontrollers and peripheral devices, such as sensors, displays, and memory chips, within electronic systems. The use of distinct addresses enables the I^2C protocol, which has a two-wire interface, to accommodate several devices on a single bus and to facilitate bidirectional data flow. The protocol is particularly valued for its flexibility, ease of use and affordability, which collectively make it an optimal choice for short-range communication in embedded devices.
The two lines that enable communication between devices on the bus in the I^2C protocol are SDA (Serial Data Line) and SCL (Serial Clock Line).
The SDA line is responsible for the transmission of data between the slave and master devices. As the line is bidirectional, the direction of data transfer may vary depending on the operational mode (read or write).
The SCL line is responsible for providing the clock pulses that are necessary for the synchronization of data transmission. The clock signal, which is necessary for the synchronization of the timing of data bits being transmitted on the SDA line, is generated by the master device.
The concurrent operation of the SDA and SCL lines facilitates the transfer of data and ensures the effective and synchronized connectivity of devices. [18]

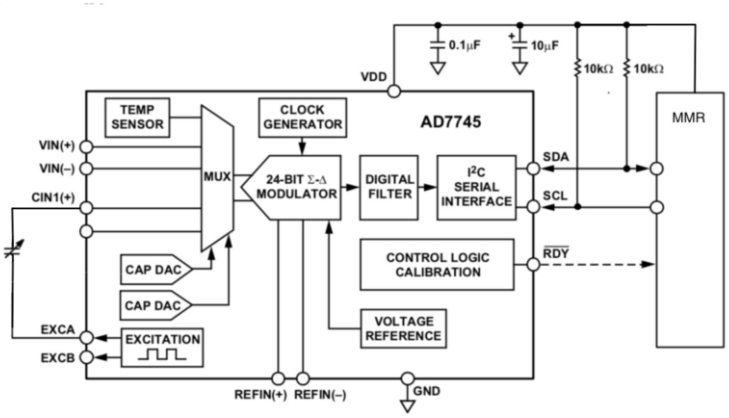

Figure 3.8: Basic Application Diagram for a Differential Capacitive Sensor [19]

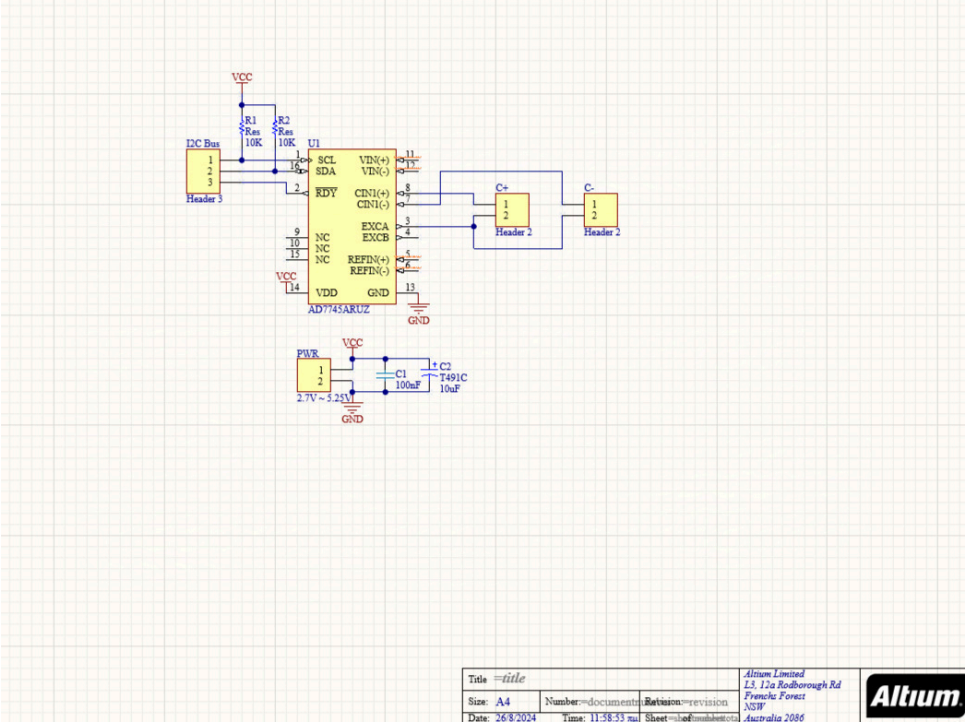

Figure 3.9: Schematic

Printed Circuit Board

As illustrated in the accompanying Figure 3.10, the PCB is presented. However, it will not be ordered in this work, as it is not a necessary component at this early stage of the experiments that will be carried out later.

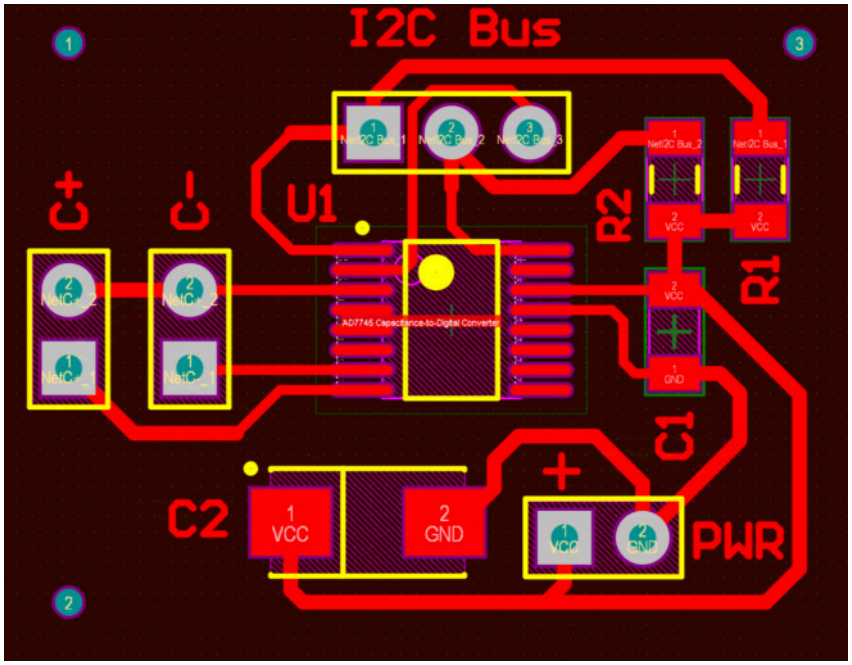

Figure 3.10: 2D Layout Mode

Figures 3.11 and 3.12 illustrate the planned configuration of the PCB and its three-dimensional (3D) layout, respectively. As can be observed in the latter illustration, elongated pins have been positioned to facilitate the connection and adhesion of the materials.

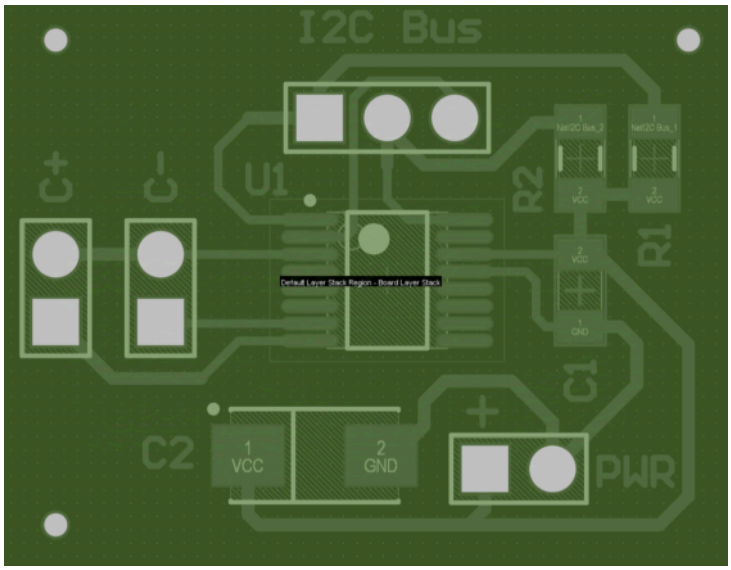

Figure 3.11: Board Planning Mode

Programming

The programming of the ESP32-S3 microcontroller by Waveshare will be conducted within the Arduino Integrated Development Environment (IDE). The code will be presented and explained in chapter 6.

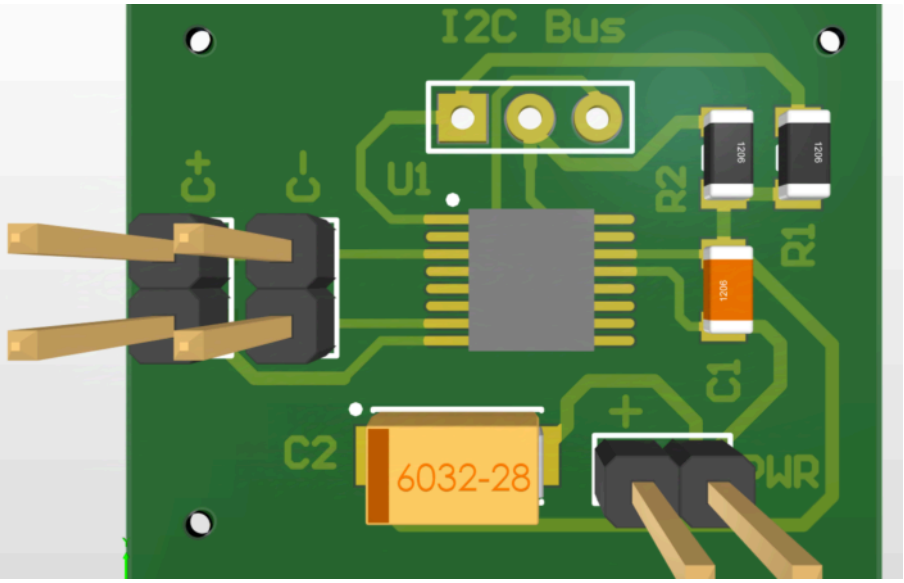

Figure 3.12: 3D Layout Mode

Conclusion

As previously stated, given the nature of this undergraduate thesis, the experiments will be conducted with the circuit constructed on a perforated board and the materials affixed by hand with a reed. Subsequently, as will be detailed in the recommendations for further enhancements, the PCB will be printed correctly and the experiments will be conducted once more, with greater professionalism, so that the research can be published.

3.3 Epilogue

The second chapter provides a comprehensive examination of the capacitance measuring circuits, accompanied by a detailed analysis of the advantages and disadvantages inherent to each proposed solution. This chapter presents a critical assessment of the effectiveness of the aforementioned solutions, with a particular emphasis on their suitability for bacterial identification. In order to make an informed decision regarding the incorporation of a particular circuit into the final experimental setup, it is essential to give careful consideration to the findings of this research. The conclusions of this chapter will have a significant impact on the precision and dependability of the study, ensuring that the selected circuit meets the rigorous standards of scientific research in microbiology.

Chapter 4

Capacitance to Digital Converter

4.1 Introduction

This chapter is dedicated to a comprehensive examination of the Capacitance-to-Digital Converter (CDC), a pivotal component of the electrical circuitry designed to identify bacteria. It provides a comprehensive examination of the selected CDC model, encompassing its technical specifications, operational principles, and integration within the circuit design; with a particular focus on its exceptional performance as a capacitance meter, offering high precision at low values. The discussion underscores the significance of precision in capacitance measurement, particularly in light of the necessity for sensitivity to detect even the slightest variations in bacterial samples. The objective of this chapter is to provide a detailed analysis of the technological intricacies of the CDC, to clarify its crucial role in the efficacy of the electronic identification process. In order to guarantee the reliability of the CDC, the chapter also addresses potential issues related to its implementation and proposes solutions.

4.2 AD7745

The AD7745 is a high-resolution, sigma-delta CDC designed by Analog Devices. The device provides a direct interface for capacitive sensors, enabling the measurement of capacitance directly and subsequent conversion to a digital format. This IC has been designed with the specific objective of enabling the precise measurement of very small capacitances, rendering it suitable for a variety of applications, including those in the automotive, industrial, and medical fields. [19]

The key features of the AD7745 include:

- **High resolution and Accuracy:** With a resolution of up to 24-bit and an effective resolution of 21-bit. Furthermore, it has a full-scale input range of ±4 pF with an accuracy of ±4 fF. [19]
- **Capacitance measurement:** The device is capable of interfacing with both single-ended and differential floating capacitive sensors. [19]
- **Temperature Sensor:** An integrated temperature sensor provides measurements with a resolution of 0.1 °C and an accuracy of ±2 °C. [19]

- **I2C Interface:** The AD7745 is equipped with a 2-wire I2C-compatible interface, facilitating straightforward integration into existing systems. [19]
- **High Power Efficiency:** The device operates with a low power consumption of 0.7 mA, rendering it suitable for applications requiring battery power. [19]

4.2.1 Detailed Examination of Performance for High-Precision Capacitance Measurement

The AD7745 is particularly well suited to applications that require the accurate measurement of minute capacitances, down to the fF level. In order to achieve the aforementioned performance, the following crucial design elements have been implemented: [19]

- **Sigma-Delta Modulation:** Utilizing a continuous sampling of the charge passing through the capacitance, the AD7745's Sigma-Delta modulator can convert the capacitance into a digital signal. A third-order digital filter is connected to the modulator to improve resolution and reduce noise. [19]
- **Capacitance Range and Resolution:** The AD7745 is capable of handling up to 17 pF of common-mode capacitance, which represents the non-changing component of the input, and has a full-scale input range of ±4 pF. The device exhibits excellent sensitivity to minute differences, with the capacity to detect capacitance changes as small as 4 aF (attofarads). [19]
- **Error Tolerance and Calibration:** The AD7745 has been designed to perform several functions, including capacitive gain calibration and system offset calibration, intending to reduce the likelihood of errors occurring. The device is designed to inherently reject power supply fluctuations and noise, which could otherwise compromise the accuracy of the measurements. The device is capable of handling parasitic capacitance to ground up to 60 pF. [19]
- **Excitation Source:** The IC is equipped with configurable excitation sources that drive the capacitive sensor with a square-wave signal. The aforementioned excitation sources facilitate capacitance measurement by inducing a charge flow proportional to the capacitance being measured. [19]
- **Capacitive Digital-to-Analog Converter (CAPDAC):** The AD7745 may be utilized for the detection of minute, fluctuating capacitances, as the CAPDAC function is employed to neutralise the influence of substantial, unchanging capacitances. This is particularly advantageous in applications such as the measurement of bacterial characteristics, where the sensor capacitance may exhibit a substantial constant component that necessitates offset correction. [19] The incorporation of the AD7745, which features a CAPDAC, is designed to facilitate the compensation of large, constant capacitances within the capacitive measuring system. This property is of critical importance in applications where a significant, constant, or common-mode component of the capacitance of the sensor is present. It is essential to subtract or balance this component in order to ensure reliable capacitance measurement, even in cases where there are only minor changes. [19]

How CAPDAC Works

- **Negative Capacitance Compensation:** The conceptualization of the CAPDAC entails the incorporation of a programmable negative capacitance into the input capacitance measurement. By essentially canceling out a major constant offset, this allows the AD7745 to focus on the variable component of the capacitance, that is, the portion that changes in response to the sensor's contact with the surrounding environment. In this example, this refers to the growth of bacteria. [19]
- **Resolution and Range:** The AD7745's CAPDAC has a resolution of seven bits, which enables the accurate modification of compensation values. In general, the total range of the CAPDAC allows for the compensation of up to 17 pF of constant capacitance. It is possible to modify the range in discrete increments. [19]
- **Balanced Inputs:** Two distinct CAPDACs are integrated into the AD7745, one of which is associated with the capacitive input pins (CIN+ and CIN-). Consequently, any static capacitance present on the sensor can be precisely balanced by differential measurements, whereby the positive and negative inputs can each have their own CAPDAC settings. [19]

Importance of CAPDAC:

- **Enhanced Measurement Accuracy:** The measuring system is capable of functioning within the AD7745's ideal input range as a consequence of CAPDAC's nullification of the substantial, constant capacitance, thereby enhancing the precision and accuracy of the capacitance measurements. [19]
- **Flexibility in Sensor Design:** The base capacitance of a sensor can vary considerably depending on a number of factors, including its dimensions, shape, and the materials used in its construction. The capacity of CAPDAC to detect even minor discrepancies in capacitance allows for the flexibility required to accommodate these variations. [19]
- **Temperature Stability:** The CAPDAC is designed in such a way that it can provide reliable measurement results in a variety of environmental circumstances. The temperature coefficient is fixed, thereby minimising drift and guaranteeing stability. [19]

The CAPDAC permits the user to select a baseline capacitance level in the circuit designed to measure bacterial attributes, thereby excluding it from further consideration. This enables the AD7745 to focus on detecting the subtle capacitance alterations induced by bacterial processes. This feature is of paramount importance for the acquisition of high-precision measurements in scenarios where the minute signals of interest may otherwise be obfuscated by the baseline capacitance of the sensor. [19]

4.2.2 Application to Bacteria Electrical Properties Measurement Circuit

In response to the project's specific inquiry, the AD7745 is employed to quantify the electrical characteristics of bacteria, with a particular emphasis on capacitance. The circuit you have developed (depicted in the diagram) establishes a connection between the AD7745 and an I2C bus, thus enabling

the integration of the former with a microcontroller or other data-acquiring apparatus. The following represents the primary components of the circuit in question:

- **Power Supply:** The AD7745 is powered by a 2.7V to 5.25V supply, with the inclusion of decoupling capacitors (C1 and C2) to stabilize the voltage and minimize the presence of noise.
- **I2C Communication:** The SCL and SDA lines are connected via pull-up resistors to the I2C bus, thereby enabling communication between the AD7745 and the microcontroller.
- **Capacitive Sensor Interface:** The sensor, which is designed to measure the capacitance affected by bacterial growth or presence, is connected to the CIN1(+) and EXCA pins of the AD7745. The differential measurement setup serves to enhance the accuracy of the measurement by compensating for any parasitic capacitances.
- **Calibration and Offset Management:** The incorporation of CAPDAC into the researcher's design serves to negate the constant offset capacitance, thereby ensuring that solely the alterations in capacitance attributable to bacterial activity are quantified.

As in the aforementioned project, in which the evaluation of bacterial properties was undertaken, the AD7745 is an optimal choice for high-precision capacitance measurement in situations where the identification of minute capacitance variations is necessary. The device is particularly well-suited to scientific and medical applications where precision is of the utmost importance, due to its combination of high resolution, low noise, and inbuilt calibration functions.

The tables (4.2.1, 4.2.2 and 4.2.3) and the Figures (4.1a, 4.1b, 4.1c, 4.1d and 4.1e) following, provide invaluable insight into the performance characteristics of the AD7745, particularly in the context of high-precision capacitance measurements. The data provides a comprehensive insight into the device's resilience to noise, fluctuations in the power supply, and non-linearities, which are pivotal factors in any context where bacterial capacitance monitoring is a requisite.

Conversion Time (ms)	Output Data Rate (Hz)	-3dB Frequency (Hz)	Root Mean Square (RMS) Noise (aF)	Effective Resolution (Bits)	P-P Resolution (Bits)
11.0	90.9	87.2	40.0	17.6	15.2
11.9	83.8	79.0	27.3	18.2	15.9
20.0	50.0	43.6	12.2	19.4	16.6
38.0	26.3	21.8	7.3	20.1	17.3
62.0	16.1	13.8	5.4	20.5	17.9
77.0	13.0	10.5	4.9	20.7	18.1
92.0	10.9	8.9	4.4	20.8	18.2
109.6	9.1	8.0	4.2	20.9	18.2

Table 4.2.1: Capacitive Input Noise and Resolution vs. Conversion Time [19]

Conversion Time (ms)	Output Data Rate (Hz)	-3dB Frequency (Hz)	RMS Noise (µV)	P-P Noise (µV)
20.1	49.8	26.4	11.4	62
32.1	31.2	15.9	7.1	42
62.1	16.1	8.0	4.0	28
122.1	8.2	4.0	3.0	20

Table 4.2.2: Voltage Input Noise and Resolution vs. Conversion Time (Internal Reference) [19]

Conversion Time (ms)	Output Data Rate (Hz)	-3dB Frequency (Hz)	RMS Noise (µV)	P-P Noise (µV)
20.1	49.8	26.4	14.9	95
32.1	31.2	15.9	6.3	42
62.1	16.1	8.0	3.3	22
122.1	8.2	4.0	2.1	15

Table 4.2.3: Voltage Input Noise and Resolution vs. Conversion Time (External 2.5V Reference) [19]

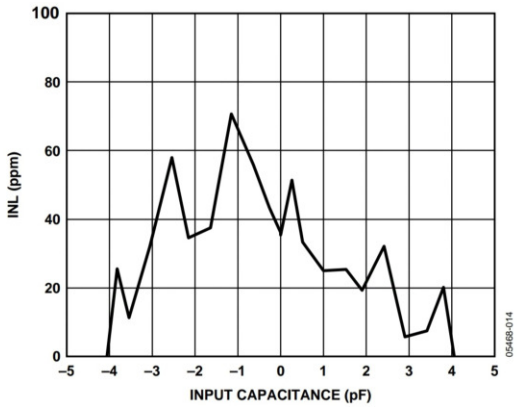

(a) Capacitance Input Integral Nonlinearity, VDD = 5 V. [19]

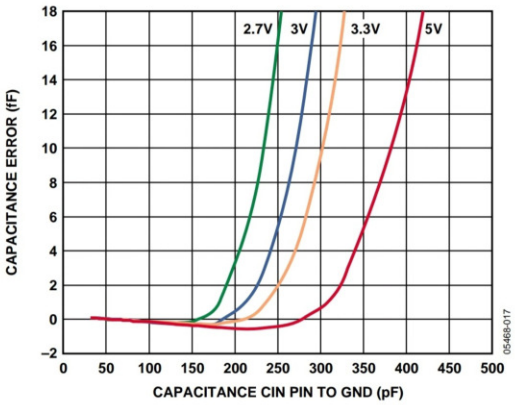

(b) Capacitance Input Error vs. Capacitance between CIN and GND [19]

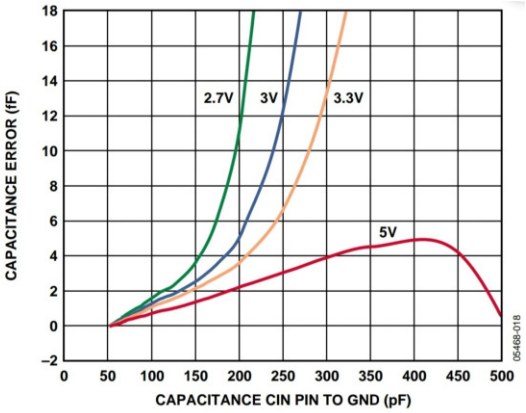

(c) Capacitance Input Error vs. Capacitance between CIN and GND, different conditions [19]

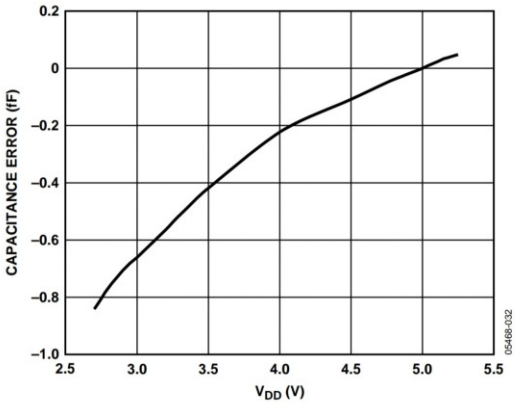

(d) Capacitance Input Power Supply Rejection (PSR)) [19]

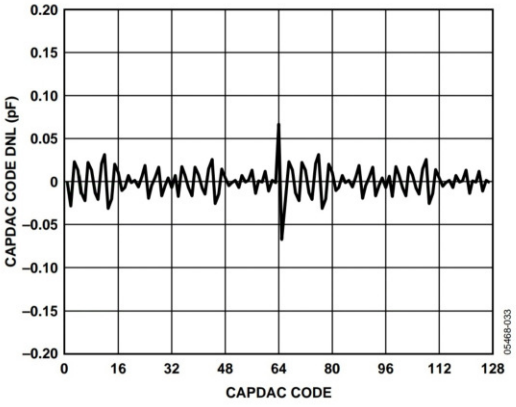

(e) CAPDAC Differential Nonlinearity (DNL) [19]

Figure 4.1: Group of Figures showing various characteristics including Capacitance Input Integral Nonlinearity, Input Error vs. Capacitance, Power Supply Rejection, and Differential Nonlinearity [19]

Figure 4.1a illustrates the integral nonlinearity for the capacitance input, showing the performance across the full input range.
Figures 4.1b and 4.1c show how input error varies as a function of capacitance between the CIN pin and ground at different supply voltages.
The graph in Figure 4.1d shows how well the AD7745 rejects noise from the power supply, which is crucial for maintaining accuracy in noisy environments.
Figure 4.1e details the performance of the CAPDAC, focusing on its nonlinearity over its operating range.

4.3 Epilogue

The third chapter reaches its conclusion by emphasizing the pivotal function of the capacitance-to-digital converter in the research process. The comprehensive examination of the CDC's constraints and capabilities presented in this chapter provides a robust basis for its deployment throughout the trial phase. The knowledge gained from this research must be applied to guarantee that the electrical circuit operates with the required accuracy, which will eventually lead to an improvement in the process's accuracy for identifying bacteria. The chapter acknowledges the crucial role played by the CDC in achieving the objectives of the study and establishes rigorous standards for its performance.

Chapter 5

Interdigitated/Interdigital Electrodes

5.1 Introduction

This chapter introduces the interdigitated/interdigital electrodes, which serve as the core sensing component in the electronic circuit for bacterial identification. The chapter provides an in-depth exploration of the design, functionality, and operational principles of these electrodes. It examines how the electrodes detect bacterial presence through changes in capacitance, focusing on the underlying physics and material properties that enable this functionality. The chapter also discusses the criteria for selecting the appropriate electrode materials, considering factors such as conductivity, durability, and compatibility with biological samples. By providing a comprehensive analysis of interdigitated electrodes, the chapter establishes their crucial role in the research and highlights their potential to enhance the accuracy and efficiency of bacterial identification.

Specifically, an analysis of the operational principles and the design of the sensor setup will be presented, which will be employed for the measurement of the electrical capacitance of bacteria. Interdigitated/interdigital electrodes represent a common planar structure employed in the fabrication of capacitive sensors and chemiresistors. It is one of the most commonly used transducers in chemical and biological sensors. Interdigitated/interdigital electrodes are composed of electrodes that form the armature of a capacitor, provided that the surface is properly insulated. In this configuration, the presence of the material to be measured affects the dielectric properties of the resulting capacitor, which is referred to as an interdigitated/interdigital capacitor. The electrodes are in direct contact with the material to be measured, which bridges the gap between a set of electrodes. This allows for the resistance between them to be easily measured. Figures 5.1 and 5.2 illustrate a variety of interdigitated/interdigital electrodes, showcasing their versatility in terms of size, material, and shape. [20] [21] [22]

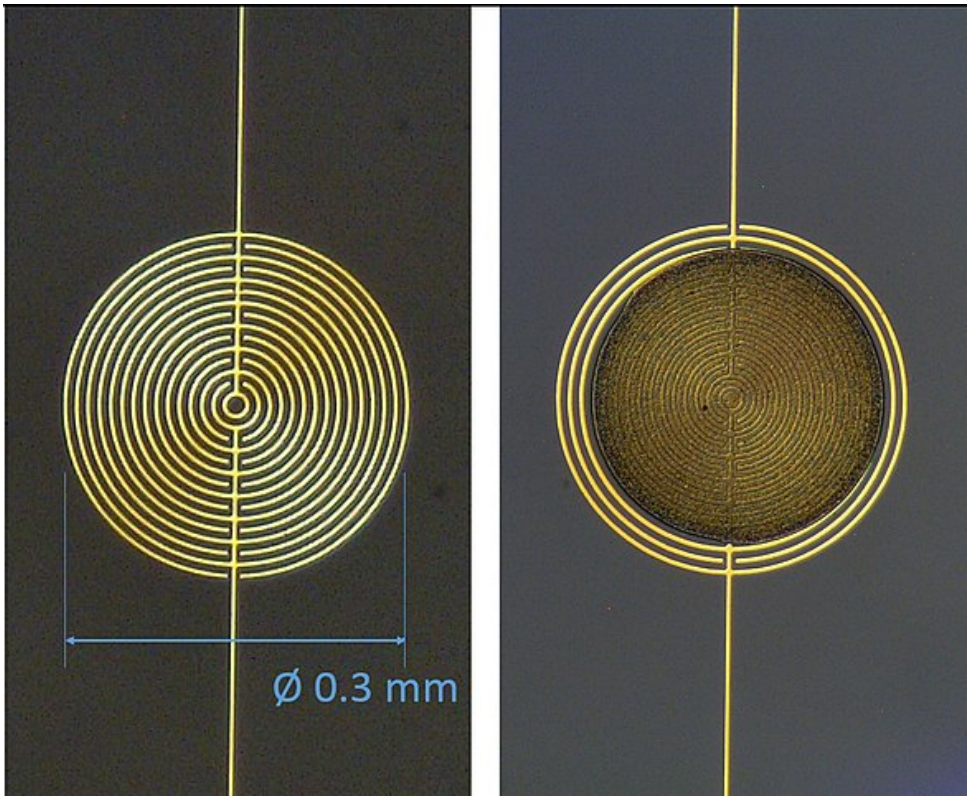

Figure 5.1: Circular interdigitated electrodes with and without a gold nanoparticle chemiresistor film
Source: Wikipedia: Chemiresistor

Figure 5.2: Interdigitated sensor
Source: Norecs

The approach of planar interdigitated/interdigital sensors has long been a subject of interest within the scientific community. The term "interdigitated/interdigital sensors" is used to describe a variety of devices, including microelectrodes, Interdigitated Transducers (IDTs), Interdigitated Microelectrode Arrays (IDAM), Interdigitated Electrode Structures (IDES), and others. Planar interdigitated/interdigital sensors, which are based on interdigitated electrode structures, are employed in a multitude of applications, including photosensitive detectors, Surface Acoustic Wave (SAW) devices, moisture sensors, sensors for chemicals and gases, Electrolyte Conductivity (EC) measurement, and the determination of components contained in aqueous solutions. The determination of moisture content in materials, fibres and titanium dioxide in pulp; the measurement of compound permeability; and the characterisation of materials are all applications of this technology. It is also used to measure tablet hardness and coating thickness in pharmaceutical products, to measure bacterial growth (biofilm) and to detect small amounts of magnetic beads on the surface of microsensors. The design and applications of interdigitated capacitive sensors were discussed by Mamishev and colleagues. [20] [23]

The number of research papers examining the development of planar interdigitated/interdigital sensors is steadily rising. Planar interdigitated/interdigital sensors have been employed to evaluate the properties of a dielectric material, including those of milk, saxophone reeds, meat, and leather utilized in the clothing and footwear industry. The evaluation of diffusion property profiles of various materials using a three-wavelength interdigitated sensor has been reported by Mamishev et al. The dielectric behaviour of liquid crystal filaments was studied with interdigitated capacitors. A novel development of interdigitated sensors for corrosion monitoring, structural condition monitoring and for environmental applications has also been documented. It can be posited that interdigitated sensors have a plethora of applications. [23]

5.2 Interdigitated/Interdigital Capacitor

Figure 5.3 depicts an interdigitated/interdigital electrode array, which will be employed in the formation of an interdigitated capacitor.

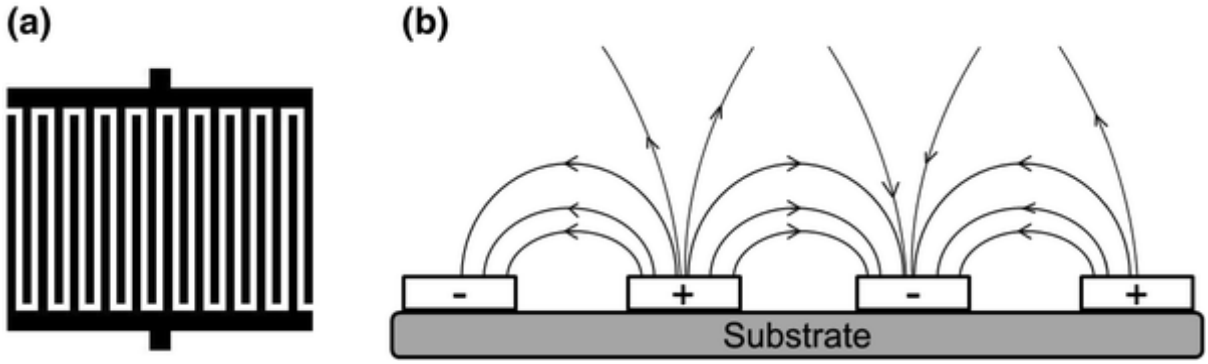

Figure 5.3: Interdigitated electrode [24]

The interdigitated capacitor can be described as a periodic, planar, comb-like structure. The periodicity of these sensors is employed to enhance their capacitance, although this is achieved at the cost of reduced electric field penetration into the sample. The electric field can penetrate deeper into the

sample, thereby increasing the capacitance of the device. A typical interdigitated capacitor is constructed from an inert substrate and electrodes arranged in a comb structure, as illustrated in Figure 5.3. The most advantageous feature of these sensors is the one-sided access. The electric, magnetic and acoustic fields are applied from one side of the sample, thereby leaving the other side exposed to the influence of the surrounding environment. This may take the form of a gas, moisture or chemical absorption, and this influence can change the properties of the sample. Interdigitated chemical sensors employ chemically sensitive layers with varying conductivity and permeability (dielectric properties) contingent on the characteristics of the sample under examination. Consequently, the capacitance of the sensor is altered. By modifying the total surface area of the sensor, the number of fingers and the distance between the electrodes, it is possible to regulate the strength of the output signal. [25]

5.2.1 Capacitor

In order to gain an understanding of interdigitated capacitors, it is first necessary to undertake a general analysis of the capacitor. A capacitor can be defined as a system comprising two adjacent parallel conductors, with an insulating material (such as air, plastic, mica, glass, or paper) interposed between them. The two conductors are referred to as the armature of the capacitor, while the insulating material is known as the dielectric of the capacitor. The dielectric constant is a constant value that is unique to each type of material and determines the dielectric properties of the material. The capacitor, by virtue of its construction, creates a homogeneous electric field, thereby enabling the storage of electric charge (Q), which in turn allows for the storage of electric energy. The Figure illustrates the configuration of the capacitor. Figure 5.4 depicts an interdigitated/interdigital electrode array, which will be employed in the formation of an interdigitated capacitor. [26]

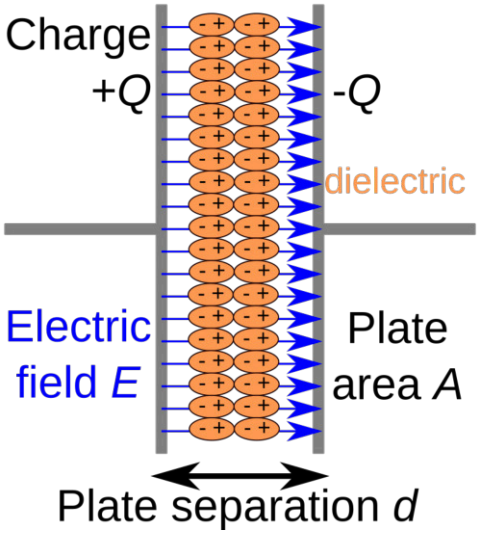

Figure 5.4: Capacitor array [26]

When a capacitor is charged, the armatures are found to have electrical charges that are approximately equal and opposite in value. The capacitor's charge (Qc) is referred to as the charge of its positively charged armature.

In order to comprehend the manner in which the geometric attributes of the capacitor influence its capacity to store charge, it is first necessary to define the term 'capacitance'. Accordingly, the term

"capacitance" is defined as the quantity of charge (Q) stored per unit potential difference. This is expressed by the following relationship:

$$C = \frac{Q}{V}$$

The unit of capacitance is 1 F = 1 Cb / V. [26]

The capacitance of a capacitor is dependent upon its geometrical characteristics, and can be expressed by the following relation:

$$C = \epsilon_r \cdot \epsilon_0 \cdot \frac{A}{d}$$

Where C is the capacitance of the capacitor, ϵ_r is the relative static permittivity or relative dielectric constant of the dielectric, ϵ_0 is the absolute dielectric constant of the vacuum and has a value $\epsilon_0 = 8.85 \times 10^{-12}\,\mathrm{C^2\,N^{-1}\,m^{-2}}$ in SI. $\epsilon_0 = 8.8554 \times 10^{-12}$ or F/m, A is the area of the positive armature and d is the distance between the armature. [26] [23]

5.2.2 Influence of the Dielectric Material

As previously suggested, a dielectric is defined as an insulator that exhibits the characteristic property of polarising its electric charges when placed in an electric field. In comparison with other insulators, dielectric materials exhibit a significant polarisation effect, which makes them useful for the production of capacitors. In such devices, the dielectric is placed between the armature and determines the basic capacitance property of the capacitor as well as the limit of the electrical voltage under which the capacitor can operate smoothly, without the generation of sparks between the armature. Figure 5.4 depicts the configuration of the capacitor, with the dielectric material situated between the armature, and illustrates the polarization of the dielectric molecules. [27]

Thus, when a dielectric is situated within an electric field, the electric charges do not traverse the material in the manner observed in an electric conductor. Instead, they exhibit a slight deviation from their average equilibrium position, thereby inducing dielectric polarisation. As a consequence of dielectric polarisation, positive charges are displaced in the direction of the field, while negative charges are displaced in the opposite direction. This results in the generation of an internal electric field, which serves to reduce the overall field strength within the dielectric material itself. In the event that a dielectric is constituted by molecules that are weakly bonded, these molecules not only become polarised but also rearrange themselves so that their axes of symmetry align with the field.

Although the term "insulator" is typically associated with low electrical conductivity, the concept of dielectric fields encompasses materials with high polarizability, which is quantified by a numerical value known as the relative permittivity. The term "insulator" is typically employed to signify the capacity of a given material to impede electrical conduction, whereas the term "dielectric" is used to describe a material's ability to store energy (through polarization). One illustrative example of a

dielectric is an electrically insulating material situated between the metal plates of a capacitor. The polarization of the dielectric by the expressed electric field results in an increase in the charge on the surface (armature) of the capacitor, given the specified electric field strength. [27]

5.2.3 Working Principle of the Interdigitated/Interdigital Sensor

The operational principle of the flat interdigitated/interdigital sensor is analogous to that of the simple capacitor with parallel armatures, wherein the electrodes (armatures) are opened to facilitate access to the Material Under Test (MUT) on one side. Figure 5.5 illustrates the electric field dynamics of a common parallel-armature capacitor and an interdigitated sensor, as well as their transient state. The electric field dynamic lines generated by the sensor penetrate the material under test, thereby modifying the impedance of the sensor. The sensor functions as a capacitor, with the capacitive response dependent on the properties of the system in question. Consequently, the capacitive response of the sensor can be employed to estimate the properties of the system. [23]

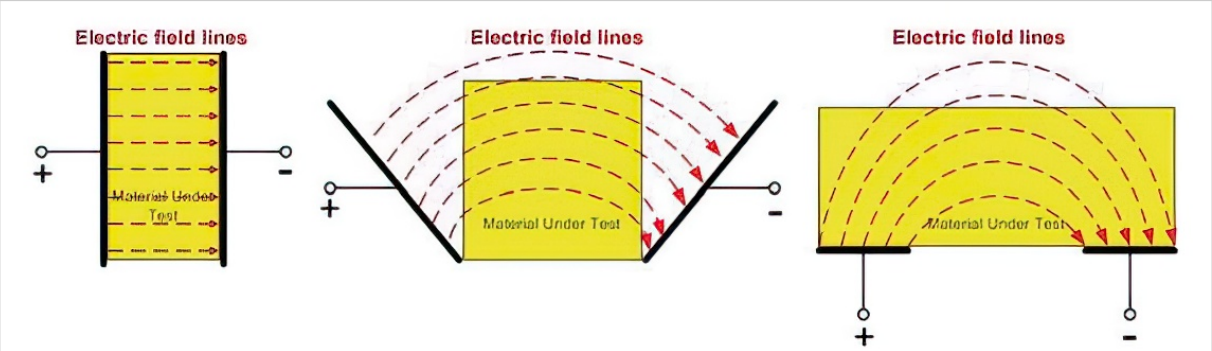

Figure 5.5: Electric field lines of parallel plate capacitors and on coplanar interdigital sensors [23]

The curved electric fields generated in interdigitated/interdigital sensors are referred to as fringing fields. These are analogous to the field fringes that emerge at the edges of a capacitor, given that the charge is unable to disperse elsewhere and, as a consequence of being repelled, accumulates at the edges.

The co-planarity of the electrodes in an interdigitated sensor ensures that the measured capacitance will yield a high signal-to-noise ratio. To facilitate the most readily discernible alteration in sensor capacitance, the electrode configuration of the interdigitated sensor can be replicated multiple times. The term “interdigitated” is used to describe a voxel-like or finger-like periodic pattern of parallel electrodes in a plane, which is employed to generate the capacitance associated with electric fields penetrating a material under test. Figure 5.2 illustrates a typical interdigitated sensor.

These sensors are typically utilised in conjunction with an AC source, which is applied as an excitation voltage between the two terminals. The electric field is generated from the positive terminal to the negative terminal. Furthermore, Mamishev posited that in the event of a semi-infinite homogeneous medium situated on the sensor surface and exhibiting periodic variation of the electric potential along the X-axis, an exponentially decreasing electric field is generated along the Z-axis, which penetrates the medium. Figure 5.6 illustrates this assertion put forth by Mamishev. [23]

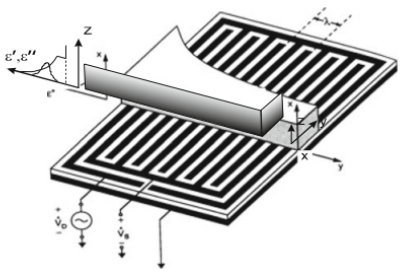

Figure 5.6: Fringing electric field of interdigital sensor [23]

Figure 5.7 depicts the lateral aspect of the interdigitated sensor, illustrating the formation of an electric field between the positive and negative electrodes. It can be observed that the penetration depths of the electric field lines vary according to the pitch of the respective parts. The term 'pitch length' is used to describe the distance between two consecutive electrodes of the same polarity in conventional interdigitated sensors. Accordingly, Figure 5.7 depicts three distinct pitch lengths (l1, l2 and l3), which illustrate the varying penetration depths with respect to the sensor pitch length. An increase in the pitch length will result in a greater penetration depth; however, this will also lead to a reduction in the strength of the electric field generated by the adjacent electrodes. [23]

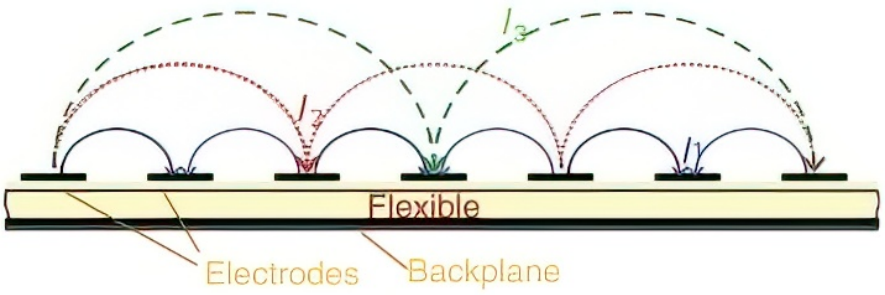

Figure 5.7: Electric field formed between positive and negative electrodes for different pitch lengths, (l1, l2 and l3) [23]

Co-planar interdigitated sensors are suitable for a variety of measurement applications. The accompanying illustration 5.8 demonstrates the detection capabilities of planar interdigitated sensors. [23]

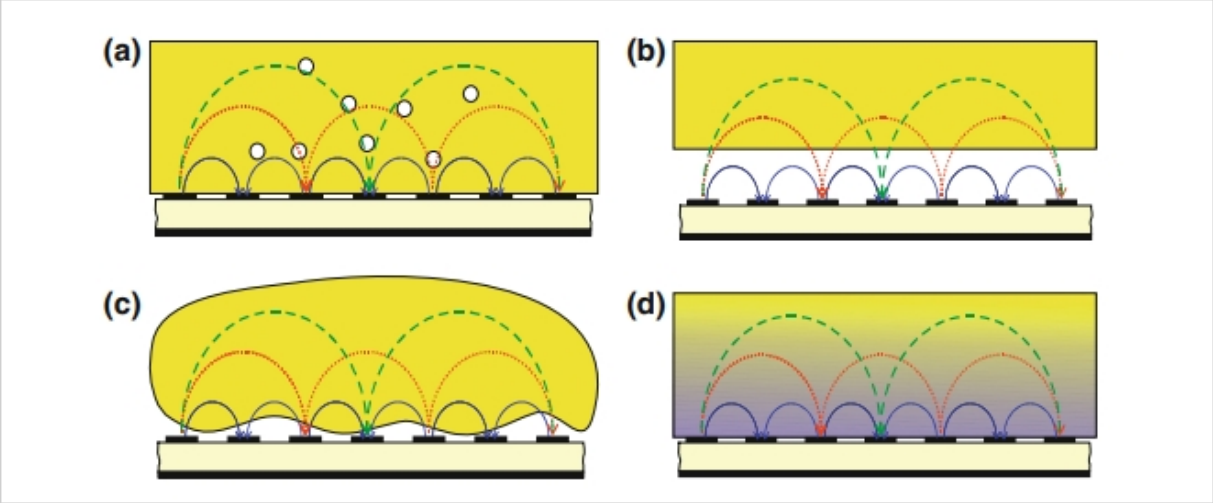

Figure 5.8: Sensing possibilities to detect various characteristic of samples. a sensing density, b sensing distance, c sensing texture, d sensing moisture [23]

As proposed, the electric field of the electrode array is significantly reduced in the direction of the vector perpendicular to the electrode surface. Furthermore, this configuration can be employed to ascertain the thickness of the dielectric material present within the electrodes by measuring the dielectric constant and capacitance. One such application is the detection of microbial growth (biofilms), which act as a dielectric material in the sensor. [20]

Capacitive sensors can be manufactured in two distinct ways: invasively and non-invasively. In the case of the invasive device, direct contact between the interdigitated electrodes and the sample is required. In contrast, the non-invasive device employs a substrate membrane, such as an insulating material, glass, polypropylene or polymer, to facilitate the interaction between the sample and the electrodes. [25]

5.2.4 Interdigitated/Interdigital Sensor Modelling

The considerable interest in scientific research into interdigitated sensors is predicated on the simplicity of these sensors and their suitability for straightforward conversion into an integrated format. Additionally, their low cost represents another advantage of these sensors. A significant drawback is the lack of suitable analytical equations for predicting their electrical response. A useful method for calculating the interdigitated capacitance is conformal mapping, whereby equations are derived based on the geometry and physical characteristics of a sensor. The precise mathematical relationships pertaining to the capacitance are relatively intricate and can only be furnished in closed form for the scenario wherein there is no masking layer. [20] [25]

Conformal mapping is a theoretical tool employed by mathematicians, engineers and scientists to facilitate the translation of information from a complex shape to a relatively simpler one, thereby enabling more straightforward analysis. Consequently, the capacitance generated by a sample of co-planar interdigitated electrodes was determined through the utilisation of conformal mapping techniques in a semi-infinite field, wherein the electrodes are coated with an identical liquid. [28]

The equation is:

$$C = \frac{Q}{2V_0} = \left[\frac{\epsilon_r \cdot \epsilon_0 \cdot l}{\pi}\right] \cdot \ln\left[\left(1 + \frac{w}{\alpha}\right) + \sqrt{\left(1 + \frac{w}{\alpha}\right)^2 - 1}\right]$$

In this equation, C represents the capacitance, ϵ_r denotes the dielectric constant of the liquid, ϵ_0 signifies the dielectric constant of the vacuum, l is the length of the electrodes, w is the width of the electrodes, and α is the total distance between the electrodes.

The aforementioned relationship indicates that the maximum capacitance can be attained by reducing the distance between the electrodes to a minimum. Figure 5.9 depicts a pair of electrodes with a protective, substrate, or insulating coating. [28]

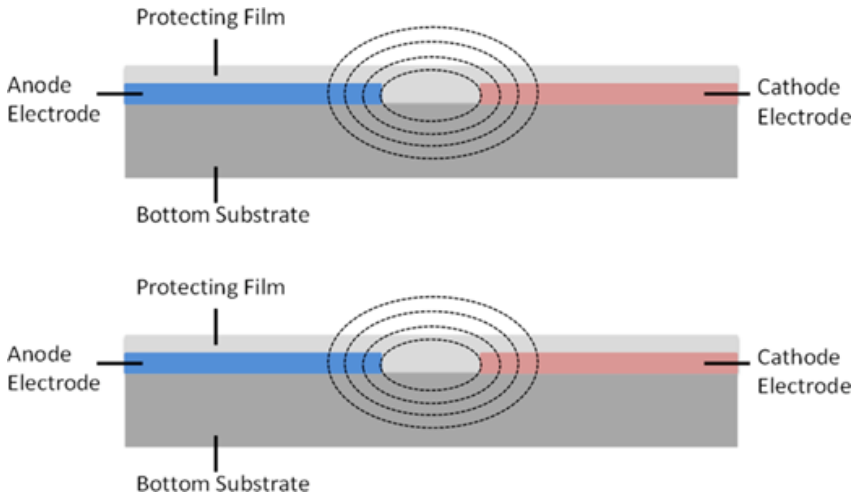

Figure 5.9: Working principle of capacitors with single coplanar electrode [28]

The protective layer in the example of the publication [28] under consideration, illustrated in Figure 5.9, is a 40 µm thick polypropylene film with an ϵ_r value of 2.2–2.34. The electric field lines traversing the protective layer do not contribute to the capacitance fluctuations discerned by the sensor. [28]

The effective width W_{eff} of the electrodes is given by the equation:

$$W_{\text{eff}} = \alpha\left(\sqrt{1 + \left(\frac{w}{\alpha}\right)^2} - 1\right)$$

In order to accurately determine the capacity of the model, it is essential to consider the impact of the protective layer. The total capacitance of a pair of coplanar electrodes can be modelled as follows:

$$C_{\text{air}} = \frac{Q}{2V_0} = \left[\frac{\epsilon_r \cdot \epsilon_0 \cdot l}{\pi}\right] \cdot \ln\left[\left(1 + \frac{w}{\alpha}\right) + \sqrt{\left(1 + \frac{w}{\alpha}\right)^2 - 1}\right]$$

and the capacitance resulting from the effect of the protective layer:

$$C_{\text{film}} = \left(\frac{\epsilon_{\text{film}} \cdot \epsilon_0 \cdot l}{\pi}\right) \cdot \ln\left[\left(1 + \frac{W_{\text{eff}}}{\alpha}\right) + \sqrt{\left(1 + \frac{W_{\text{eff}}}{\alpha}\right)^2 - 1}\right]$$

In result, the total capacitance is:

$$C = C_{\text{air}} + C_{\text{film}}$$

If it is assumed that the number of electrodes with the same polarity is N, then the total number of pairs of co-planar electrodes will be 2N - 1. Consequently, the total capacity of the printed co-planar electrodes can be estimated as follows:

$$C_{\text{total}} = C(2N - 1)$$

As illustrated in the accompanying Figure 5.9, when a material comes into contact with the sensor above its protective layer, the material modifies the electric field around the sensor, thereby increasing the total capacitance. The system can be modelled as a parallel combination of the co-planar capacitance of the sensor and the capacitance of the material. The actual effect of the material is based on the relative permeability of ϵ_r, which acts as a multiplier of the capacitance. [28]

The penetration depth of the fringing electric fields situated above the interdigitated electrodes is proportional to the distance λ/2 between the centres, the sensing electrodes and the driven electrodes. Figure 5.10demonstrates the concept of multiple depth penetration for three distinct sensor wavelengths. [29]

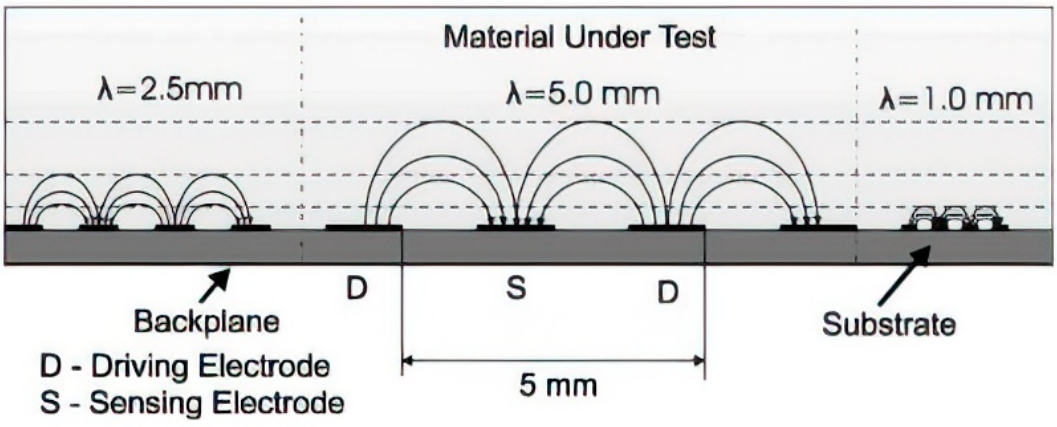

Figure 5.10: A conceptual view of multiwavelength dielectrometry. The penetration depth of electric field lines is proportional to the electrode spatial period [29]

Consequently, a reduction in electrode distance will result in an increase in capacitance, although this will be accompanied by a limitation in depth of penetration.

If one were to observe the plane from a top perspective, rather than a cross-sectional view of the interdigitated sensor, the behaviour of the electric field would be evident, as illustrated in the accompanying Figure 5.11.

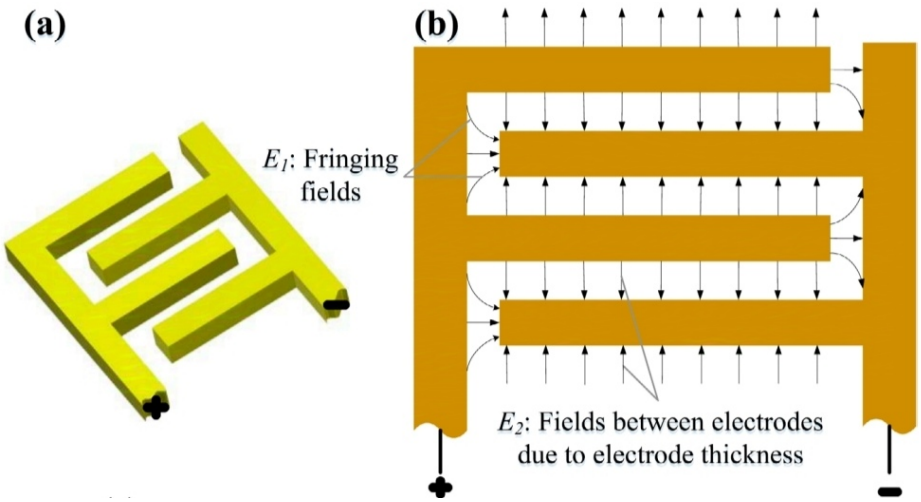

Figure 5.11: Electric fields and capacitances in the interdigitated electroadhesive system: (a) is the interdigital electrodes in 3D and (b) is the top view of the interdigital electrodes [30]

It has been observed that once more, at the peripheries of the electrode field, fringes emerge. In the event that the length of the electrodes is significantly greater than their width and thickness, and the area of the electrodes is considerably larger than the gap between the electrodes on the surface of the substrate, it is possible to disregard all field fringes E_1 that result from edge/edge phenomena. The thickness of the electrodes also permits the observation of electric fields E_2, which, despite their capacity to generate considerable attractive forces between the electrodes, exert a similar influence on their sides, thereby cancelling each other out. [30]

Furthermore, due to the presence of E_2 and the deposition of electrodes within a dielectric field, it is evident that the electrodes will not come into contact with one another. Furthermore, the individual forces between adjacent or overlapping fields are assumed to be insignificant. As a result of the aforementioned considerations, the fields between the electrodes and the substrate E_3 are the sole determinants of the fields between the co-planar electrodes E_4. These fields originate from the positive electrodes and traverse the dielectric material and the substrate, terminating at the negative electrodes. Inside the interdigitated electroadhesive system, as illustrated in Figure 5.12 E_3, the fields of E3 are insignificant in comparison to those of E_4. Consequently, the half side of E_4 that is in closest proximity to the substrate wall is the primary contributor to the attractive forces developed between the electrodes and the substrate. [30]

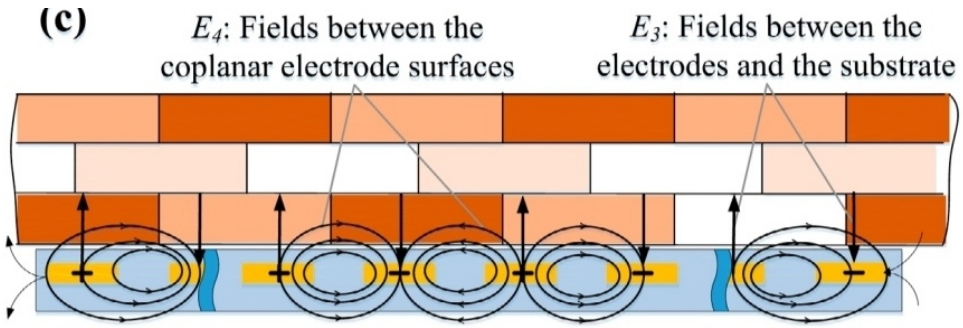

Figure 5.12: Electric fields and capacitances in the interdigitated electroadhesive system: (c) is the cross-sectional view of the interdigital electroadhesive pad attached on a wall substrate [30]

In light of the aforementioned evidence, it is possible to construct an equivalent circuit representing the capacitance developed in the co-planar interdigitated electrodes. This is illustrated in the accompanying Figure 5.13. [30]

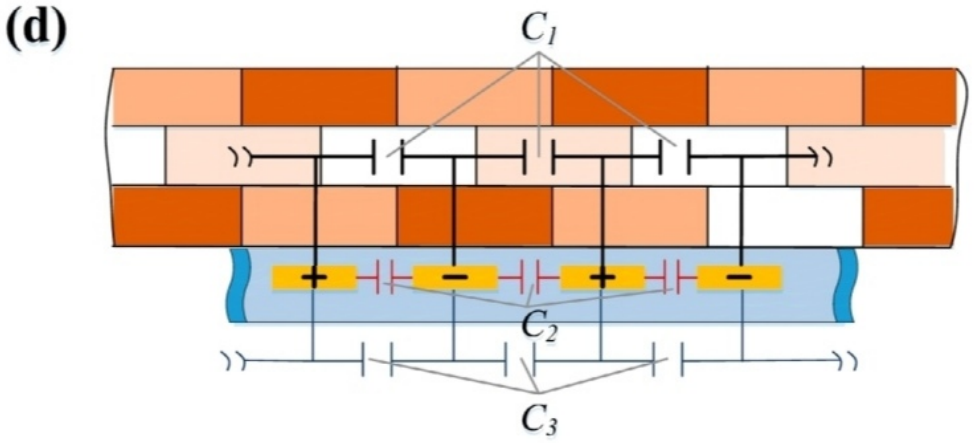

Figure 5.13: Electric fields and capacitances in the interdigitated electroadhesive system: (d) is the equivalent circuit for the coplanar interdigital capacitance [30]

In this configuration, the co-planar capacitances C_1 and C_3 are based on the parallel reinforcements E_4 and the simple capacitance C_2 between the electrodes, which is created due to the influence of E_2. In light of the aforementioned assumptions and the aforementioned simplification, it can be concluded that the electrostatic forces between the electrode and the substrate are dependent solely on C_1. [30]

A number of techniques have been developed for calculating the co-planar capacitance within an interdigitated electrostatic system. These include the continuum model, the finite element method, non-dimensionalised plots, approximate relations and conformal mapping methods. The conformal mapping method is an effective approach for transforming complex and co-planar geometries into a simplified representation of parallel reinforcement. It is a widely utilized method in this field of study. The existing approximate relations were only applied to insulating substrates, as the theoretical model, which is more computationally efficient and can be used for both conductive and insulating substrates, is therefore necessary. [30]

An alternative method for calculating the capacitance of an interdigitated capacitor is presented in the

following mathematical relationship [31]:

$$C_{\text{IDC}} = \frac{\epsilon_r \cdot 10^{-3} \cdot K(k)}{18\pi \cdot K'(k)} \cdot (N-1)l \quad \text{[pF]}$$

The capacitance is a function of the length (l) of the electrodes (fingers of the total number of electrodes (N)), the width (w) of the electrodes, the space between them and the effective dielectric constant ($\epsilon_r e$). The outcome of this function is expressed in picofarads (pF). [31]

The approximation of the ratio between the elliptic integrals of the first type and the complement of $K'(k)$ is as follows:

- For $0.707 \leq k \leq 1$:

$$K(k) = \frac{1}{\pi} \ln\left(\frac{2\left(1+\sqrt{k}\right)}{1-\sqrt{k}}\right)$$

- For $0 \leq k \leq 0.707$:

$$K'(k) = \frac{\pi}{\ln\left(\frac{2\left(1+\sqrt{k'}\right)}{1-\sqrt{k'}}\right)}$$

Therefore,

$$\frac{K(k)}{K'(k)} = \frac{\frac{1}{\pi} \ln\left(\frac{2\left(1+\sqrt{k}\right)}{1-\sqrt{k}}\right)}{\frac{\pi}{\ln\left(\frac{2\left(1+\sqrt{k'}\right)}{1-\sqrt{k'}}\right)}}$$

where:

$$k' = \sqrt{1-k^2}$$

and

$$k = \tan^2\left(0.25 \cdot \left(\frac{w\pi}{w+g}\right)\right)$$

The units of measurement for all lengths of these relationships must be given in um. [31]

In order to ascertain which of the two models yields the most accurate results, the actual implementation of an interdigitated capacitor, which has been published, is presented for analysis. In this instance,

the characteristics of the interdigitated capacitor are known, as they have been fully calculated, simulated and measured. Accordingly, in accordance with the design review methodology proposed by Agilent Technologies, the capacitor depicted in the accompanying Figure 5.14 was subjected to a detailed examination. [32]

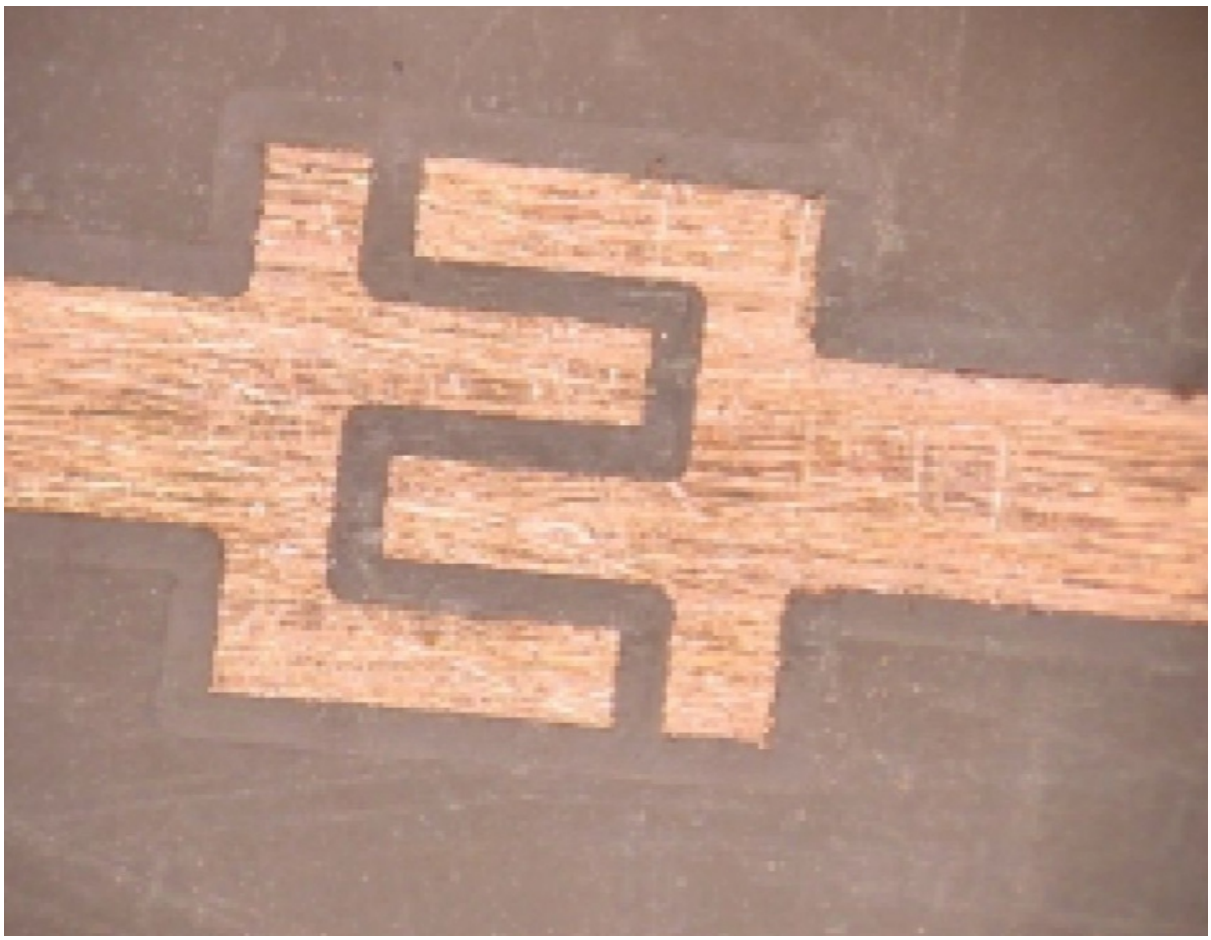

Figure 5.14: Four Finger MIDCAP Element Under Test [32]

The above capacitor has the following geometric characteristics:

$$
\begin{aligned}
w &= 508\,\mu\text{m}\,(20\,\text{mils}) \\
g &= 254\,\mu\text{m}\,(10\,\text{mils}) \\
g_E &= 254\,\mu\text{m}\,(10\,\text{mils})\ \text{gap at the end of the fingers} \\
l &= 1270\,\mu\text{m}\,(50\,\text{mils}) \\
N &= 4 \\
\epsilon_r &= 3.05\ \text{substrate dielectric constant} \\
t &= 35.56\,\mu\text{m}\,(1.4\,\text{mils})\ \text{metal thickness} \\
h &= 508\,\mu\text{m}\,(20\,\text{mils})\ \text{substrate thickness}
\end{aligned}
$$

The simulated and measured results give the following values:

$$\begin{aligned} \text{EMPOWER (Simulation)}: &\quad C_{\text{eff}} = 0.082\,\text{pF} \\ \text{MIDCAP (Simulation)}: &\quad C_{\text{eff}} = 0.089\,\text{pF} \\ \text{Hardware (Measurements)}: &\quad C_{\text{eff}} = 0.068 - 0.077\,\text{pF} \end{aligned}$$

In light of the aforementioned results, the models described earlier will be employed to illustrate which of them represents the optimal approach. In conclusion, the following can be stated:

$$k = \tan^2\left(0.25 \cdot \frac{w\pi}{w+g}\right) = \tan^2\left(0.25 \cdot \frac{508\,\mu\text{m} \cdot \pi}{508\,\mu\text{m} + 254\,\mu\text{m}}\right) = 0.3333$$

$$k' = \sqrt{1-k^2} = \sqrt{1-(0.3333)^2} = 942.809 \times 10^{-3}$$

Given that the condition $0 \leq k \leq 0.707$ is satisfied, the ratio between the elliptic integrals can be expressed as follows:

$$\frac{K(k)}{K'(k)} = \frac{\pi}{\ln\left(\frac{2 \cdot \left(1+\sqrt{k'}\right)}{1-\sqrt{k'}}\right)} = \frac{\pi}{\ln\left(\frac{2 \cdot \left(1+\sqrt{942.809 \times 10^{-3}}\right)}{1-\sqrt{942.809 \times 10^{-3}}}\right)} = 639.631 \times 10^{-3}$$

Finally, the capacitance in pF, can be expressed as:

$$C_{\text{IDC}} = \frac{\epsilon_r \cdot 10^{-3} \cdot K(k) \cdot (N-1) \cdot l}{18\pi \cdot K'(k)} = \frac{3.05 \times 10^{-3} \cdot 639.631 \times 10^{-3} \cdot (4-1) \cdot 1270\,\mu\text{m}}{18\pi} = 0.131\,\text{pF}$$

A value that is approximately equivalent to the actual value.

5.3 Use as a Biosensor

In this research thesis, interdigitated/interdigital electrodes will be employed as biosensors for the measurement of bacterial capacity.

The concept of success is derived from the fundamental principle that all phenomena in life can be explained by the science of chemistry, which in turn is based on the laws of physics and biology. It is evident that the diverse shapes, sizes, and colours observed in different bacterial species are indicative of their unique chemical compositions. This suggests that they will also exhibit disparate electrical properties, including those pertaining to capacitance.

A total of six distinct bacterial cultures, comprising three Gram-positive and three Gram-negative strains, will be employed in this investigation.

In the first part of the research, the objective is to ascertain whether the bacteria exhibit electrical properties, specifically capacitance, and to determine the methodology for its measurement. Subsequently, the hypothesis that different bacteria may exhibit disparate capacitance values will be tested, contingent on the outcomes of the preceding experiments. Subsequently, an investigation will be conducted to ascertain whether the values of the Gram-positive bacteria exhibit convergence, and a similar analysis will be performed for the Gram-negative bacteria. Ultimately, if the values of the Gram-positive bacteria are markedly disparate from those of the Gram-negative bacteria, it can be postulated that an innovative and cost-effective method for their separation and subsequent identification based on their electrical properties may be attainable.

The interdigitated electrode (IDE) boasts a distinctive structural configuration that renders it particularly well-suited to a multitude of biological and medicinal applications. The aforementioned design renders IDEs an extremely efficacious biosensor. The interdigitated comb-like structures that comprise the electrodes generate a substantial surface area in a compact configuration, thereby enhancing the biosensor's sensitivity and specificity. The extensive surface area facilitates deeper interaction between target analytes, including bacteria, DNA, and proteins, and the sensor surface, which is crucial for the detection of biomolecules at low concentrations. The capacity of IDEs to operate in both faradaic and non-faradaic modes serves to enhance their sensitivity to an even greater extent. When a biomolecule interacts with the electrode surface in faradaic mode, IDEs measure changes in electron transfer resistance and double-layer capacitance. Conversely, in non-faradaic mode, they detect variations in capacitance caused by alterations in the dielectric properties of the material between the electrodes. These characteristics facilitate the provision of accurate, real-time readings, which are crucial for applications in environmental monitoring and medical diagnostics. [33] [34]

In regard to the functionality of Integrated Development Environment (IDE)s as biosensors, the design of these environments is of paramount importance. The dimensions of the electrodes, including their width, spacing, total surface area, and overall shape, have a significant impact on the sensitivity and accuracy of the sensor. To illustrate, a reduction in the distance between the electrode fingers results in an augmented effective surface area, thereby enhancing the sensor's capability to discern even the minutest fluctuations in the analyte's electrical characteristics. It has been demonstrated that there is an inverse relationship between the impedance and capacitance of an IDE sensor. Consequently, the impedance decreases with an increase in surface area, facilitating the identification of target molecules with greater accuracy. This connection is particularly advantageous for the identification of cancer cells, as the larger surface area facilitates the precise identification of cancer cells in their early stages. Furthermore, the use of nanomaterials or electrode surface alterations may enhance the sensitivity of IDEs, enabling the detection of a broader range of biomolecules, including proteins, DNA fragments, and whole cells. The versatility of IDEs in a range of biosensing applications is evidenced by their capacity to adapt in terms of both design and material utilisation. [34] [35] [36]

The identification of bacterial infections represents a highly compelling application of IDEs as biosensors, given the paramount importance of their high sensitivity and specificity. It is possible to collect

and identify bacterial cells by functionalising IDEs with specific antibodies or other recognition components. For instance, IDEs have been employed to quantify the alterations in electrical conductivity that occur when bacteria attach to the functionalised electrode surface, thereby enabling the identification of Escherichia coli. In this context, the high sensitivity of IDEs enables the identification of individual bacterial cells, which is highly beneficial for applications pertaining to food safety and medical diagnostics. Furthermore, IDEs' label-free detection capabilities obviate the necessity for complex sample preparation, rendering them the optimal choice for rapid and cost-effective bacterial detection. IDEs are a crucial instrument in the battle against bacterial infections and pollution, as they are capable of identifying pathogens in real-time with high specificity and sensitivity. [9] [12] [37] [13].

5.4 Chemical Study

The interdigitated/interdigital electrodes currently available on the market are composed of either a titanium and gold (Ti/Au) or a chromium and gold (Cr/Au) combination, with a substrate comprising either a single-crystal Silicon (Si) (P-type), a surface of Silicon Dioxide (SiO_2) SiO_2, or a quartz glass, double-sized polished. Gold, titanium and chromium are relatively inert metals, with gold exhibiting the lowest reactivity. The objective of the study is to identify which material is the most chemically inert and thermally stable, and therefore the most suitable substrate for the given application. In terms of chemical treatment, this refers to the cleaning agents used to eliminate and sterilise bacteria, as well as the temperatures employed in the decontamination furnace. It should be noted that chromium exhibits superior mechanical stability. With regard to the substrates, both are based on silicon (SiO_2), but quartz glass is more durable. It should be noted that Ti/Au and Cr/Au are not even alloys. The substrate is comprised of a SiO_2 base, with the addition of a metal alloy between titanium and gold, and finally, gold. The majority of these materials are in the form of coatings, rather than alloys. Therefore, the focus is on gold, which exhibits high resistance to any temperature or chemical treatment that the interdigitated/interdigital electrodes will undergo in this study. Gold, as a metal, is highly inert, which is the reason for its extensive use. [38]

Some metals are renowned for their relative stability and inertness, including gold, titanium and chromium. Given its position within the electrochemical series, gold is regarded as the most inert of the three metals. The characteristics of these metals may be altered by alloying them with gold, particularly in regard to their resistance to chemicals, thermal stability, and mechanical durability. The objective of this investigation is to ascertain whether the alloy Ti/Au (titanium-gold) or Cr/Au (chromium-gold) is more inert and more suitable for handling abrasive chemicals and high temperatures. Furthermore, an evaluation of these alloys' mechanical stability will be conducted based on the existing literature.

Inertness and Chemical Resistance

Chromium-Gold Alloy (Cr/Au):

Chemical Resistance: Alloys comprising chromium and gold are renowned for their exceptional resilience to corrosion, particularly when subjected to atmospheric conditions. A persistent oxide layer

(Cr_3O_4) forms on the surface of chromium, providing a protective barrier against further oxidation and corrosion. This characteristic is beneficial in circumstances where the alloy is subjected to oxidising agents or harsh chemicals. [38] [39]

Applications: Chromium-gold (Cr/Au) alloys are employed extensively in the manufacture of electronic components and coatings for engineering applications where long-term stability is of paramount importance, due to their reliable resistance to corrosion. [38] [39]

Inertness: The primary factor contributing to the inertness of Cr/Au alloys is the chromium content, which enhances the alloy's resilience to chemical deterioration under diverse environmental circumstances. Nevertheless, chromium displays greater reactivity than titanium, which may result in enhanced surface oxidation in specific circumstances. [38] [40]

Titanium-Gold Alloy (Ti/Au):

Chemical Resistance: Titanium-gold alloys are renowned for their exceptional resilience to a multitude of chemical agents, particularly in environments characterised by the presence of potent acids and elevated chloride concentrations. TiO_2 represents a solid and inert oxide layer formed by titanium, offering superior corrosion resistance. For biomedical applications where exposure to bodily fluids and other corrosive substances is common, titanium-gold alloys are particularly well suited. [40] [41]

Applications: Ti/Au alloys are employed in a multitude of applications where robust corrosion resistance and biocompatibility are prerequisites, including in sensors designed for use in harsh environments and medical implants. The alloy exhibits notable stability at elevated temperatures and resistance to oxidation, as evidenced by previous studies. [41] [42]

Inertness: In general, titanium is more chemically inert than chromium, particularly when exposed to strong acids or chloride ions. This indicates that Ti/Au alloys may offer superior protection against abrasive chemical conditions in comparison to Cr/Au alloys. [40] [41]

Thermal Stability

Chromium-Gold Alloy (Cr/Au):

Thermal Resistance: The ability of Cr/Au alloys to function and maintain structural integrity at high temperatures is due to their thermal resilience. In contexts where high-temperature processes are required, such as in microelectronics and aerospace engineering, this feature is of paramount importance. [39] [42]

Degradation: However, at elevated temperatures, chromium can penetrate the gold layer, which may ultimately result in alterations to the alloy's microstructure and a reduction in its protective properties. [39]

Titanium-Gold Alloy (Ti/Au):

Thermal Resistance: The capacity of Ti/Au alloys to withstand mechanical and chemical stability under thermal stress is ascribed to titanium, which also contributes to the alloys' robust resistance to elevated temperatures. Due to its resilience to thermal degradation, the alloy is suitable for utilisation in contexts where corrosion resistance and stability at elevated temperatures are requisite. [40] [41]

Degradation: The oxide layer that titanium (TiO_2) forms is highly stable at elevated temperatures, which contributes to the overall enhanced thermal stability of the alloy. When subjected to elevated temperatures over an extended period, the titanium oxide layer displays a reduced propensity for deterioration in comparison to the chromium oxide layer observed in Cr/Au alloys. [40]

Mechanical Stability

Chromium-Gold Alloy (Cr/Au):

Mechanical Stability: The remarkable mechanical stability of chromium-gold alloys is a well-established phenomenon, particularly in thin-film applications. The strong bond between chromium and gold renders the former less susceptible to delamination or mechanical failure under stress. [38] [39]

Research Findings: The study described in the publication "Influence of Ti and Cr Adhesion Layers on Ultrathin Au Films" indicates that when used as an adhesive layer under gold films, chromium offers superior mechanical stability to titanium. This stability is of particular significance in scenarios where the alloy is subjected to mechanical stress or wear. [38] [39]

Titanium-Gold Alloy (Ti/Au):

Mechanical Stability: Although Ti/Au alloys are typically less robust than Cr/Au alloys, particularly in thin-film applications, they are renowned for their remarkable mechanical stability. Titanium exhibits a strong affinity for gold, yet the bond formed is comparatively weaker than that of chromium. Consequently, in certain scenarios, titanium may be more susceptible to mechanical failure. [40]

Research Findings: Ti/Au alloys remain a viable option for a multitude of applications, despite a slight decline in their mechanical stability. This is particularly the case when the priority is biocompatibility and corrosion resistance, rather than maximum mechanical strength. [40]

Based on the analysis of available research and literature:

Inertness and Chemical Resistance: Alloys comprising titanium and gold (Ti/Au) are renowned for their remarkable chemical resistance and inertness, particularly in environments where strong acids or chlorides are present. In comparison to the chromium oxide layer of chromium-gold (Cr/Au) alloys, titanium (TiO3) exhibits a superior capacity to form oxide layers, thereby providing enhanced protection.

Thermal Stability: Both alloys demonstrate excellent thermal stability. However, due to the stability of the TiO2 layer, Ti/Au alloys may exhibit superior integrity preservation at elevated temperatures.

Mechanical Stability: Due to their exceptional mechanical stability, chromium-gold (Cr/Au) alloys are more appropriate for applications where the material will be subjected to mechanical stress or where adhesion strength is of paramount importance, as in thin-film applications.

In conclusion, the particular requirements of the intended application should inform the decision as to whether Ti/Au or Cr/Au alloys are selected. Ti/Au alloys are likely to be the optimal selection when chemical resistance and thermal stability are of paramount importance. In circumstances where mechanical stability and adhesion strength are of paramount importance, Cr/Au alloys may prove to be the optimal selection.

The materials under examination comprise quartz glass and single-crystal silicon (p-type), with a surface layer of SiO_2. Given their established resistance to chemicals and high temperatures, these materials are well-suited for a multitude of high-performance applications, including optical devices, microelectronics, and sensors. The objective of this study is to ascertain whether the material, whether silicon covered with SiO2 or quartz glass, exhibits greater resistance to chemicals and high temperatures.

Material Composition and Properties

Single-Crystal Silicon (P-Type with SiO_2 Surface):

Composition: Group III elements, including boron, are introduced into single-crystal silicon (p-type) as dopants to facilitate the introduction of "holes" as the predominant charge carriers. The principal objectives of the deposition of a SiO_2 (SiO_2) surface layer are to enhance chemical resistance and electrical insulation. [43] [44]

Properties:

Chemical Resistance: The SiO_2 layer on silicon exhibits robust resistance to a wide range of chemical substances, particularly acids and bases. Nevertheless, it can be dissolved by hydrofluoric acid (HF). Consequently, silicon may be effectively safeguarded by SiO_2 in a multitude of contexts. [44] [41]

Thermal Resistance: Single-crystal silicon exhibits excellent thermal stability, with a temperature resistance of up to 1,500 °C. The SiO_2 layer has a somewhat lower melting point of approximately 1,100 °C, yet it still exhibits thermal stability. [43] [45] [42]

Quartz Glass:

Composition: One crystalline form of SiO_2 is quartz glass. It is of high purity and is typically employed in contexts where chemical inertness, high heat resistance, and transparency are necessary. [44] [45]

Properties:

Chemical Resistance: Quartz glass exhibits remarkable resistance to a wide range of chemical agents, including acids, bases, and organic solvents. Quartz glass is susceptible to hydrofluoric acid, in a manner analogous to the SiO_2 layer on silicon. However, it is regarded as one of the most chemically inert materials. [45] [41]

Thermal Resistance: Quartz glass has a melting point of approximately 1,670 °C, which demonstrates its exceptional resilience to high temperatures. Furthermore, the material exhibits a markedly low coefficient of thermal expansion, which enhances its stability under thermal cycling and sudden temperature fluctuations. [45] [46]

Comparative Analysis

Chemical Resistance:

Single-Crystal Silicon with SiO_2 Surface: The SiO_2 layer exhibits notable chemical resistance, particularly in the presence of strong acids and bases. One significant disadvantage, however, is the materials' vulnerability to hydrofluoric acid. [44] [41]

The SiO_2 layer provides protection for the silicon substrate in HF-free settings, thereby ensuring the preservation of its chemical and structural integrity. [44] [45]

Quartz Glass: The ability of a substance to resist chemical reactivity is defined as chemical inertness. Quartz glass is renowned for its capacity to withstand such reactivity. It exhibits resistance to a wide range of chemical agents, including hydrofluoric acid. It is often assumed that the SiO_2 layer on silicon exhibits reduced chemical resistance compared to quartz glass. This can be attributed to the fact that quartz glass is a bulk substance, as opposed to a coating on the surface. [45] [41]

In comparison to silicon coated in SiO_2, quartz glass is a more reliable option due to its uniform composition and chemical resistance in highly corrosive environments. [45]

Conclusion on Chemical Resistance: The homogeneity and bulk characteristics of quartz glass afford a somewhat superior overall chemical resistance when compared to the SiO_2 layer over silicon. Nevertheless, in scenarios where there is no exposure to hydrofluoric acid, both materials demonstrate excellent resistance.

Thermal Resistance:

Single-Crystal Silicon with SiO_2 Surface: Silicon is a suitable material for high-temperature applications due to its high melting point, which is approximately 1,500 °C. However, with regard to thermal resistance, the SiO_2 layer, whose melting point is approximately 1,100 °C, represents the upper limit. [43] [45] [42]

The combination of SiO_2 and silicon provides considerable thermal stability; however, exposure to

temperatures approaching the melting point of the SiO_2 layer may pose a risk to it. [43] [42]

Quartz Glass: The thermal resistance of SiO_2-coated silicon is inferior to that of quartz glass. Quartz glass displays resilience in high temperatures due to its low thermal expansion and melting point of approximately 1,670 °C. [45] [46]

Furthermore, quartz glass displays an augmented capacity to withstand thermal shock, which renders it less susceptible to fractures or structural alterations during sudden temperature fluctuations. [45] [46]

Conclusion on Thermal Resistance: Quartz glass exhibits superior thermal resistance compared to silicon covered with SiO_2 due to its elevated melting point and enhanced thermal stability.

Practical Considerations and Applications

Application Environments: Quartz glass is the optimal material for use in applications where chemical resistance is of paramount importance, particularly in environments where hydrofluoric acid (HF) or other highly corrosive chemicals may be employed.

We would like to highlight that quartz glass is the material of choice for high-temperature applications due to its remarkable thermal stability.

Mechanical Considerations: Although this examination is primarily concerned with the chemical and thermal stability of single-crystal silicon, it is essential to acknowledge the advantages that this material offers as a semiconductor in mechanical applications, particularly in microelectronics. Nevertheless, these variables fall outside the remit of this comparison. [43] [44] Based on the comprehensive analysis of the materials in question:

Chemical Resistance: In terms of chemical resistance, quartz glass typically demonstrates superior performance compared to silicon coated with SiO2. This is particularly the case when the material is required to demonstrate consistent resistance across its entire surface.

Thermal Resistance: Quartz glass exhibits superior heat resistance compared to silicon coated with SiO2; therefore, it is a more optimal selection for applications involving elevated temperatures.

The data thus lends support to the original theory that quartz glass is more resilient. With regard to resistance to heat and chemicals, quartz glass demonstrates superior performance compared to single-crystal silicon with a SiO2 surface layer.

In order to prevent an increase in the sensor's inherent capacitance, interdigitated/interdigital electrodes should have a low relative electrical permeability (dielectric constant). This is with regard to the substrate, as the electrical permeability of the substrate is of interest, given that it should not have a high impedance capacitance. It is essential that the dielectric constant of the substrate is as low as possible. In general, electrodes with high sensitivity are preferable when their dimensions are small. In general, sensitivity increases with an increase in the width of the electrodes, which corresponds to an increase in length (and thus active surface area). Furthermore, sensitivity increases with an increase in

the number of electrodes (fingers). The geometric dimensions and the number of electrodes are related in such a way that the overall capacitance of the element can be calculated. The following section will demonstrate, based on this relationship, which factor has the greatest influence on the overall result. It is evident that an increase in the number of electrodes will result in an enhancement of both capacitance and sensitivity. However, in order to maintain the overall dimensions of the sensor, it is necessary to reduce the width of the electrodes. The following section will examine which of the two factors is of greater consequence. [47] [48]

It is common practice in the field of biomedical sensors to utilise interdigitated or interdigital electrodes, or IDEs, as a sensor application. The electrical characteristics of the substrate on which the electrodes are placed represent one of numerous variables that influence the efficacy of these sensors. The objective here is to ascertain the thermal, chemical and dielectric constants (or relative electrical permeability) of two substrates: quartz glass and monocrystalline silicon with a surface SiO2 layer.

Dielectric Constant (Electrical Permeability)

The relative electrical permeability, or dielectric constant, is a pivotal factor that markedly influences the capacitance and impedance of sensors. In the construction of capacitive sensors, the use of substrates with lower dielectric constants is often preferable, as this reduces impedance and improves sensor accuracy.

Monocrystalline Silicon (P-type, with surface SiO_2 layer):

Si: The dielectric constant of silicon is relatively high, with a value of approximately 11.7.

Surface SiO_2 Layer: SiO_2 is a material that is frequently employed as a passivation or insulating layer on silicon substrates. Its dielectric constant is approximately 3.9, as evidenced by research. [43]

Composite Dielectric Constant: In the case of a substrate with a SiO_2 layer, the effective dielectric constant can be conceptualised as a summation of the dielectric constants of silicon and SiO_2.

Conversely, the SiO_2 layer serves to reduce the effective dielectric constant at the interface, which may result in enhanced capacitive sensing performance.

Quartz Glass:

Quartz (SiO_2): The crystalline SiO_2 material, otherwise known as quartz glass, has a dielectric constant of approximately 3.8. This value is considerably lower when considered in aggregate, but is in close proximity to the dielectric constant of the SiO_2 layer on silicon substrates. [46]

Thermal Resistance

The capacity of a substrate to withstand elevated temperatures without undergoing degradation is defined as its thermal resistance. In the context of biomedical applications, where sensors may be subjected to sterilisation procedures, this is of particular importance.

Monocrystalline Silicon (with SiO_2 layer):

Silicon: Silicon exhibits excellent thermal resistance, with a temperature tolerance reaching 1,500 °C.

SiO_2 Layer: Furthermore, the SiO_2 layer exhibits favourable thermal stability up to 1,100 °C. [44]

Overall Thermal Resistance: High.

Quartz Glass:

Quartz Glass: Quartz is renowned for its exceptional thermal resistance, with a melting point of approximately 1,670 °C. Furthermore, it exhibits low thermal expansion, thereby ensuring high stability under temperature fluctuations. [45]

Overall Thermal Resistance: Very high.

Chemical Resistance

An additional essential quality is the ability to withstand chemical attack, particularly in biomedical settings where sensors may be subjected to a range of chemical agents during sterilisation or when in contact with biological fluids.

Monocrystalline Silicon (with SiO_2 layer):

Silicon: Silicon exhibits moderate resistance to chemical attack, yet it can be etched by strong acids and alkalis.

SiO_2 Layer: The addition of a SiO_2 layer serves to enhance the chemical resistance of the material, particularly against alkalis and the majority of acids, with the exception of hydrofluoric acid (HF), which is capable of dissolving SiO_2. [44]

Overall Chemical Resistance: High, except in the presence of HF.

Quartz Glass:

Quartz Glass: The level is elevated, with the exception of instances where HF is present.

Overall Chemical Resistance: Very high.

Geometric Characteristics

The geometric properties of the substrate exert a considerable influence on the sensor's performance, particularly in the determination of capacitance and sensitivity. However, as no precise measurements were provided, the typical properties of these materials as substrates were considered.

Monocrystalline Silicon (with SiO_2 layer):

Thickness: The typical range is between a few micrometres and several hundred micrometres, depending on the intended application.

Surface Roughness: It can be regulated at the nanometre level, which is crucial for applications that require high precision.

Overall Geometric Characteristics: The product is highly customisable and can be double-sided polished for enhanced performance. [29]

Quartz Glass:

Thickness: It can be comparable to silicon, which is frequently utilised in thin-film applications.

Surface Roughness: Furthermore, it can be regulated at the nanometre level.

Overall Geometric Characteristics: The processing of quartz glass is generally more challenging, yet it offers high precision and stability. [34]

Comparative Analysis and Recommendations

The dielectric constant, thermal resistance, and chemical resistance of quartz glass have been demonstrated to exceed those of monocrystalline silicon with a surface SiO_2 layer when employed as substrates for interdigital electrodes in biomedical capacitive sensors.

Dielectric Constant: The dielectric constant of quartz glass (3.8) is slightly lower than that of the SiO_2 layer on silicon (3.9), which results in quartz glass exhibiting superior impedance capacitance reduction properties.

Thermal Resistance: Quartz glass is capable of withstanding elevated temperatures and exhibits reduced thermal expansion, thereby conferring enhanced stability under thermal stress.

Chemical Resistance: Quartz glass exhibits enhanced chemical resistance, particularly against a more diverse array of chemicals, including resistance to etching by the majority of acids.

Table 5.4.1: Comparison of Properties: Monocrystalline Silicon (P-type, with surface SiO2) vs. Quartz Glass [43] [45] [44] [29] [46]

Property	Monocrystalline Silicon (P-type, with surface SiO2)	Quartz Glass
Dielectric Constant	Si: 11.7, SiO2 layer: 3.9	3.8
Thermal Resistance	High (Si: up to 1,500 °C, SiO2: up to 1,100 °C)	Very High (1,670 °C)
Chemical Resistance	High, except for HF	Very High, except for HF
Geometric Characteristics	Highly customizable, can be double-side polished	High precision, stable

Quartz glass is the optimal substrate for interdigital electrodes in biological capacitive sensors due to its lower dielectric constant, superior temperature resistance, and enhanced chemical resistance. Nevertheless, monocrystalline silicon with a SiO2 layer remains a formidable competitor, particularly when integration with other silicon-based devices necessitates specific silicon characteristics.

The accompanying table presents a comprehensive comparison of the geometric properties of quartz glass and monocrystalline silicon (with surface SiO2) as substrates for interdigital electrodes in biomedical capacitive sensors. The table encompasses a multitude of attributes, including thickness, dimensional stability, surface roughness, and machinability.

Table 5.4.2: Geometric Characteristics of Monocrystalline Silicon (P-type, with surface SiO2) vs. Quartz Glass [43] [45] [44] [29] [46]

Characteristic	Monocrystalline Silicon (P-type, with surface SiO2)	Quartz Glass
Thickness Range	Typically 200-500 µm (can be thinner or thicker depending on application)	Typically 100-500 µm (can be customized)
Surface Roughness	Ultra-smooth, typically ≤ 1 nm RMS after polishing	Ultra-smooth, typically ≤ 1-2 nm RMS
Dimensional Stability	Excellent; minimal warping or deformation	Exceptional; highly stable under thermal and mechanical stress
Thermal Expansion Coefficient	Low (2.6 x 10^{-6} /K for Si; SiO2 surface layer further stabilizes it)	Very Low (0.5 x 10^{-6} /K)

Continued on next page

Table 5.4.2 – continued from previous page

Characteristic	Monocrystalline Silicon (P-type, with surface SiO2)	Quartz Glass
Flatness	Can achieve ≤ 2 µm over a 200 mm wafer, high precision	Typically ≤ 3 µm over similar dimensions
Edge Quality	Can be precisely controlled, with beveled edges for better mechanical strength	Excellent edge quality, but more brittle and susceptible to chipping during processing
Mechanical Strength	High (due to the crystalline structure), but susceptible to micro-cracking	Moderate; lower mechanical strength compared to silicon, but highly stable and resistant to thermal shock
Machinability	High; can be easily etched or cut with precision tools	Moderate; more difficult to machine due to brittleness, requires specialized techniques
Double-Sided Polishing	Available; reduces surface roughness and improves performance in high-precision applications	Available, but more challenging due to material hardness
Patterning Precision	High precision; suitable for sub-micron patterning	High precision; suitable for micro- and nano-scale patterning but harder to achieve due to material hardness
Transparency	Opaque in the visible spectrum, transparent in infrared (SiO2 layer is transparent in UV-Visible)	Transparent across a wide spectrum (UV-Visible-Infrared (IR)), useful for optical applications

Analysis of the table 5.4.2

Thickness Range: The thickness of the two substrates can be varied to suit the intended application. In general, monocrystalline silicon is thicker, which is beneficial for mechanical stability. In contrast, quartz glass is available in thinner sheets, which could be advantageous for certain biological applications that require a thin substrate. [29] [46]

Surface Roughness: The production of ultra-smooth surfaces, which are essential for high-precision

sensor applications, is achievable with both materials. Nevertheless, silicon is typically capable of attaining a slightly higher degree of smoothness due to the utilisation of more sophisticated polishing techniques. [29] [46]

Dimensional Stability: Quartz glass is distinguished by a remarkably low thermal expansion coefficient, which endows it with exceptional dimensional stability, particularly when subjected to elevated temperatures. Similarly, silicon displays remarkable stability, although it is somewhat more susceptible to temperature-related influences. [29] [46]

Thermal Expansion Coefficient: Quartz glass exhibits a markedly lower thermal expansion coefficient than other materials, rendering it less susceptible to expansion or contraction in response to temperature fluctuations. This property contributes to enhanced dimensional stability. [43] [45]

Flatness: While both materials are capable of achieving high levels of flatness, silicon wafers tend to exhibit greater consistency due to the advanced production techniques employed in the semiconductor industry. [29] [46]

Edge Quality: Both materials are capable of producing high-quality edges, although the precision of control achievable with silicon edges is superior. Quartz glass may also achieve an acceptable level of edge quality; however, due to its brittle nature, it is more susceptible to chipping. [29] [46]

Mechanical Strength: Silicon is typically more robust and resilient to mechanical stress than quartz glass, which reduces the likelihood of fracturing during handling and manufacturing. [29] [46]

Machinability: The utilisation of precise tools facilitates the machining and etching of silicon, thereby enhancing its suitability for the creation of intricate patterns. The brittle nature of quartz glass restricts its machinability, necessitating the utilisation of specific processes. [29] [46]

Double-Sided Polishing: Both materials can be polished on both sides to reduce surface roughness; however, due to its high hardness, this procedure is more challenging with quartz glass. [29] [46]

Patterning Precision: Both substrates facilitate high-precision patterning; however, the compatibility of silicon with semiconductor processing methods enables the creation of more intricate sub-micron patterns. [29] [46]

Transparency: Quartz glass is a potentially useful material for applications requiring optical transparency due to its clear quality across a wide range of wavelengths. Although silicon is invisible to the human eye in the visible light spectrum, it may be employed in applications utilising infrared radiation. Furthermore, the SiO_2 layer enables the material to exhibit transparency across the ultraviolet to visible light spectrum. [43] [45]

In regard to geometric properties, monocrystalline silicon (SiO_2 surface) is the optimal choice for applications necessitating intricate patterning and structural integrity. This is due to its superior mechanical strength, enhanced machinability, and slightly improved surface flatness and smoothness. Nevertheless, quartz glass exhibits remarkable transparency and exceptional dimensional stability, particularly when exposed to elevated temperatures. For this reason, it is an appropriate selection for optical ap-

plications and situations with significant temperature fluctuations.
It is possible that biomedical capacitive sensors may be constructed from both types of material; the choice of material may depend on the particular needs of the intended use, such as the need for improved thermal stability or optical transparency.

Comprehensive Analysis of Interdigital Electrode Sensitivity and Geometry

It is of paramount importance to achieve high sensitivity in compact dimensions when designing interdigital electrodes (IDEs) for capacitive sensing, particularly in biomedical applications. The relationship between electrode geometry (width, length, and number of electrodes) and sensor performance (capacitance and sensitivity) is complex and involves a number of trade-offs. The objective of this investigation is to ascertain which of the three factors – electrode width, length, or number – has the greatest influence on capacitance and sensitivity when integrated circuits are constructed. Furthermore, the objective is to predict the outcomes of modifying these parameters while maintaining the overall dimensions of the sensor.

Theoretical Background

Capacitance C of an interdigital capacitor is given by the general equation:

$$C = \epsilon_r \cdot \epsilon_0 \cdot \left(\frac{N \cdot L \cdot W}{d} \right)$$

Where:

ϵ_r is the relative permittivity (dielectric constant) of the substrate [46],

ϵ_0 is the permittivity of free space,

N is the number of electrode pairs [42],

L is the length of the electrodes (which contributes to the active surface area),

W is the width of the electrodes and

d is the distance between adjacent electrodes. [29]

The sensitivity S of the sensor is directly proportional to the capacitance and can be expressed as:

$$S \propto C$$

Given these relationships, we explore the impact of varying N, L, and W while maintaining the overall dimensions of the sensor constant.

Impact of Electrode Number N and Length L

Increase in the Number of Electrodes N: It is possible to enhance the sensitivity (S) of the sensor by increasing the number of electrode pairs (N), while maintaining the sensor's length (L) and width (W) at a constant level. This will result in an overall increase in capacitance (C). [48]

In order to maintain the overall dimensions of the sensor, it is necessary to reduce the width (W) of each electrode as a consequence of the addition of electrodes. Therefore, any increase in the number of electrodes must be weighed against the available space.

Increase in Electrode Length L: The active surface area of the electrodes increases in proportion to the length (L), which in turn increases the capacitance (C), sensitivity (S), and other related parameters. [47]

However, the sensor's dimensions impose a restriction on the total surface area that can be utilised for the electrodes. If the length L is increased while the total area remains constant, either the number of electrodes N or the electrode width W must be reduced. This may have unintended consequences.

Impact of Electrode Width W

Reduction of Electrode Width W: To keep the sensor's overall dimensions the same, a decrease in electrode width (W) must be made in conjunction with an increase in electrode number (N). The ability of each electrode to contribute to capacitance will decrease with a fall in W, potentially offsetting the sensitivity gain that results with an increase in N. As a result, although a decrease in W may result in a reduction in total capacitance, an increase in N increases capacitance; this creates a complicated connection that needs to be carefully balanced. [29]

Trade-offs and Final Outcome

It is extremely important to optimize the electrode shape in order to achieve a balance between these effects and maintain good sensitivity.

Electrode Number N: An increase in N enhances capacitance; however, if W is insufficient, the gain may be offset by a reduction in the individual electrode contribution.

Electrode Length L: An increase in L will typically enhance the capacitance of a circuit, provided that this is not achieved at the expense of a significant reduction in N. [47]

Electrode Width W: It is essential to exercise caution and implement effective strategies to prevent the diminishing returns that may result from an increase in N. [48]

The ultimate result will be contingent upon the particular application and the desired level of sensitivity. It is likely that the most favourable outcome will be achieved through the implementation of a balanced strategy, comprising a modest increase in N and L, coupled with a simultaneous reduction in W.

Practical Example with Bacteria Dimensions

In the context of biological applications, such as bacterial detection, it is of paramount importance to ensure that the electrode diameters (W) and distance (d) are aligned with the scale of the target analytes. For instance, in order to guarantee optimal contact and measurement sensitivity, electrode spacing and widths must be maintained within the same range, given that bacteria typically range in size from 1 to 2 μm. [46]

Equations and Relationships from Relevant Literature

A review of the relevant literature, with particular focus on the papers "Dielectric Sensing (Capacitive) on Cooking Oil's TPC Level" and "Frying Oil Evaluation by a Portable Sensor Based on Dielectric Constant Measurement," revealed the following formulas to be particularly relevant: [47] [48]

$$C = \frac{\epsilon_r \cdot \epsilon_0 \cdot N \cdot L}{d + W}$$

In this context, $d + W$ represents the spacing between electrodes and the influence of electrode width. [29]

Key Findings

From "Dielectric Sensing (capacitive) on cooking oil's TPC level": The findings of this study indicate that an increase in the number of electrodes results in enhanced sensitivity, provided that the electrode width is optimised to prevent a significant reduction in capacitance due to a decline in the contribution of each individual electrode. [47]

From "Frying Oil Evaluation by a Portable Sensor Based on Dielectric Constant Measurement": The findings of this investigation illustrate that the utilisation of longer electrodes markedly enhances capacitance, thereby underscoring the pivotal role of electrode length in the design of sensors. [48]

In conclusion, the number of electrodes (N), length (L), and width (W) of interdigital electrodes must be considered in a balanced manner during the design process. While an increase in N and L typically enhances sensitivity, it is essential to exercise caution to avoid a concomitant reduction in W, which could diminish the overall capacitance. The final result will depend on the specific application, but the objective should be to optimise all three variables in order to achieve the greatest sensitivity within the defined dimensional constraints. [46] [42] [29] [41]

In light of the aforementioned findings and extensive research, it can be concluded that the most appropriate interdigitated/interdigital electrodes to buy was those with 240 fingers with a 3 um gap between fingers. The substrate is monocrystalline silicon (Single crystal silicon (P type), surface Sio2), and the metal layers on top are Ti/Au (titanium and gold). The dimensions of the purchased sensors are 4mm*7mm*3um as shown in Figure 5.15. The optimal configuration is one with a greater number of

fingers and a minimal gap between them, utilising a more durable alloy. At the product information, it is claimed that these interdigitated/interdigital electrodes can withstand from -150 degrees celcius to 400-500 degrees celcius, but the company mentioned up to 350 degrees celcius for sure. Figure 5.16 illustrates the interdigitated sensor.

The above study was conducted exclusively for research purposes. Given that the experiments to be conducted in this case represent a single, unified project, there is no discernible distinction between the interdigitated/interdigital electrodes that were available for purchase; they are all of an equally high caliber and robust in design.

Figure 5.15: The dimensions of the interdigitated/interdigital electrode purchased

Figure 5.16: Real life dimensions and picture of the interdigitated electrode that will be used as a sensor for the bacterial capacitance measurement

The following link was instrumental in the preparation of this subsection. It offers a comprehensive database of chemical elements, allowing users to search for specific elements and retrieve detailed information, including literature citations:
`https://refractiveindex.info/`

5.5 Cleaning Process

Following the selection of appropriate sensors, it was determined that there is no risk of corrosion or damage from any chemical used for sterilisation and disinfection in microbiology laboratories, or following their placement in a disinfection furnace (operating at 180 °C to ensure effective disinfection without damaging the instruments).

In this instance, however, only basic room disinfectants will be employed, under the supervision of Dr. Varlamis G. Sotirios. The individual who has kindly relinquished their professional space to conduct these experiments and made significant personal and professional contributions in terms of knowledge and resources.
In particular, the surface of the sensor will be first wiped with a dry swab and then wiped again with a swab moistened in disinfectant solution, following the application of these disinfectant chemicals to the surface via spraying. Subsequently, prior to the deposition of the subsequent bacterial culture sample, a further wipe with a dry swab will be conducted.

5.6 Epilogue

A comprehensive analysis of the interdigitated/interdigital electrodes is presented in the fourth chapter's conclusion, emphasising their pivotal role as the primary sensing component of the electronic circuit. An understanding of the performance of the electrodes in the detection of bacterial samples is contingent upon an examination of the electrodes' design and material characteristics, as presented in this chapter. The findings presented in this chapter will inform the subsequent phases of the experiment, ensuring that the electrodes are configured as optimally as possible for reliable and precise bacterial identification. Furthermore, the chemical constituents of the electrode were elucidated, and the rationale behind the selection of the most appropriate one was presented. Additionally, the procedure for cleaning the electrodes following contact with the bacterial culture was outlined. The chapter reiterates the importance of selecting and constructing these components with precision, as they are fundamental to the success of the research project.

Chapter 6

Electronic Biosensor

6.1 Introduction

This chapter offers a comprehensive account of the design, construction, and programming of the completed electronic biosensor, accompanied by a synopsis of the research presented in preceding chapters. It is concerned with the methodology employed to integrate the interdigitated electrodes, capacitance-to-digital converter, and capacitance measuring circuit into a unified biosensor system. It discusses the technological challenges encountered throughout the process and the strategies employed to address them. Furthermore, it examines the programming of the biosensor, with a particular emphasis on the development of software algorithms for the interpretation of sensor data and the facilitation of bacterial identification. The research process reaches a pivotal point in this chapter, wherein the theoretical designs are transformed into a functional prototype. In short, it introduces the concept of the integrated circuit as a final product as well as its potential use as a high-precision biosensor for identifying bacteria.

6.2 Design, construction and programming

Design and Construction

The following section provides a detailed account of the circuit's construction, accompanied by photographic documentation.

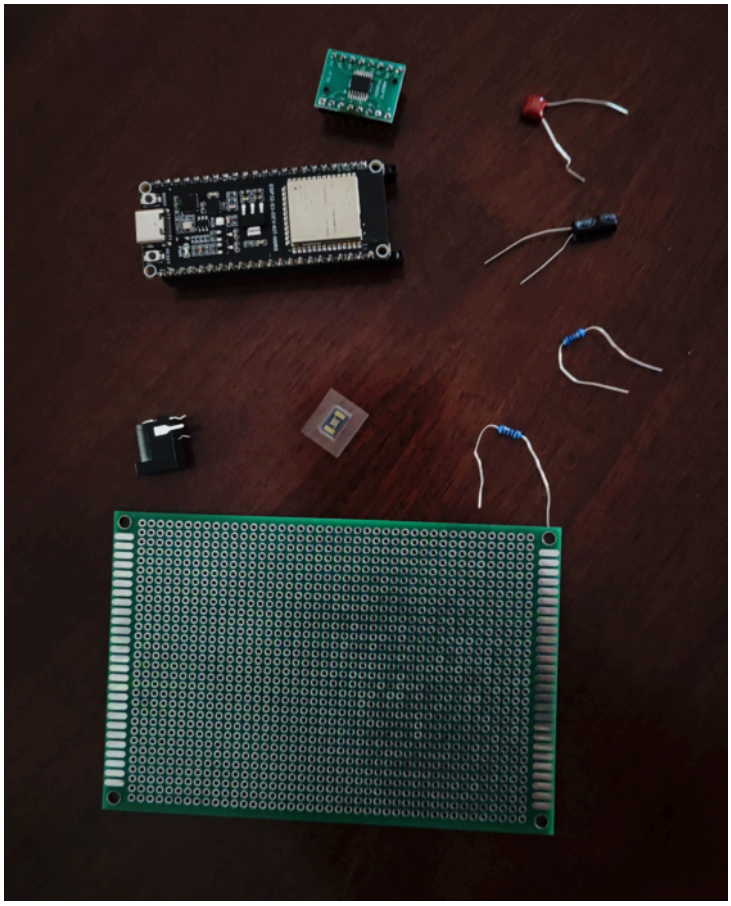

Figure 6.1: All the components of the circuit board

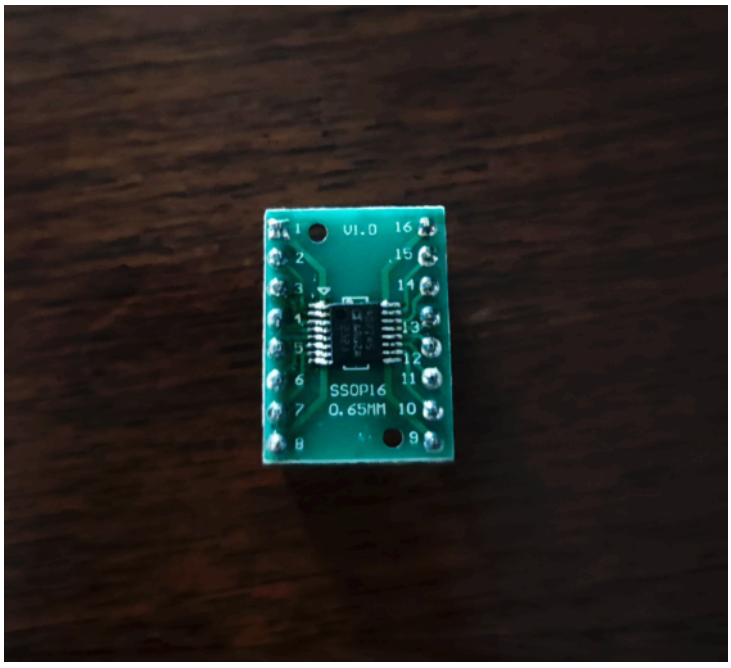

Figure 6.2: The integrated circuit AD7745 onto an SMD-to-DIP board, ready for the placement to the prefboard

Once the requisite materials had been procured, the AD7745 IC, being an Surface-Mount Device (SMD) component, was mounted on an SMD-to-DIP board (soldered with a hot air gun) for subsequent placement on the perfboard, as shown in Figure 6.2.

Secondly, the materials were placed on the perforated board to ascertain their optimal positions. The capacitors were situated in close proximity to one another and in close relation to the power supply, while the sensor was positioned at a sufficient distance from the other components to facilitate measurement (and subsequently cleaned from the bacterial culture sample using a flame and chemicals) without disrupting the surrounding elements.

Subsequently, the materials were affixed to the board with a soldering iron and reed, and the wiring was completed with jumper jumpers (typically used on a breadboard). The connection was established by creating pathways with the reed.

The sensor wiring was conducted using bare copper wire, which facilitates optimal current conduction without complications. Hot glue was employed as the medium for the sensor wiring. The glue was employed for the specific purpose of affixing the sensor to the prefboard and insulating the bare copper wire.

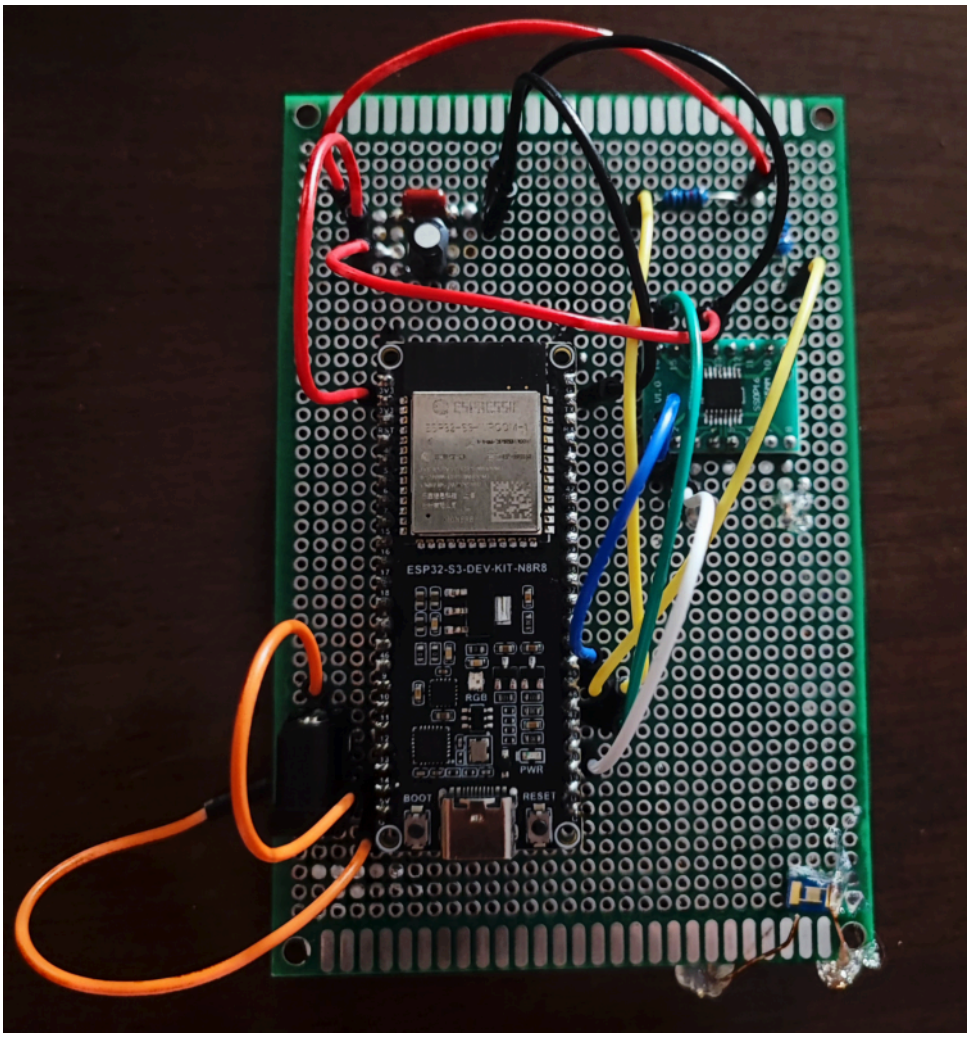

Figure 6.3: The first circuit design

As shown in figure 6.3, the orange wires are intended for the purpose of supplying power to the ESP32 via the power jack, with the expectation that this will be done from a 5V/3A power supply.
The red and black wires are intended for use with all other power supplies and grounds within the circuit, respectively.
The yellow wires pertain to the wiring of the pull-up resistors.
The green, blue and white wires are for the SDA, SCL and RDY, respectively, and are used for I2C BUS connectivity.

Table 6.2.1: Price List of the initial circuit

A/A	Component	Quantity	Price
1	Perforated Board	1	7€
2	ESP32-S3	1	5€
3	Power Supply 5V 3A	1	4€
4	Dc Power Jack	1	0.2€
5	AD7745ARUZ ADC	1	13€
6	Resistor 10k	2	0.2€
7	Capacitor 100nF	1	0.2€
8	Capacitor 10uF	1	0.2€
9	Interdigitated Electrode	1	25€
10	Female Pin Headers 40 pin	2	1€
11	SMD to DIP Adapter	1	3€
12	Hot Glue	1	0.5€
13	Hot Glue Gun	1	15€
14	Soldering Iron Pen	1	15€
15	Solder/Kalay	1	11€
16	Male-to-Male Pin Headers	2	0.5€
X	**Summarize**	**Total**	100.8€

However, the original circuit was found to be inoperable due to a malfunctioning power supply, which was determined to be the result of a faulty microcontroller. Consequently, an alternative design was devised, employing a slightly altered methodology and greater attention to detail.

Initially, an ESP32-WROOM-32, produced by ESPRESSIF, was employed. Subsequently, the capacitors and resistors were replaced with SMD, which are situated at the base of the circuit board, and one additional component was incorporated into the power supply circuit.

Two capacitors were incorporated into the 5V power supply: a 100uF capacitor and a 470nF multilayer capacitor. A 10 μF capacitor was connected in parallel with a 100 nF multilayer capacitor at the 3.3 V

output, as illustrated in the original schematic. Finally, a 100nF multilayer capacitor was installed in the AD7745 integrated circuit.
Multilayer capacitors are a specific type of decoupling capacitor that are situated in close proximity to the peripheral supplies on each component and are typically identified by their yellow colour. Additionally, these components possess a low Equivalent Series Resistance (ESR), enabling them to facilitate high current delivery and mitigate peak fluctuations in peripheral operations.

Additionally, 10k resistors were positioned on the bottom side to the SDA and SCL respectively, in order for the I2C protocol to initialize properly. Despite their relatively high value, the proximity of the bus spacing renders this inconsequential.

As the sensor cable (copper wire) is enameled (i.e. coated with a varnish on the outside), the edges were abraded slightly at the point of contact with the sensor in order to facilitate a more optimal electrical connection. This is due to the fact that the wire is composed of a coil and an insulating material, which necessitates the removal of the latter in order to facilitate the flow of current.
On the reverse of the board, the copper wire was insulated with an electrical insulator in lieu of the previous use of hot glue.
The interdigitated/interdigital electrode, which serves as a sensor, was affixed with hot glue.

Programming

The following section presents the microcontroller's programming, which ensures the circuit's optimal functionality. The complete code is provided in Appendix D, with a detailed explanation of each command.
In order to ensure the correct programming of the code to be inserted in the ESP32 microcontroller and its subsequent execution in accordance with the desired operation and result of the experiment, the following datasheets and associated documentation were studied and utilised: [49], [50], [51] and [52].
In the absence of an explicit command within the code specifying the desired measurement interval, the measurements are taken at the maximum sampling rate supported by the AD7745. In accordance with the specifications outlined in the datasheet, the measurements obtained and displayed by the sensor are taken at AD7745's default fastest measurement speed, which is **11 ms per conversion (around 90.9 measurements per second, which equates to around 90.9 Hz)**. Consequently, the values received by the sensor are displayed at **11 ms** intervals continuously until the program is terminated. [19]
The baud rate at Arduino IDE platform is set at 115200 as the optimum rate for the specific measurements.

Figure 6.4: The microcontroller ESP32-S3-DEV-KIT-WROOM-1-N8R8 that will be programmed for the proper operation of the circuit

6.2.1 Final Result

The final circuit, as illustrated in the accompanying Figure, has been constructed using the specified materials and exhibits no signs of deterioration. The connections are intact and free from short circuits, and the power supplies have been evaluated and deemed satisfactory. Overall, the final hardware is of an excellent standard. The Power Jack has been installed with the intention of facilitating the future integration of an LCD monitor, thereby enhancing portability and wireless functionality.

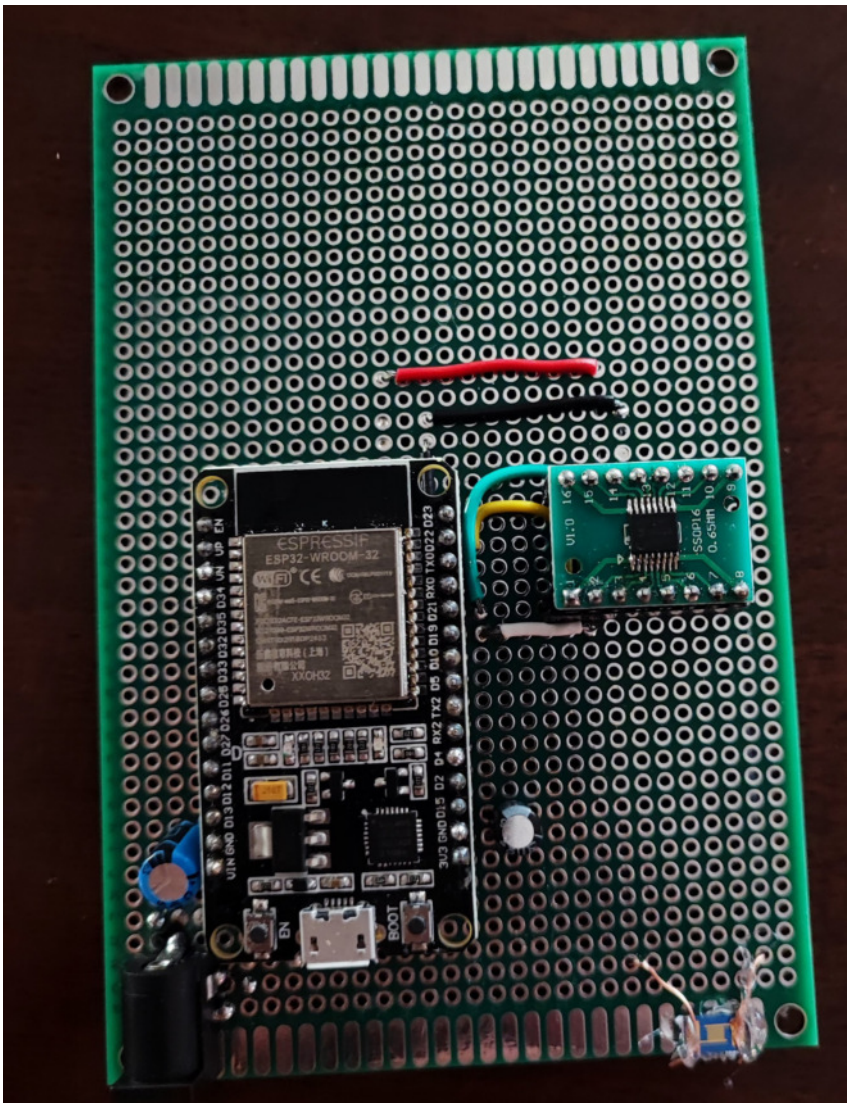

Figure 6.5: The final circuit, ready to take low value measurements with high accuracy

Figure 6.6 depicts the reverse of the circuit board, as well as the 100nF capacitors, which are coloured brown.

Lastly, Figure 6.8 shows the 2 circuits in comparison side by side.

Ultimately, Figure 6.7 illustrates the supplementary capacitors from the original schematic, situated within the 5V supply.

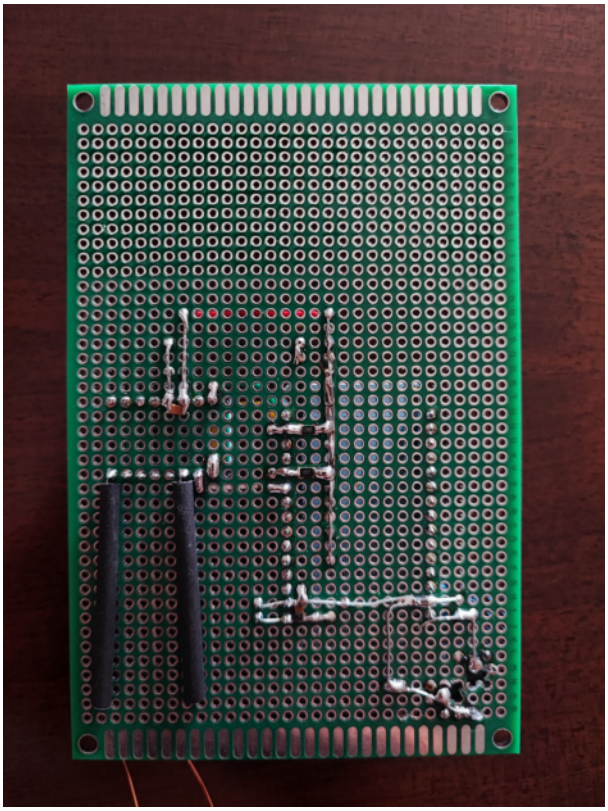

Figure 6.6: The black components are 10k SMD resistors, while the brown components are SMD multilayer capacitors

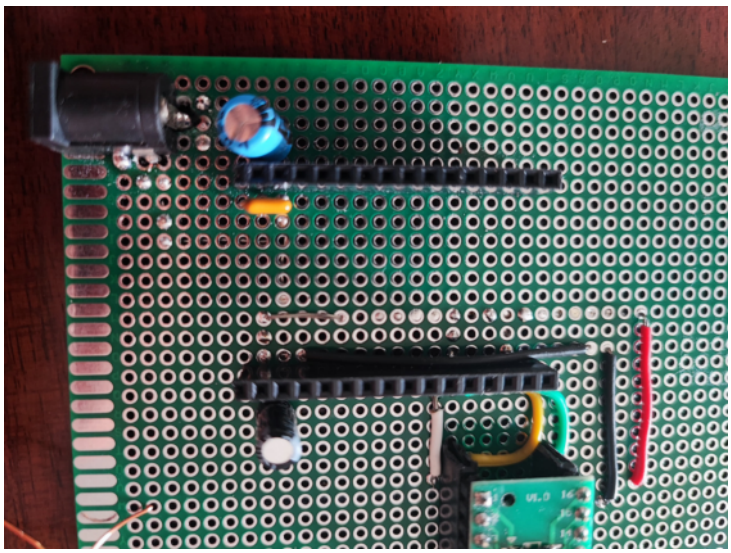

Figure 6.7: The supplementary capacitors incorporated into the 5V power supply, the yellow one is multilayer (though THT)

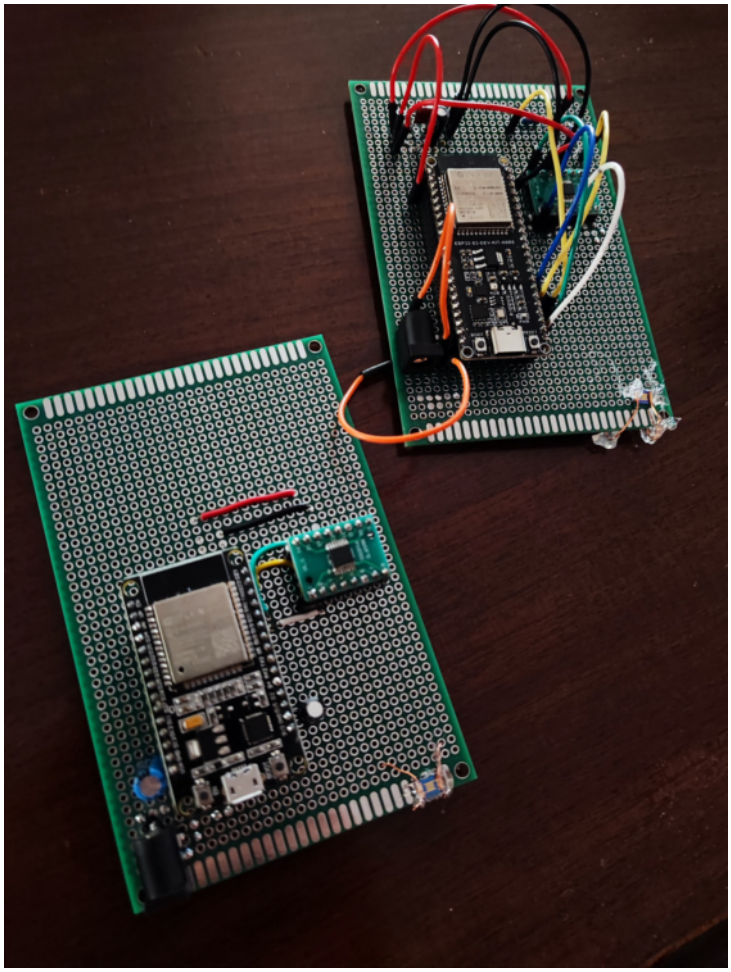

Figure 6.8: The 2 circuits together in comparison

Table 6.2.2: Price List of the final circuit

A/A	Component	Quantity	Price
1	Perforated Board	1	7€
2	ESP32-WROOM-32	1	16€
3	Dc Power Jack	1	0.2€
4	AD7745ARUZ ADC	1	13€
5	Resistor 10k	2	0.2€
6	Capacitor 10uF	1	0.2€
7	Capacitor 100uF	1	0.1€
8	SMD Multilayer Capacitor 470nF	1	0.05€
9	SMD Multilayer Capacitor 100nF	2	0.1€
10	Interdigitated Electrode	1	25€
11	Female Pin Headers 40 pin	2	1€
12	SMD-to-DIP Adapter	1	3€
13	Hot Glue	1	0.5€
14	Hot Glue Gun	1	15€
15	Soldering Iron Pen	1	15€
16	Solder/Kalay	1	11€
17	Male-to-Male Pin Headers	2	0.5€
X	**Total**	**Total**	**107.85€**

6.3 Epilogue

The successful construction of the electronic biosensor represents a significant milestone in the research endeavour, marking the conclusion of the fifth chapter. The chapter provides details on the planning and construction phases, offering valuable insights into the practical challenges inherent in the development of a biosensor system. The completed biosensor is the culmination of the technical work conducted as part of the research project and is now ready for testing in an experimental setting. The chapter also provides an overview of how the innovative use of electrical circuits in the biosensor may revolutionise the process of identifying bacteria, and establishes the framework for the subsequent performance evaluation.

Chapter 7

Comparative Study

7.1 Introduction

This chapter presents a comprehensive analysis of the evaluated circuits and sensors, conducted in both theoretical and in vitro environments. Moreover, is offers an assessment of the performance of each circuit, with a particular emphasis on key parameters such as sensitivity, precision, and dependability. Furthermore, the potential for utilization of these circuits within a laboratory setting is investigated, considering factors such as cost-effectiveness, user-friendliness and compatibility with existing microbiological protocols. The objective of this chapter is to ascertain the optimal methodology for bacterial identification by conducting a systematic comparison of the evaluated circuits and sensors. The findings of the comparative study will be instrumental in optimizing the biosensor's final design and ensuring its suitability for real-world applications.

7.2 Theoretical Study

As will be demonstrated in the following sections, the electronic interface based on the principle of double measurement [16] was found to exhibit insufficient linearity, while the current sense amplifier [17], despite its impeccable design, was determined to be more expensive than the one constructed with the AD7745. Accordingly, the final study as well as the experiments in the microbiology laboratory were conducted using the latter (CDC utilizing the integrated circuit AD7745).

7.2.1 Circuit Comparison

In laboratory experiments conducted in the laboratories of the Electronics Department of the School of Information and Electronic Engineering of the International Hellenic University, it was determined that the circuit of Preethichandra. D.M.G. and Shida. K. exhibited no linearity, rendering it unsuitable for research purposes. Figures 7.1, 7.2, 7.3 and 7.4 illustrate the methodology employed in the study. [16]

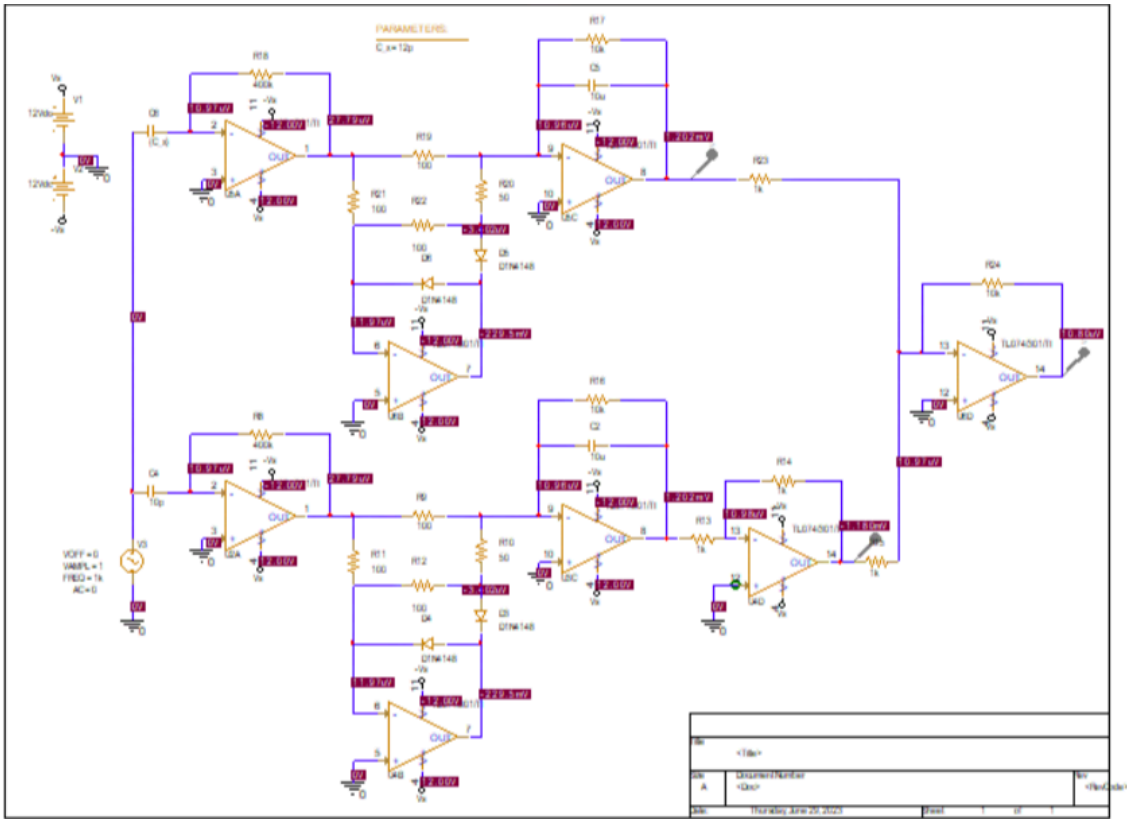

Figure 7.1: Schematic in PSpice software [1]

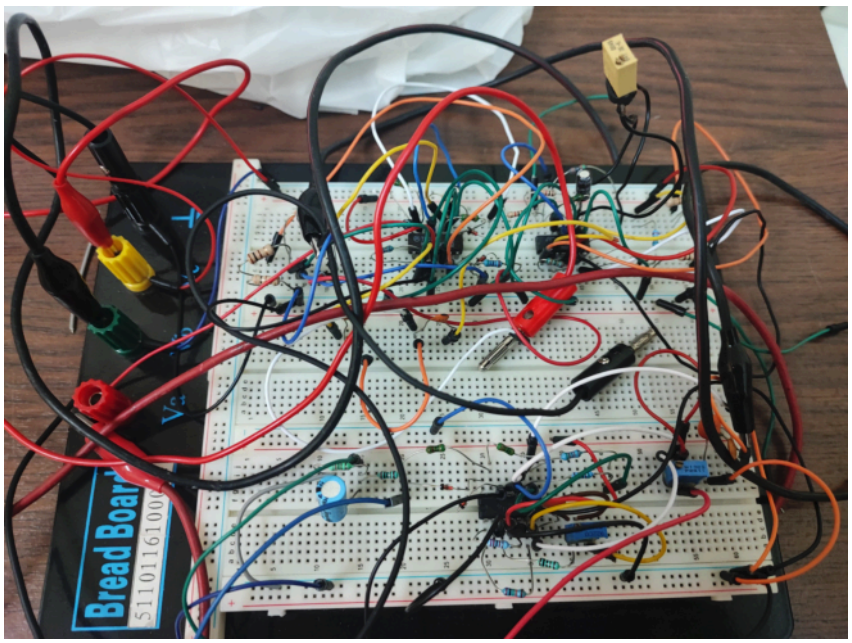

Figure 7.2: Constructed circuit on a breadboard

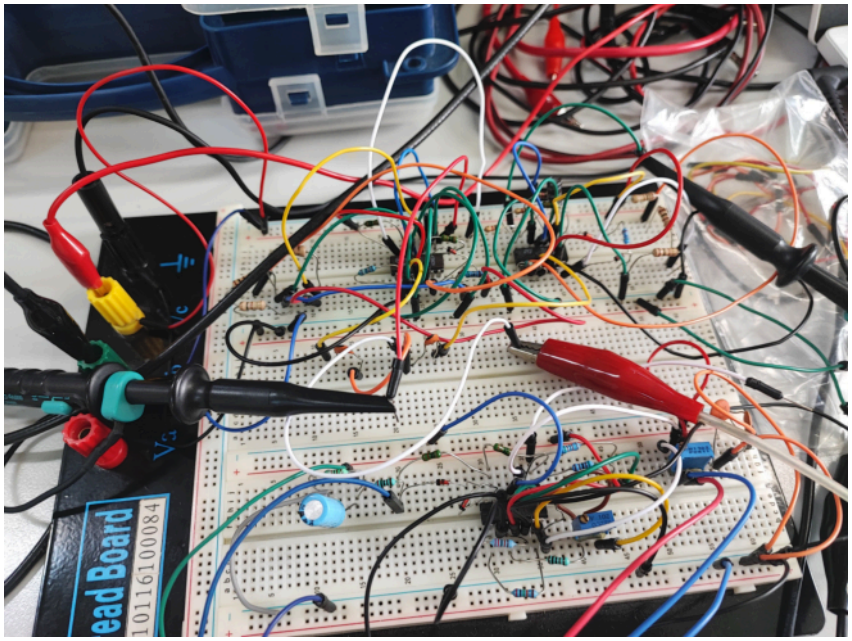

Figure 7.3: Circuit ready for measurements

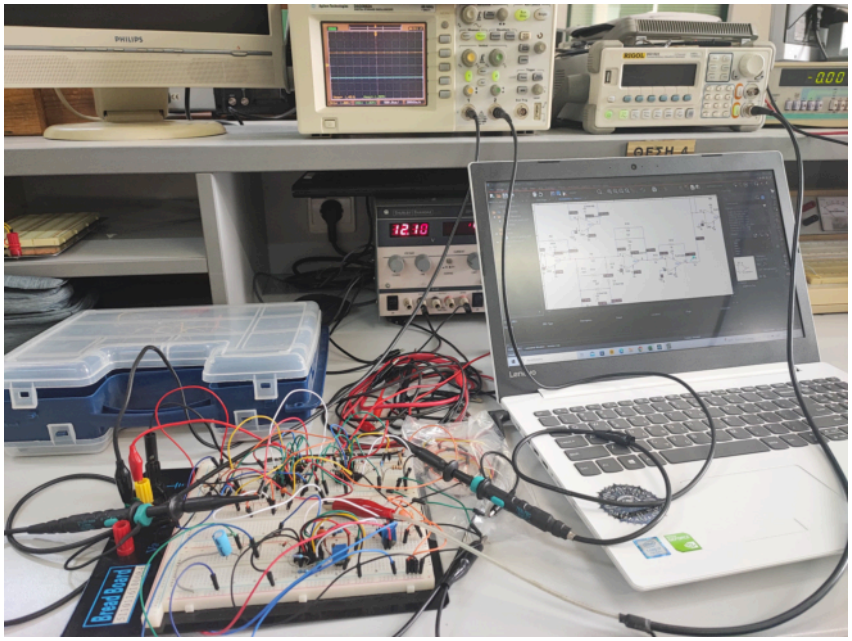

Figure 7.4: Taking measurements on real time

Concerning the circuit designed by Ramanathan. Prabhu et al., while an optimal circuit was identified, it was noted that, in comparison to the one devised by the author, it is more expensive to construct. Consequently, it was also rejected. [17]

Accordingly, the circuit designed by the author of the capacitance to digital converter with IC AD7745 is deemed more suitable, as it is compact and less costly compared to the others. It will be employed for the final bacterial measurements of the research in the microbiological laboratory of the researcher's scientific collaborator, Dr. Varlamis G. Sotirios.

7.3 In Vitro Study

A scientific study conducted in a controlled laboratory setting, such as a Petri dish, test tube, or culture flask, is referred to as an "in vitro" study. The Latin term "in vitro" is derived from the phrase "in glass," which reflects the conventional use of glassware in these investigations. These investigations constitute an indispensable component of biological and medical research, representing the initial phase of more comprehensive "in vivo" (within the living) examinations. A comprehensive account of in vitro studies, encompassing their applications, advantages, and limitations, is presented below. [53]

Key Characteristics of In Vitro Studies

Controlled Environment: In vitro research is conducted in a controlled laboratory setting, with precise regulation of key parameters such as pH, temperature, and nutritional availability. This obviates the necessity for additional elements present in an entire organism to impede the isolation and examination of specific biological processes or responses by researchers. [53]

Use of Biological Materials: The study of biological materials, including cells, tissues, proteins, enzymes, and DNA, which have been isolated from an organism, is a common practice in this field of research. In order to ensure the continued functionality and viability of these materials, they are stored in environments that closely resemble their native habitat. [53]

Focus on Mechanisms: In vitro experiments are a common means of investigating the fundamental principles of biological processes. For example, scientists may investigate the impact of a medication on a specific cell type, the interactions between proteins, or the conditions surrounding gene expression. [53]

Applications of In Vitro Studies

Drug Development: In vitro investigations constitute an indispensable component of the preliminary stages of drug development. Before embarking upon animal or human trials, researchers may ascertain how a medication interacts with cells or tissues, evaluate its efficacy, and identify any potential toxicity. [54]

Genetic Research: In vitro methods are employed by scientists to investigate the regulation and function of genes. This may entail the utilization of CRISPR technology for the precise editing of genes or the modification of genes within cells, with subsequent observation of the resulting consequences. [54]

Toxicology: Toxicology relies heavily on in vitro models because they make it easier to evaluate the possible negative consequences of a wide range of substances, such as chemicals, medicines, and cosmetics. These tests could provide some first information on the possible effects of chemicals on human health. [54]

Research on Cancer: In vitro studies are employed by researchers to gain further insight into the

biology of cancer cells, to investigate how cancer cells respond to different treatments, and to accelerate the development of personalized therapies. [54]

Research on Stem Cells: Research into stem cell differentiation and potential therapeutic applications is conducted in vitro.

Advantages of In Vitro Studies

Ethical Considerations: One potential advantage of in vitro studies is that they may reduce the necessity for animal experimentation, which is frequently a significant ethical concern in research. The utilization of cells and tissues in controlled conditions enables researchers to eliminate or postpone the use of live animals. [55]

Cost-Effectiveness: As these investigations are often completed in a shorter timeframe and require fewer resources than in vivo research, they are typically less expensive. [55]

High Control and Reproducibility: A significant advantage of in vitro research is the high degree of control and reproducibility it enables. The controlled circumstances of in vitro experiments facilitate higher repeatability of results and greater accuracy in experimental design. [55]

Rapid Data Collection: In vitro studies frequently employ more straightforward systems than whole organisms, facilitating data collection and enabling expedited experimental iterations. [55]

Limitations of In Vitro Studies

Lack of Complexity: The lack of complexity in comparison to a living organism represents a significant limitation. The inability to accurately reproduce the interactions and conditions observed in a living organism in vitro may limit the generalizability of the findings. [55]

Progression to In Vivo: It is not always feasible to extrapolate research findings from in vitro experiments to in vivo settings. For instance, discrepancies in immunological responses, metabolic processes, and other variables may result in a pharmacological agent that exhibits efficacy in vitro failing to elicit the same outcome in a human organism. [55]

Artificial Conditions: On occasion, the artificial environment of the in vitro culture produces results that are not wholly representative of what would occur in the natural world. When cells are separated from their natural tissue environment, they may display behaviors that differ from those typically observed in vivo. [55]

Limited Scope: In vitro studies frequently concentrate on specific aspects of a biological process, which may restrict their generalisability. In most cases, a comprehensive understanding can only be achieved through further in vitro research conducted with other animals or in different settings. [55]

Conclusion

In vitro investigations represent a pivotal instrument in the realms of biological and medical research. They offer a secure, ethically sound, and cost-effective avenue for exploring a vast array of scientific inquiries. Nevertheless, due to their intrinsic limitations, they cannot wholly supplant in vivo research, despite the insights they offer and their indispensable role in preliminary testing and hypothesis formation. The results of in vitro research frequently require validation in more intricate biological systems before they can be properly comprehended and used in practical settings. [53]

In this case, the In Vitro study will be the experiments on bacterial cultures with the final device as an electronic biosensor, at the microbiological laboratory, of the researcher's scientific collaborator, Dr. Varlamis G. Sotirios.

7.3.1 Bacterial Capacitance

This subsection presents the photographic documentation of the experimental procedures conducted in the microbiology laboratory, along with the outcome of the research project on bacteria.
Concerning the sample of each bacterial culture to be applied to the sensor (interdigitated/interdigital electrode), the quantity will be identical for all cultures, as the measurement results must be based on the same reference.

Furthermore, a comprehensive table containing all the obtained values is provided. The table is divided into three sections, one for each of the three cultures of Gram-positive bacteria, one for each of the three cultures of Gram-negative bacteria and one for the fungus. Within each section, the data is presented for each type of bacteria separately.

The microorganism (bacteria and fungus) in question are *Escherichia coli* (Gram Negative), *Proteus mirabilis* (Gram Negative), *Pseudomonas aeruginosa* (Gram Negative), *Staphylococcus aureus* (Gram Positive), *Streptococcus viridans* (Gram Positive), *Enterococcus faecium* (Gram Positive) and *Candida albicans* (fungus).

Subsequently, the data from the table is imported into MATLAB, where graphs are generated to illustrate the range of variation in capacity values for each bacterial culture sample separately.

Measurement procedure:

To ensure consistency and accuracy, each bacterial culture sample will be measured identically, ensuring that all measurements are comparable. Each sample placed on the sensor is 10uL.

The quantity of bacteria will thus remain constant and distributed uniformly across the entire surface of the sensor. The sensor's dense finger structure enables measurement at a close distance to the surface. Consequently, in the event of a substantial bacterial accumulation on the surface, the resulting measurements are deemed to be free from any potential inaccuracies.

The subsequent section presents a series of visual representations, comprising photographs, tables and

graphs, which illustrate the measurement outcomes.

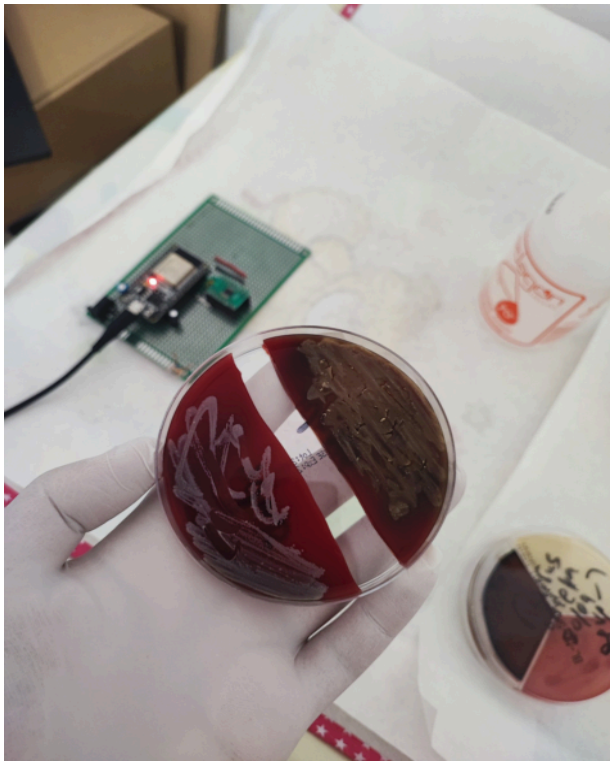

Figure 7.5: Cultures of *Streptococcus viridans* and *Staphylococcus aureus*

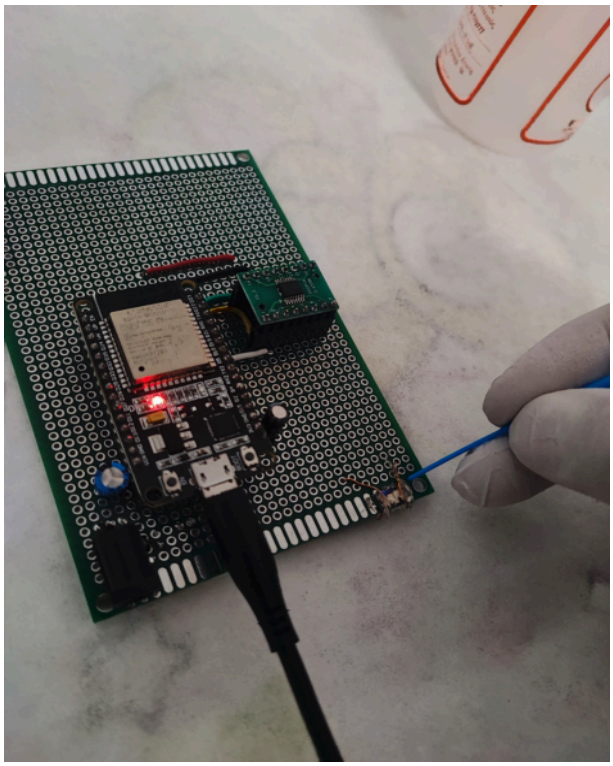

Figure 7.6: Applying the fungus (*Candida albicans*) onto the sensor

Figure 7.7: Taking measurements in real-time in the microbiological laboratory

Table 7.3.1: Capacitance values of various bacteria, fungus, and air samples in pF from the measurements taken in the laboratory

	Bacteria						**Fungus**	**Air**
	Gram Positive			**Gram Negative**				
	Staphylococcus aureus	*Streptococcus viridans*	*Enterococcus faecium*	*Escherichia coli*	*Proteus mirabilis*	*Pseudomonas aeruginosa*		
Capacitance(pF)	3.84	1.38	1.5	0.63	0.96	1.08	2.67	0.44

7.4 MATLAB

7.4.1 Code

The code written in the MATLAB environment that generated the graphs presented in this study is provided in Appendix E for reference.

7.4.2 Graphs

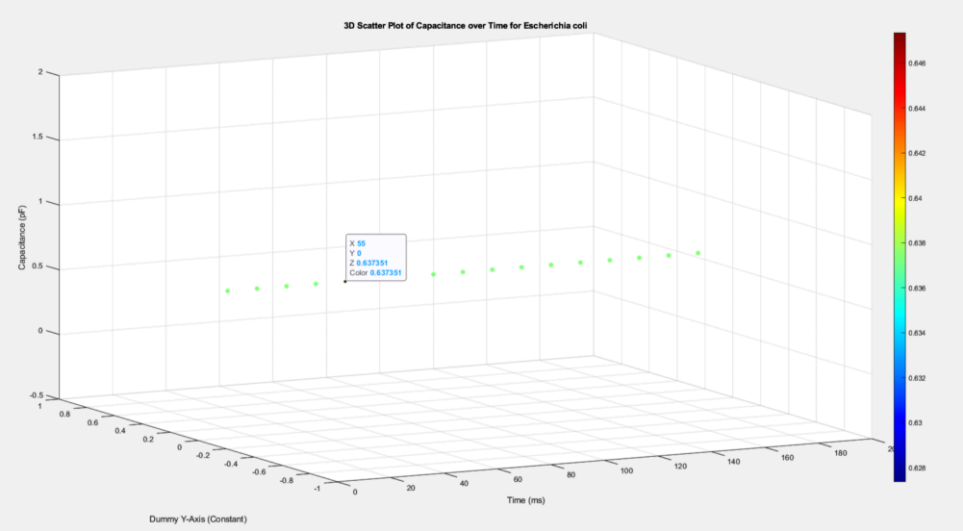

Figure 7.8: *Escherichia Coli* Plot

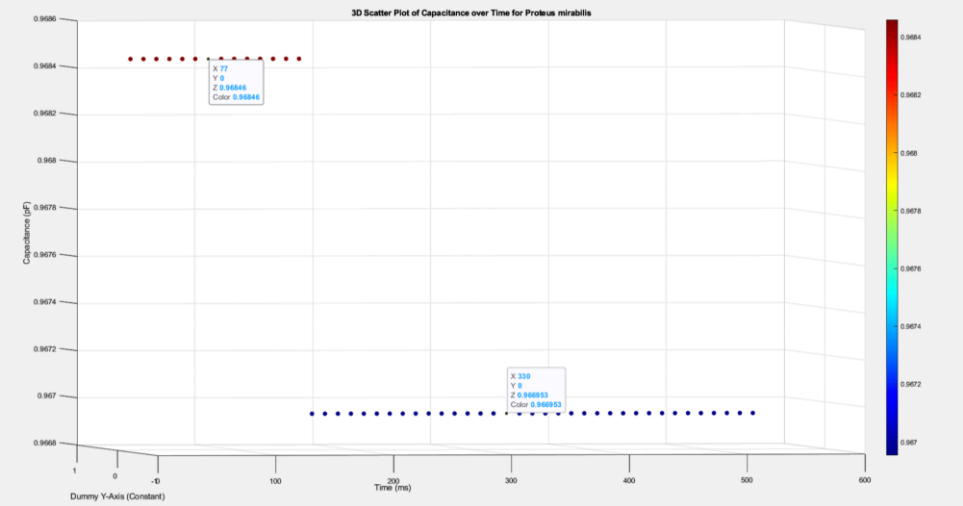

Figure 7.9: *Proteus mirabilis* Plot

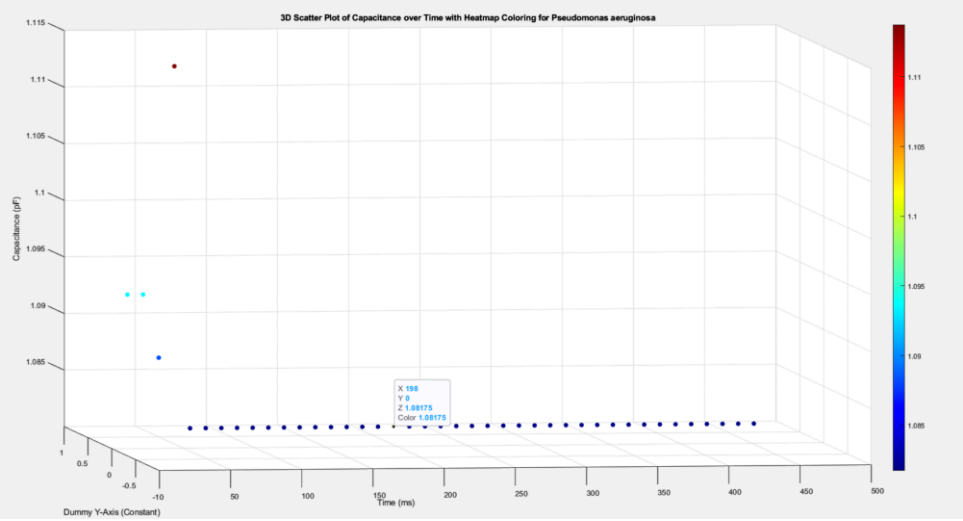

Figure 7.10: *Pseudomonas aeruginosa* Plot

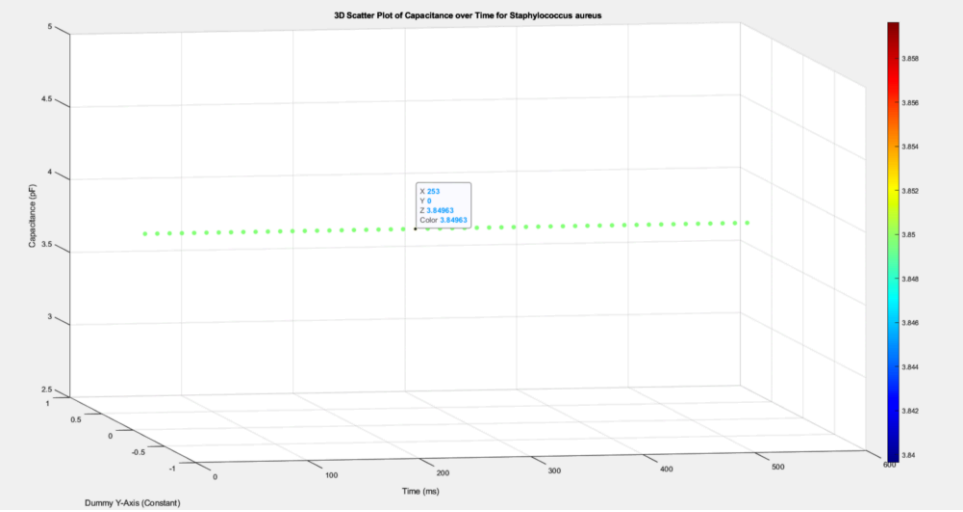

Figure 7.11: *Staphylococcus aureus* Plot

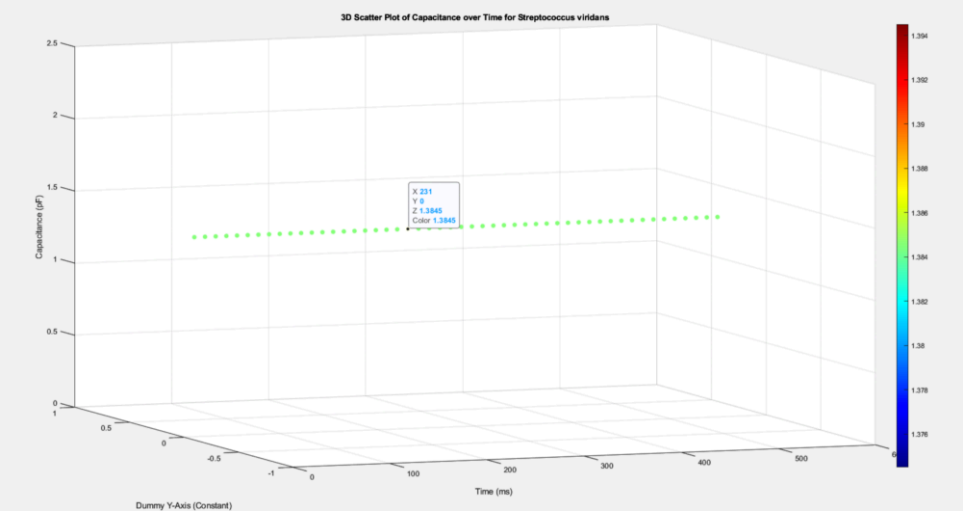

Figure 7.12: *Streptococcus viridans* Plot

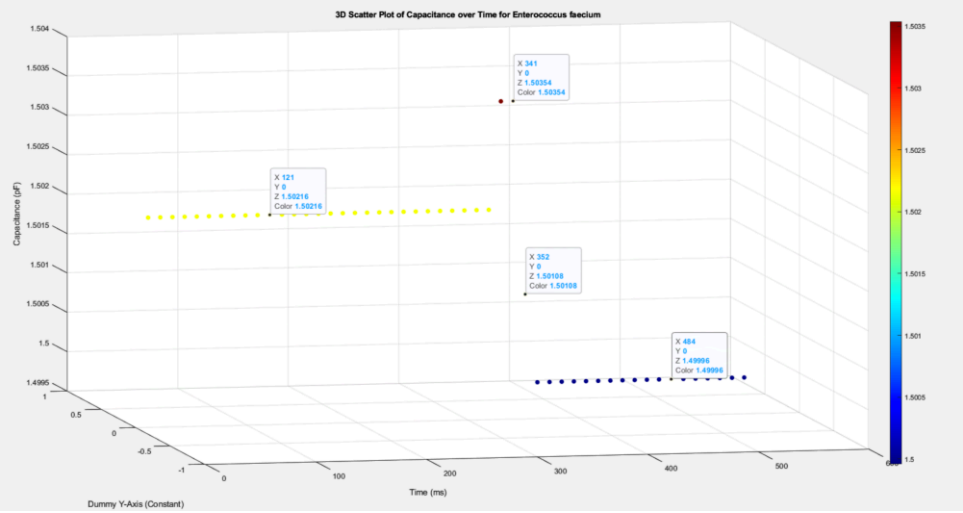

Figure 7.13: *Enterococcus faecium* Plot

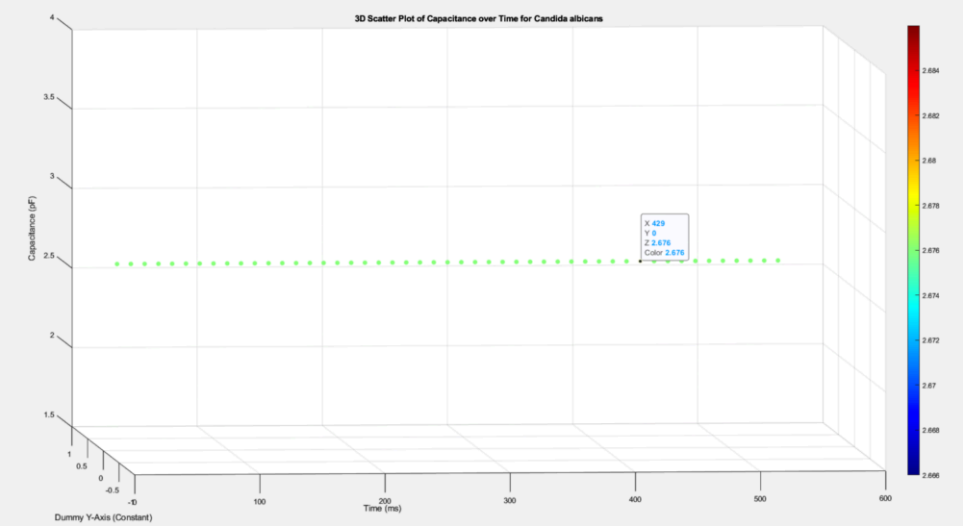

Figure 7.14: *Candida albicans* Plot

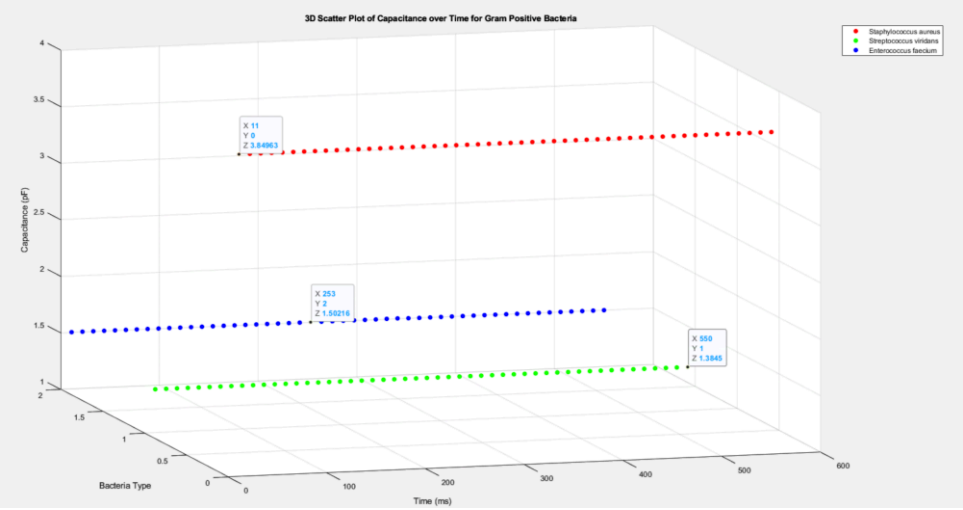

Figure 7.15: Plot of Gram Positive Bacteria

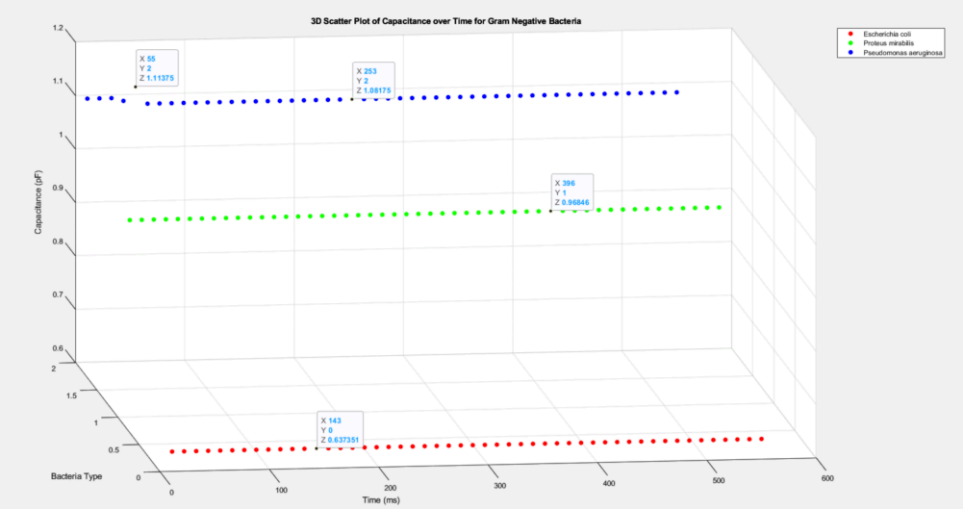

Figure 7.16: Plot of Gram Negative Bacteria

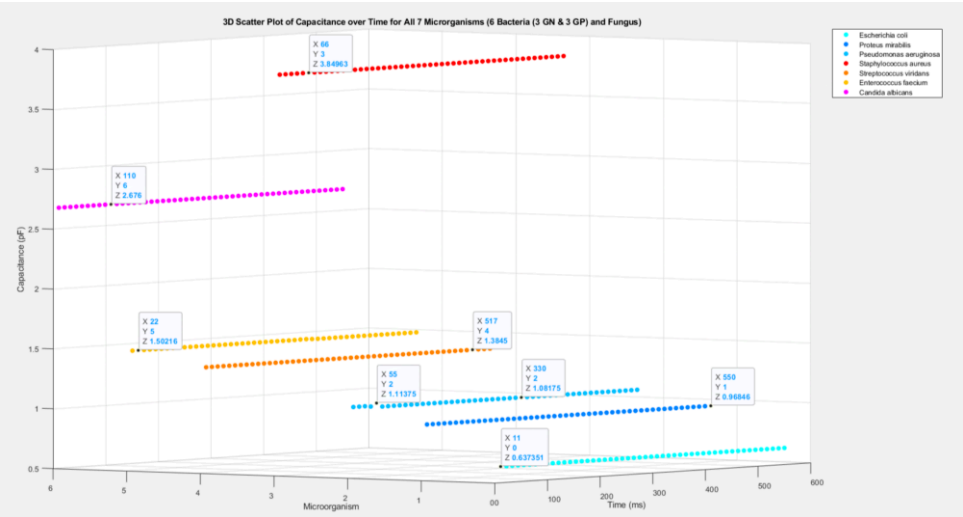

Figure 7.17: Plot of every microorganism together for comparison

It can be observed that the six bacteria exhibit disparate capacity values.

However, the three Gram-positive bacteria display a narrower range of values (except *Staphylococcus aureus*), while the three Gram-negative bacteria exhibit a broader range of values, albeit still within proximity.

The range of the Gram positives and Gram negatives differs significantly, indicating that the Gram-positive bacteria possess distinct electrical properties (including different capacitance values) compared to the Gram-negative bacteria. This approach thus provides an answer to the initial question of bacterial identification, as outlined at the outset of this paper.

7.5 Epilogue

The sixth chapter presents a comprehensive examination of the comparative research, accompanied by a data-driven rationale for the final circuit and sensor configuration. The subsequent stages of the study project will be informed by the findings presented in the chapter, which are pivotal in guaranteeing that the selected system can meet the rigorous demands of bacterial identification in both clinical and laboratory settings. So as to establish rigorous expectations for the performance of the selected biosensor configuration in subsequent tests, the chapter emphasizes the necessity for comprehensive testing and assessment in the development of cutting-edge technologies.

Chapter 8

Conclusions

8.1 Introduction

The findings of the research are synthesized in the concluding chapter, which provides a comprehensive summary of the study's contributions to the field of bacterial identification. This chapter revisits the study objectives stated in the introduction and offers a critical assessment of their degree of fulfillment. The potential implications of the developed electronic biosensor are further explored in the chapter, with a particular focus on how it could address the limitations of conventional bacterial identification techniques. Furthermore, this chapter examines the challenges that arise throughout the research process and the methods used to overcome them. The chapter presents a critical analysis of the study findings, establishing a foundation for future research directions and potential avenues of inquiry.

8.2 An innovative and Efficient Analog Electronic Biosensor Interface

The completed project presents a distinctive analog electrical circuit designed for the detection of microorganisms. The circuit, which employs the AD7745 capacitance-to-digital converter, is distinguished as an economical and highly effective solution. This research addresses the shortcomings of previous bacterial identification techniques by prioritizing three key factors: cost-effectiveness, measurement accuracy and ease of design.

Components and Design

The AD7745 integrated circuit is renowned for its exceptional precision in monitoring minute capacitance alterations, which are a vital element in the detection of bacterial activity. It serves as the core component of the biosensor interface circuit. The circuit incorporates a sensor (C+), resistors, and capacitors for noise filtering, thereby ensuring signal stability across a wide frequency range. The I2C protocol facilitates communication between the microcontroller and the circuit. The system is powered by a 5V/3A power source, and the integrity of the communication lines' signals is preserved by

the use of pull-up resistors.

This circuit is ideally suited to use in microbiology laboratories, as it has been specifically designed to detect alterations in bacterial capacitance. The device's accuracy is enhanced by its small size and capacity to detect capacitance at fF levels, rendering it an appropriate tool for identifying the electrical characteristics of bacterial cells in a laboratory setting.

Advantages

1. **Cost-Effective:** The proposed course of action is economically viable. The use of widely accessible components, including the AD7745, ensures the maintenance of high accuracy at a reasonable cost. This facilitates the utilization of the circuit for a greater variety of purposes.
2. **High Sensitivity:** The circuit exhibits a high degree of sensitivity. The circuit's exceptional sensitivity, which is necessary for accurate bacterial identification, is derived from its capacity to discern minute capacitance fluctuations at the femtofarad level.
3. **Noise Reduction:** Furthermore, the circuit exhibits noise reduction capabilities. The results are accurate due to the configuration of the capacitors (100nF and 10µF) in parallel, which serves to filter both high- and low-frequency noise.
4. **Compact Design:** The circuit's compact dimensions facilitate integration into a multitude of experimental configurations. The circuit's compact dimensions facilitate integration into laboratory settings.
5. **Future-Ready:** The configuration is designed to accommodate future developments. The study proposes the utilization of neural networks and machine learning as potential avenues for enhancing the precision and utility of the biosensor.

Conclusion of the Project

The successful completion of the project was marked by the creation of an electronic biosensor interface for bacterial identification that is highly sensitive, compact, and cost-effective. Intending to accurately detect capacitance changes resulting from bacterial metabolic processes, the circuit employs the AD7745 capacitance-to-digital converter. This innovative approach provides an effective alternative to more complex and costly techniques for identifying microbial pathogens.

In conclusion, the final product is set to transform the field of bacterial identification by offering laboratories an accurate and cost-effective instrument. It would be capable of expanding its capabilities to assess other qualities, such as conductivity, and integrating it with three-dimensional printing technology for the fabrication of bespoke enclosures, among other enhancements. The application of neural networks and machine learning could facilitate the automation and enhancement of bacterial detection procedures, thereby rendering this biosensor an adaptable instrument for microbiological study.

8.3 Proposals for Further Research

It is evident that the outcome of this endeavor is worthy of commendation. It is, however, particularly noteworthy that this piece is undergoing a significant amount of ongoing research until a final product is ready for mass sale and use in every microbiology laboratory by healthcare scientists.

As a preliminary step, the fabrication of a standard printed circuit board (PCB) can be initiated. Subsequently, an enclosure for the PCB can be designed and 3D printed, with the sensor protruding so that measurements can be taken. Subsequently, the aforementioned process will be conducted to ascertain another electrical property, namely conductivity.

Upon completion of the aforementioned steps, the research can be advanced to encompass additional domains, including machine learning, neural networks, optimization algorithms, automatic control systems, peak detection algorithms, 3D design and 3D printing, analog and digital electronics, and programming. Additionally, the investigation can delve into the diverse cultures of bacteria. It should be noted that the aforementioned categories also encompass fungi, which can be dangerous to humans. This includes bacteria such as Pseudomonas aeruginosa.

The author's proposed methodology for the aforementioned research project is as follows:

1. **As previously conducted (with integrated devices),** the development of bacterial culture and experimentation on the diverse electrical properties (conductivity and capacitance) of various bacteria will be undertaken. Prior to undertaking further research at this stage, a comparative study will be conducted between the existing circuit and the one developed by Ph.D. candidate Delimaras Vasileios, Dr Kyriakos Tsiakmakis and Dr Argyrios T. Hatzopoulos. This is a circuit that can be used for both capacitance and conductance measurement with high accuracy. Additionally, Doctoral Candidate Delimaras Vasileios and Doctor Varlamis Sotirios are the inaugural participants in this prospective research, having contributed to the aforementioned work. [56]

2. **Subsequently,** the sensor could be modified with Molecularly Imprinted Polymers (MIPs). In general, the sensitivity of the sensor can be increased and made selective to only the substances of interest in the measurements. This can be achieved by spreading a solid substance, such as a polymer material, on its surface, which will selectively form chemical bonds with the substance that the researchers are interested in measuring. As a consequence of this, the sensor will become selective to the substance in question, given that it is only held on its surface. As part of this process, the selectivity of MIPs will be modified to be selective only to the substances that the researchers are interested in measuring. It should be noted that a single sensor will not be capable of measuring all substances. In essence, MIPs with X modification will exhibit sensitivity to Y substance. Thus, a single surface may comprise two or three sensors with varying degrees of selectivity, enabling the detection of different substances. It may be the case that during the liquid-liquid phase of these polymers, an admixture occurs with substances that form bonds with the target substances (i.e. the substances to be measured). Upon polymerization, the material takes on a solid form, whereby only the substances being sought adhere to its surface. [57] [58]

[59] [60] [61] [62]

3. **In the event that the aforementioned assertion (1) is indeed factual,**—that is, that distinct bacterial species possess disparate electrical properties—the rate of growth of the bacteria within an incubation furnace (operating at 37 degrees Celsius) will be monitored through the use of computer vision. If this hypothesis is invalid, a paper will be written on the subject and the research will continue as usual, utilizing different classes of microorganisms, which undoubtedly possess disparate electrical properties. Such categories include the combination of fungus with streptococcus.

4. **The subsequent phase** will entail the development of an automated control system for regulating the growth rate of bacteria (specifically, their size) through the use of infrared radiation (UV) as a suppressor, which will be LED-controlled by the aforementioned automated control system.

5. **An optimization algorithm** will be developed to regulate the growth conditions (e.g., temperature, humidity, lighting, carbon dioxide, and oxygen) of the bacterial colonies to achieve the maximum growth rate and size.

6. **A spectrophotometer** should be constructed or utilized in order to facilitate the separation of similar bacteria, given that it has the capacity to measure absorbance across the entire spectrum.

7. **Additionally,** Dielectrophoresis (DEP) could be employed in some capacity.

8. **Finally,** the aforementioned methods can be employed as inputs to a neural network, enabling the identification of bacteria with an integrated construct that will typically display the name and genus of each microorganism.

In conclusion, the aforementioned procedures, in addition to numerous others, will be carried out to create a final device that can be sold on a global scale for use in the healthcare industry. This device will facilitate bacterial identification conveniently, offering a cost-effective, accurate, and rapid alternative to existing methods.

8.4 Epilogue

The 8th chapter of this thesis provides a comprehensive overview of the study's significant contributions to the field of bacterial identification. The electronic biosensor that has been created has the potential to enhance the efficiency, precision and affordability of bacterial detection. Furthermore, the chapter presents prospective research avenues, emphasizing the necessity for continuous evaluation and optimization of the biosensor to achieve its full potential. The chapter adopts a forward-looking perspective, focusing on the ongoing importance of innovation in addressing the challenges associated with bacterial identification. Further investigation and advancement in this crucial field of study is required.

REFERENCES

[1] F. D. Lowy. (2008) Bacterial classification, structure and function. Accessed: Columbia University. [Online]. Available: https://api.semanticscholar.org/CorpusID:49963607

[2] A. Freiwald and S. Sauer, "Phylogenetic classification and identification of bacteria by mass spectrometry," *Nat Protoc*, vol. 4, no. 5, pp. 732–742, 2009, DOI: 10.1038/nprot.2009.37. [Online]. Available: https://www.nature.com/articles/nprot.2009.37

[3] A. S. Janda JM, "Bacterial identification for publication: When is enough enough?" *Journal of Clinical Microbiology*, vol. 40, no. 6, pp. 1887–1891, 2002, DOI: 10.1128/jcm.40.6.1887-1891.2002. [Online]. Available: https://doi.org/10.1128/jcm.40.6.1887-1891.2002

[4] F. Walter, T. Arianna, B. Simona, G. Emilia, and L. Antonella, "Recent advances and ongoing challenges in the diagnosis of microbial infections by maldi-tof mass spectrometry," *Frontiers in Microbiology*, vol. 9, 2018, DOI: 10.3389/fmicb.2018.01097. [Online]. Available: https://www.frontiersin.org/journals/microbiology/articles/10.3389/fmicb.2018.01097/full

[5] D. Maneg, J. Sponsel, I. Müller, B. Lohr, J. Penders, K. Madlener, Hunfeld, and Klaus-Peter, "Advantages and limitations of direct pcr amplification of bacterial 16s-rdna from resected heart tissue or swabs followed by direct sequencing for diagnosing infective endocarditis: A retrospective analysis in the routine clinical setting," *BioMed Research International*, vol. 2016, no. 1, pp. 792–874, 2016, DOI: 10.1155/2016/7923874. [Online]. Available: https://onlinelibrary.wiley.com/doi/10.1155/2016/7923874

[6] V. Muigg, H. M. Seth-Smith, K.-M. Adam, M. Weisser, V. Hinić, A. Blaich, T. Roloff, U. Heininger, H. Schmid, M. Kohler, L. Graf, D. M. Winterflood, P. Schlaepfer, and D. Goldenberger, "Novel organism verification and analysis (nova) study: identification of 35 clinical isolates representing potentially novel bacterial taxa using a pipeline based on whole genome sequencing," *BMC Microbiol*, vol. 24, no. 14, 2024, DOI: 10.1186/s12866-023-03163-7. [Online]. Available: https://bmcmicrobiol.biomedcentral.com/articles/10.1186/s12866-023-03163-7

[7] J.-M. R. Silpak Biswas, "Use of maldi-tof mass spectrometry for identification of bacteria that are difficult to culture," *Journal of Microbiological Methods*, vol. 92, no. 1, pp. 14–24, 2013, DOI: 10.1016/j.mimet.2012.10.014. [Online]. Available: https://www.sciencedirect.com/science/article/abs/pii/S0167701212003478?via%3Dihub

[8] D. S. Chertow, "Next-generation diagnostics with crispr," *Science360*, vol. 360, no. 6387, pp. 381–382, 2018, DOI: 10.1126/science.aat4982. [Online]. Available: https://www.science.org/doi/10.1126/science.aat4982

[9] S. Brosel-Oliu, N. Abramova, N. Uria, and A. Bratov, "Impedimetric transducers based on interdigitated electrode arrays for bacterial detection – a review," *Analytica Chimica Acta*, vol. 1088, pp. 1–19, 2019, DOI: 10.1016/j.aca.2019.09.026. [Online]. Available: https://www.sciencedirect.com/science/article/pii/S0003267019310979

[10] V. G. P., L. W., H. G., D. B. M., B. K., S. J., V. A., S. W., H. L., and M. R., "Nanoscaled interdigitated electrode arrays for biochemical sensors," *Proceedings of International Solid State Sensors and Actuators Conference (Transducers '97)*, vol. 2, pp. 907–910, 1997, DOI: 10.1109/SENSOR.1997.635249. [Online]. Available: https://ieeexplore.ieee.org/abstract/document/635249

[11] S. N. F., T. R. C., and W. Christine, "Electrical conductivity measurements using microfabricated interdigitated electrodes," *Analytical Chemistry*, vol. 65, no. 9, pp. 1199–1202, 1993, DOI: 10.1021/ac00057a016. [Online]. Available: https://pubs.acs.org/doi/abs/10.1021/ac00057a016

[12] Y.-C. Lu, Y.-S. Chuang, Y.-Y. Chen, A.-C. Shu, H.-Y. Hsu, H.-Y. Chang, and T.-R. Yew, "Bacteria detection utilizing electrical conductivity," *Sensors and Actuators A: Physical*, vol. 23, no. 12, pp. 1856–1861, 2008, DOI: 10.1016/j.bios.2008.03.005. [Online]. Available: https://www.sciencedirect.com/science/article/pii/S0956566308001127

[13] W. H. Grove, *Interdigitated Array Electrode Sensors: Their Design, Efficiency and Applications*. Chancellor's Honors Program Projects, 1999. [Online]. Available: https://trace.tennessee.edu/utk_chanhonoproj/310/

[14] R. Prabhu, R. Sudha, J. Prateek, N. Hardik, P. Saurav, A. P, and T. Rao, "Low value capacitance measurements for capacitive sensors - a review," *Sensors and Transducers*, vol. 148, no. 1, pp. 1–10, 2013. [Online]. Available: https://www.proquest.com/openview/521bc25a9e12296b5767ca0232b84181/1?pq-origsite=gscholar&cbl=52938#

[15] V. Delimaras, "Sensor of oil quality measurement based on changes in electric permitivity," Master's Thesis, International Hellenic University, Thessaloniki, 2019, [Unpublished].

[16] P. D.M.G. and S. K., "A simple interface circuit to measure very small capacitance changes in capacitive sensors," *IEEE Transactions on Instrumentation and Measurement*, vol. 50, no. 6, pp. 1583–1586, 2001, DOI: 10.1109/19.982949. [Online]. Available: https://ieeexplore.ieee.org/abstract/document/982949

[17] H. M. R., M. M. R., I. S. K., E. S. A., Q. W., and P. E., "A low-power capacitance measurement circuit with high resolution and high degree of linearity," in *2008 51st Midwest Symposium on Circuits and Systems*. IEEE, 2008, DOI: 10.1109/MWSCAS.2008.4616786, pp. 261–264. [Online]. Available: https://ieeexplore.ieee.org/abstract/document/4616786

[18] W. contributors. (26 August 2024) I²c. [Online]. Available: https://en.wikipedia.org/w/index.php?title=I%C2%B2C&oldid=1232229587

[19] A. Devices, *AD7745/AD7746 24-Bit Capacitance-to-Digital Converter with Temperature Sensor Data Sheet*, Analog Devices, Norwood, MA, 2005, rev. 0. [Online]. Available: https://www.analog.com/media/en/technical-documentation/data-sheets/AD7745_7746.pdf

[20] S. Schaur and B. Jakoby, "A numerically efficient method of modeling interdigitated electrodes for capacitive film sensing," *Procedia Engineering*, vol. 25, pp. 431–434, 2011, DOI: 10.1016/j.proeng.2011.12.107. [Online]. Available: https://www.sciencedirect.com/science/article/pii/S1877705811057766

[21] G. González, E. S. Kolosovas-Machuca, E. López-Luna, H. Hernández-Arriaga, and F. J. González, "Design and fabrication of interdigital nanocapacitors coated with hfo2," *Sensors*, vol. 15, no. 1, pp. 1998–2005, 2015, DOI: 10.3390/s150101998. [Online]. Available: https://www.mdpi.com/1424-8220/15/1/1998

[22] W. contributors. (24 August 2024) Chemiresistor. [Online]. Available: https://en.wikipedia.org/w/index.php?title=Chemiresistor&oldid=1218700041

[23] P.-L. Y. Mohd Syaifudin Abdul Rahman, Subhas Chandra Mukhopadhyay, "Novel sensors for food inspection: Modelling, fabrication and experimentation," in *Smart Sensors, Measurement and Instrumentation*, S. Sariaslani and G. M. Gadd, Eds. Springer Cham, 2014, vol. 1, pp. 1–140. [Online]. Available: https://link.springer.com/book/10.1007/978-3-319-04274-9#bibliographic-information

[24] G. N. e. a. Bilican I., Guler M.T., "Capacitive solvent sensing with interdigitated microelectrodes," *Microsyst Technol*, vol. 22, no. 3, pp. 659–668, 2016, DOI: 10.1007/s00542-015-2617-1. [Online]. Available: https://link.springer.com/article/10.1007/s00542-015-2617-1#citeas

[25] A. Vuković Rukavina, "Non-invasive liquid recognition based on interdigital capacitor," *Sensors and Actuators A: Physical*, vol. 228, pp. 145–150, 2015, DOI: 10.1016/j.sna.2015.03.019. [Online]. Available: https://www.sciencedirect.com/science/article/pii/S0924424715001314

[26] W. contributors. (24 August 2024) Capacitor. [Online]. Available: https://en.wikipedia.org/w/index.php?title=Capacitor&oldid=1240014029

[27] ——. (24 August 2024) Dielectric. [Online]. Available: https://en.wikipedia.org/w/index.php?title=Dielectric&oldid=1240178662

[28] H. Qin, Y. Cai, J. Dong, and Y.-S. Lee, "Direct printing of capacitive touch sensors on flexible substrates by additive e-jet printing with silver nanoinks," *Journal of Manufacturing Science and Engineering*, vol. 139, no. 3, p. 031011, 2016, DOI: 10.1115/1.4034663. [Online]. Available: https://asmedigitalcollection.asme.org/manufacturingscience/article/139/3/031011/377019/Direct-Printing-of-Capacitive-Touch-Sensors-on

[29] A. Mamishev, K. Sundara-Rajan, F. Yang, Y. Du, and M. Zahn, "Interdigital sensors and transducers," *Proceedings of the IEEE*, vol. 92, no. 5, pp. 808–845, 2004, DOI: 10.1109/JPROC.2004.826603. [Online]. Available: https://ieeexplore.ieee.org/document/1288505

[30] J. Guo, T. Bamber, M. Chamberlain, L. Justham, and M. Jackson, "Optimization and experimental verification of coplanar interdigital electroadhesives," *Journal of Physics D: Applied Physics*, vol. 49, no. 41, p. 415304, 2016, DOI: 10.1088/0022-3727/49/41/415304. [Online]. Available: https://iopscience.iop.org/article/10.1088/0022-3727/49/41/415304/meta

[31] W. Withayachumnankul, C. Fumeaux, and D. Abbott, "Compact electric-lc resonators for metamaterials," *Opt. Express*, vol. 18, no. 25, pp. 25 912–25 921, 2010, DOI: 10.1364/OE.18.025912. [Online]. Available: https://opg.optica.org/oe/fulltext.cfm?uri=oe-18-25-25912&id=208428

[32] A. Technologies. (2008) Overview on interdigital capacitor design. [Online]. Available: https://www.yumpu.com/en/document/view/9552220/overview-on-interdigital-capacitor-design-agilent-technologies

[33] M. N. S., R. M. M., A. M. M. A. B., H. D. S. C., I. S. S. M., T. L. F. A., D. N. S., and M. S. A. Z., "Interdigitated electrodes as impedance and capacitance biosensors: A review," *AIP Conference Proceedings*, vol. 1885, no. 1, p. 020276, 2017, DOI: 10.1063/1.5002470. [Online]. Available: https://pubs.aip.org/aip/acp/article-abstract/1885/1/020276/886511/Interdigitated-electrodes-as-impedance-and

[34] A. Nasrin, N. Anindya, A. M. E. E., H. Tao, and M. S. Chandra, "Interdigital sensors: Biomedical, environmental and industrial applications," *Sensors and Actuators A: Physical*, vol. 305, p. 111923, 2020, DOI: 10.1016/j.sna.2020.111923. [Online]. Available: https://www.sciencedirect.com/science/article/pii/S0924424719321090

[35] B. T. e. a. Quoc T.V., Ngoc V.N., "High-frequency interdigitated array electrode-based capacitive biosensor for protein detection," *Sensors and Actuators A: Physical*, vol. 13, p. 403–415, 2019, DOI: 10.1007/s13206-019-3412-3. [Online]. Available: https://link.springer.com/article/10.1007/s13206-019-3412-3

[36] H.-W. Jung, Y. W. Chang, G. yeon Lee, S. Cho, M.-J. Kang, and J.-C. Pyun, "A capacitive biosensor based on an interdigitated electrode with nanoislands," *Analytica Chimica Acta*, vol. 844, pp. 27–34, 2014, DOI: 10.1016/j.aca.2014.07.006. [Online]. Available: https://www.sciencedirect.com/science/article/pii/S0003267014008307

[37] L. Wang, M. Veselinovic, L. Yang, B. J. Geiss, D. S. Dandy, and T. Chen, "A sensitive dna capacitive biosensor using interdigitated electrodes," *Biosensors and Bioelectronics*, vol. 87, pp. 646–653, 2017, DOI: 10.1016/j.bios.2016.09.006. [Online]. Available: https://www.sciencedirect.com/science/article/pii/S095656631630879X

[38] T. Matteo, B. da Silva Fanta Alice, J. Flemming, W. J. Birkedal, and H. Anpan, "Influence of ti and cr adhesion layers on ultrathin au films," *ACS Applied Materials and Interfaces*, vol. 9, no. 42, pp. 37 374–37 385, 2017, DOI: 10.1021/acsami.7b10136. [Online]. Available: https://pubs.acs.org/doi/abs/10.1021/acsami.7b10136

[39] S. V. R. Suzhe Liang, Matthias Schwartzkopf and P. Müller-Buschbaum, "State of the art of ultra-thin gold layers: formation fundamentals and applications," *Nanoscale Adv.*, vol. 4, pp. 2533–2560, 2022, DOI: 10.1039/D2NA00127F. [Online]. Available: https://pubs.rsc.org/en/content/articlehtml/2022/na/d2na00127f

[40] H. P. H., "Gold/chromium metallizations for electronic devices," *Gold Bulletin*, vol. 13, no. 3, pp. 98–106, 1980, DOI:10.1007/BF03214772. [Online]. Available: https://www.researchgate.net/publication/226114335_Goldchromium_metallizations_for_electronic_devices

[41] C. W. D. and R. D. G., *Materials Science and Engineering: An Introduction*, 9th ed. Wiley, 2018. [Online]. Available: https://books.google.gr/books?hl=el&lr=&id=dmoTEQAAQBAJ&oi=fnd&pg=PA19&dq=Materials+Science+and+Engineering+AN+INTRODUCTION+10th+edition+s&ots=O-EtmNwUk4&sig=3j1CAuJXi3RM3Q-Vj_V4rv19yWA&redir_esc=y#v=onepage&q=Materials%20Science%20and%20Engineering%20AN%20INTRODUCTION%2010th%20edition%20s&f=false

[42] S. K. R. and J. V., *Handbook of Thin Film Deposition Processes and Techniques*, 2nd ed. Elsevier, 2012. [Online]. Available: https://www.sciencedirect.com/book/9780815514428/handbook-of-thin-film-deposition-processes-and-techniques

[43] M. Majhi, "Growth and characterizations of sio2 thin films on silicon substrates," *ethesis@nitr*, 2013. [Online]. Available: https://core.ac.uk/outputs/53189554/?source=oai

[44] N. S.S. and G. V.A., "Electronic structure of silicon dioxide (a review)," *Phys. Solid State*, vol. 56, no. 2, pp. 209–223, 2014, DOI: 10.1134/S106378341402022X. [Online]. Available: https://link.springer.com/article/10.1134/S106378341402022X

[45] T. C. Edwards and M. B. Steer, *Foundations for Microstrip Circuit Design*, 4th ed. Chichester, UK: John Wiley & Sons, Ltd., 2016, appendix B: Material Properties. [Online]. Available: https://onlinelibrary.wiley.com/doi/10.1002/9781118936160.app2

[46] L. Reto Keller, Business Development Manager at Optics Balzers AG. Balzers, *Manufacturing interdigital electrodes for capacitive sensing using thin film deposition*, Optics Balzers, Neugrüt 35, LI-9496 Balzers, 2001, oBA 002 AE (2001-1). [Online]. Available: https://www.materionbalzersoptics.com/userdata/pdf_files/oba-002-ae-optics-balzers-manufacturing-interdigital-electrodes-0120.pdf

[47] K. N. Khamil and M. A. Mood, "Dielectric sensing (capacitive) on cooking oil's tpc level," *Journal of Telecommunication, Electronic and Computer Engineering*, vol. 9, no. 3, pp. 27–32, 2017, DOI: 10.1021/acsami.7b10136. [Online]. Available: https://jtec.utem.edu.my/jtec/article/view/1228

[48] M. Liu, X. Qin, Z. Chen, L. Tang, B. Borom, N. Cao, D. Barnes, K. Cheng, J. Chen, T. Wang, and J. Rao, "Frying oil evaluation by a portable sensor based on dielectric constant measurement," *Sensors*, vol. 19, no. 24, pp. 1–11, 2019, DOI: 10.3390/s19245375. [Online]. Available: https://www.mdpi.com/1424-8220/19/24/5375

[49] Espressif, *ESP32-Arduino Documentation*, 2023, c1a40558. [Online]. Available: https://espressif-docs.readthedocs-hosted.com/projects/arduino-esp32/en/latest/index.html

[50] Waveshare, *ESP32-S3 Datasheet*, Espressif System, 2023, version 1.6. [Online]. Available: https://files.waveshare.com/upload/f/f7/Esp32-s3_datasheet_en_%281%29.pdf

[51] ——, *ESP32-S3 Technical Reference Datasheet*, Espressif Systems, 2023, version 1.2. [Online]. Available: https://files.waveshare.com/upload/9/9e/Esp32-s3_technical_reference_manual_en_%281%29.pdf

[52] ——, *ESP32-S3-WROOM-1 Datasheet*, Espressif Systems, 2023, version 1.2. [Online]. Available: https://files.waveshare.com/upload/8/87/Esp32-s3-wroom-1_wroom-1u_datasheet_en.pdf

[53] T. Raissa, B. S. M., and B. J. J., "An overview of in vitro methods to study microglia," *Frontiers in Cellular Neuroscience*, vol. 12, 2018, DOI: 10.3389/fncel.2018.00242. [Online]. Available: https://www.frontiersin.org/journals/cellular-neuroscience/articles/10.3389/fncel.2018.00242

[54] S. Arora, J. M. Rajwade, and K. M. Paknikar, "Nanotoxicology and in vitro studies: The need of the hour," *Toxicology and Applied Pharmacology*, vol. 258, no. 2, pp. 151–165, 2012, DOI: 10.1016/j.taap.2011.11.010. [Online]. Available: https://www.sciencedirect.com/science/article/pii/S0041008X11004467

[55] G. Schmalz, "Use of cell cultures for toxicity testing of dental materials—advantages and limitations," *Journal of Dentistry*, vol. 22, pp. S6–S11, 1994, DOI: 10.1016/0300-5712(94)90032-9. [Online]. Available: https://www.sciencedirect.com/science/article/pii/0300571294900329

[56] V. Delimaras, K. Tsiakmakis, and A. T. Hatzopoulos, "Analog interface based on capacitance multiplier for capacitive sensors and application to evaluate the quality of oils," *AIMS Electronics and Electrical Engineering*, vol. 7, no. 4, pp. 243–270, 2023, DOI: 10.3934/electreng.2023015. [Online]. Available: https://www.aimspress.com/article/doi/10.3934/electreng.2023015

[57] P. A. Cormack and A. Z. Elorza, "Molecularly imprinted polymers: synthesis and characterisation," *Journal of Dentistry*, vol. 804, pp. 173–182, 5 2004, DOI: 10.1016/j.jchromb.2004.02.013. [Online]. Available: https://linkinghub.elsevier.com/retrieve/pii/S1570023204001412

[58] K. Haupt and K. Mosbach, "Molecularly imprinted polymers and their use in biomimetic sensors," *Chemical Reviews*, vol. 100, pp. 2495–2504, 1994, DOI: 10.1021/cr990099w. [Online]. Available: https://pubs.acs.org/doi/full/10.1021/cr990099w

[59] K. Haupt, "Topics in current chemistry," in *Molecular Imprinting*. Springer Berlin, Heidelberg, 2014, DOI: 10.1007/978-3-642-28421-2, pp. XIV, 350. [Online]. Available: https://link.springer.com/book/10.1007/978-3-642-28421-2

[60] A. A. Lahcen and A. Amine, "Recent advances in electrochemical sensors based on molecularly imprinted polymers and nanomaterials," *Electroanalysis*, vol. 31, pp. 188–201, 2019, DOI: 10.1002/elan.201800623. [Online]. Available: https://analyticalsciencejournals.onlinelibrary.wiley.com/doi/abs/10.1002/elan.201800623

[61] G. Vasapollo, R. D. Sole, L. Mergola, M. R. Lazzoi, A. Scardino, S. Scorrano, and G. Mele, "Molecularly imprinted polymers: Present and future prospective," *International Journal of Molecular Sciences*, vol. 12, pp. 5908–5945, 2011, DOI: 10.3390/ijms12095908. [Online]. Available: https://www.mdpi.com/1422-0067/12/9/5908

[62] R. Schirhagl, "Bioapplications for molecularly imprinted polymers," *Analytical Chemistry*, vol. 86, pp. 250–261, 2014, DOI: 10.1021/ac401251j. [Online]. Available: https://pubs.acs.org/doi/full/10.1021/ac401251j

[63] L. A. Kirsebom, S. Dasgupta, and B. M. Fredrik Pettersson, "Chapter four - pleiomorphism in mycobacterium," in *Advances in Applied Microbiology*, S. Sariaslani and G. M. Gadd, Eds. Academic Press, 2012, vol. 80, pp. 81–112. [Online]. Available: https://www.sciencedirect.com/science/article/pii/B9780123943811000040

[64] P. Sarangan, S. Dharanidevi, N. K. Das, and S. Raj, "Prevalence, phenotypic characterization and antibiotic susceptibility of non-fermentative gram negative bacilli isolates at a tertiary care centre," *International Journal of Current Microbiology and Applied Sciences*, vol. 5, pp. 442–454, 11 2016, DOI: 10.20546/ijcmas.2016.511.051. [Online]. Available: https://www.ijcmas.com/abstractview.php?ID=1105&vol=5-11-2016&SNo=51

[65] D. Narayan and M. Krishnan, "Prodigiosin inhibits motility and activates bacterial cell death revealing molecular biomarkers of programmed cell death," *AMB Express*, vol. 6, no. 50, 7 2016, DOI: 10.1186/s13568-016-0222-z. [Online]. Available: https://amb-express.springeropen.com/articles/10.1186/s13568-016-0222-z

[66] K. Arshak, E. Moore, G. M. Lyons, J. Harris, and S. Clifford, "A review of gas sensors employed in electronic nose applications," *Sensor Review*, vol. 24, no. 2, pp. 181–198, Jun. 2004. [Online]. Available: https://www.emerald.com/insight/content/doi/10.1108/02602280410525977/full/html

[67] R. Igreja and C. Dias, "Analytical evaluation of the interdigital electrodes capacitance for a multi-layered structure," *Sensors and Actuators A: Physical*, vol. 112, no. 2, pp. 291–301, 2004, DOI: 10.1016/j.sna.2004.01.040. [Online]. Available: https://www.sciencedirect.com/science/article/pii/S0924424704000779

[68] K. Christopher and E. Bruno, *Identification of Bacterial Species*, M. A. O'Donnell, Ed. Department of Biological Sciences, University of Alberta, 2003, vol. 24. [Online]. Available: https://www.ableweb.org/biologylabs/wp-content/uploads/volumes/vol-24/8-christopher.pdf

Appendix A

BACTERIA AND THEIR IDENTIFICATION METHODS

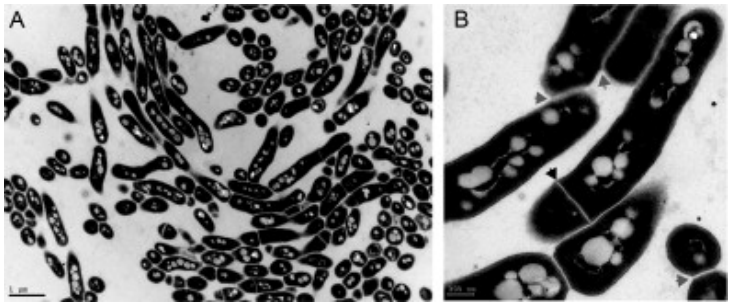

Appendix Figure A.1: *Mycobacterium* [63]

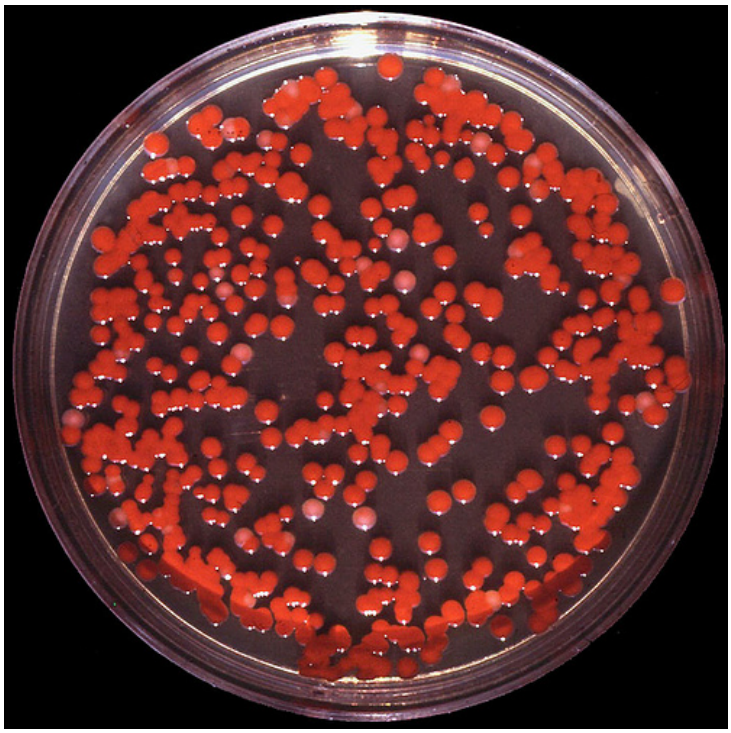

Appendix Figure A.2: *Serratia marcescens*
Source: Medbullets

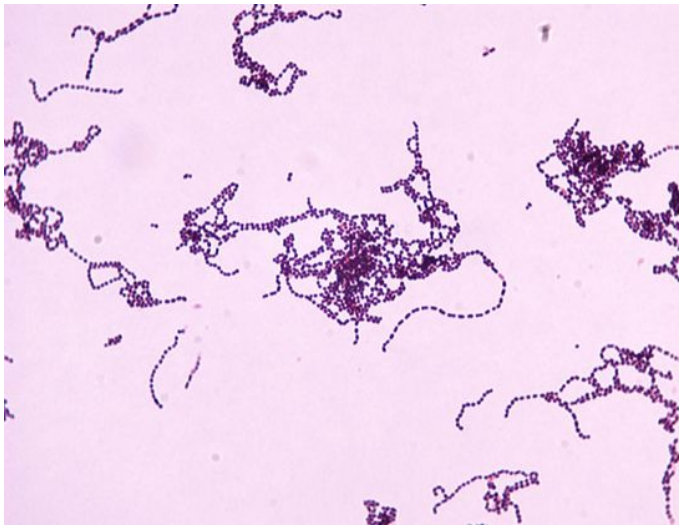

Appendix Figure A.3: *Streptococcus pyogenes*
Source: Infectious Disease Advisor

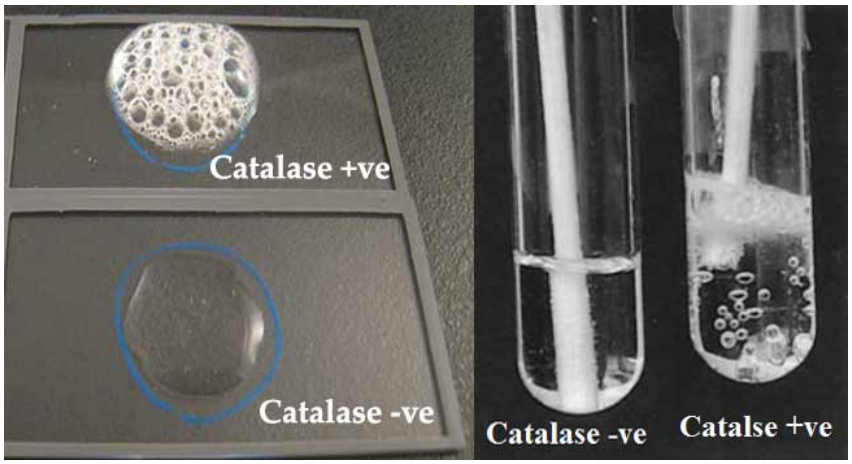

Appendix Figure A.4: Catalase Test
Source: Online Microbiology Notes - MicrobiologyInfo.com

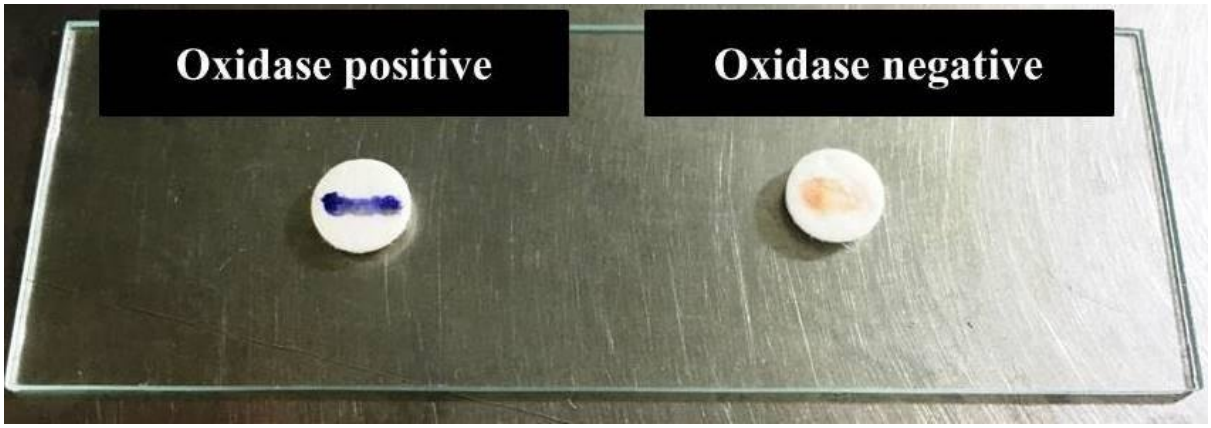

Appendix Figure A.5: Oxidase Test [64]

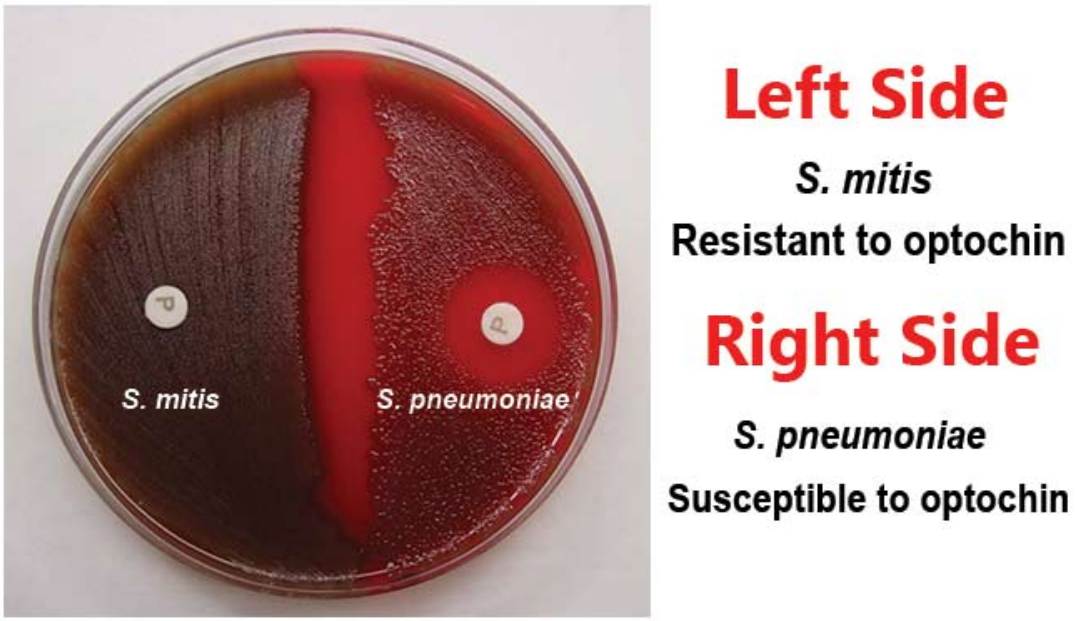

Appendix Figure A.6: Optochin Test
Source: Online Microbiology Notes - MicrobiologyInfro.com

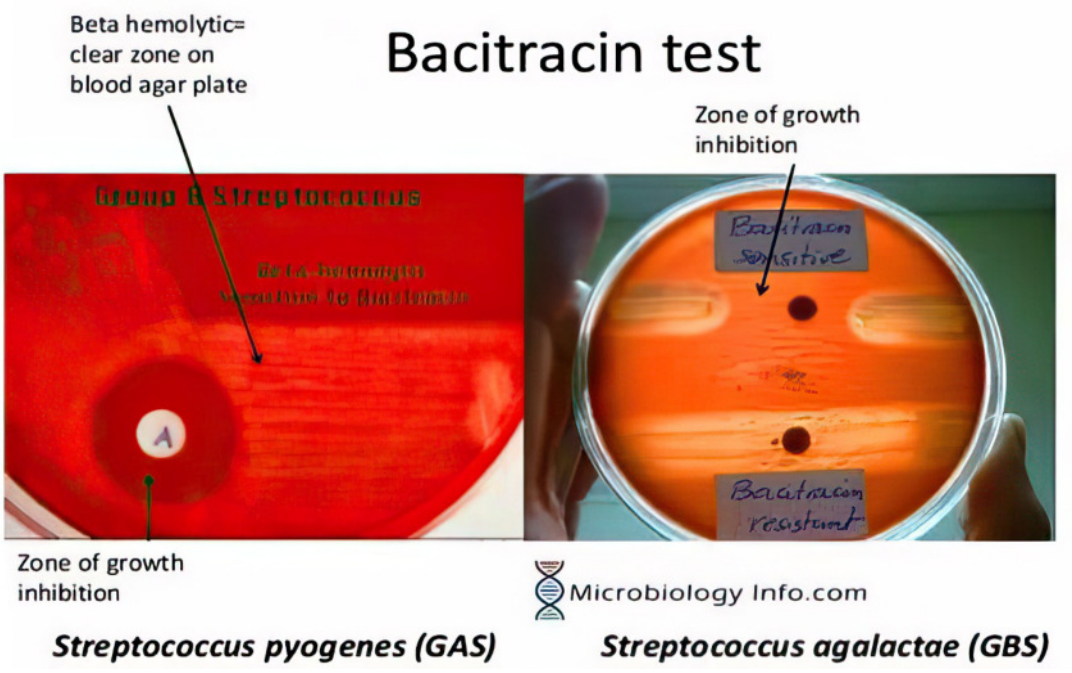

Appendix Figure A.7: Bacitracin Test
Source: Online Microbiology Notes - MicrobiologyInfro.com

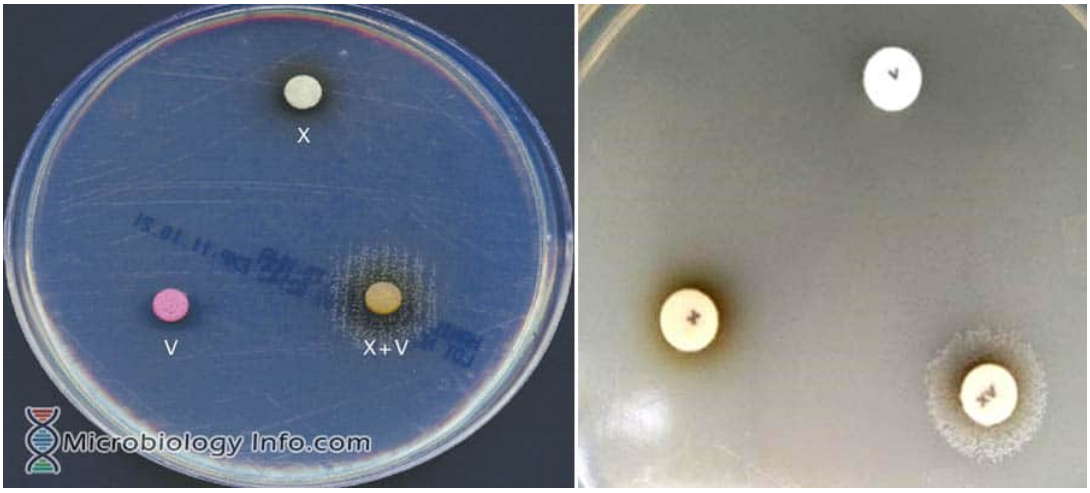

Appendix Figure A.8: X and V Factors Test
Source: Online Microbiology Notes - MicrobiologyInfo.com

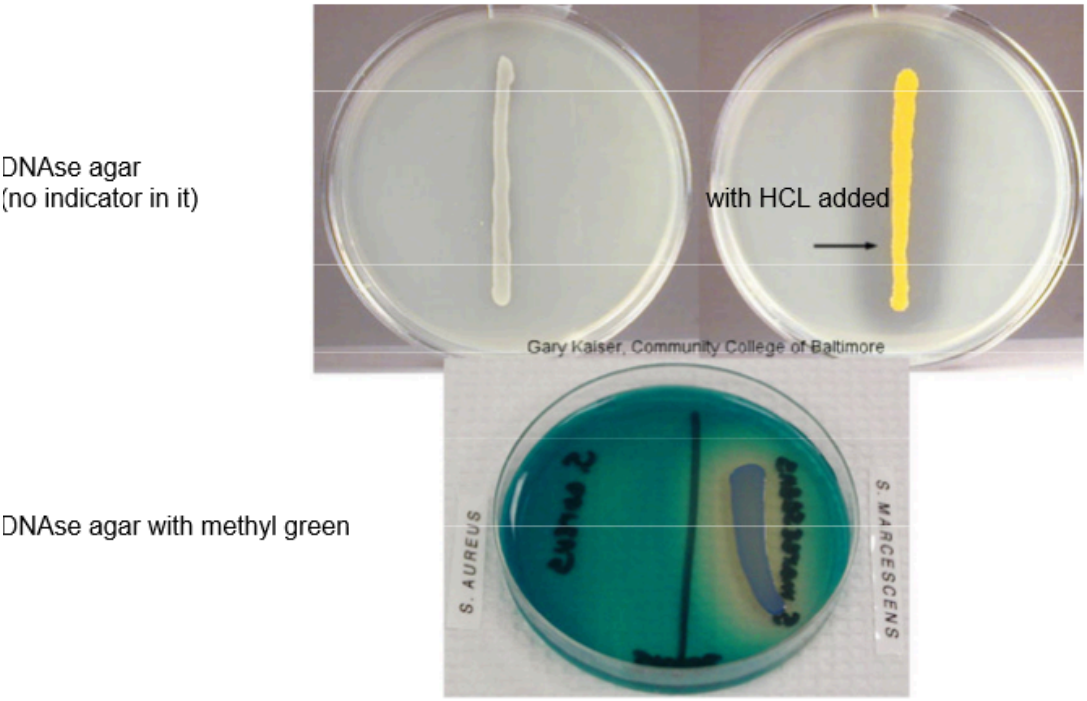

Appendix Figure A.9: Thermolabite Nuclease (DNase) Test
Source: LibreTexts / Biology / 33: Deoxyribonuclease (DNase) Test

Appendix Figure A.10: Esculin Test
Source: Online Microbiology Notes - MicrobiologyInfro.com

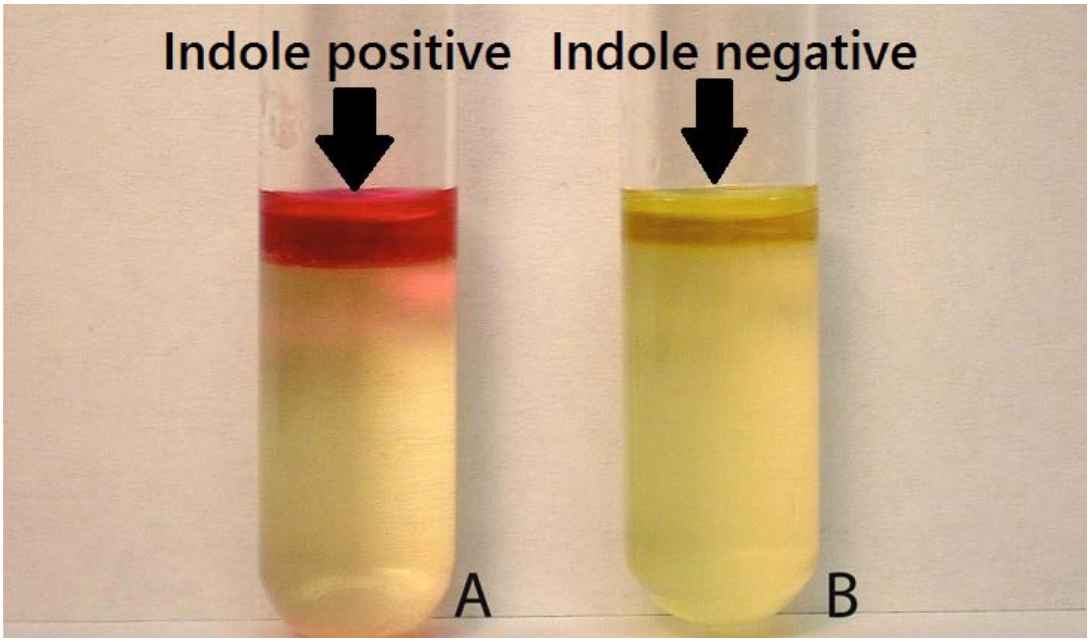

Appendix Figure A.11: Indole Test
Source: Online Microbiology Notes - MicrobiologyInfro.com

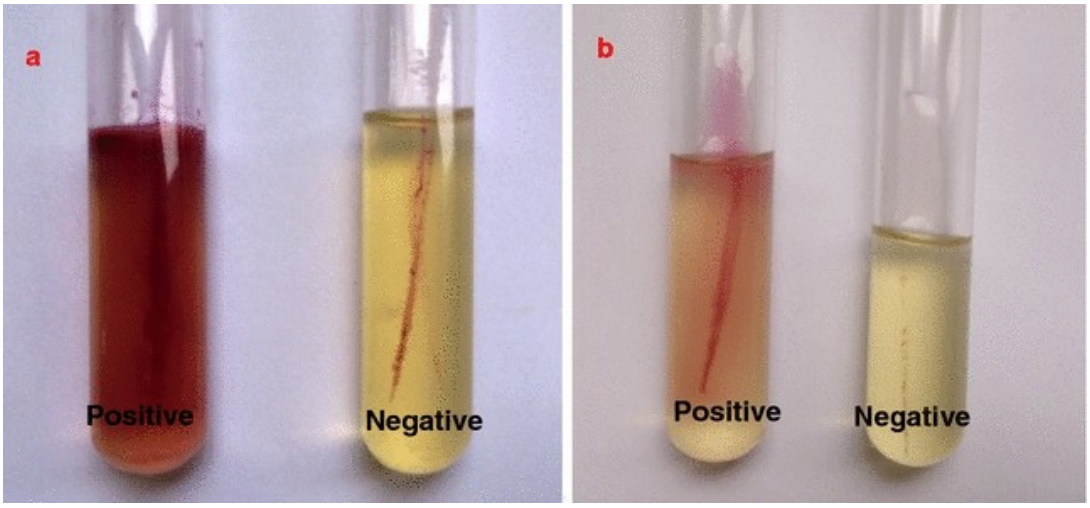

Appendix Figure A.12: Motility Test [65]

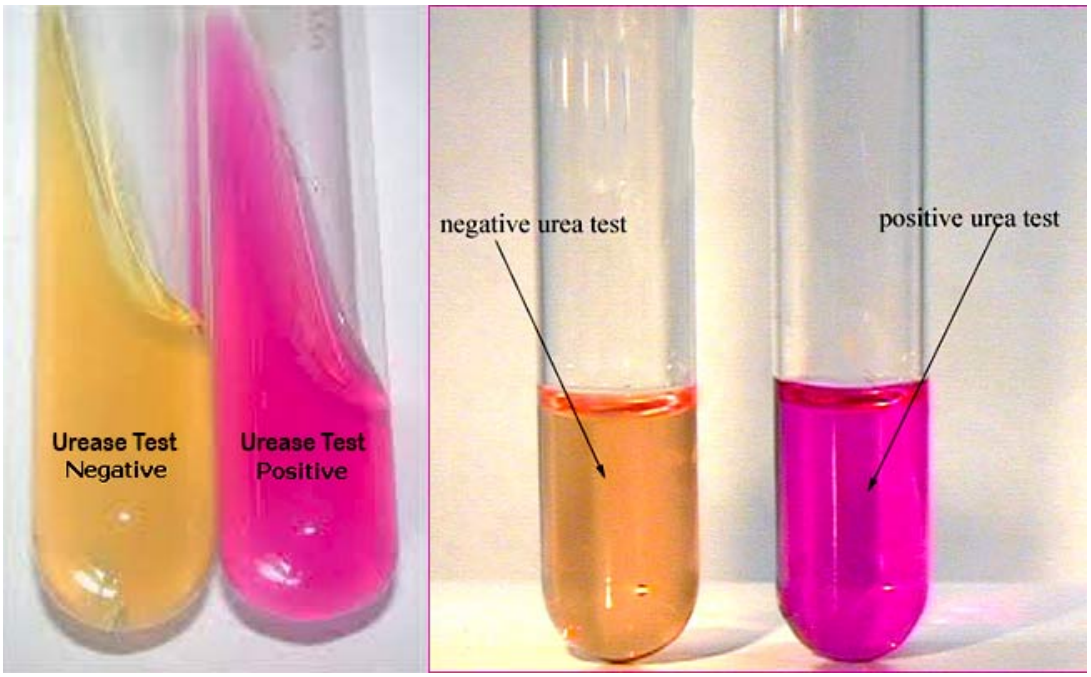

Appendix Figure A.13: Urease Test
Source: Online Microbiology Notes - MicrobiologyInfro.com

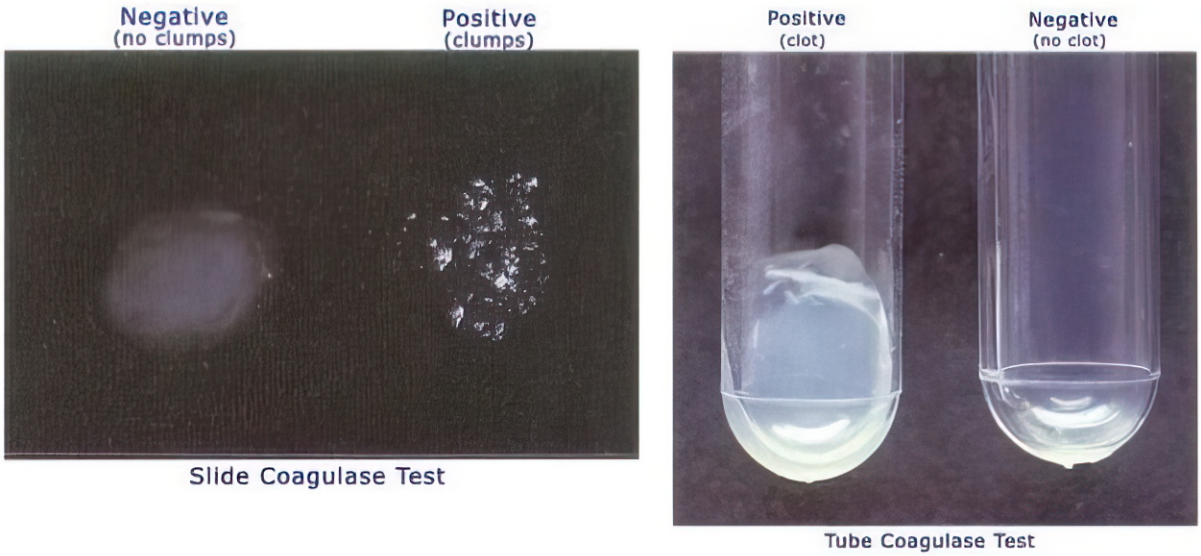

Appendix Figure A.14: Coagulase (Pectase) Test
Source: Online Microbiology Notes - MicrobiologyInfro.com

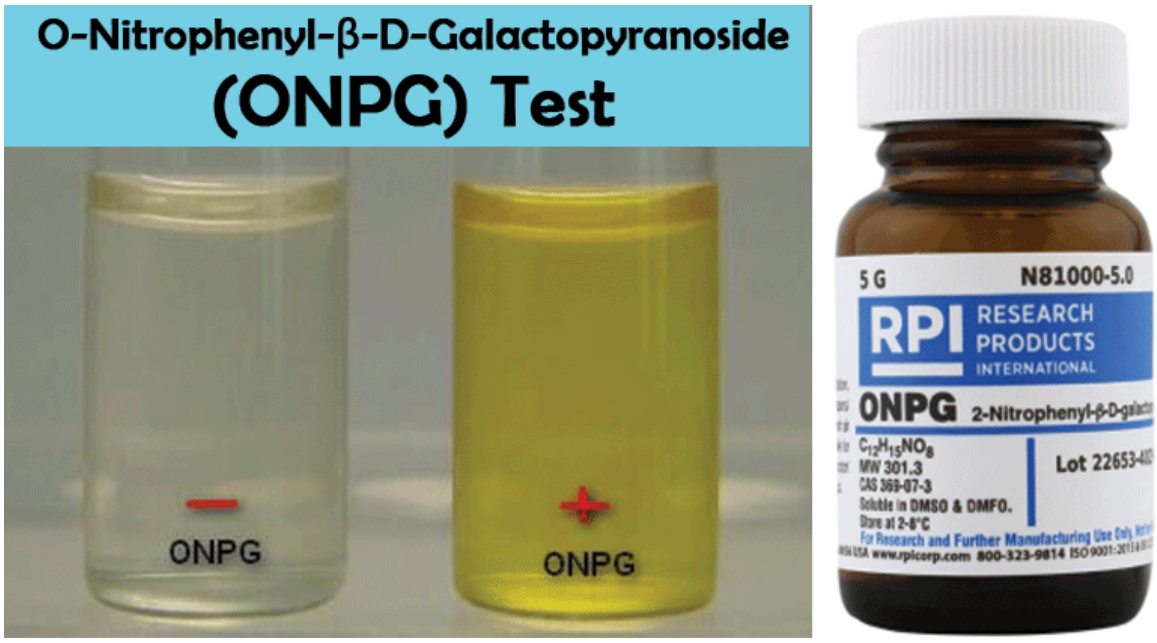

Appendix Figure A.15: O-NPG Test
Source: Online Biology Notes / Biology Practical / Microbiology Practical

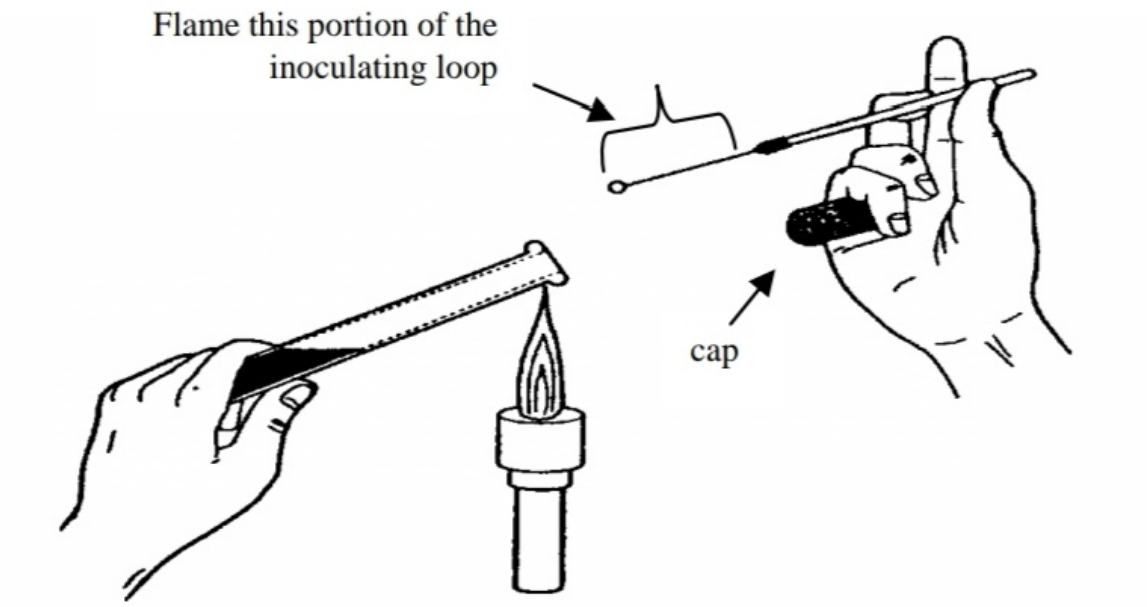

Appendix Figure A.16: Removing cells from a liquid culture using an inoculating loop [68]

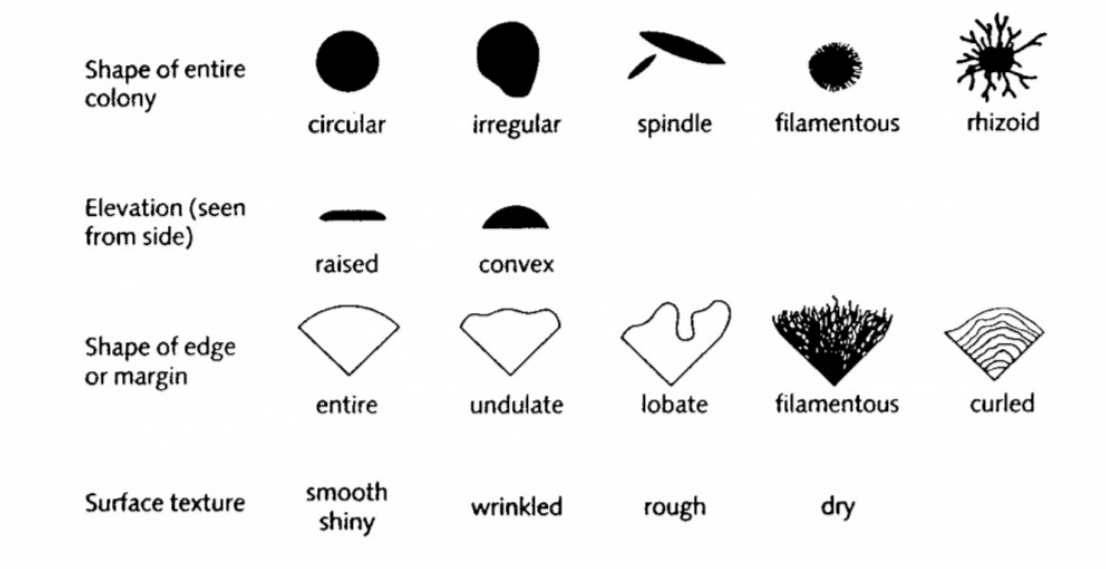

Appendix Figure A.17: Some terms used to describe colony morphology [68]

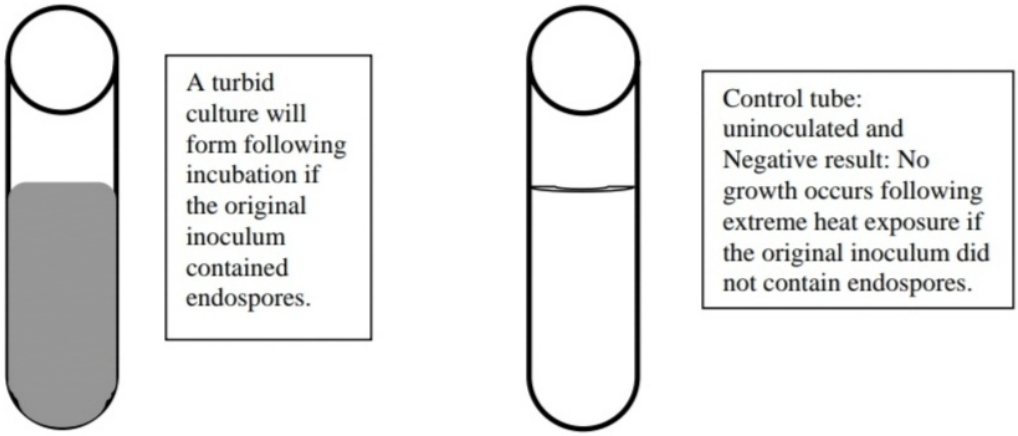

Appendix Figure A.18: Endospore Test [68]

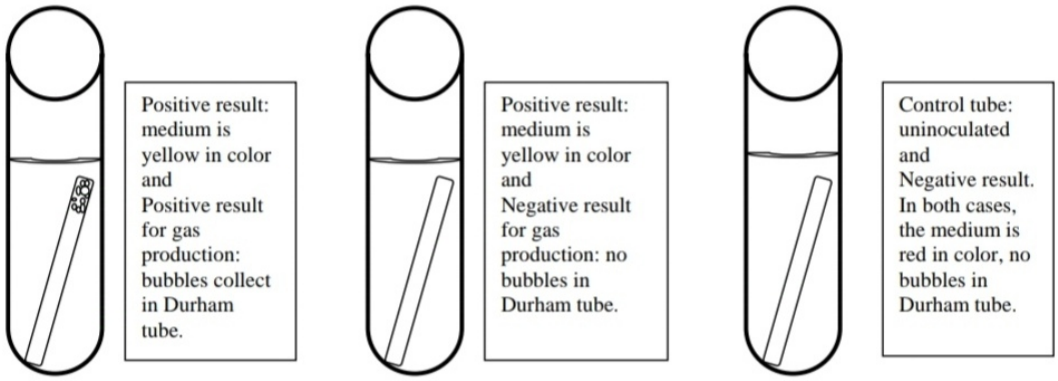

Appendix Figure A.19: Glucose Fermentation Test [68]

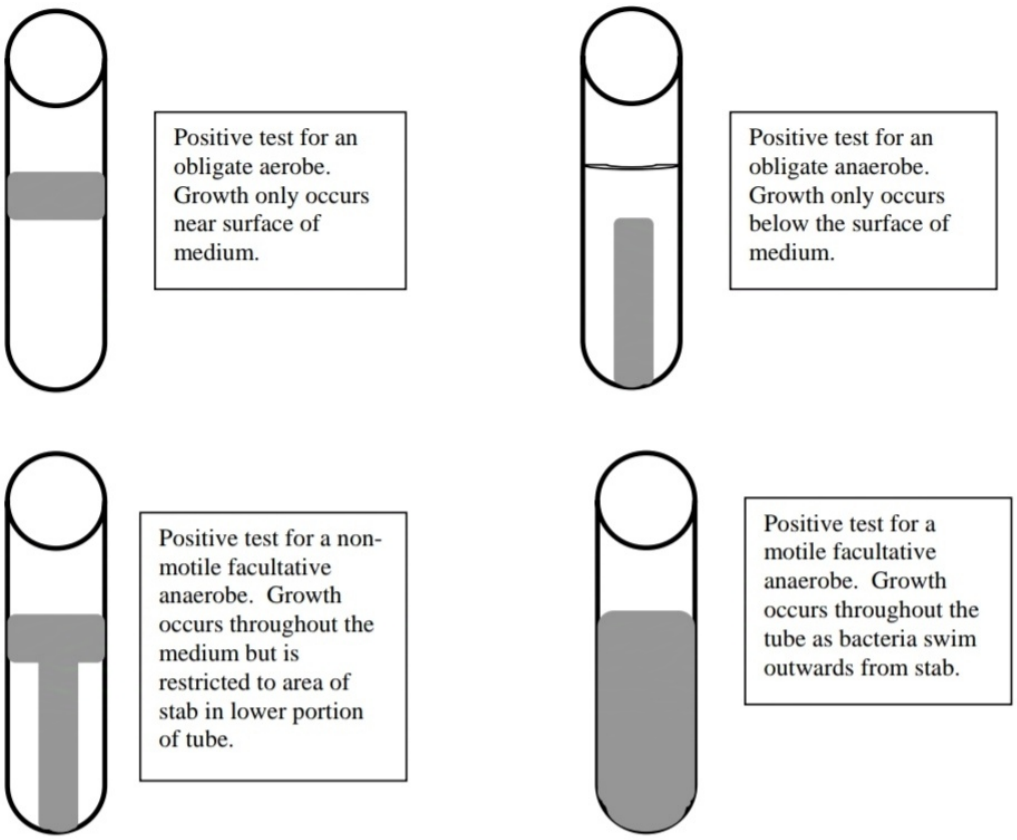

Appendix Figure A.20: Oxygen Requirements for Growth Test [68]

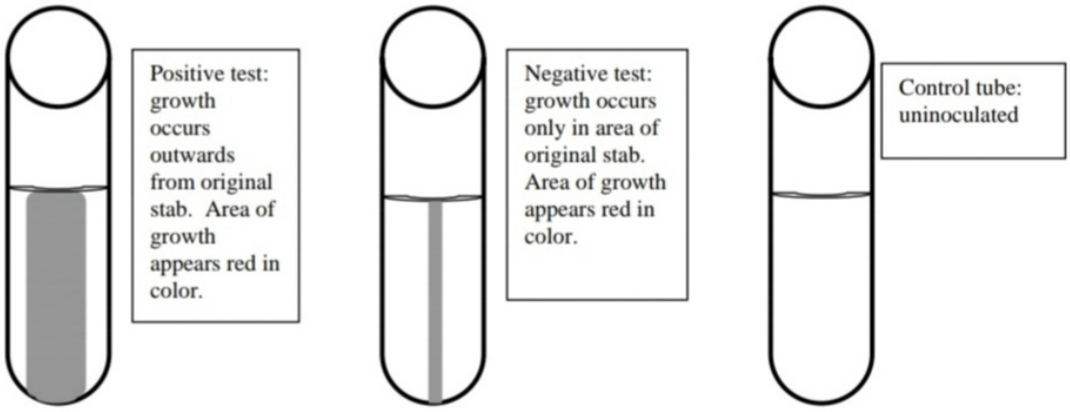

Appendix Figure A.21: Motility Test [68]

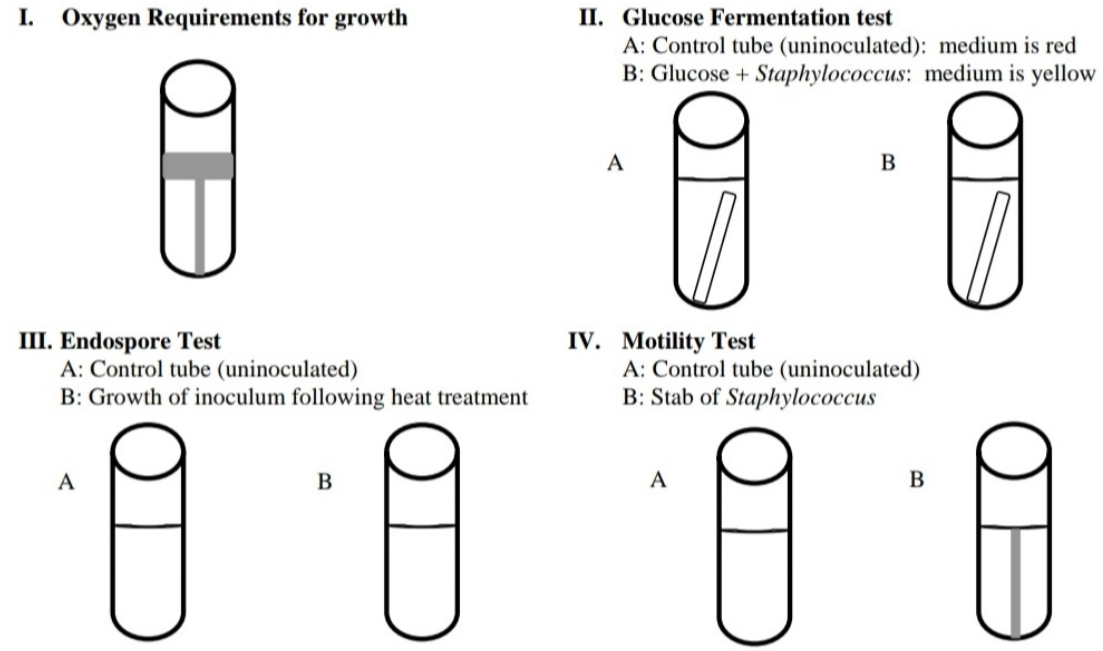

Appendix Figure A.22: Staphyloccoccus Test Results [68]

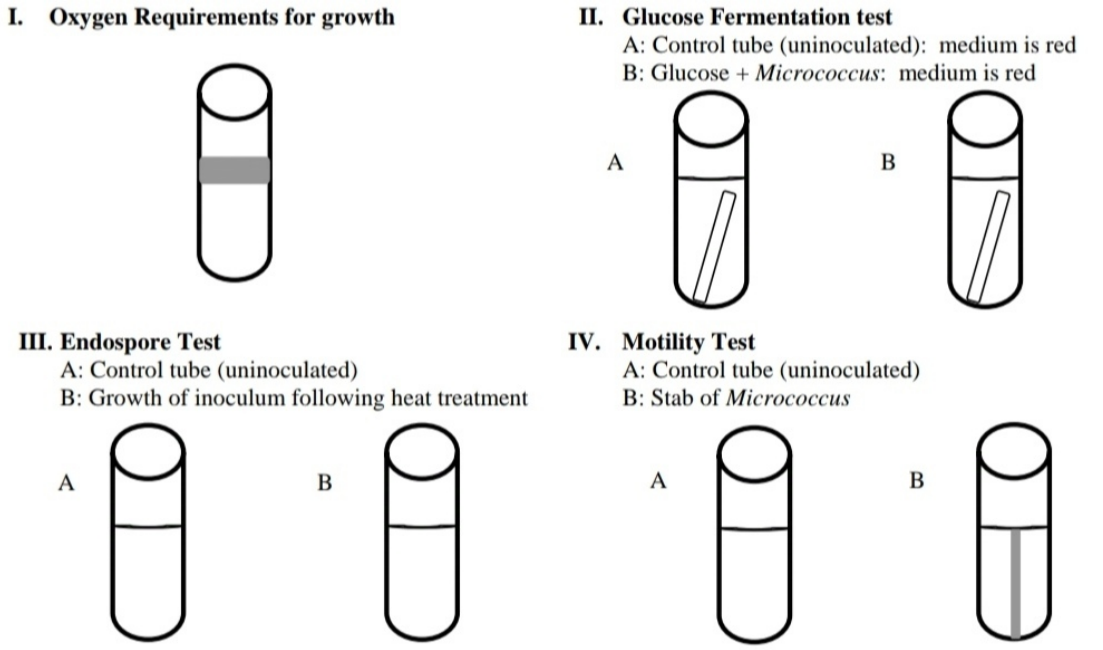

Appendix Figure A.23: Micrococcus Test Results [68]

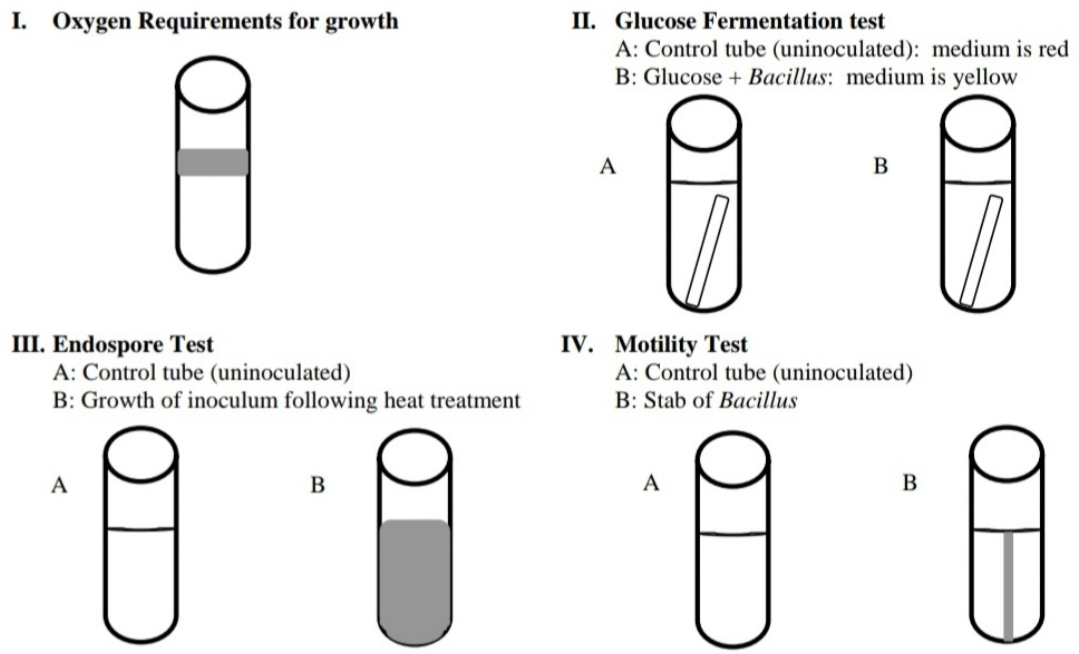

Appendix Figure A.24: Bacillus Test Results [68]

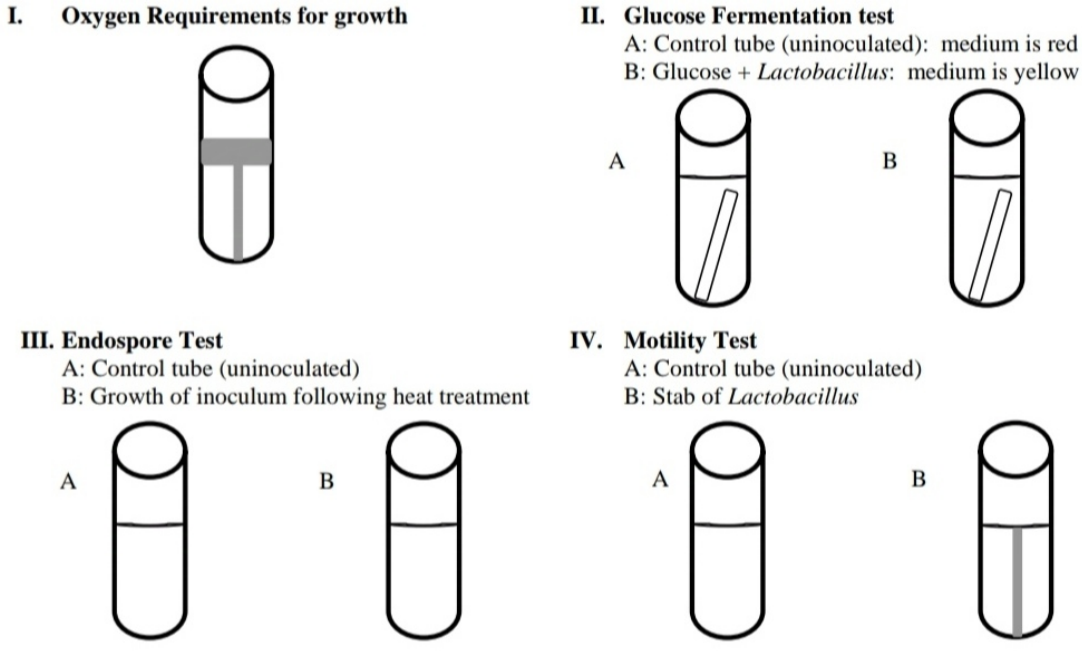

Appendix Figure A.25: Lactobacillus Test Results [68]

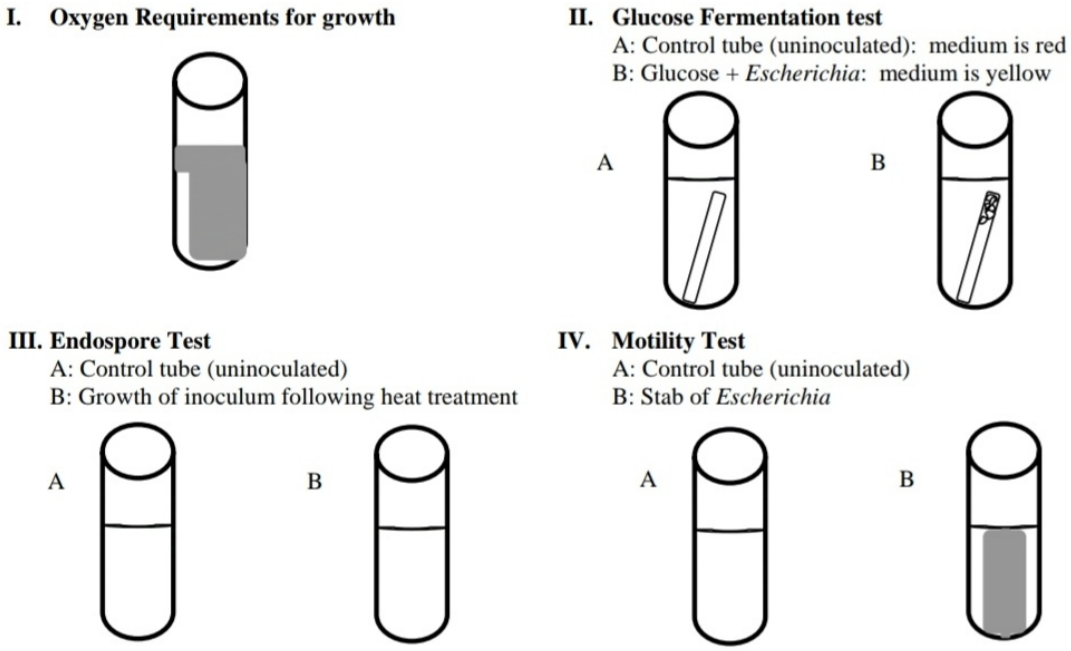

Appendix Figure A.26: Escherichia Test Results [68]

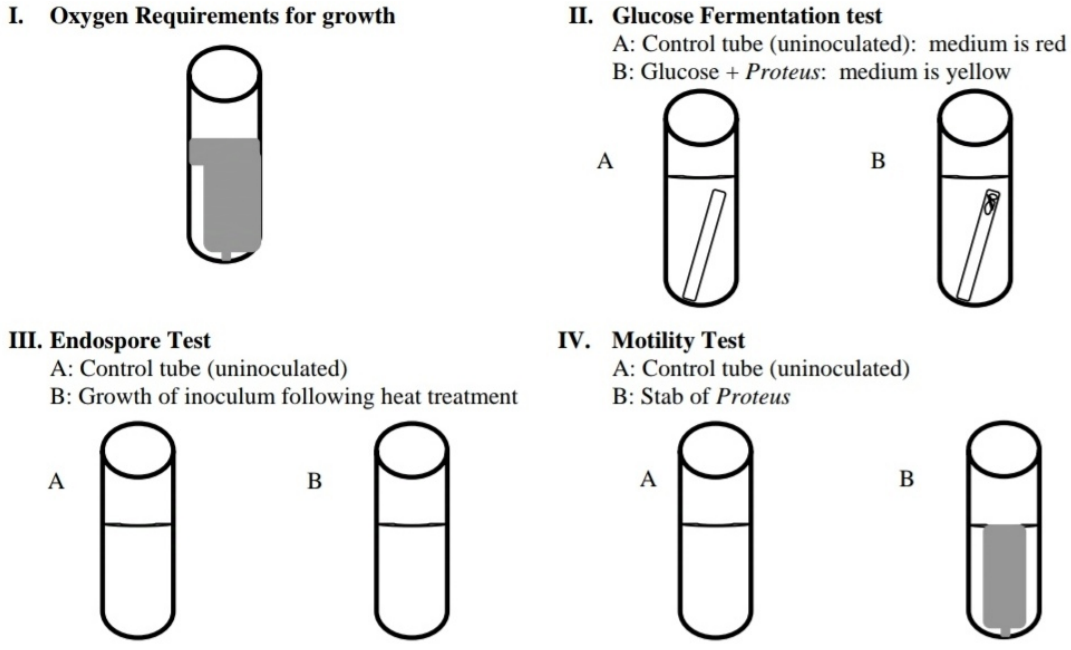

Appendix Figure A.27: Proteus Test Results [68]

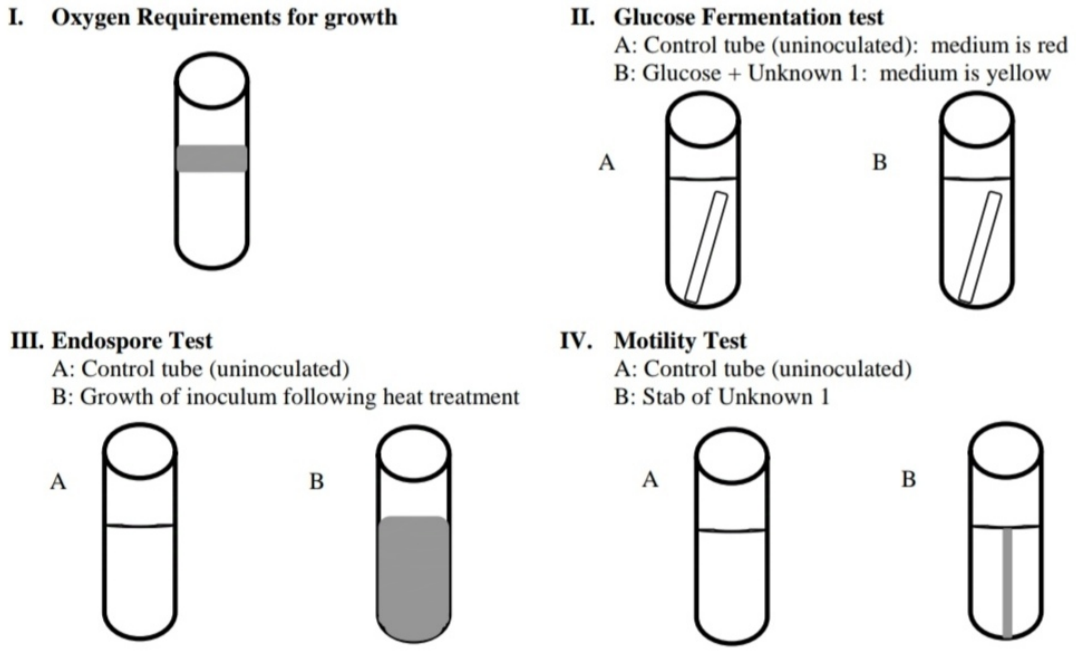

Appendix Figure A.28: Unknown 1 Test Results [68]

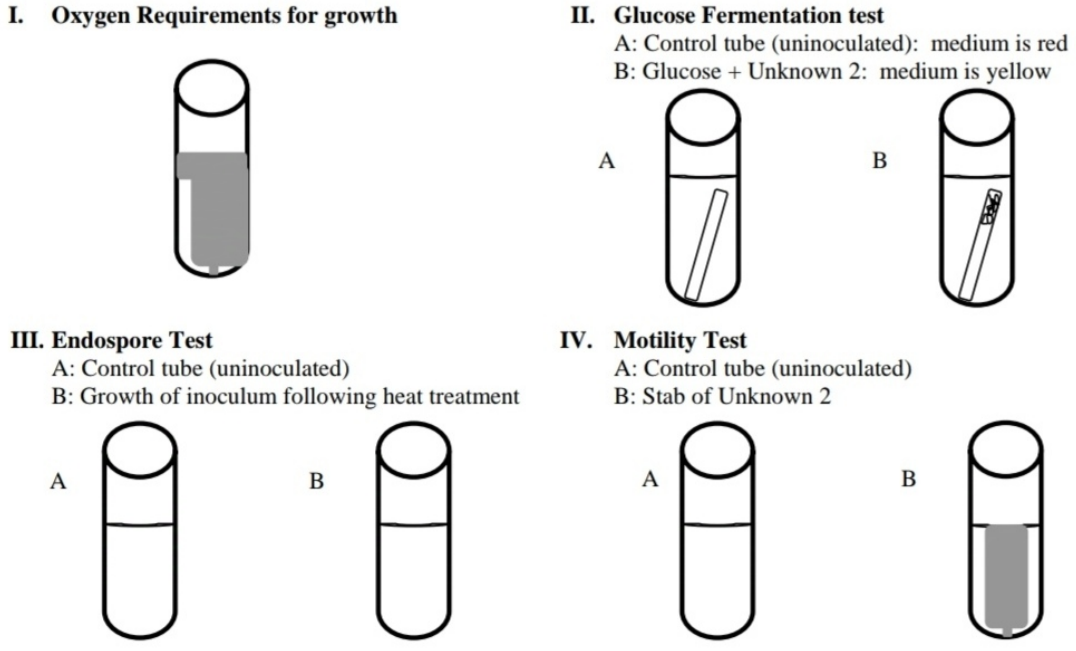

Appendix Figure A.29: Unknown 2 Test Results [68]

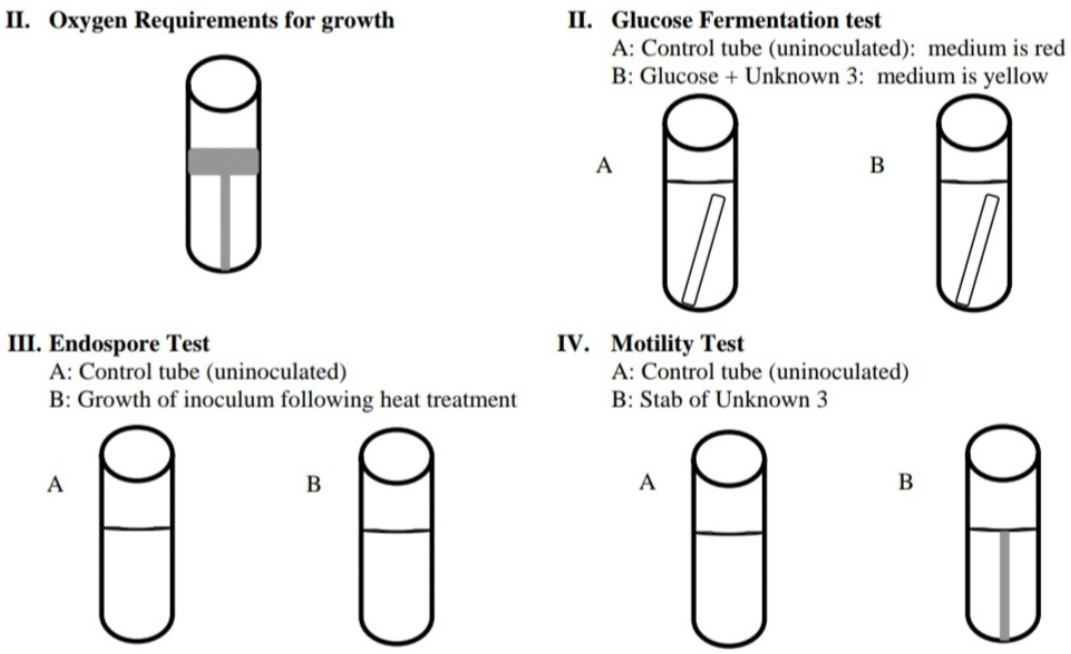

Appendix Figure A.30: Unknown 3 Test Results [68]

Appendix B

AD7745

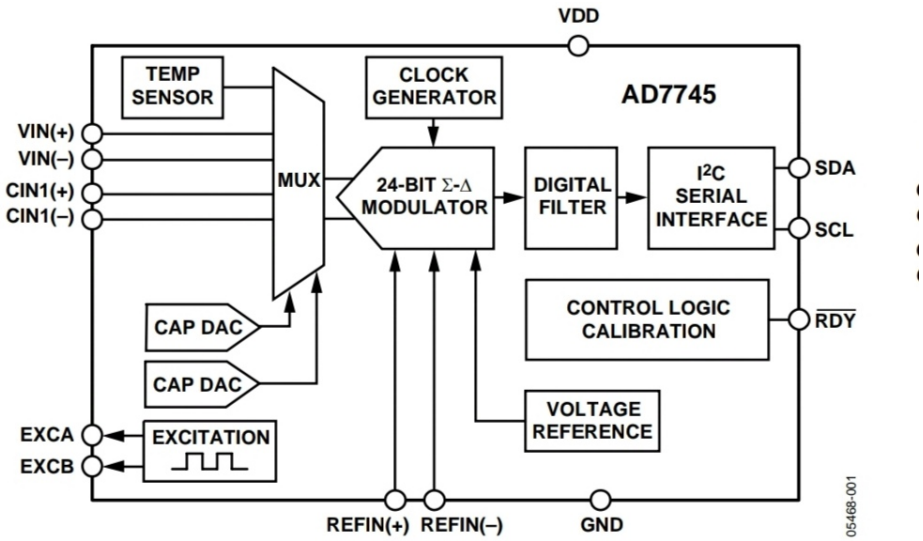

Appendix Figure B.1: Functional Block Diagram of AD7745 [19]

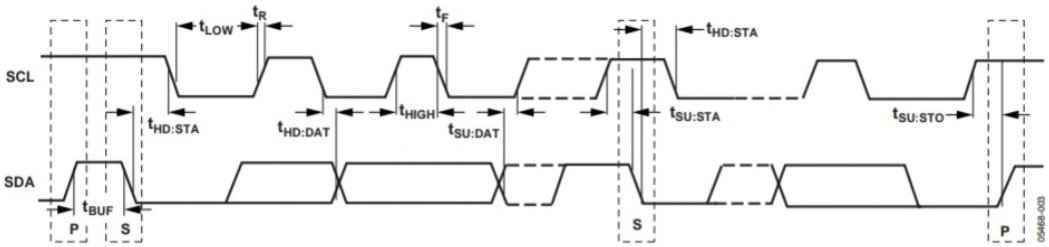

Appendix Figure B.2: Serial Interface Timing Diagram [19]

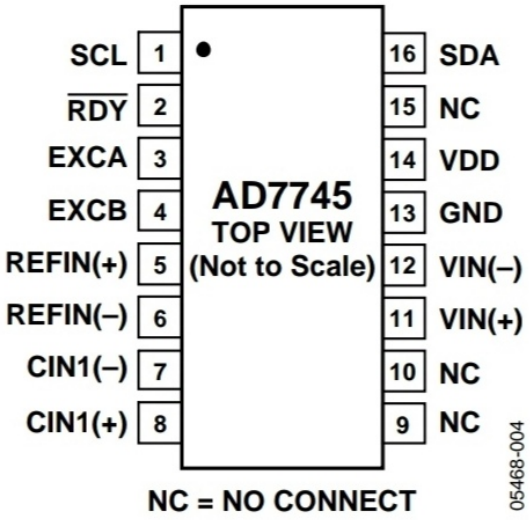

Appendix Figure B.3: AD7745 Pin Configuration (16-Lead TSSOP) [19]

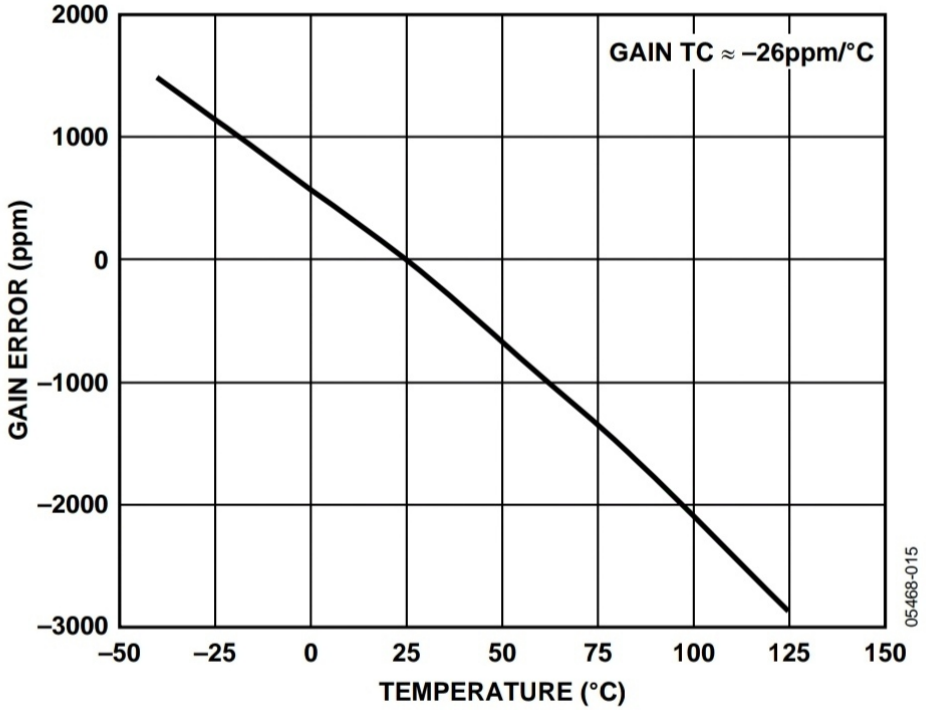

Appendix Figure B.4: Capacitance Input Offset Drift vs. Temperature, VDD = 5 V, CIN and EXC Pins Open Circuit [19]

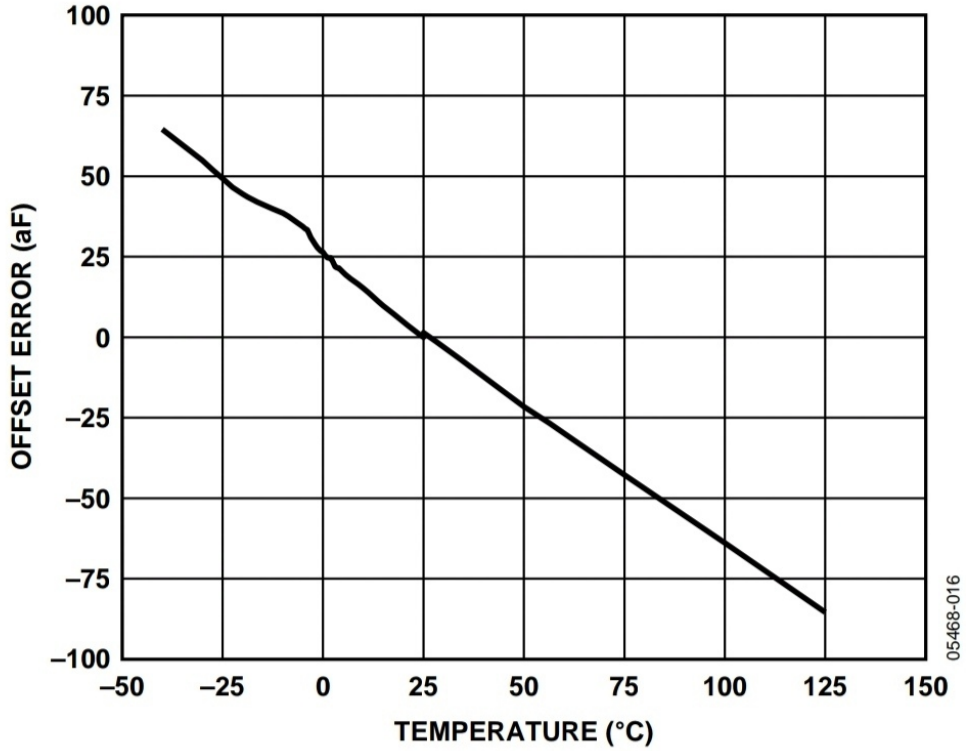

Appendix Figure B.5: Capacitance Input Gain Drift vs. Temperature, VDD = 5 V, CIN(+) to EXC = 4 pF [19]

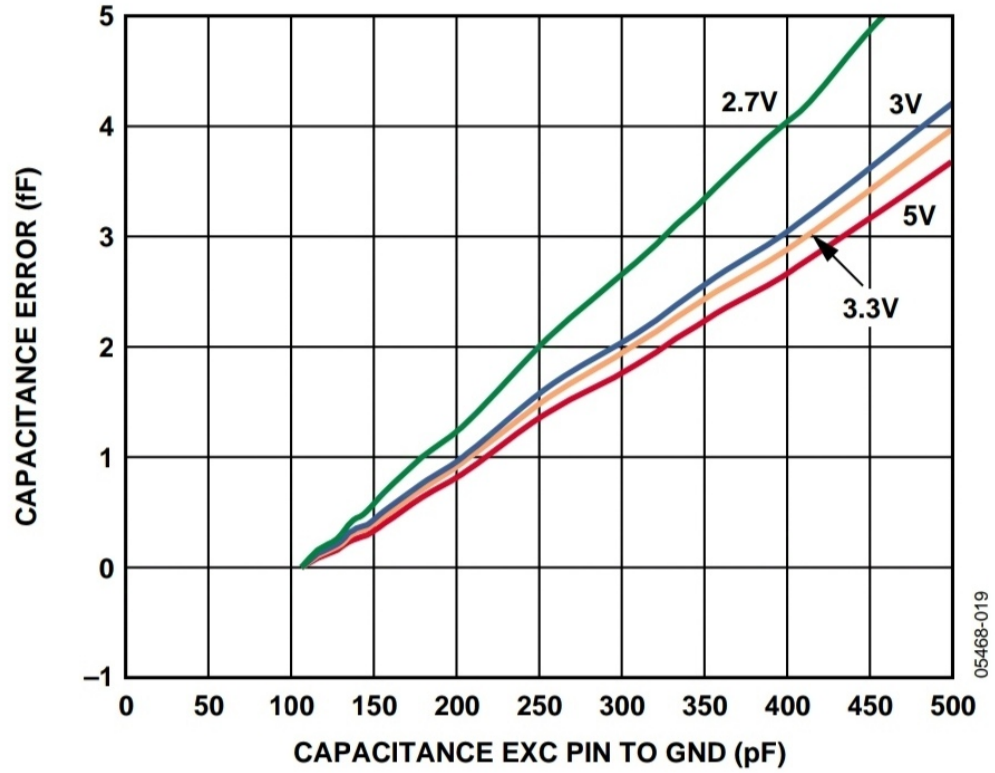

Appendix Figure B.6: Capacitance Input Error vs. Capacitance between EXC and GND, CIN(+) to EXC = 21 pF, CIN(–) to EXC = 23 pF, VDD = 2.7 V, 3 V, 3.3 V, and 5 V [19]

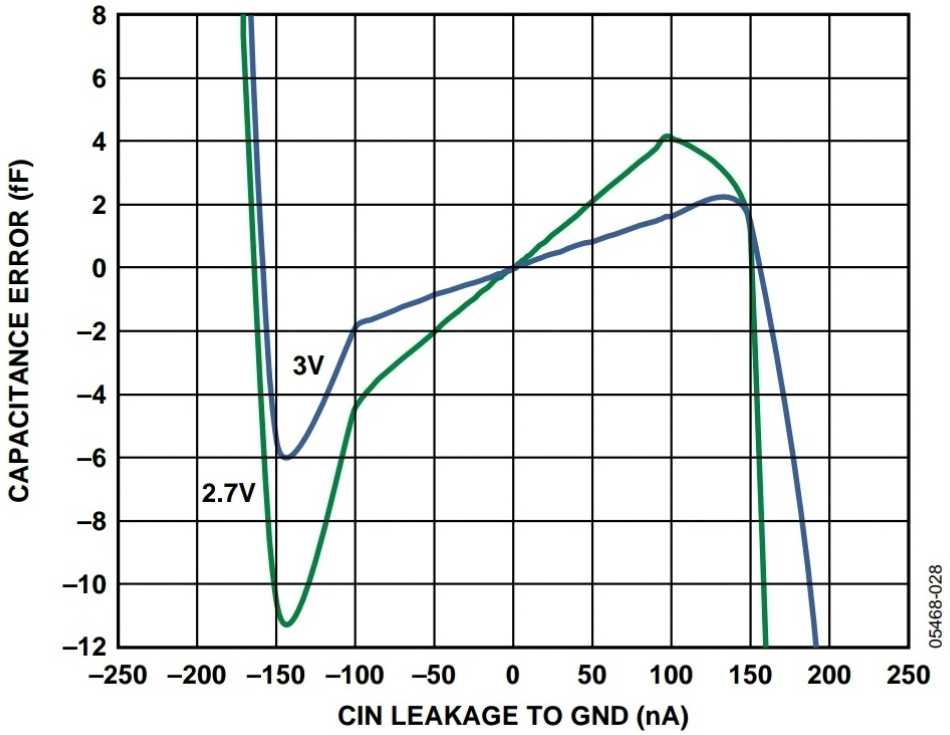

Appendix Figure B.7: Capacitance Input Error vs. Leakage Current to GND, CIN(+) to EXC = 4 pF, CIN(–) to EXC = 0 pF, VDD = 2.7 V and 3 V [19]

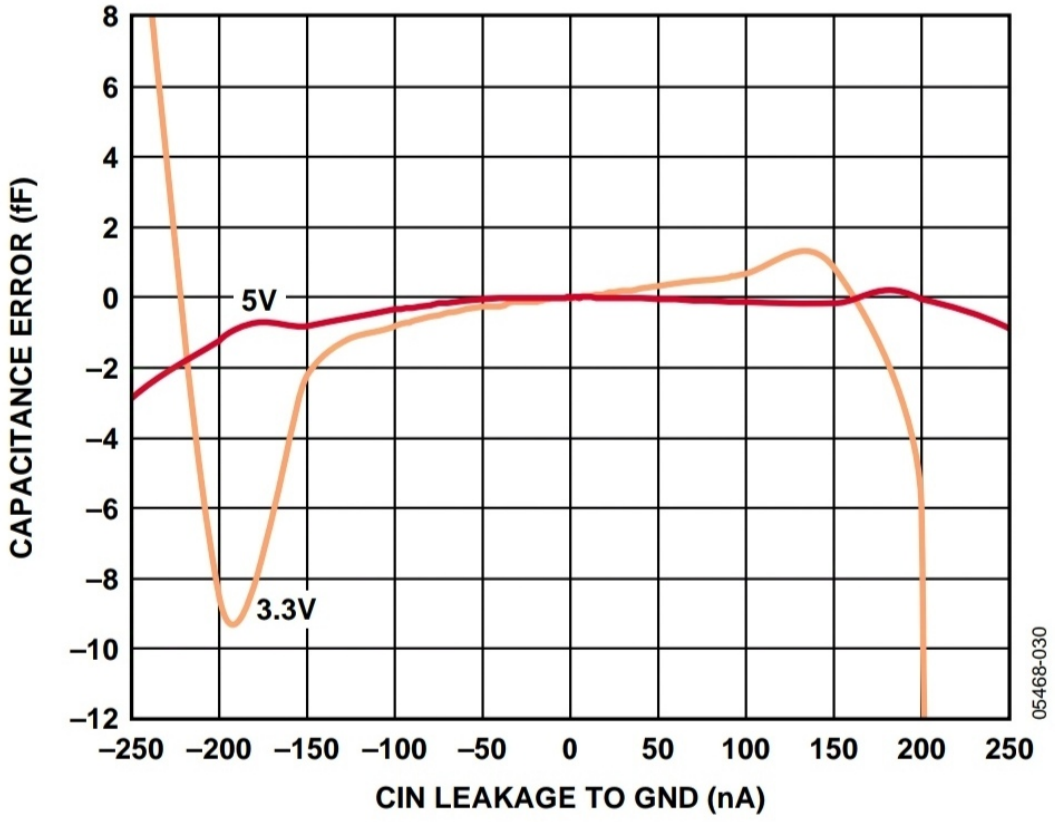

Appendix Figure B.8: Capacitance Input Error vs. Leakage Current to GND, CIN(+) to EXC =4 pF, CIN(–) to EXC = 0 pF, VDD=3.3 V and 5 V [19]

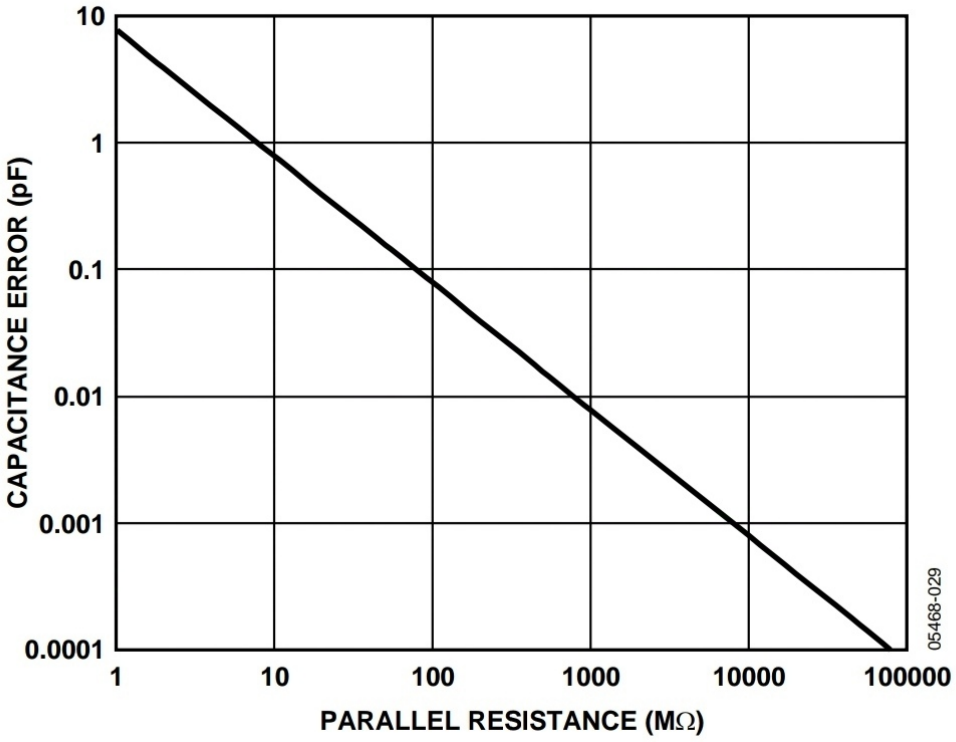

Appendix Figure B.9: Capacitance Input Error vs. Resistance in Parallel with Measured Capacitance [19]

Appendix Figure B.10: Capacitance Input Error vs. Serial Resistance, CIN(+) to EXC = 21 pF, CIN(−) to EXC = 23 pF, VDD = 5 V [19]

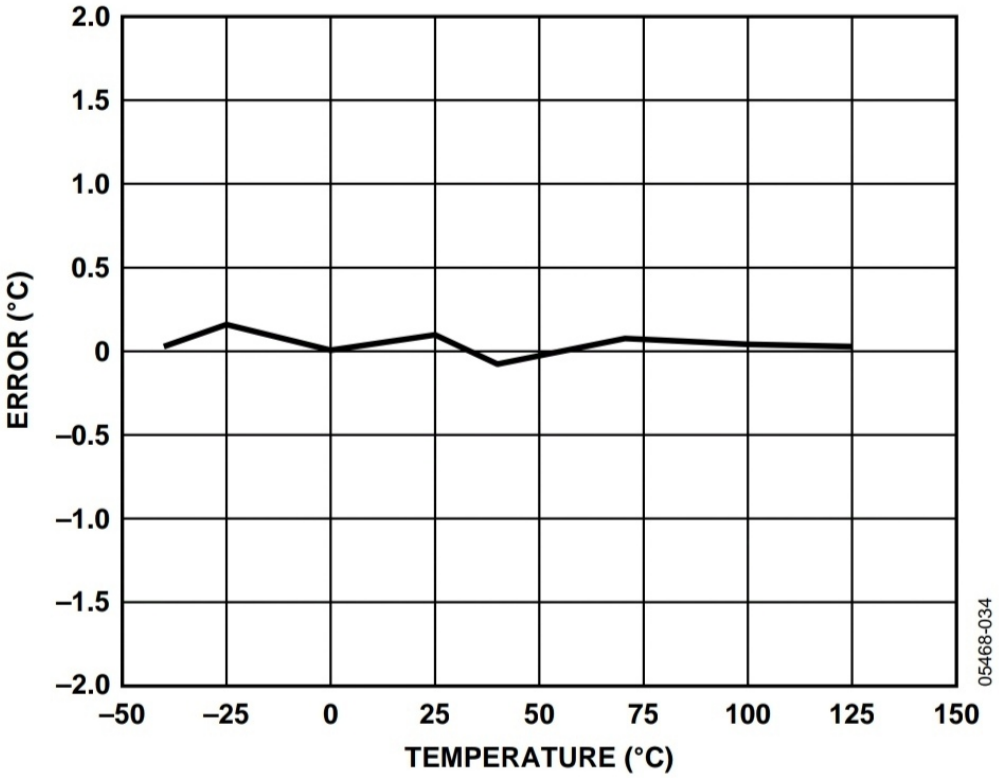

Appendix Figure B.11: Internal Temperature Sensor Error vs. Temperature [19]

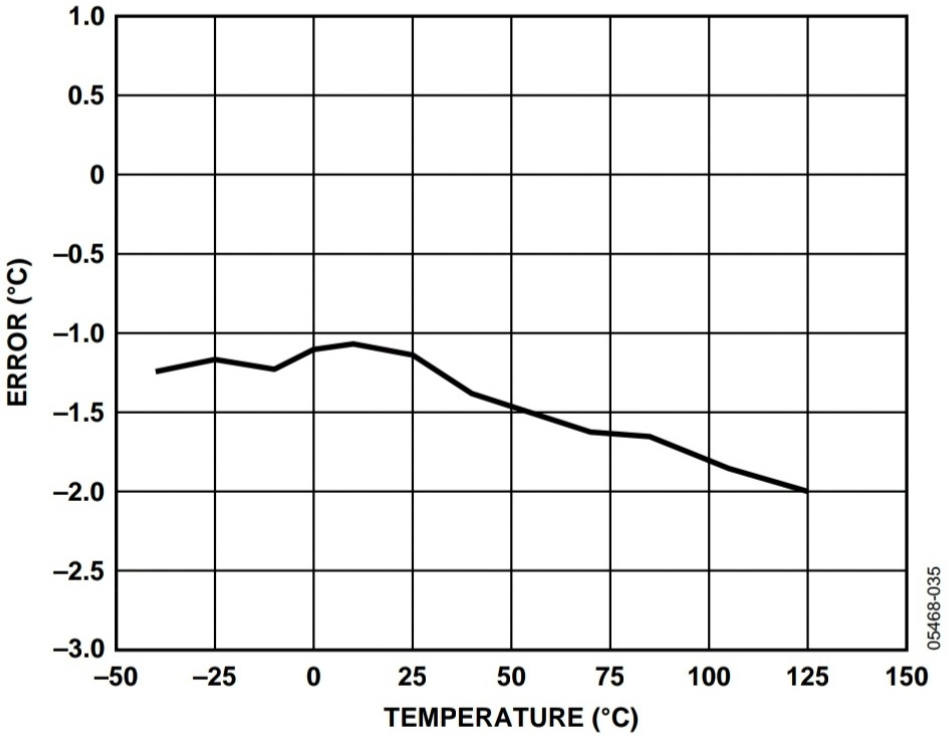

Appendix Figure B.12: External Temperature Sensor Error vs. Temperature [19]

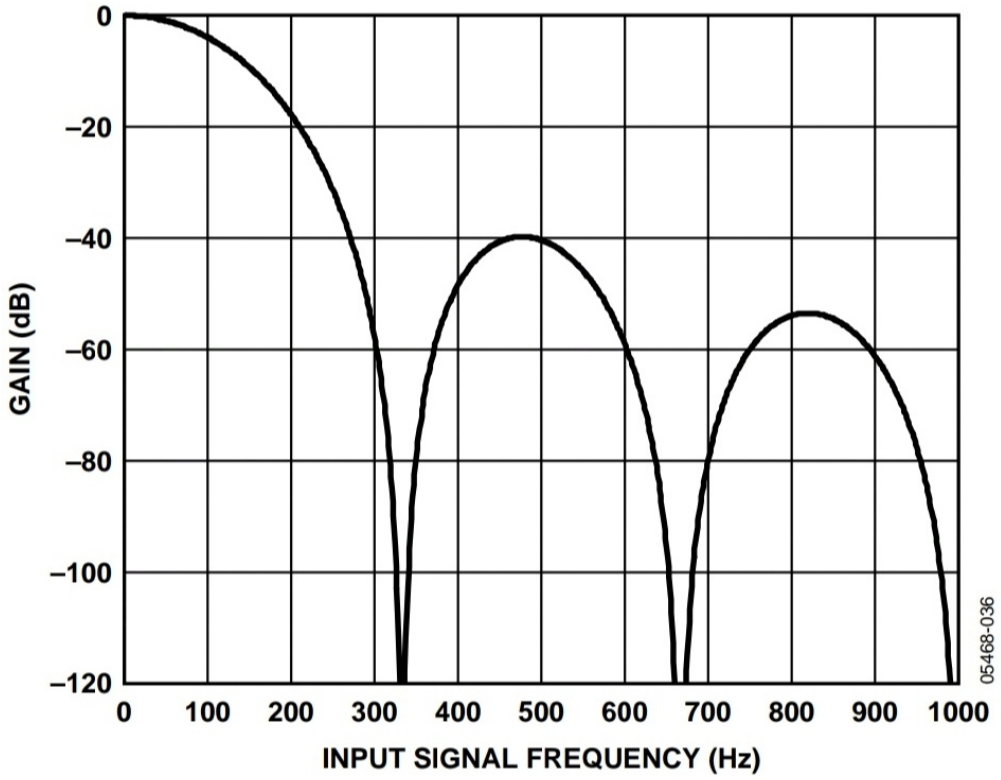

Appendix Figure B.13: Capacitance Channel Frequency Response, Conversion Time = 11 ms [19]

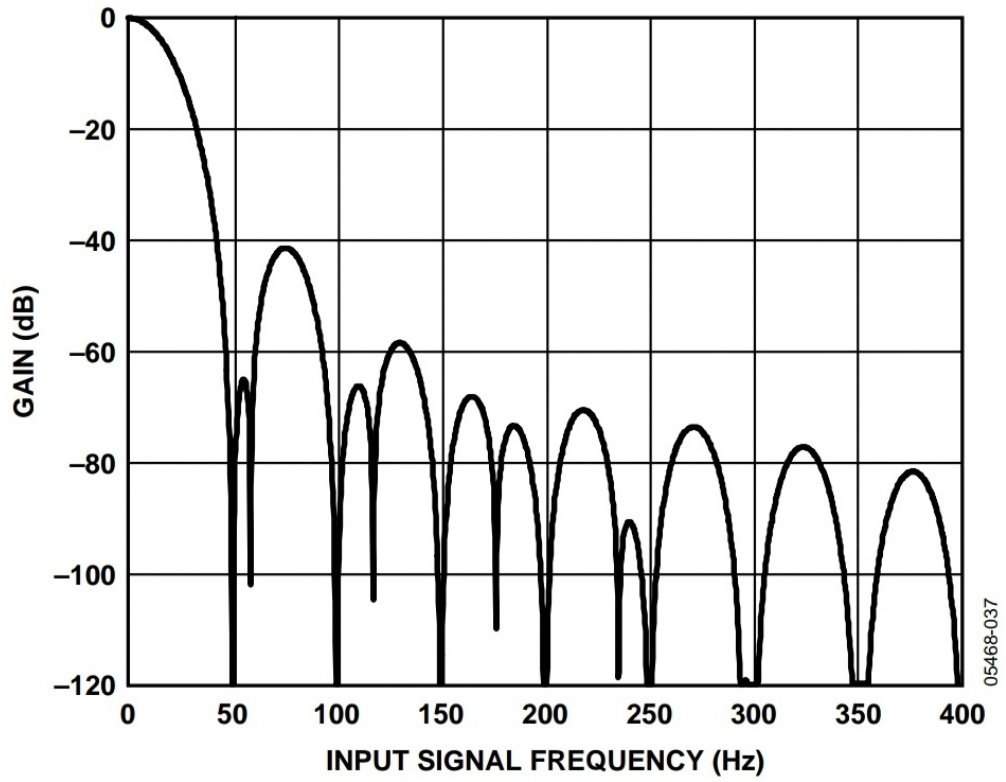

Appendix Figure B.14: Capacitance Channel Frequency Response, Conversion Time = 62 ms [19]

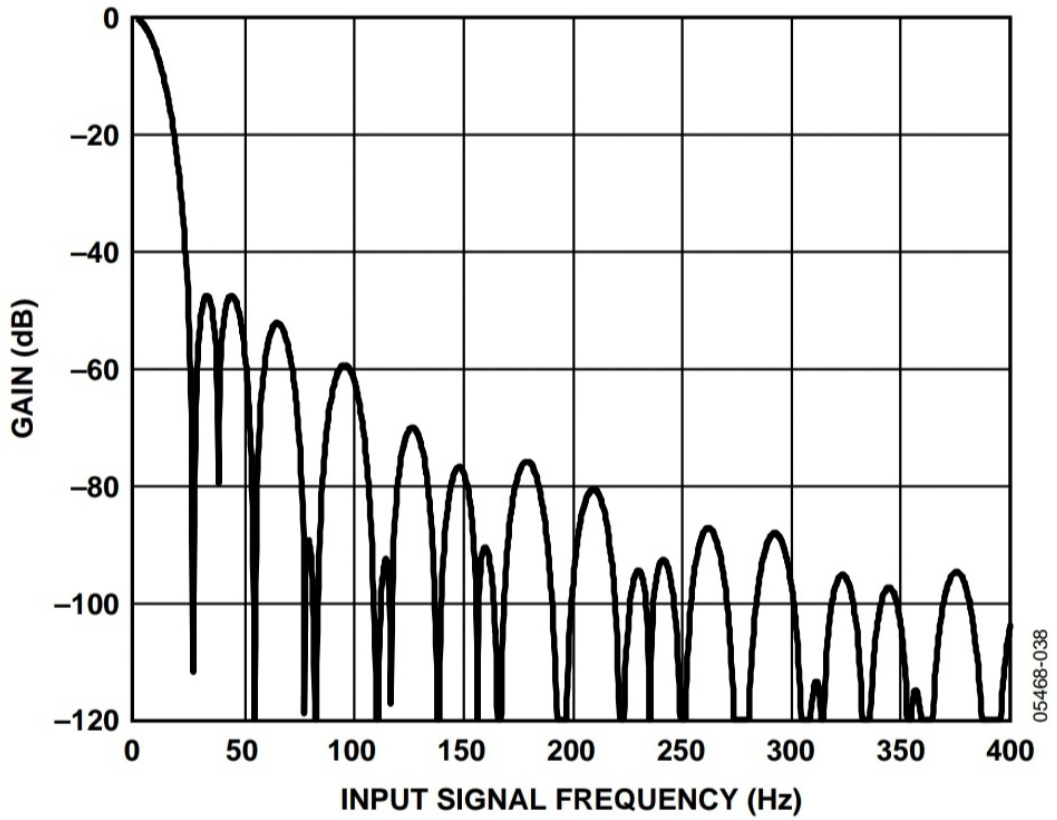

Appendix Figure B.15: Capacitance Channel Frequency Response, Conversion Time = 109.6 ms [19]

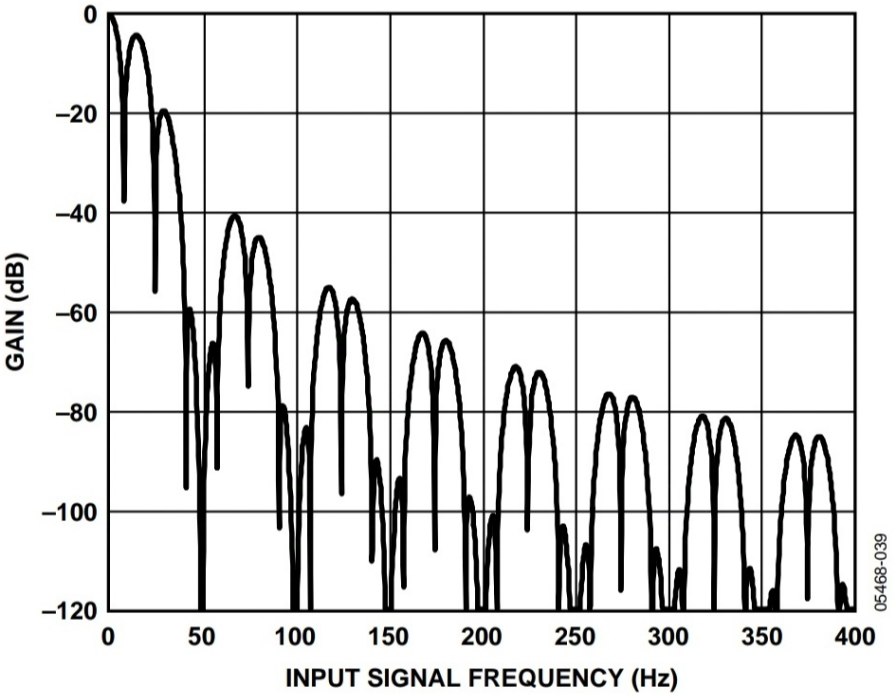

Appendix Figure B.16: Voltage Channel Frequency Response, Conversion Time = 122.1 ms [19]

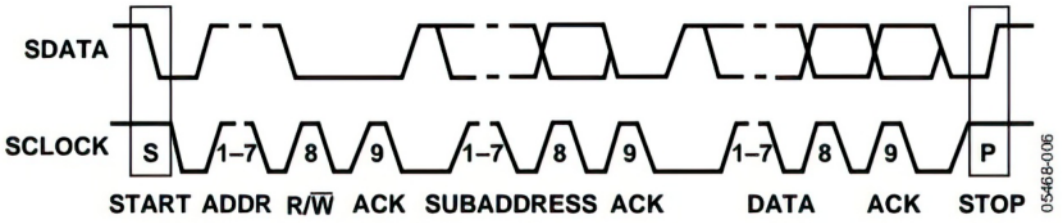

Appendix Figure B.17: Bus Data Transfer [19]

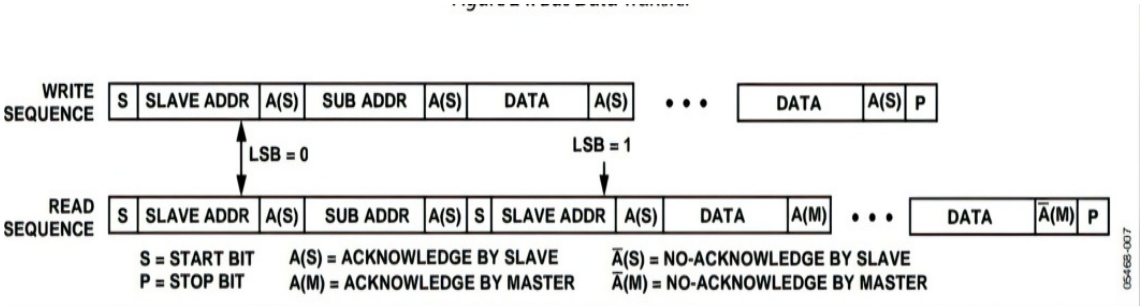

Appendix Figure B.18: Write and Read Sequences [19]

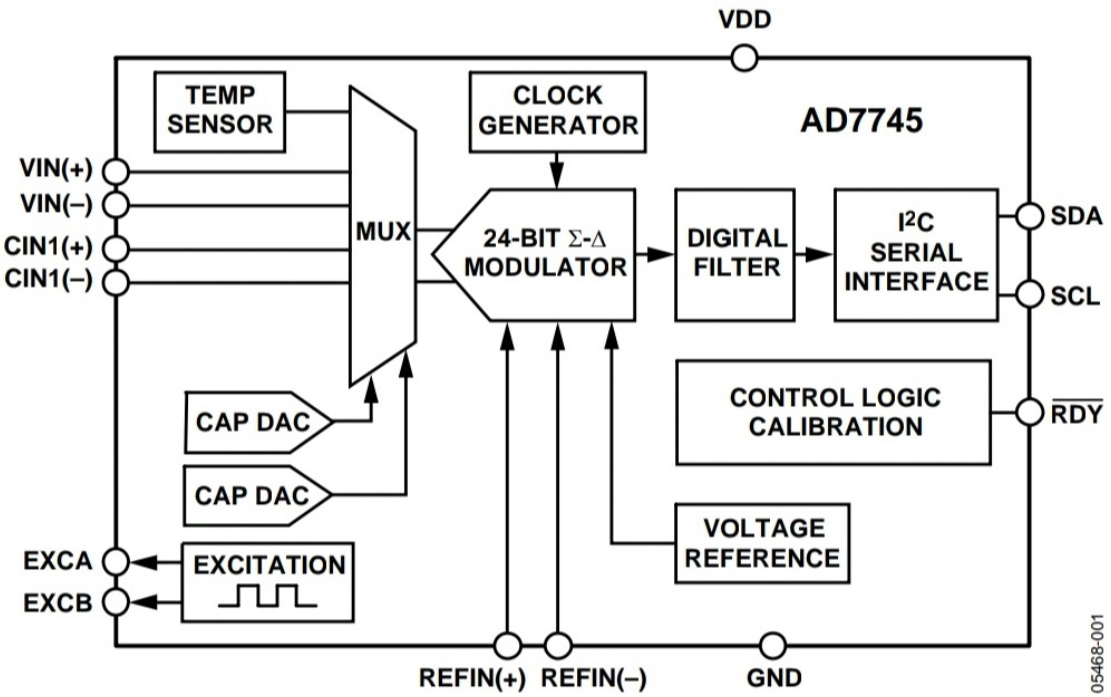

Appendix Figure B.19: AD7745 Block Diagram [19]

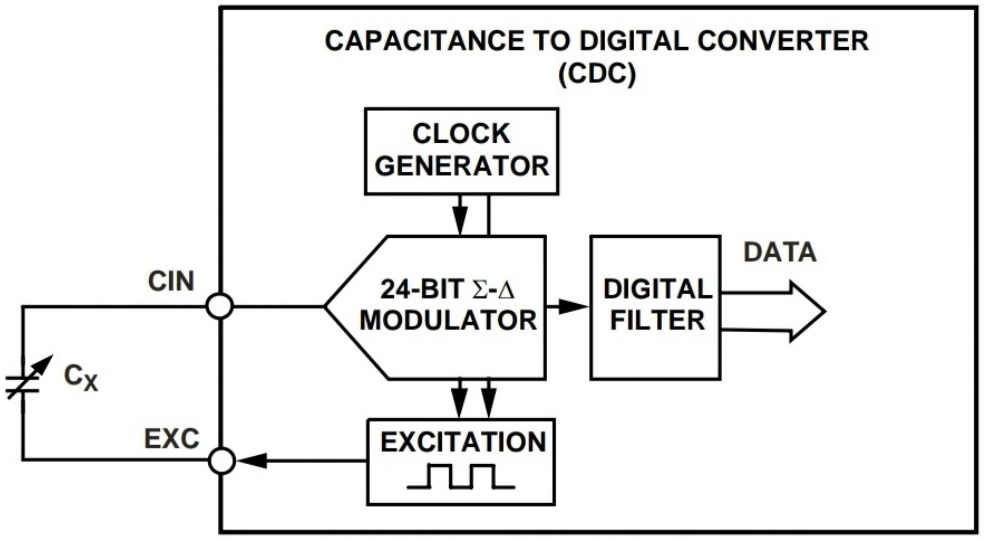

Appendix Figure B.20: CDC Simplified Block Diagram [19]

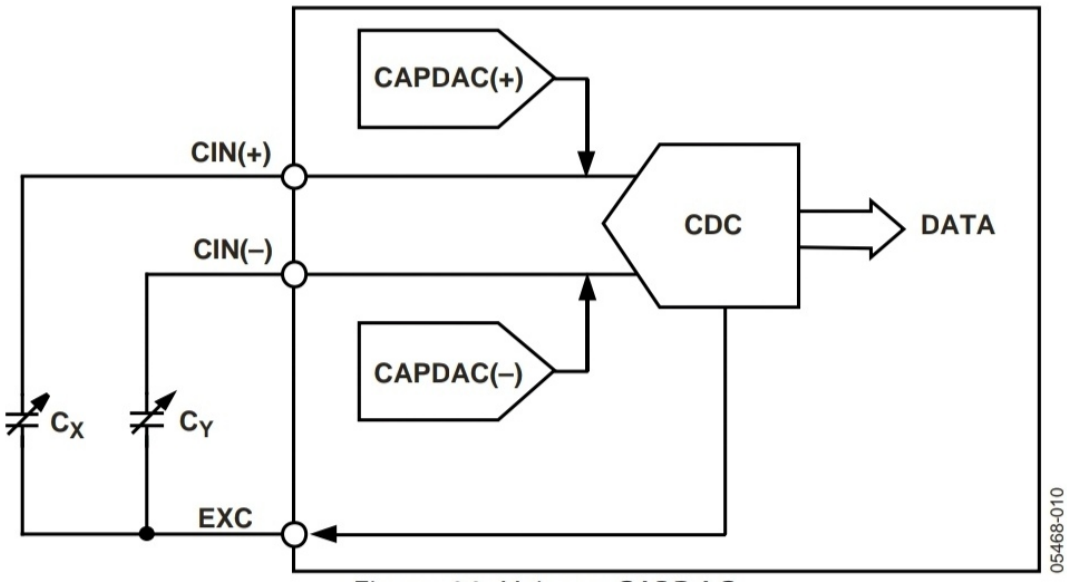

Appendix Figure B.21: Using a CAPDAC [19]

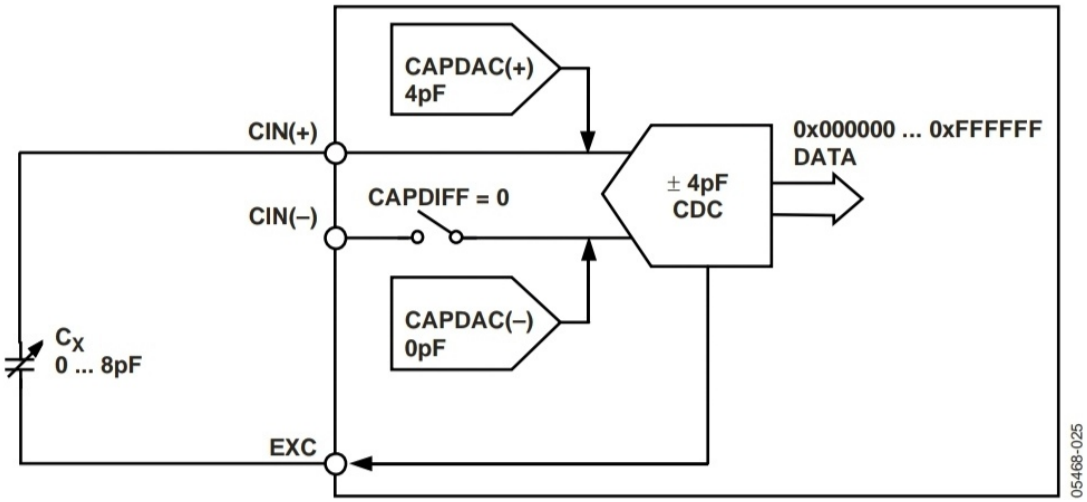

Appendix Figure B.22: Using CAPDAC in Single-Ended Mode (1) [19]

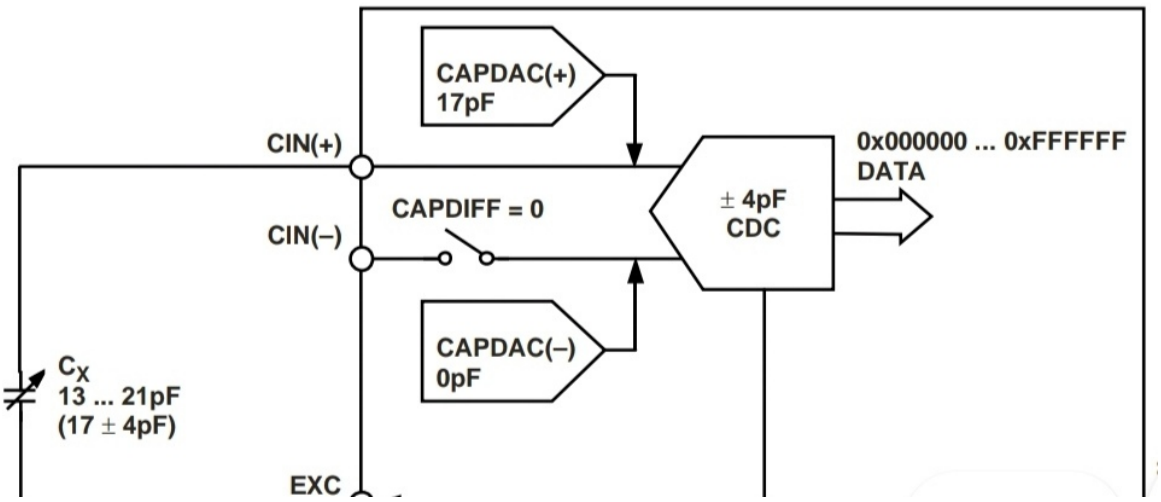

Appendix Figure B.23: Using CAPDAC in Single-Ended Mode (2) [19]

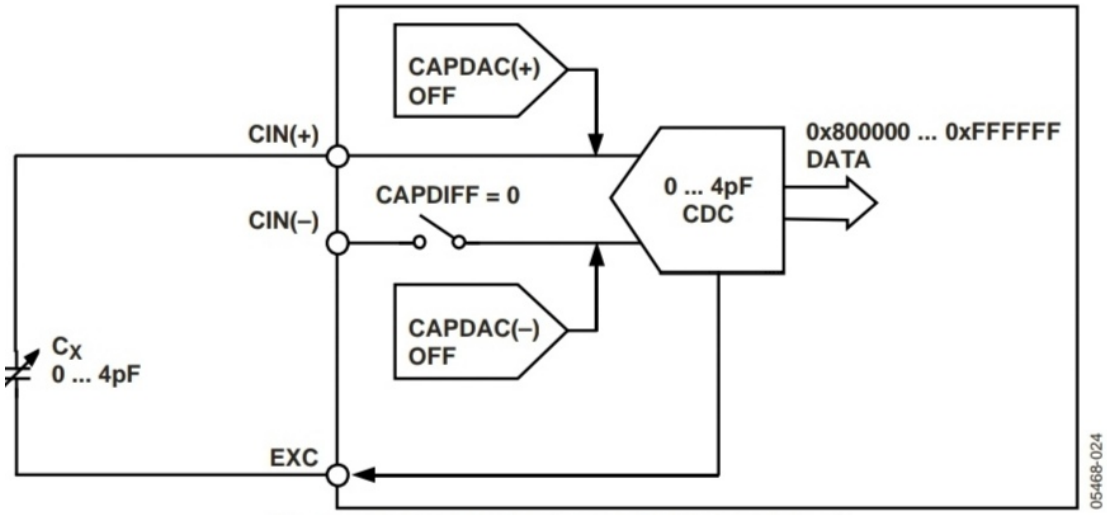

Appendix Figure B.24: CDC Single-Ended Input Mode [19]

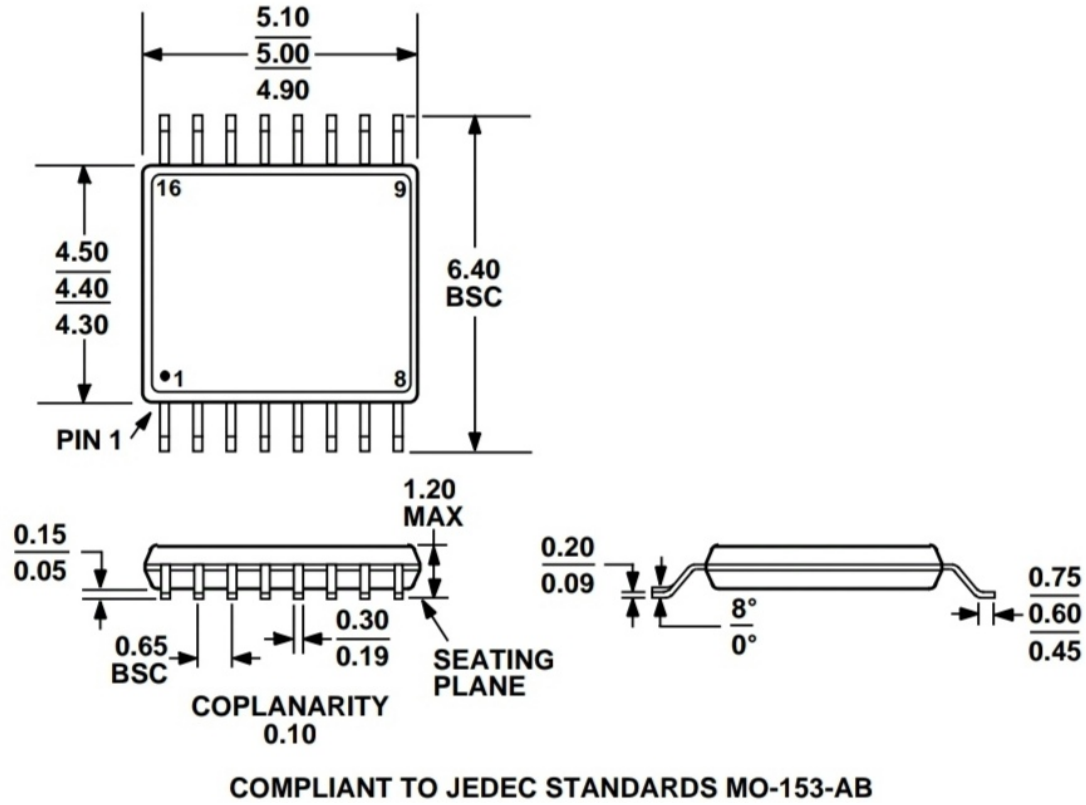

Appendix Figure B.25: 16-Lead Thin Shrink Small Outline Package (TSSOP) (RU-16) Dimensions shown in millimeters [19]

Appendix C

INTERDIGITATED/INTERDIGITAL ELECTRODES

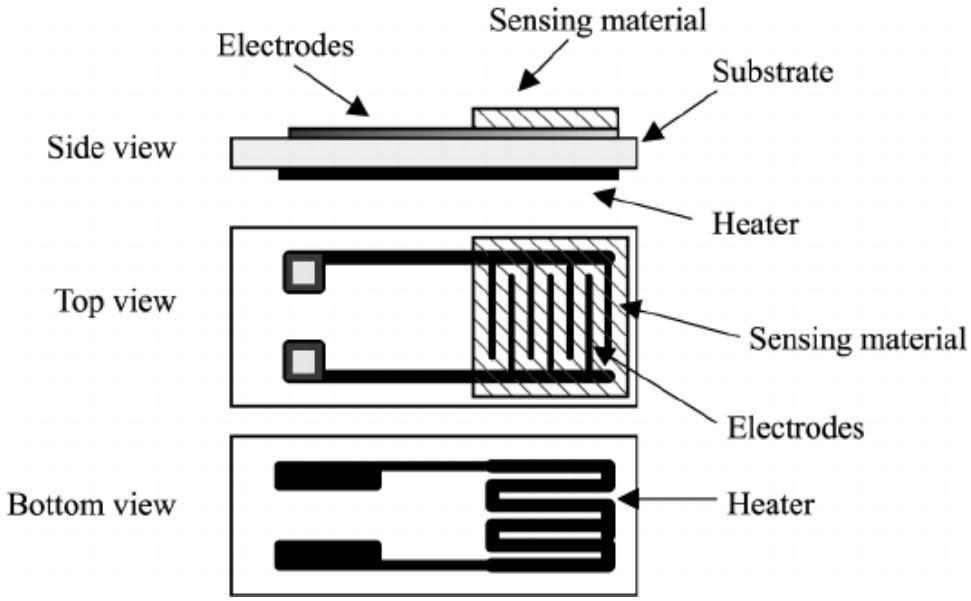

Appendix Figure C.1: Typical structure of a conductivity sensor interdigitated electrodes [66]

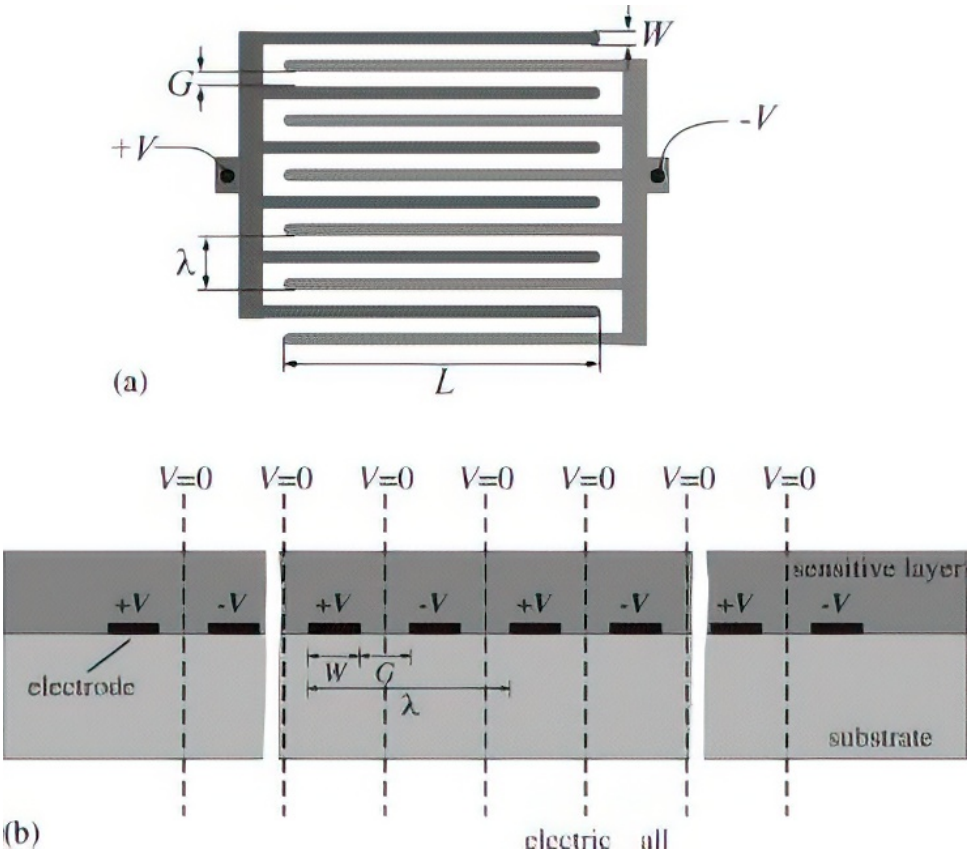

Appendix Figure C.2: (a) Layout of electrode plane, (b) Cross-section of a periodic IDC-S showing the electric potential boundary planes distribution [67]

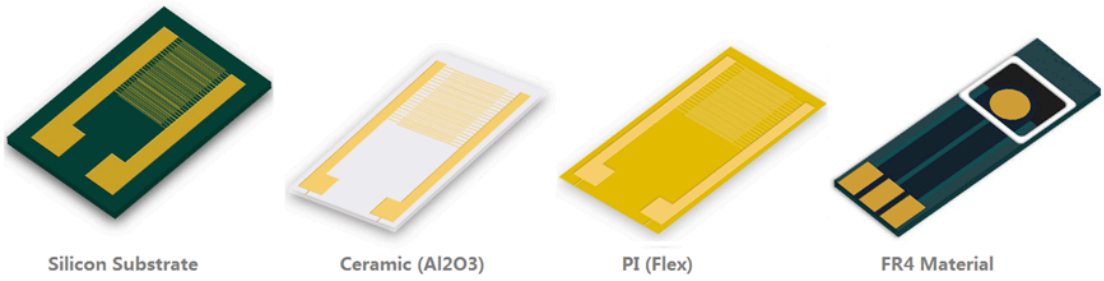

Appendix Figure C.3: Different types of electrodes
Source: Panda PCB / Products / Interdigital Electrodes (IDEs)

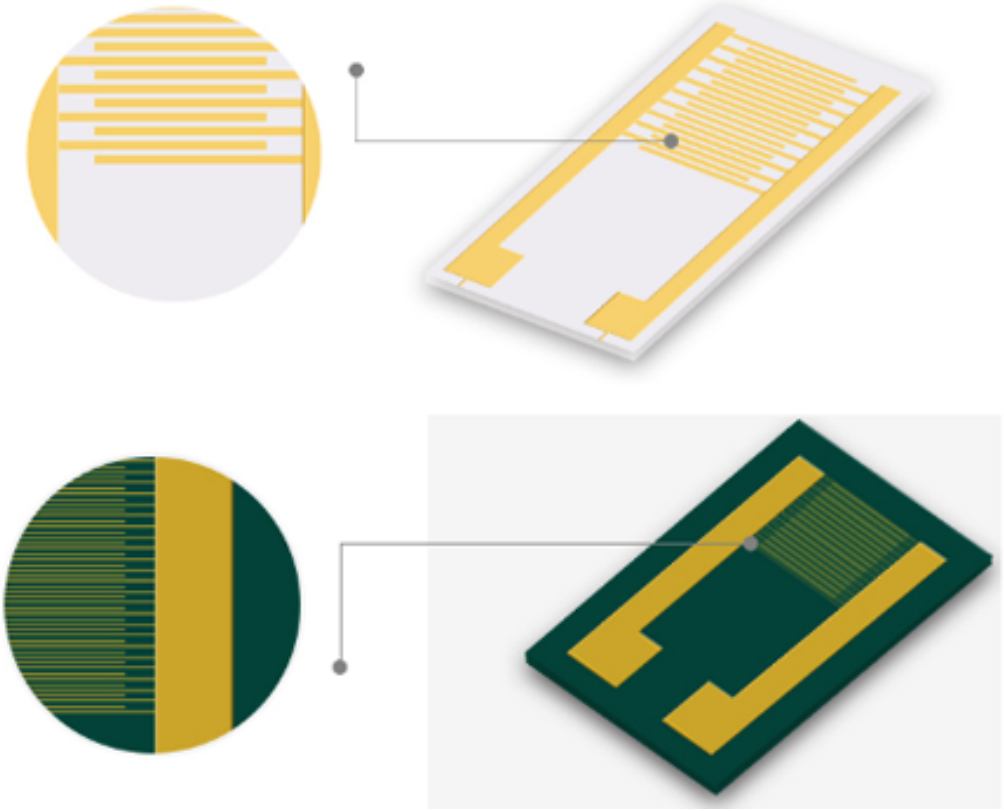

Appendix Figure C.4: A magnifying view of 2 types of electrodes shown in figure C.3
Source: Panda PCB / Products / Interdigital Electrodes (IDEs)

Appendix D

ESP32 CODE USED FOR PROGRAMMING THE MICROCONTROLLER OF THE CIRCUIT

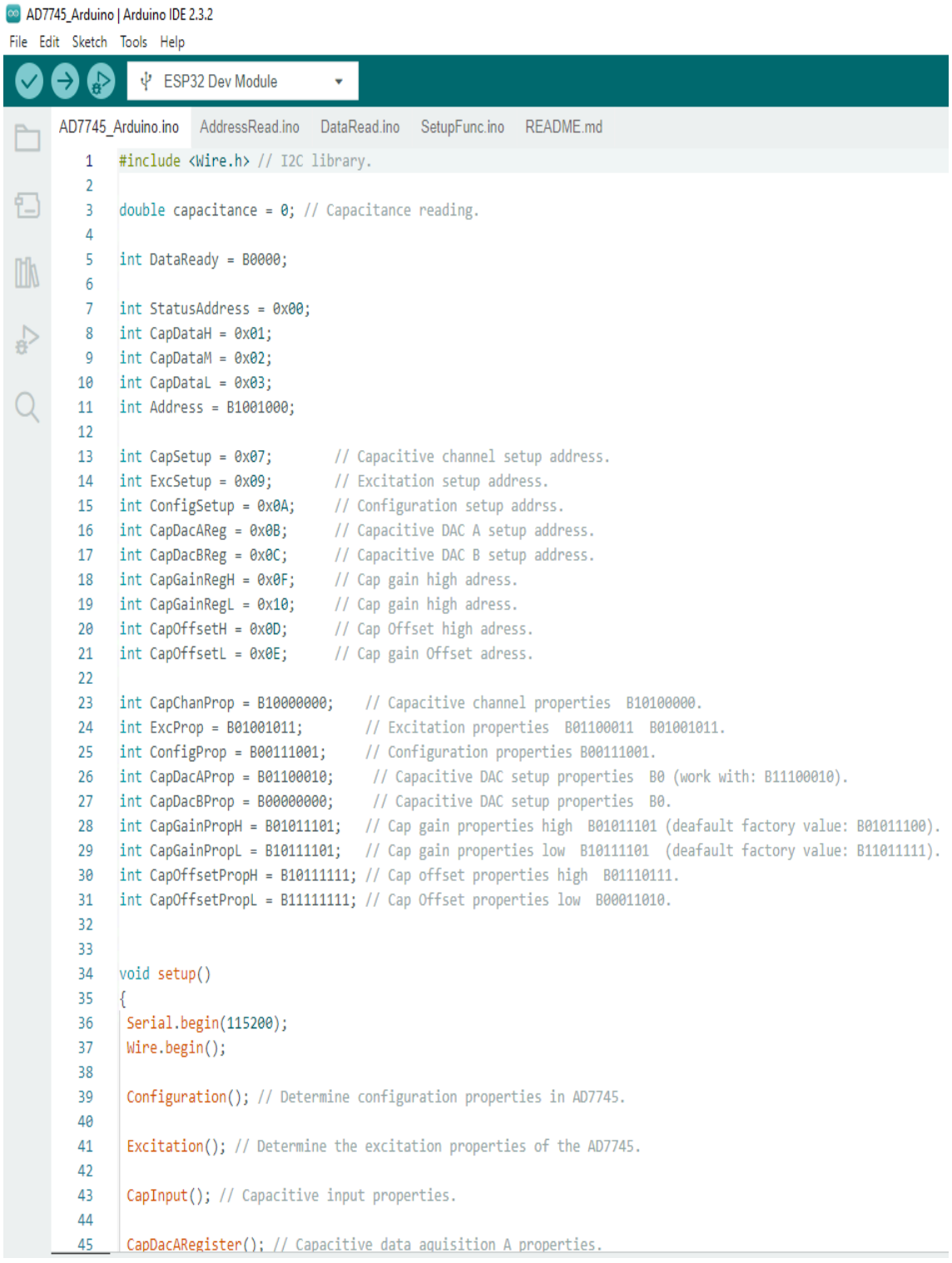

Appendix Figure D.1: Main code, part 1

Appendix Figure D.2: Main code, part 2

Appendix Figure D.3: Code used for debugging, part 1

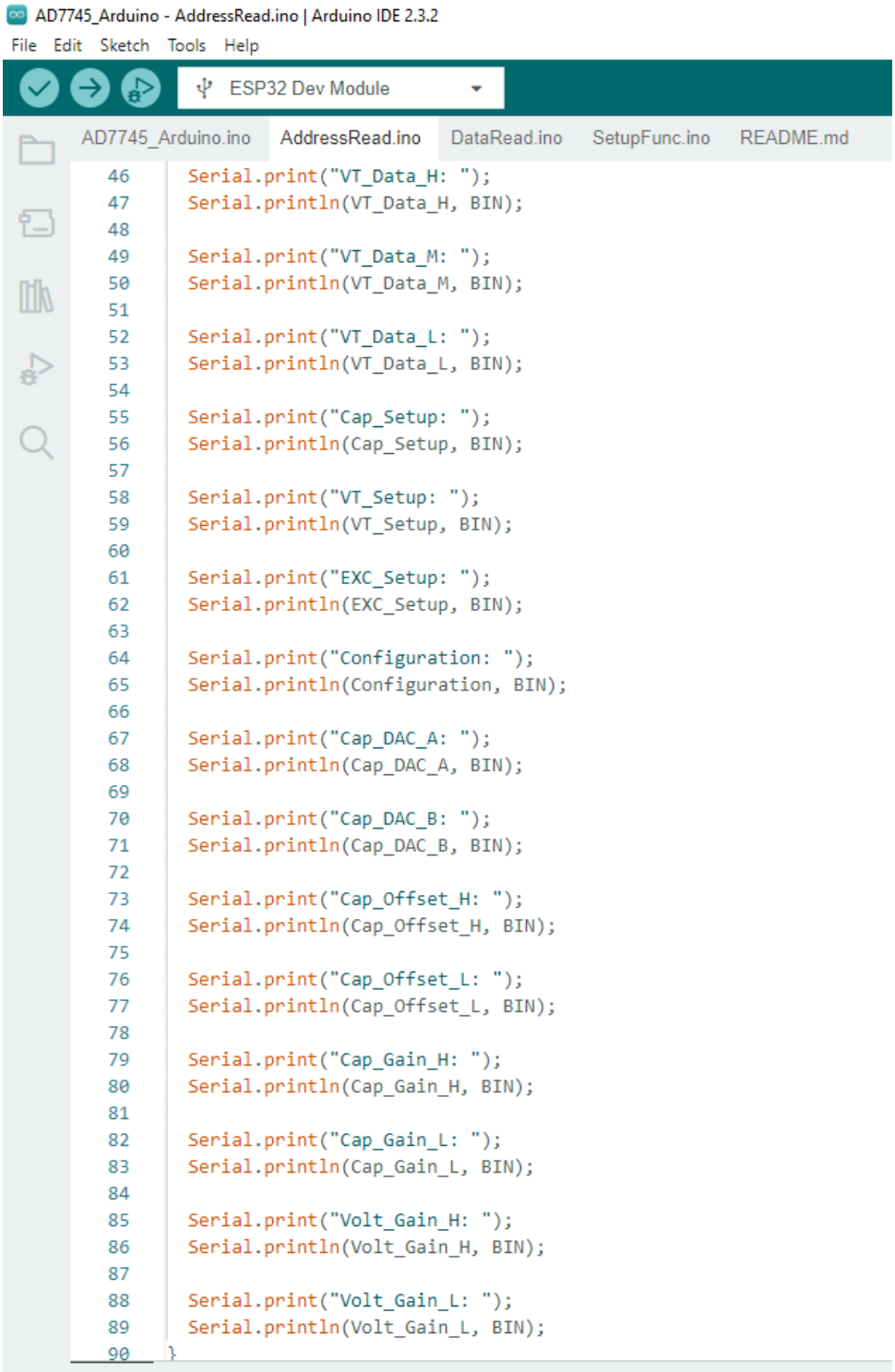

Appendix Figure D.4: Code used for debugging, part 2

Appendix Figure D.5: Code used for debugging, part 3

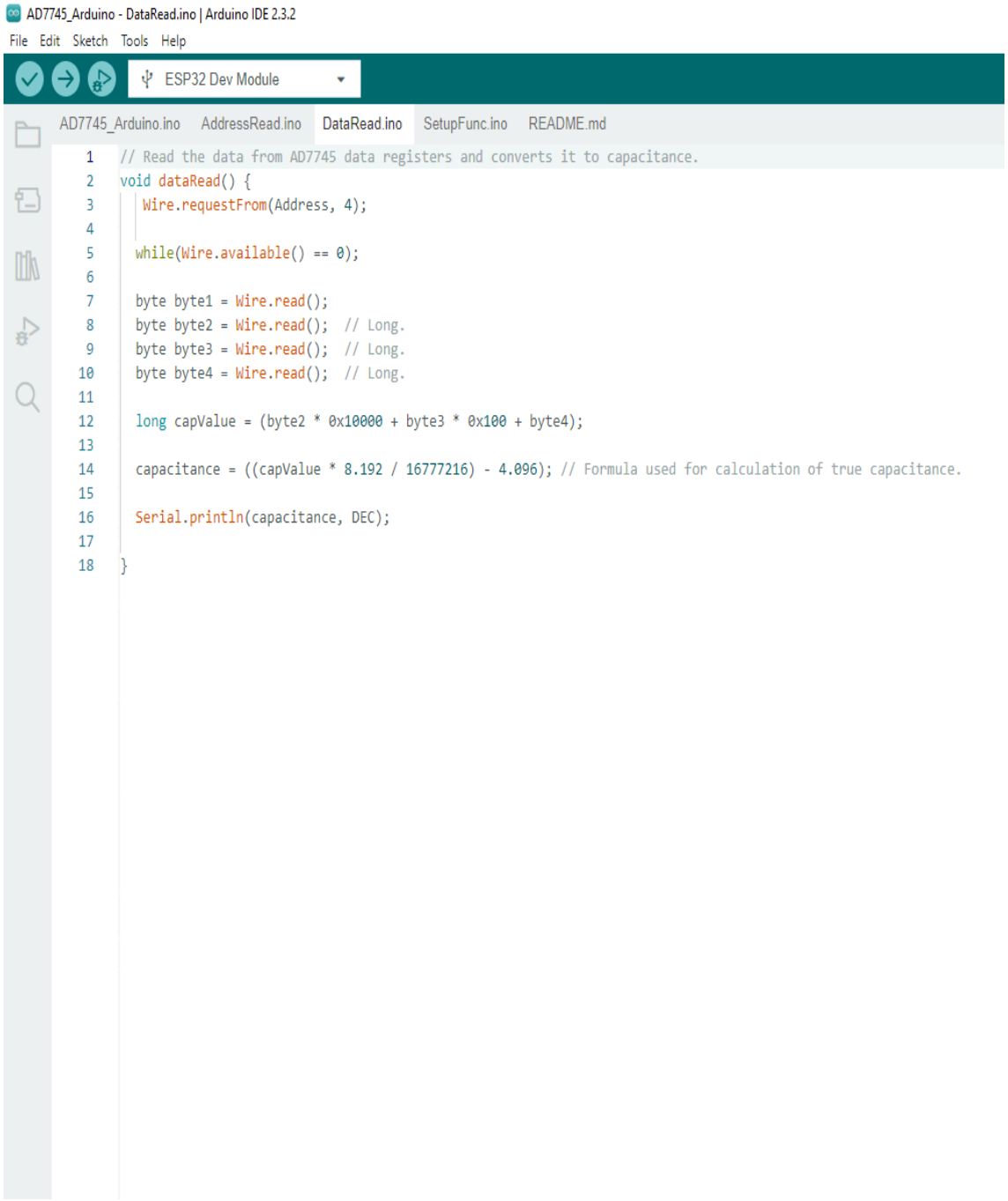

Appendix Figure D.6: Code that reads the data and converts it to capacitance

Appendix Figure D.7: Code with the setup function, part 1

Appendix Figure D.8: Code with the setup function, part 2

Appendix Figure D.9: Code with the setup function, part 3

Appendix E

MATLAB CODE USED FOR GRAPHS IN CHAPTER 7

```
% Time values (X-axis) from 11 ms to 187 ms at 11 ms intervals
time_values = 11:11:187;

% Capacitance values (Z-axis) for Escherichia coli
capacitance_values = [0.6373505859, 0.6373505859, 0.6373505859, 0.6373505859, ...
                      0.6373505859, 0.6373505859, 0.6373505859, 0.6373505859, ...
                      0.6373505859, 0.6373505859, 0.6373505859, 0.6373505859, ...
                      0.6373505859, 0.6373505859, 0.6373505859, 0.6373505859, ...
                      0.6373505859];

% Create a 3D scatter plot with color-coded points
figure;
scatter3(time_values, zeros(size(time_values)), capacitance_values, 36, capacitance_values, 'filled');
colormap(jet);  % Use a jet color map ranging from blue to red
colorbar;

% Set the color axis manually to provide some range if values are constant
constant_value = capacitance_values(1);
caxis([constant_value - 0.01, constant_value + 0.01]);  % Providing a small artificial range

% Enhance the plot
xlabel('Time (ms)');
ylabel('Dummy Y-Axis (Constant)');
zlabel('Capacitance (pF)');
title('3D Scatter Plot of Capacitance over Time for Escherichia coli');
grid on;
```

Appendix Figure E.1: MatLab code developed for *Escherichia Coli* plot

```
% Time values (X-axis) from 11 ms to 539 ms at 11 ms intervals
time_values = 11:11:539;

% Capacitance values (Z-axis) for Proteus mirabilis
capacitance_values = [0.9684599609, 0.9684599609, 0.9684599609, 0.9684599609, ...
                      0.9684599609, 0.9684599609, 0.9684599609, 0.9684599609, ...
                      0.9684599609, 0.9684599609, 0.9684599609, 0.9684599609, ...
                      0.9684599609, 0.9684599609, 0.9669531250, 0.9669531250, ...
                      0.9669531250, 0.9669531250, 0.9669531250, 0.9669531250, ...
                      0.9669531250, 0.9669531250, 0.9669531250, 0.9669531250, ...
                      0.9669531250, 0.9669531250, 0.9669531250, 0.9669531250, ...
                      0.9669531250, 0.9669531250, 0.9669531250, 0.9669531250, ...
                      0.9669531250, 0.9669531250, 0.9669531250, 0.9669531250, ...
                      0.9669531250, 0.9669531250, 0.9669531250, 0.9669531250, ...
                      0.9669531250, 0.9669531250, 0.9669531250, 0.9669531250, ...
                      0.9669531250];

% Create a 3D scatter plot with color-coded points
figure;
scatter3(time_values, zeros(size(time_values)), capacitance_values, 36, capacitance_values, 'filled');
colormap(jet);  % Use a jet color map ranging from blue to red
colorbar;  % Adds a color scale
caxis([min(capacitance_values) max(capacitance_values)]);  % Set the color axis limits to match capacitance values

% Enhance the plot
xlabel('Time (ms)');
ylabel('Dummy Y-Axis (Constant)');
zlabel('Capacitance (pF)');
title('3D Scatter Plot of Capacitance over Time for Proteus mirabilis');
grid on;
```

Appendix Figure E.2: MatLab code developed for *Proteus mirabilis* plot

```matlab
% Time values (X-axis) from 11 ms to 451 ms at 11 ms intervals
time_values = 11:11:451;

% Capacitance values (Z-axis)
capacitance_values = [1.0936015625, 1.0936015625, 1.0880063477, 1.1137465820, ...
                      1.0817465820, 1.0817465820, 1.0817465820, 1.0817465820, ...
                      1.0817465820, 1.0817465820, 1.0817465820, 1.0817465820, ...
                      1.0817465820, 1.0817465820, 1.0817465820, 1.0817465820, ...
                      1.0817465820, 1.0817465820, 1.0817465820, 1.0817465820, ...
                      1.0817465820, 1.0817465820, 1.0817465820, 1.0817465820, ...
                      1.0817465820, 1.0817465820, 1.0817465820, 1.0817465820, ...
                      1.0817465820, 1.0817465820, 1.0817465820, 1.0817465820, ...
                      1.0817465820, 1.0817465820, 1.0817465820, 1.0817465820, ...
                      1.0817465820, 1.0817465820, 1.0817465820, 1.0817465820, ...
                      1.0817465820];

% Create a 3D scatter plot with color-coded points
figure;
scatter3(time_values, zeros(size(time_values)), capacitance_values, 36, capacitance_values, 'filled');
colormap(jet);  % Use a jet color map ranging from blue to red
colorbar;  % Adds a color scale
caxis([min(capacitance_values) max(capacitance_values)]);  % Set the color axis limits to match capacitance values

% Enhance the plot
xlabel('Time (ms)');
ylabel('Dummy Y-Axis (Constant)');
zlabel('Capacitance (pF)');
title('3D Scatter Plot of Capacitance over Time with Heatmap Coloring for Pseudomonas aeruginosa');
grid on;
```

Appendix Figure E.3: MatLab code developed for *Pseudomonas aeruginosa* plot

```matlab
% Time values (X-axis)
time_values = 11:11:550;

% Capacitance values (Z-axis) for Staphylococcus aureus
capacitance_values = [3.8496347656, 3.8496347656, 3.8496347656, 3.8496347656, ...
                      3.8496347656, 3.8496347656, 3.8496347656, 3.8496347656, ...
                      3.8496347656, 3.8496347656, 3.8496347656, 3.8496347656, ...
                      3.8496347656, 3.8496347656, 3.8496347656, 3.8496347656, ...
                      3.8496347656, 3.8496347656, 3.8496347656, 3.8496347656, ...
                      3.8496347656, 3.8496347656, 3.8496347656, 3.8496347656, ...
                      3.8496347656, 3.8496347656, 3.8496347656, 3.8496347656, ...
                      3.8496347656, 3.8496347656, 3.8496347656, 3.8496347656, ...
                      3.8496347656, 3.8496347656, 3.8496347656, 3.8496347656, ...
                      3.8496347656, 3.8496347656, 3.8496347656, 3.8496347656, ...
                      3.8496347656, 3.8496347656, 3.8496347656, 3.8496347656, ...
                      3.8496347656, 3.8496347656, 3.8496347656, 3.8496347656, ...
                      3.8496347656, 3.8496347656];

% Create a 3D scatter plot with color-coded points
figure;
scatter3(time_values, zeros(size(time_values)), capacitance_values, 36, capacitance_values, 'filled');
colormap(jet);  % Use a jet color map ranging from blue to red
colorbar;

% Manually adjust the color axis to prevent errors from identical values
constant_value = capacitance_values(1);  % Since all values are the same
caxis([constant_value - 0.01, constant_value + 0.01]);  % Add a small range to the color axis

% Enhance the plot
xlabel('Time (ms)');
ylabel('Dummy Y-Axis (Constant)');
zlabel('Capacitance (pF)');
title('3D Scatter Plot of Capacitance over Time for Staphylococcus aureus');
grid on;
```

Appendix Figure E.4: MatLab code developed for *Staphylococcus aureus* plot

```
% Time values (X-axis)
time_values = 11:11:550;

% Capacitance values (Z-axis) for Streptococcus viridans
capacitance_values = [1.3845039062, 1.3845039062, 1.3845039062, 1.3845039062, ...
                      1.3845039062, 1.3845039062, 1.3845039062, 1.3845039062, ...
                      1.3845039062, 1.3845039062, 1.3845039062, 1.3845039062, ...
                      1.3845039062, 1.3845039062, 1.3845039062, 1.3845039062, ...
                      1.3845039062, 1.3845039062, 1.3845039062, 1.3845039062, ...
                      1.3845039062, 1.3845039062, 1.3845039062, 1.3845039062, ...
                      1.3845039062, 1.3845039062, 1.3845039062, 1.3845039062, ...
                      1.3845039062, 1.3845039062, 1.3845039062, 1.3845039062, ...
                      1.3845039062, 1.3845039062, 1.3845039062, 1.3845039062, ...
                      1.3845039062, 1.3845039062, 1.3845039062, 1.3845039062, ...
                      1.3845039062, 1.3845039062, 1.3845039062, 1.3845039062, ...
                      1.3845039062, 1.3845039062, 1.3845039062, 1.3845039062, ...
                      1.3845039062, 1.3845039062];

% Create a 3D scatter plot with color-coded points
figure;
scatter3(time_values, zeros(size(time_values)), capacitance_values, 36, capacitance_values, 'filled');
colormap(jet);  % Use a jet color map ranging from blue to red
colorbar;

% Manually adjust the color axis to prevent errors from identical values
constant_value = capacitance_values(1);  % Since all values are the same
caxis([constant_value - 0.01, constant_value + 0.01]);  % Add a small range to the color axis

% Enhance the plot
xlabel('Time (ms)');
ylabel('Dummy Y-Axis (Constant)');
zlabel('Capacitance (pF)');
title('3D Scatter Plot of Capacitance over Time for Streptococcus viridans');
grid on;
```

Appendix Figure E.5: MatLab code developed for *Streptococcus viridans* plot

```
% Time values (X-axis)
time_values = 11:11:550;

% Capacitance values (Z-axis) for Enterococcus faecium
capacitance_values = [1.5021625977, 1.5021625977, 1.5021625977, 1.5021625977, ...
                      1.5021625977, 1.5021625977, 1.5021625977, 1.5021625977, ...
                      1.5021625977, 1.5021625977, 1.5021625977, 1.5021625977, ...
                      1.5021625977, 1.5021625977, 1.5021625977, 1.5021625977, ...
                      1.5021625977, 1.5021625977, 1.5021625977, 1.5021625977, ...
                      1.5021625977, 1.5021625977, 1.5021625977, 1.5021625977, ...
                      1.5021625977, 1.5021625977, 1.5021625977, 1.5021625977, ...
                      1.5021625977, 1.5035375977, 1.5035375977, 1.5010800781, ...
                      1.4999584961, 1.4999584961, 1.4999584961, 1.4999584961, ...
                      1.4999584961, 1.4999584961, 1.4999584961, 1.4999584961, ...
                      1.4999584961, 1.4999584961, 1.4999584961, 1.4999584961, ...
                      1.4999584961, 1.4999584961, 1.4999584961, 1.4999584961, ...
                      1.4999584961, 1.4999584961];

% Create a 3D scatter plot with color-coded points
figure;
scatter3(time_values, zeros(size(time_values)), capacitance_values, 36, capacitance_values, 'filled');
colormap(jet);  % Use a jet color map ranging from blue to red
colorbar;
caxis([min(capacitance_values) max(capacitance_values)]);  % Set the color axis limits to match capacitance values

% Enhance the plot
xlabel('Time (ms)');
ylabel('Dummy Y-Axis (Constant)');
zlabel('Capacitance (pF)');
title('3D Scatter Plot of Capacitance over Time for Enterococcus faecium');
grid on;
```

Appendix Figure E.6: MatLab code developed for *Enterococcus faecium* plot

```
% Time values (X-axis) from 11 ms to 539 ms at 11 ms intervals
time_values = 11:11:539;

% Capacitance values (Z-axis) for Candida albicans
capacitance_values = [2.6759970703, 2.6759970703, 2.6759970703, 2.6759970703, ...
                      2.6759970703, 2.6759970703, 2.6759970703, 2.6759970703, ...
                      2.6759970703, 2.6759970703, 2.6759970703, 2.6759970703, ...
                      2.6759970703, 2.6759970703, 2.6759970703, 2.6759970703, ...
                      2.6759970703, 2.6759970703, 2.6759970703, 2.6759970703, ...
                      2.6759970703, 2.6759970703, 2.6759970703, 2.6759970703, ...
                      2.6759970703, 2.6759970703, 2.6759970703, 2.6759970703, ...
                      2.6759970703, 2.6759970703, 2.6759970703, 2.6759970703, ...
                      2.6759970703, 2.6759970703, 2.6759970703, 2.6759970703, ...
                      2.6759970703, 2.6759970703, 2.6759970703, 2.6759970703, ...
                      2.6759970703, 2.6759970703, 2.6759970703, 2.6759970703, ...
                      2.6759970703, 2.6759970703, 2.6759970703, 2.6759970703, ...
                      2.6759970703];

% Create a 3D scatter plot with color-coded points
figure;
scatter3(time_values, zeros(size(time_values)), capacitance_values, 36, capacitance_values, 'filled');
colormap(jet);  % Use a jet color map ranging from blue to red
colorbar;

% Set the color axis manually to provide some range if values are constant
constant_value = capacitance_values(1);
caxis([constant_value - 0.01, constant_value + 0.01]);  % Providing a small artificial range

% Enhance the plot
xlabel('Time (ms)');
ylabel('Dummy Y-Axis (Constant)');
zlabel('Capacitance (pF)');
title('3D Scatter Plot of Capacitance over Time for Candida albicans');
grid on;
```

Appendix Figure E.7: MatLab code developed for *Candida albicans* plot

```
% Time values (X-axis)
time_values = 11:11:550;

% Capacitance values for Staphylococcus aureus
capacitance_s_aureus = [3.8496347656, 3.8496347656, 3.8496347656, 3.8496347656, ...
                        3.8496347656, 3.8496347656, 3.8496347656, 3.8496347656, ...
                        3.8496347656, 3.8496347656, 3.8496347656, 3.8496347656, ...
                        3.8496347656, 3.8496347656, 3.8496347656, 3.8496347656, ...
                        3.8496347656, 3.8496347656, 3.8496347656, 3.8496347656, ...
                        3.8496347656, 3.8496347656, 3.8496347656, 3.8496347656, ...
                        3.8496347656, 3.8496347656, 3.8496347656, 3.8496347656, ...
                        3.8496347656, 3.8496347656, 3.8496347656, 3.8496347656, ...
                        3.8496347656, 3.8496347656, 3.8496347656, 3.8496347656, ...
                        3.8496347656, 3.8496347656, 3.8496347656, 3.8496347656, ...
                        3.8496347656, 3.8496347656, 3.8496347656, 3.8496347656, ...
                        3.8496347656, 3.8496347656, 3.8496347656, 3.8496347656, ...
                        3.8496347656, 3.8496347656];

% Capacitance values for Streptococcus viridans
capacitance_s_viridans = [1.3845039062, 1.3845039062, 1.3845039062, 1.3845039062, ...
                          1.3845039062, 1.3845039062, 1.3845039062, 1.3845039062, ...
                          1.3845039062, 1.3845039062, 1.3845039062, 1.3845039062, ...
                          1.3845039062, 1.3845039062, 1.3845039062, 1.3845039062, ...
                          1.3845039062, 1.3845039062, 1.3845039062, 1.3845039062, ...
                          1.3845039062, 1.3845039062, 1.3845039062, 1.3845039062, ...
                          1.3845039062, 1.3845039062, 1.3845039062, 1.3845039062, ...
                          1.3845039062, 1.3845039062, 1.3845039062, 1.3845039062, ...
                          1.3845039062, 1.3845039062, 1.3845039062, 1.3845039062, ...
                          1.3845039062, 1.3845039062, 1.3845039062, 1.3845039062, ...
                          1.3845039062, 1.3845039062, 1.3845039062, 1.3845039062, ...
                          1.3845039062, 1.3845039062, 1.3845039062, 1.3845039062, ...
                          1.3845039062, 1.3845039062];

% Capacitance values for Enterococcus faecium
capacitance_e_faecium = [1.5021625977, 1.5021625977, 1.5021625977, 1.5021625977, ...
                         1.5021625977, 1.5021625977, 1.5021625977, 1.5021625977, ...
                         1.5021625977, 1.5021625977, 1.5021625977, 1.5021625977, ...
```

Appendix Figure E.8: MatLab code (part 1) developed for the plot that illustrates the Gram Positive Bacteria

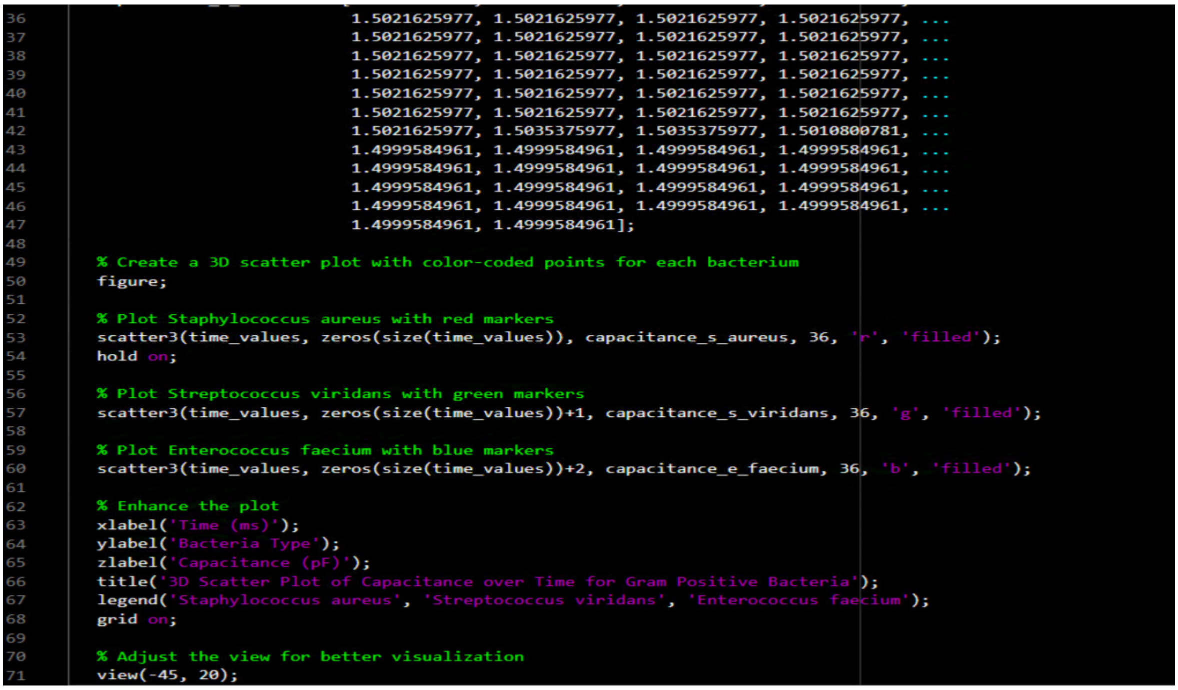

```
                         1.5021625977, 1.5021625977, 1.5021625977, 1.5021625977, ...
                         1.5021625977, 1.5021625977, 1.5021625977, 1.5021625977, ...
                         1.5021625977, 1.5021625977, 1.5021625977, 1.5021625977, ...
                         1.5021625977, 1.5021625977, 1.5021625977, 1.5021625977, ...
                         1.5021625977, 1.5021625977, 1.5021625977, 1.5021625977, ...
                         1.5021625977, 1.5021625977, 1.5021625977, 1.5021625977, ...
                         1.5021625977, 1.5035375977, 1.5035375977, 1.5010800781, ...
                         1.4999584961, 1.4999584961, 1.4999584961, 1.4999584961, ...
                         1.4999584961, 1.4999584961, 1.4999584961, 1.4999584961, ...
                         1.4999584961, 1.4999584961, 1.4999584961, 1.4999584961, ...
                         1.4999584961, 1.4999584961, 1.4999584961, 1.4999584961, ...
                         1.4999584961, 1.4999584961];

% Create a 3D scatter plot with color-coded points for each bacterium
figure;

% Plot Staphylococcus aureus with red markers
scatter3(time_values, zeros(size(time_values)), capacitance_s_aureus, 36, 'r', 'filled');
hold on;

% Plot Streptococcus viridans with green markers
scatter3(time_values, zeros(size(time_values))+1, capacitance_s_viridans, 36, 'g', 'filled');

% Plot Enterococcus faecium with blue markers
scatter3(time_values, zeros(size(time_values))+2, capacitance_e_faecium, 36, 'b', 'filled');

% Enhance the plot
xlabel('Time (ms)');
ylabel('Bacteria Type');
zlabel('Capacitance (pF)');
title('3D Scatter Plot of Capacitance over Time for Gram Positive Bacteria');
legend('Staphylococcus aureus', 'Streptococcus viridans', 'Enterococcus faecium');
grid on;

% Adjust the view for better visualization
view(-45, 20);
```

Appendix Figure E.9: MatLab code (part 2) developed for the plot that illustrates the Gram Positive Bacteria

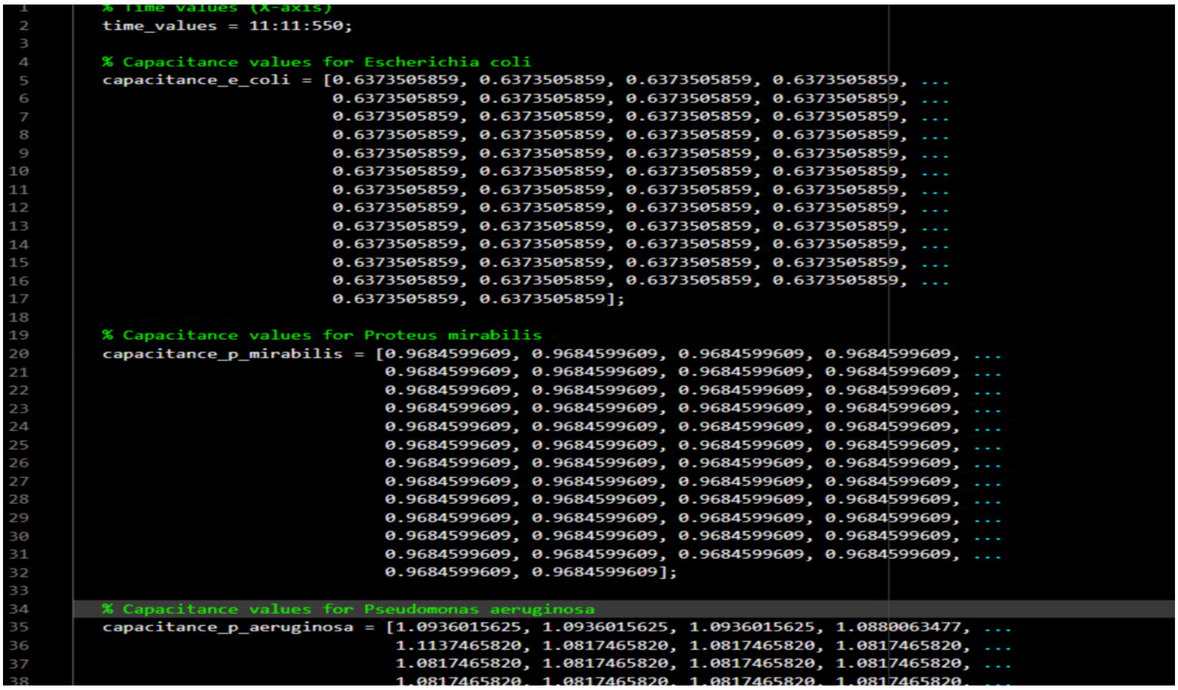

```
% Time values (X-axis)
time_values = 11:11:550;

% Capacitance values for Escherichia coli
capacitance_e_coli = [0.6373505859, 0.6373505859, 0.6373505859, 0.6373505859, ...
                      0.6373505859, 0.6373505859, 0.6373505859, 0.6373505859, ...
                      0.6373505859, 0.6373505859, 0.6373505859, 0.6373505859, ...
                      0.6373505859, 0.6373505859, 0.6373505859, 0.6373505859, ...
                      0.6373505859, 0.6373505859, 0.6373505859, 0.6373505859, ...
                      0.6373505859, 0.6373505859, 0.6373505859, 0.6373505859, ...
                      0.6373505859, 0.6373505859, 0.6373505859, 0.6373505859, ...
                      0.6373505859, 0.6373505859, 0.6373505859, 0.6373505859, ...
                      0.6373505859, 0.6373505859, 0.6373505859, 0.6373505859, ...
                      0.6373505859, 0.6373505859, 0.6373505859, 0.6373505859, ...
                      0.6373505859, 0.6373505859, 0.6373505859, 0.6373505859, ...
                      0.6373505859, 0.6373505859, 0.6373505859, 0.6373505859, ...
                      0.6373505859, 0.6373505859];

% Capacitance values for Proteus mirabilis
capacitance_p_mirabilis = [0.9684599609, 0.9684599609, 0.9684599609, 0.9684599609, ...
                           0.9684599609, 0.9684599609, 0.9684599609, 0.9684599609, ...
                           0.9684599609, 0.9684599609, 0.9684599609, 0.9684599609, ...
                           0.9684599609, 0.9684599609, 0.9684599609, 0.9684599609, ...
                           0.9684599609, 0.9684599609, 0.9684599609, 0.9684599609, ...
                           0.9684599609, 0.9684599609, 0.9684599609, 0.9684599609, ...
                           0.9684599609, 0.9684599609, 0.9684599609, 0.9684599609, ...
                           0.9684599609, 0.9684599609, 0.9684599609, 0.9684599609, ...
                           0.9684599609, 0.9684599609, 0.9684599609, 0.9684599609, ...
                           0.9684599609, 0.9684599609, 0.9684599609, 0.9684599609, ...
                           0.9684599609, 0.9684599609, 0.9684599609, 0.9684599609, ...
                           0.9684599609, 0.9684599609, 0.9684599609, 0.9684599609, ...
                           0.9684599609, 0.9684599609];

% Capacitance values for Pseudomonas aeruginosa
capacitance_p_aeruginosa = [1.0936015625, 1.0936015625, 1.0936015625, 1.0880063477, ...
                            1.1137465820, 1.0817465820, 1.0817465820, 1.0817465820, ...
                            1.0817465820, 1.0817465820, 1.0817465820, 1.0817465820, ...
                            1.0817465820, 1.0817465820, 1.0817465820, 1.0817465820, ...
```

Appendix Figure E.10: MatLab code (part 1) developed for the plot that illustrates the Gram Negative Bacteria

```matlab
                              1.0817465820, 1.0817465820, 1.0817465820, 1.0817465820, ...
                              1.0817465820, 1.0817465820, 1.0817465820, 1.0817465820, ...
                              1.0817465820, 1.0817465820, 1.0817465820, 1.0817465820, ...
                              1.0817465820, 1.0817465820, 1.0817465820, 1.0817465820, ...
                              1.0817465820, 1.0817465820, 1.0817465820, 1.0817465820, ...
                              1.0817465820, 1.0817465820, 1.0817465820, 1.0817465820, ...
                              1.0817465820, 1.0817465820, 1.0817465820, 1.0817465820, ...
                              1.0817465820, 1.0817465820, 1.0817465820, 1.0817465820, ...
                              1.0817465820, 1.0817465820, 1.0817465820, 1.0817465820, ...
                              1.0817465820, 1.0817465820, 1.0817465820, 1.0817465820, ...
                              1.0817465820, 1.0817465820];

% Create a 3D scatter plot with color-coded points for each bacterium
figure;

% Plot Escherichia coli with red markers
scatter3(time_values, zeros(size(time_values)), capacitance_e_coli, 36, 'r', 'filled');
hold on;

% Plot Proteus mirabilis with green markers
scatter3(time_values, zeros(size(time_values))+1, capacitance_p_mirabilis, 36, 'g', 'filled');

% Plot Pseudomonas aeruginosa with blue markers
scatter3(time_values, zeros(size(time_values))+2, capacitance_p_aeruginosa, 36, 'b', 'filled');

% Enhance the plot
xlabel('Time (ms)');
ylabel('Bacteria Type');
zlabel('Capacitance (pF)');
title('3D Scatter Plot of Capacitance over Time for Gram Negative Bacteria');
legend('Escherichia coli', 'Proteus mirabilis', 'Pseudomonas aeruginosa');
grid on;

% Adjust the view for better visualization
view(-45, 20);
```

Appendix Figure E.11: MatLab code (part 2) developed for the plot that illustrates the Gram Negative Bacteria

```matlab
% Time values (X-axis)
time_values = 11:11:550;

% Capacitance values for Gram-Negative Bacteria
capacitance_e_coli = [0.6373505859, 0.6373505859, 0.6373505859, 0.6373505859, ...
                      0.6373505859, 0.6373505859, 0.6373505859, 0.6373505859, ...
                      0.6373505859, 0.6373505859, 0.6373505859, 0.6373505859, ...
                      0.6373505859, 0.6373505859, 0.6373505859, 0.6373505859, ...
                      0.6373505859, 0.6373505859, 0.6373505859, 0.6373505859, ...
                      0.6373505859, 0.6373505859, 0.6373505859, 0.6373505859, ...
                      0.6373505859, 0.6373505859, 0.6373505859, 0.6373505859, ...
                      0.6373505859, 0.6373505859, 0.6373505859, 0.6373505859, ...
                      0.6373505859, 0.6373505859, 0.6373505859, 0.6373505859, ...
                      0.6373505859, 0.6373505859, 0.6373505859, 0.6373505859, ...
                      0.6373505859, 0.6373505859, 0.6373505859, 0.6373505859, ...
                      0.6373505859, 0.6373505859, 0.6373505859, 0.6373505859, ...
                      0.6373505859, 0.6373505859];

capacitance_p_mirabilis = [0.9684599609, 0.9684599609, 0.9684599609, 0.9684599609, ...
                           0.9684599609, 0.9684599609, 0.9684599609, 0.9684599609, ...
                           0.9684599609, 0.9684599609, 0.9684599609, 0.9684599609, ...
                           0.9684599609, 0.9684599609, 0.9684599609, 0.9684599609, ...
                           0.9684599609, 0.9684599609, 0.9684599609, 0.9684599609, ...
                           0.9684599609, 0.9684599609, 0.9684599609, 0.9684599609, ...
                           0.9684599609, 0.9684599609, 0.9684599609, 0.9684599609, ...
                           0.9684599609, 0.9684599609, 0.9684599609, 0.9684599609, ...
                           0.9684599609, 0.9684599609, 0.9684599609, 0.9684599609, ...
                           0.9684599609, 0.9684599609, 0.9684599609, 0.9684599609, ...
                           0.9684599609, 0.9684599609, 0.9684599609, 0.9684599609, ...
                           0.9684599609, 0.9684599609, 0.9684599609, 0.9684599609, ...
                           0.9684599609, 0.9684599609];

capacitance_p_aeruginosa = [1.0936015625, 1.0936015625, 1.0936015625, 1.0880063477, ...
                            1.1137465820, 1.0817465820, 1.0817465820, 1.0817465820, ...
                            1.0817465820, 1.0817465820, 1.0817465820, 1.0817465820, ...
                            1.0817465820, 1.0817465820, 1.0817465820, 1.0817465820, ...
                            1.0817465820, 1.0817465820, 1.0817465820, 1.0817465820, ...
```

Appendix Figure E.12: MatLab code (part 1) developed for the plot that illustrates every single microorganism in comparison with each other

```
                          1.0817465820, 1.0817465820, 1.0817465820, 1.0817465820, ...
                          1.0817465820, 1.0817465820, 1.0817465820, 1.0817465820, ...
                          1.0817465820, 1.0817465820, 1.0817465820, 1.0817465820, ...
                          1.0817465820, 1.0817465820, 1.0817465820, 1.0817465820, ...
                          1.0817465820, 1.0817465820, 1.0817465820, 1.0817465820, ...
                          1.0817465820, 1.0817465820, 1.0817465820, 1.0817465820, ...
                          1.0817465820, 1.0817465820, 1.0817465820, 1.0817465820, ...
                          1.0817465820, 1.0817465820, 1.0817465820, 1.0817465820, ...
                          1.0817465820, 1.0817465820, 1.0817465820, 1.0817465820, ...
                          1.0817465820, 1.0817465820, 1.0817465820, 1.0817465820, ...
                          1.0817465820, 1.0817465820];

  % Capacitance values for Gram-Positive Bacteria
  capacitance_s_aureus = [3.8496347656, 3.8496347656, 3.8496347656, 3.8496347656, ...
                          3.8496347656, 3.8496347656, 3.8496347656, 3.8496347656, ...
                          3.8496347656, 3.8496347656, 3.8496347656, 3.8496347656, ...
                          3.8496347656, 3.8496347656, 3.8496347656, 3.8496347656, ...
                          3.8496347656, 3.8496347656, 3.8496347656, 3.8496347656, ...
                          3.8496347656, 3.8496347656, 3.8496347656, 3.8496347656, ...
                          3.8496347656, 3.8496347656, 3.8496347656, 3.8496347656, ...
                          3.8496347656, 3.8496347656, 3.8496347656, 3.8496347656, ...
                          3.8496347656, 3.8496347656, 3.8496347656, 3.8496347656, ...
                          3.8496347656, 3.8496347656, 3.8496347656, 3.8496347656, ...
                          3.8496347656, 3.8496347656, 3.8496347656, 3.8496347656, ...
                          3.8496347656, 3.8496347656, 3.8496347656, 3.8496347656, ...
                          3.8496347656, 3.8496347656];

  capacitance_s_viridans = [1.3845039062, 1.3845039062, 1.3845039062, 1.3845039062, ...
                            1.3845039062, 1.3845039062, 1.3845039062, 1.3845039062, ...
                            1.3845039062, 1.3845039062, 1.3845039062, 1.3845039062, ...
                            1.3845039062, 1.3845039062, 1.3845039062, 1.3845039062, ...
                            1.3845039062, 1.3845039062, 1.3845039062, 1.3845039062, ...
                            1.3845039062, 1.3845039062, 1.3845039062, 1.3845039062, ...
                            1.3845039062, 1.3845039062, 1.3845039062, 1.3845039062, ...
                            1.3845039062, 1.3845039062, 1.3845039062, 1.3845039062, ...
                            1.3845039062, 1.3845039062, 1.3845039062, 1.3845039062, ...
                            1.3845039062, 1.3845039062, 1.3845039062, 1.3845039062, ...
                            1.3845039062, 1.3845039062, 1.3845039062, 1.3845039062, ...
```

Appendix Figure E.13: MatLab code (part 2) developed for the plot that illustrates every single microorganism in comparison with each other

```
                            1.3845039062, 1.3845039062, 1.3845039062, 1.3845039062, ...
                            1.3845039062, 1.3845039062, 1.3845039062, 1.3845039062, ...
                            1.3845039062, 1.3845039062, 1.3845039062, 1.3845039062, ...
                            1.3845039062, 1.3845039062];

  capacitance_e_faecium = [1.5021625977, 1.5021625977, 1.5021625977, 1.5021625977, ...
                           1.5021625977, 1.5021625977, 1.5021625977, 1.5021625977, ...
                           1.5021625977, 1.5021625977, 1.5021625977, 1.5021625977, ...
                           1.5021625977, 1.5021625977, 1.5021625977, 1.5021625977, ...
                           1.5021625977, 1.5021625977, 1.5021625977, 1.5021625977, ...
                           1.5021625977, 1.5021625977, 1.5021625977, 1.5021625977, ...
                           1.5021625977, 1.5021625977, 1.5021625977, 1.5021625977, ...
                           1.5021625977, 1.5035375977, 1.5035375977, 1.5010800781, ...
                           1.4999584961, 1.4999584961, 1.4999584961, 1.4999584961, ...
                           1.4999584961, 1.4999584961, 1.4999584961, 1.4999584961, ...
                           1.4999584961, 1.4999584961, 1.4999584961, 1.4999584961, ...
                           1.4999584961, 1.4999584961, 1.4999584961, 1.4999584961, ...
                           1.4999584961, 1.4999584961];

  % Capacitance values for Candida albicans (Fungus)
  capacitance_c_albicans = [2.6759970703, 2.6759970703, 2.6759970703, 2.6759970703, ...
                            2.6759970703, 2.6759970703, 2.6759970703, 2.6759970703, ...
                            2.6759970703, 2.6759970703, 2.6759970703, 2.6759970703, ...
                            2.6759970703, 2.6759970703, 2.6759970703, 2.6759970703, ...
                            2.6759970703, 2.6759970703, 2.6759970703, 2.6759970703, ...
                            2.6759970703, 2.6759970703, 2.6759970703, 2.6759970703, ...
                            2.6759970703, 2.6759970703, 2.6759970703, 2.6759970703, ...
                            2.6759970703, 2.6759970703, 2.6759970703, 2.6759970703, ...
                            2.6759970703, 2.6759970703, 2.6759970703, 2.6759970703, ...
                            2.6759970703, 2.6759970703, 2.6759970703, 2.6759970703, ...
                            2.6759970703, 2.6759970703, 2.6759970703, 2.6759970703, ...
                            2.6759970703, 2.6759970703, 2.6759970703, 2.6759970703, ...
                            2.6759970703, 2.6759970703];

  % Create a 3D scatter plot with color-coded points for each microorganism
  figure;

```

Appendix Figure E.14: MatLab code (part 3) developed for the plot that illustrates every single microorganism in comparison with each other

```
                                2.6759970703, 2.6759970703, 2.6759970703, 2.6759970703, ...
                                2.6759970703, 2.6759970703, 2.6759970703, 2.6759970703, ...
                                2.6759970703, 2.6759970703, 2.6759970703, 2.6759970703, ...
                                2.6759970703, 2.6759970703, 2.6759970703, 2.6759970703, ...
                                2.6759970703, 2.6759970703, 2.6759970703, 2.6759970703, ...
                                2.6759970703, 2.6759970703, 2.6759970703, 2.6759970703, ...
                                2.6759970703, 2.6759970703, 2.6759970703, 2.6759970703, ...
                                2.6759970703, 2.6759970703];

% Create a 3D scatter plot with color-coded points for each microorganism
figure;

% Plot Gram-Negative Bacteria (similar shades)
scatter3(time_values, zeros(size(time_values)), capacitance_e_coli, 36, 'c', 'filled'); hold on;
scatter3(time_values, zeros(size(time_values))+1, capacitance_p_mirabilis, 36, [0 0.5 1], 'filled');
scatter3(time_values, zeros(size(time_values))+2, capacitance_p_aeruginosa, 36, [0 0.75 1], 'filled');

% Plot Gram-Positive Bacteria (similar shades)
scatter3(time_values, zeros(size(time_values))+3, capacitance_s_aureus, 36, 'r', 'filled');
scatter3(time_values, zeros(size(time_values))+4, capacitance_s_viridans, 36, [1 0.5 0], 'filled');
scatter3(time_values, zeros(size(time_values))+5, capacitance_e_faecium, 36, [1 0.75 0], 'filled');

% Plot Candida albicans (Fungus - distinct color)
scatter3(time_values, zeros(size(time_values))+6, capacitance_c_albicans, 36, 'm', 'filled');

% Enhance the plot
xlabel('Time (ms)');
ylabel('Microorganism');
zlabel('Capacitance (pF)');
title('3D Scatter Plot of Capacitance over Time for All 7 Microrganisms (6 Bacteria (3 GN & 3 GP) and Fungus)');
legend('Escherichia coli', 'Proteus mirabilis', 'Pseudomonas aeruginosa', ...
       'Staphylococcus aureus', 'Streptococcus viridans', 'Enterococcus faecium', 'Candida albicans');
grid on;

% Adjust the view for better visualization
view(-45, 20);
```

Appendix Figure E.15: MatLab code (part 4) developed for the plot that illustrates every single microorganism in comparison with each other